# Activity-dependent coordination of protein synthesis and protein degradation through a neuronal-specific plasma membrane 20S proteasome complex

by
Kapil V. Ramachandran

A dissertation submitted to Johns Hopkins University in conformity with the requirements for the degree of Doctor of Philosophy

Baltimore, Maryland
March 2018

## Abstract

In the nervous system, rapidly occurring processes such as neuronal transmission and calcium signaling are affected by short-term inhibition of proteasome function. It is unclear how proteasomes are able to acutely regulate such processes, as this action is inconsistent with their canonical role in proteostasis. We discovered a mammalian nervous-system-specific membrane 20S proteasome complex that directly and rapidly modulates neuronal function by degrading intracellular proteins into extracellular peptides that can stimulate neuronal signaling. This proteasome complex is closely associated with neuronal plasma membranes, exposed to the extracellular space, and catalytically active. Selective inhibition of the membrane proteasome complex by a cell-impermeable proteasome inhibitor blocked the production of extracellular peptides and attenuated neuronal-activity-induced calcium signaling. Moreover, we observed that membrane-proteasome-derived peptides were sufficient to induce neuronal calcium signaling.

Analyzing the composition of the neuronal membrane proteasome (NMP), we did not find canonical ubiquitin-proteasome components required for recognizing a ubiquitiylated protein. This raised the fundamental question of how substrates were being targeted to the NMP for degradation into extracellular peptides. Remarkably, we observed newly synthesized polypeptides were rapidly turned over by the NMP in a stimulation-dependent manner. This turnover correlated with enhanced production of NMP-derived peptides in the extracellular space. Using parameters determined in these experiments, we constructed Markov process chain models *in silico* which predicted that the kinetics of this process necessitate coordination of translation and degradation. In a series of biochemical analyses, this predicted coordination was instantiated by NMP-mediated and ubiquitin-independent degradation of ribosome-associated nascent polypeptides. Using in-depth, global, and unbiased mass spectrometry, we identified the nascent protein substrates of the NMP. Among these substrates, we found that immediate-early gene products c-Fos and Npas4 are targeted by the NMP during ongoing activity-dependent protein

synthesis, prior to activity-induced transcriptional responses. Our findings challenge the prevailing notion that proteasomes function primarily to maintain proteostasis, and highlight a form of neuronal communication that takes place through the NMP. Together, these findings generally define an activity-dependent protein quality control program unique to the nervous system through the neuronal membrane proteasome.

Thesis advisor: Seth S. Margolis, Ph.D.

Thesis reader: Jeremy Nathans, M.D., Ph.D.

## Acknowledgements

I find myself writing this section last, because it is the by far the hardest to write, and one that I will probably rewrite the most because there are so many people that were so critical to this endeavor. They say it takes a village, and that's an underestimate. I want to first thank the mentors that believed in me at the beginning of my career. Nigel Atkinson is an unbelievable scientist and mentor, and gave me so much freedom to explore science as a High School student. Without him, I am not sure I would have had the same love for science and sheer curiosity that I do now. My next mentors, Geoff Pitt and Peggy Kirby fostered that naïve curiosity and instilled in me a sense of rigor and scientific depth. More than anything else, they let me find my own confidence as a scientist by challenging me and pushing me to be more critical and more careful. These and my other mentors before graduate school still advise me, and I will always continue to interact with them as friends and colleagues and mentors.

When I came to graduate school, I foolishly thought that I knew that I had a good biological framework to construct experiments and even thought I knew what scientific questions I wanted to tackle. I could not have been more wrong. I was taught by example what true scientific breadth and depth was, and so many students and faculty at Hopkins continuously reminded me of how much I have left to learn. Thank you to everyone for being so open, so willing to discuss the science, so willing the share reagents, time and space. In particular, I want to thank my thesis committee members Jeremy Nathans, Geraldine Seydoux, and Mike Caterina. They all pushed me to be more critical, more careful, and also more well-rounded as a scientist. My committee always made me step back and look at my science and career trajectories from an unbiased perspective, and were so instrumental to handling every situation I came across in graduate school. On that note, Carolyn Machamer has been such a genuine and phenomenal source of ideas and advice, and I am so glad I had the opportunity to call her a mentor and friend. I could not have envisioned or even imagined a more wonderful institution to grow up in as a

person and as a scientist. I will miss this place a lot, and I don't think any future institution that I am at can emulate it.

Graduate school is a process where perserverance is key, and it would not have been nearly as fun and fulfilling as it was without the wonderful friends that supported me here. Becca, Leah, and Tyler formed my base, and have been the very best friends and colleagues. Then, we brought the next class and the class after and so on, and it's been a barrage of a bigger and closer group. Eric, Leah, Jordan, PJ, Hannah and Rick, Bram, and Mich – y'all kept me going for the next few years. And then, there's the Goley lab. Seriously, you all are such goofballs and brilliant thinkers, and you made graduate school awesome. Erin – thanks for putting up with our shenanigans. Kousik, Chris, PJ, Liz, Allison, and Selam – oy. How do I start - Phudball, stupid hallway antics, late nights, food runs, serious science conversation (despite not working on anything similar), reverse translation conversations. I hope I can find friends and scientists like you all in my hallways forever.

And then there's the other part of that hallway, the Margolis lab. I had to put this near the end, because how or what do I say? You all were a constant source of encouragement, dealing with all the same highs and lows. We made an awesome team, and every lab meeting we had solid ideas and contributions. And to boot, you were a ton of fun – razor glove, haunted houses, post happy hour beers, movie nights, lunch breaks. I hope it stays the way it's been because we had a ton of fun over the past few years. We may not work on related topics, but that was the beauty of it, because we approached everything from a different perspective and that made each of our projects stronger. This brings me to Seth. Seth, you gave me the freedom to explore scientifically, and never said no when I had ideas that went against the grain. I don't believe any other mentor would have fostered this project in their labs like you did. And to boot, your generosity is what enables me to bring this project with me to Harvard as a Junior Fellow and continue to work on it. You were a constant source of encouragement and further instilled in me a sense of scientific rigor and wonder. You taught me the importance of simplicity in both

experiments and in communicating the science. They say that imitation is the sincerest form of flattery, and I hope to emulate aspects of Seth's mentorship in the future. To top it, Seth showed me that it is possible to be a rigorous, honest, and careful scientist while still being a great mentor and having a amazing life outside of lab. Sometimes, it is hard to believe that it is possible that anyone can do it all, but Seth gave me the blueprint and confidence that it can be done. Thank you, Seth.

I'm almost done. I would like to thank the BCMB program, especially Sharon and Arhonda. You are rockstars. Thank you to the many flies, zebrafish, and mice over the years, I hope that your lives come to benefit science and that I have done right by your contributions. To my family: Appa and Amma, I hope I have made you proud, and that I continue to make you proud. You two are the exemplars of parents and people, and I am amazed by the endless bounds of your love. I have learned about justice, philosophy, religion, duty, and kindness from you. I love you.

I hope that the effort and knowledge that I generate and will generate contributes to the advancement of science, to the pursuit of truth, and to human health. I hope that the mentors at Hopkins and before are proud of who they have raised, and I can't wait to keep pushing the boundaries forward. Thanks all.

## Table of Contents

## List of Tables

## List of Figures

Figure 5.3. Stimulation-induced NMP-dependent peptides (SNAPPs) protect against Aβ1-42 binding and downstream molecular cascades

## List of Acronyms

UPS – Ubiquitin proteasome system

NMP – Neuronal membrane proteasome

PM – Plasma membrane

Bio-Epox/EpB – Biotin-Epoxomicin

ATP – Adenosine triphosphate

tRNA – transfer ribonucleic acid

# Chapter 1

# Introduction

The ability to interact and communicate with the environment around us relies on fundamental intracellular events within neurons that enable robust and rapid neuronal communication. Neuronal communication takes place over multiple timescales, from rapid neurotransmission events (~1ms) to long-scale peptide and hormone communication (~hrs). This large variation in timescales is determined by an accompanying diversity in the molecular underpinnings of neuronal communication. Analyzing these molecular mechanisms, there are some contributors to neuronal communication that remain unexplored. For example, inhibition of the proteasome, the major machine and pathway that enables intracellular protein degradation, has previously been shown to affect the speed and intensity of neuronal transmission within seconds to minutes. This remains entirely inconsistent with what is known about the function for proteasomes in degrading proteins and regulating protein homeostasis over hours to days. This fundamental contradiction provided the rationale to explore unidentified functions for proteasomes in the nervous system to rapidly regulate neuronal signaling.

### 1.1 Protein homeostasis

Over their lifetime, cells experience a huge number of extracellular and intracellular cues. A small subset of examples include hormone and growth signals, cell-cell communication or contact-based signals, extracellular remodeling, organellar or DNA damage events, or generally aging-induced changes. In most cell types, these perturbations modulate gene and protein expression, which eventually leads to changes in both the identity and abundance of synthesized proteins. Such large-scale events generate stress on an already busy and dynamic system. Over the past few decades, a substantial number of studies have demonstrated that these fluctuations and stresses can have detrimental consequences for cell viability and outcomes. These effects are largely buffered by a series of intracellular pathways that regulate translation, protein folding, and protein degradation(Sontag, Samant, and Frydman 2017; Brehme et al. 2014; Labbadia and Morimoto 2015). We define protein homeostasis as the collective set of inter and intracellular mechanisms that enable a cell to retain a balanced proteome despite perturbations that can lead to

large changes in gene and protein expression. Protein homeostasis (or proteostasis) permits a system to maintain biochemical homeostasis when challenged with various stimuli.

Neurons display a particular and unique sensitivity to alterations in proteostasis(Brehme et al. 2014). Such vulnerabilities are most clearly demonstrated by the vast number of genetic disorders of protein aggregation that are characterized by severe phenotypes in the nervous system. Examples include Alzheimer's disease, Parkinson's disease, Amyotrophic Lateral Sclerosis, Huntington's disease, Frontotemporal Dementia, and so on. Moreover, disorders such as Autism spectrum disorder, Angelman Syndrome, Fragile X mental retardation disorder, and others have been linked to dysfunctions in both the protein synthesis or protein degradation machinery. Mechanisms that dictate the sensitivity of the nervous system over other tissues are only beginning to be uncovered and require far more investigation. There is a plethora of information regarding general mechanisms of proteostasis. For the purposes of providing background for my work, I will focus on core mechanisms of regulating protein synthesis and protein degradation.

The ribosome is the center of protein synthesis in all cells, generating the proteome that defines cellular composition and function(Alberts B 2002). At the ribosome, newly synthesized polypeptides leave the exit tunnel and must undergo the complex task of folding into the proper conformation. All the while, the remainder of the protein is continuing to be synthesized. This makes the ribosome an ideal platform for ensuring that protein synthesis occurs properly, without aggregation or misfolding(Pechmann, Willmund, and Frydman 2013). Nascent polypeptides are also therefore one of the most vulnerable populations in the cell to cellular perturbations(Dimitrova et al. 2009; Kramer et al. 2009; Ito et al. 2011; Pechmann, Willmund, and Frydman 2013; Gloge et al. 2014; Balchin, Hayer-Hartl, and Hartl 2016). As nascent polypeptides emerge from the exit tunnel, they begin folding co-translationally. A set of eukaryotic chaperones regulate this process, such as the nascent polypeptide-associated complex (NAC), HSP70, and the TRiC/CCT complex. As the polypeptide is being synthesized, nascent

chains can be detected from within the exit tunnel prior to exit, and the appropriate machinery recruited to the ribosome and the new nascent chain. Following synthesis, some substrates continue to need assistance in achieving the correct folded state. Prefoldin, TRiC/CCT, Hsp90, and a few other factors assist with complex proteins that cannot just be dealt with by ribosome-bound chaperones(Kirstein-Miles et al. 2013; Frydman et al. 1992; Frydman et al. 1994; Melville et al. 2003; Kim et al. 2010; Albanese, Reissmann, and Frydman 2010). For topologically challenging proteins, substrates need to be shuttled to complex chaperonins such as TRiC for sustained and protected folding. For other substrates such as Endoplasmic Reticulum (ER)-destined proteins, the signal sequence is recognized by signal recognition particle SRP. SRP competes or interacts with NAC, and traffics nascent chains to the appropriate fate(Thrift et al. 1991; Ng and Walter 1994; Ogg and Walter 1995; Powers and Walter 1996; Wiedmann et al. 1994; Siegel 1995; Gamerdinger et al. 2015).

Despite this large and robust repertoire of mechanisms to ensure polypeptide fidelity, a portion of synthesized proteins will contain translation or folding defects. These defects are only exaggerated by cellular stresses, and therefore, mechanisms to eliminate these improper proteins are critical to cellular viability. Two major systems of protein degradation are employed to ensure the fidelity of the proteome – 1) proteasome-mediated protein degradation and 2) autophagy or lysosome-mediate protein degradation.

First, the ubiquitin-proteasome system is the dominant form of protein degradation in almost all cells. First, a protein is tagged for degradation through an enzymatic cascade of E1 ubiquitin-activating enzymes that transfer ubiquitin to an E2. These E2 conjugate the ubiquitin to the E3 ubiquitin ligase, which finally marks a candidate substrate for ubiquitylation and subsequent degradation by the proteasome(Coux, Tanaka, and Goldberg 1996; Ciechanover 1998; Groll et al. 2000; Tsai 2014; Collins and Goldberg 2017). Proteasomes are large multisubunit catalytic machines that are made of a core 20S particle and a 19S cap. The 19S cap contains a number of proteins that contain ubiquitin-binding domains to recognize a ubiquitylated substrate,

deubiquitinases that remove the ubiquitylated protein, and then ATPases that use ATP hydrolysis to unfold the candidate substrate for its subsequent degradation. This step is thought to be necessary prior to degradation by the core 20S proteasome, because the pore of the 20S is fairly narrow (~6A°), which requires a substrate to be nearly linearized(Coux, Tanaka, and Goldberg 1996; Ciechanover 1998; Groll et al. 2000; Tsai 2014; Collins and Goldberg 2017). The core 20S degrades these proteins into peptide fragments. Typically, these peptides are turned over by exo- and endopeptidases within a few seconds and converted into single amino acids for reuse. This is why the proteasome is generally considered to be a degradation machine responsible for the ubiquitin-dependent turnover of proteins and sometimes to regenerate free amino acids.

The ubiquitin-proteasome system is the canonical system for degrading proteins, though there are cases where the proteasome is thought to have functions that are independent of ubiquitylation. Historically, there have been dozens of reports of ubiquitin-independent degradation of particular protein substrates. In particular, substrates such as c-Fos, p21, and ornithine decarboxylase have all been shown to be degraded without requiring tagging by ubiquitin(Hoyt, Zhang, and Coffino 2003; Asher et al. 2005; Bodenstein, Sunahara, and Neubig 2007; Tsvetkov, Reuven, and Shaul 2009; Tsvetkov et al. 2009; Adler et al. 2010). This has been shown to be driven through just the 20S proteasome, without the 19S cap. However, most scenarios in cells have focused on the capped 26S proteasome. Rising evidence does suggest that 20S proteasomes exist without 19S caps in cells, though these data are still actively debated and in progress(Ben-Nissan and Sharon 2014). In general, 20S proteasome-mediated ubiquitin-independent degradation is thought to be of unstructured or intrinsically disordered proteins(Coux, Tanaka, and Goldberg 1996; Asher et al. 2005; Tsvetkov et al. 2008; Rabl et al. 2008; Adler et al. 2010; Ben-Nissan and Sharon 2014). This seems likely since the 20S cannot itself unfold a substrate or recognize a ubiquitylated protein, and there must be some structure that can intrinsically be threaded through the narrow pore of the 20S

These structural constraints on what can enter the 20S therefore dictates that the majority of proteasome substrates must be processed through the ubiquitin pathway. How then do cells handle large aggregates, which are challenging to unfold using proteasomal ATPases? Typically, autophagy and lysosomal degradation handle such large cargo which can range from groups of proteins to entire organelles(Jiang et al. 2013; Yang and Klionsky 2010; Kaushik and Cuervo 2012; Wickner, Maurizi, and Gottesman 1999; Doyle, Genest, and Wickner 2013). In some cases, proteins are released from aggregates through chaperones and targeted to the autophagy machinery, and in other cases, the machinery is recruited to the aggregates. Regardless of how the autophagy machinery sees its cargo, the cargo is then loaded into a double-membrane vesicle and trafficked to the lysosome. This is thought to be driven by the concerted actions of over 40 autophagy-releated genes which function at the various steps of this process. While the progression through autophagy has largely been thought to be vectorial and sequential, recent data runs contradictory to this paradigm. Certainly, the pathways is critically important over longer timescales (~hrs to days) to determine protein turnover or that of large aggregates. However, because of the complexity and intrinsic speed of the mechanisms involved, autophagy is unlikely to provide major contributions to rapid cellular events, such as neuronal communication. Both the protein synthesis and protein degradation machinery are far more poised to participate in such mechanisms. While seemingly contradictory to their canonical role in regulating global protein homeostasis, such rapid mechanisms are tantalizing to consider and could open new domains in biology.

### 1.2 Protein synthesis and proteasome-mediated protein degradation in the nervous system

Mounting evidence suggests that both ribosomes and proteasomes are regulated in tissue-specific manners. For example, recent reports reveal the expression of tRNAs that are unique to the nervous system. Interfering with or mutations in this tRNA leads to severe neurodegenerative phenotypes(Ishimura et al. 2014). In addition, components that regulate the translation life cycle have been shown to be unique to certain tissues, such as erythrocytes(Mills et al. 2016).

Translation is even regulated at the level of codon usage across tissues, which have clear effects on translation efficiency(Plotkin, Robins, and Levine 2004; Dittmar, Goodenbour, and Pan 2006). How these different modes of translational regulation come together to modulate a tissue-specific outcome is largely unexplored. Finally, while older studies suggest that the composition of ribosomes themselves may be different in different tissues, these studies have not been rigorously followed up using modern approaches.

What about tissue-specific proteasome expression? There are many modes of regulation of the UPS to focus on. For example, TRIM32 is a tissue-specific ubiquitin ligase that is restricted to skeletal muscle(Lazzari and Meroni 2016). This serves as a way of modulating substrate selectivity in different tissues. There are also a number of situations where the proteasome composition itself is altered. First and foremost, three major types of core 20S proteasomes have been identified in different tissues. The most classic example for tissue-specific proteasome expression is in the immune system. Here, the so-called immunoproteasome contains three unique subunits that are highly enriched in the immune system that swap places into the normal proteasome(Rock et al. 2014; Ettari et al. 2017; Freudenburg et al. 2013; Basler, Kirk, and Groettrup 2013; Johnston-Carey, Pomatto, and Davies 2015; Winter et al. 2017). This subunit replacement results in a proteasome that is more finely tuned towards generating longer peptides. In fact, these peptides go on to be processed and presented as antigenic peptides that allow cells to dictate self vs non-self. Therefore, this tissue-specific proteasome degradation system lies at the heart of how the immune system functions. In addition, the thymoproteasome has shown to utilize a different β5 subunit, the production of CD4+ T cells that are generated in the thymus(Murata, Takahama, and Tanaka 2008). These cells are necessary for mounting a strong antigenic response against viral infections and other challenges to the immune system. Finally, the most extensive modulation in proteasome composition has been observed in spermatids(Zimmerman and Sutovsky 2009; Rivkin et al. 2009; Kong, Diaz, and Morales 2009;

Yokota, Harada, and Sawada 2010; D'Amours et al. 2010; Sanchez et al. 2011; Rosales et al. 2011; Sasanami et al. 2012; Uechi, Hamazaki, and Murata 2014; Richburg, Myers, and Bratton 2014). These proteasome subunits undergo extensive alternative splicing, generating a series of different types of proteasomes in different parts of the sperm. Studies looking into this further have shown different capping structures in different regions of sperm. For example, nuclear spermatoproteasomes have been shown to be capped by PA200 which enables efficient degradation of histones. Perhaps the most unusual and intriguing observation of spermatoproteasomes is their localization to plasma membranes. A few groups have made this observation, though they have not at all been followed up on or studied in great detail.

Indeed, such tissue-specific regulation is also observed in the nervous system. This seems logical as neurons, as large polarized and spatially segregated cells, need to solve the challenging problem of local protein synthesis and degradation near sites of activity without relying on transcriptional responses. Local protein synthesis has been detected over the past two deacdes using chemical reporters of protein synthesis. Initially, these studies were motivated by observations that ribosomes were localized at the base of dendritic spines, and even in axon terminals(Steward and Levy 1982; Steward and Falk 1991; Steward and Worley 2001). Later studies developed reporters which typically utilize either unnatural amino acid incorporation and detection by mass spectrometry, or incorporation of puromycin to disrupt the translating nascent polypeptide and subsequent detection using antibodies against puromycin(Aakalu et al. 2001; Dieterich et al. 2010; Landgraf et al. 2015). These techniques have all suggested that translation occurs both pre- and post-synaptically, though there continues to be debate about this(Tcherkezian et al. 2010). In addition to spatial regulation of protein synthesis, there is also evidence of the role for neuronal activity to modulate protein synthesis. Based on some of the puromycin-based reporters, the Schuman group has reported that neuronal activity bi-directionally modulates the amount of protein synthesis(Aakalu et al. 2001; Bingol and Schuman 2006; Dieterich et al. 2010). Additional evidence based on puromycylation and other

pharmacological experiments reveals that neuronal activity relieves ribosomal stalling on dendritic mRNAs(Graber et al. 2013). This suggests that a large portion of mRNAs in dendrites are held in translationally repressed states, such as in stress granules(Ramaswami, Taylor, and Parker 2013; Wheeler et al. 2016; Protter and Parker 2016; Protter et al. 2018). Somehow, neuronal activity may play a critical role in activating or translating these transcripts. Regardless, the role for activity in protein translation seems to be an emerging modality of post-transcriptional regulation of the proteome.

Another mechanism by which the proteome can be remodeled is through proteasome-mediated protein degradation. Proteasomes have been shown to be distributed all across the neuron, from the nucleus, soma, dendrites, axons, and even in dendritic spines(Asano et al. 2015; Campbell and Holt 2001; Ehlers 2003; Bingol and Schuman 2006; Tai and Schuman 2008b). Components of the UPS do exist at spines as well, such as the E3 ubiquitin ligases IDOL, Trim3, and Ube3A(Liu et al. 2008; Albrecht et al. 1997; Tai et al. 2010; Schreiber et al. 2015; Lazzari and Meroni 2016). Other components have been shown to be enriched in the brain such as the ligase RNF182(Liu et al. 2008). Unusually, the initiating components of the ubiquitin cascade (E1s and E2s) have not been studied in dendrites or axons. Some investigation has also gone into biochemical separation of neuronal cultures, and purification of proteasome complexes to determine whether these proteasomes are 20S or single- or double-capped 26S proteasomes(Tai et al. 2010). These data surprisingly revealed that a significant fraction of proteasomes are 20S. In support of the different types of proteasomes in the nervous system, cryo-electron tomography analysis of proteasomes in intact hippocampal neurons reveals proteasomes in different capping states(Asano et al. 2015). In contrast to the biochemical methods, the majority of proteasomes detected by Cryo-ET methods are singly or doubly capped. These data are interpreted to mean that the the majority of proteasomes are in substrate processing modes. However, these data should be re-evaluated in the context of the significant amount of work on 20S proteasome-mediated ubiquitin-independent degradation. In addition, the capping of proteasomes seems to be

fairly dynamic, where some proteasomes are capped and uncapped depending on the activity state of the neuron. In response to excitatory neuronal stimuli, a large fraction of singly- and doubly-capped proteasomes have been shown to disassemble into uncapped 20S proteasomes. Again, much like protein synthesis, components of the protein degradation machinery seem to be modulated by neuronal activity(Ehlers 2003; Bingol and Schuman 2006). This extends to both the localization of proteasomes segregating to dendritic spines, and enzymatic activity of proteasome-mediated protein degradation increasing in response to stimulation.

Therefore, neuronal activity-dependent biochemical programs drive the enzymatic activity of both ribosomes and proteasomes. In addition, activity promotes the localization of both complexes to the same subcellular compartments. This leaves a fundamental but outstanding question: do the ribosome and proteasome coordinate their actions in any manner? Such a coordination could result in either or both ubiquitylation and degradation of polypeptides undergoing translation. Indeed, such co-translational mechanisms have been both postulated and observed(Robertson and Wheatley 1979; Wheatley, Giddings, and Inglis 1980; Wheatley, Grisolia, and Hernandez-Yago 1982; Wheatley and Inglis 1980). Historical studies on the fate of newly synthesized proteins have been extensively conducted and followed up on, though not in neuronal tissues. A major conclusion of these studies is that newly synthesized proteins can be incredibly susceptible to rapid turnover, potentially through co-translational mechanisms. However, compelling evidence for such turnover is largely lacking, with a few major exceptions. In contrast, substantial evidence has recently emerged for co-translational ubiquitylation. This is largely driven by Listerin1 (Ltn1) and the Ribosome Quality Control (RQC) complex(Brandman et al. 2012; von der Malsburg, Shao, and Hegde 2015; Yonashiro et al. 2016; Bengtson and Joazeiro 2010). Ltn1 is a ubiquitin ligase that is a component of the RQC complex. These proteins mediate a protein quality control response to recognize stalled ribosomes, separate the ribosomes, and eliminate the partial polypeptide through the ubiquitin-proteasome system. As a more general mechanism, co-translational ubiquitylation has been clearly demonstrated for a

variety of substrates in yeast that depends on a large series of ubiquitin ligases(Duttler, Pechmann, and Frydman 2013). A few studies have even gone on to show that some substrates are co-translationally degraded, potentially without the need for ubiquitylation. Beyond these types of near-direct interactions between UPS components and the ribosome, secondary consequences of signaling pathways have linked protein synthesis and degradation together. Of note, mammalian Target of Rapamycin (mTOR), a key metabolic sensor in mammalian cells, has clearly been shown to be involved in both proteasomal degradation and protein synthesis(Kelleher, Govindarajan, and Tonegawa 2004; Wu, Volta, et al. 2009; Zhao et al. 2015; Zhao, Garcia, and Goldberg 2016). Though interplay was posited by a few studies, these studies have come under question based on methodologies that they employ. More general mechanisms have also been proposed for the interplay between proteasomes and ribosomes. Proteasome inhibition has reproducibly shown to inhibit protein synthesis(Ding et al. 2006; Obeng et al. 2006). This likely occurs through the activation of the unfolded protein response, leading to phosphorylation of elongation initiation factor 2 alpha (eIF2α) and subsequent inhibition of protein synthesis.

The overall functions of protein synthesis and degradation in the nervous system have been studied for the better half of a century. Initially, this work was done using inhibitors against protein synthesis, and in particular, Puromycin. Puromycin is an aminoacyl-tRNA mimic that modified the growing nascent polypeptide and prematurely releases the nascent chain from the ribosome(Nathans and Neidle 1963; Nathans 1964). The earliest experiments with Puromycin in the nervous system injected tritiated radiolabeled Puromycin into the brains of mice, and monitored the fate of puromycylated peptides in the brain(Flexner et al. 1962; Flexner, Flexner, and Stellar 1963; Flexner et al. 1964; Flexner and Flexner 1967; Flexner and Flexner 1968; Roberts and Flexner 1969; Flexner et al. 1971). These studies revealed an unusually long lifetime of these radiopeptides, and that these peptides spread from the site of injection far into other regions of the brain. While the Flexners posited that these peptides could serve as tracers of

learning and memory, no follow up experiments were done for more than two decades. The next major set of experiments to address these questions injected Puromycin and cycloheximide into the brains of mice undergoing behavior tasks. These and many subsequent experiments determined the requirement for protein synthesis in learning and memory using a variety of paradigms in both amygdala and hippocampus. A corresponding plethora of data has been generated using inhibitors of protein degradation, which by and large have similar consequences in similar brain regions in similar behavioral tasks. Based on some fairly uncompelling data, these changes have been correlated to changes in the ubiquitylation state of proteins. However, changes in substrate levels in response to neuronal activity or under different behavioral paradigms needs to be clearly demonstrated.

Outside of behavioral contexts, many compelling studies on protein synthesis and degradation have been done. These have largely focused on the use of inhibitors of the synthesis and degradation machinery on long-term potentiation (LTP) and depression (LTD). These mechanisms are thought to be fundamental to the core function of the nervous system to encode information. LTP is defined as a stimulation-dependent sustained increase in synaptic strength that is thought to underlie learning and memory, while LTD is the opposite phenomenon(Nicoll and Roche 2013). Protein synthesis and protein degradation have been shown to be critical for the maintenance of LTP and LTD(Kelleher, Govindarajan, and Tonegawa 2004; Fonseca et al. 2006; Fonseca, Nagerl, and Bonhoeffer 2006; Klein, Castillo, and Jordan 2015). Intriguingly, neither have been shown to be involved in the induction of LTP (early-LTP). This is likely because calcium influx and the resulting receptor insertion events are critical for short LTP. However, the mechanisms underlying late-LTP and late-LTD are unknown. In addition, both protein synthesis and protein degradation have been shown to be critical for synaptic tagging and capture(Cai et al. 2010). This is thought to be a phenomenon underlying heterosynaptic plasticity, where one set of inputs influence the dynamic range of plasticity of an alternate set of inputs. The primary inputs are thought to modulate the alternate pathway by marking these neurons with so called “synaptic

tags". The tags are likely protein in origin, as they rely on protein synthesis to be established(Ding, Cecarini, and Keller 2007). Intriguingly though, they also rely on protein degradation. This seems unusual since if they were simply a set of proteins that were made, then protein degradation should not be necessary. Therefore, there seems to be a more complex phenomenon underlying synaptic tagging that may depend on the coordination of protein synthesis and degradation.

**1.3 Neuronal communication and small peptides**

Neuronal communication takes place over multiple timescales, from rapid neurotransmission events (~1ms) to long-scale peptide and hormone communication (~hrs). This diversity in timescale is driven by diversity in the molecular underpinnings of these events. Neurotransmission is dictated by fast and transient release of specific neurotransmitters which act on specific receptors(Hyman 2005). The duration of action for these molecules act is determined and regulated by specific reuptake mechanisms in both neurons and glial cells. The action of neurotransmitters tends to be fairly transient, and gives a short and directed signal in a determined manner. In contrast, hormone signaling begins with a series of signaling events, which drives the transcription of genes encoding the hormone products(Nestler et al. 2015). Subsequently, the pre-peptide neuropeptides must be processed to their active forms, and eventually exported and transported to their targets. The relative timescales of these actions provides critical information about their functions in the nervous system: while fast neurotransmission underlies fast membrane depolarization events, slow peptide hormone signaling is largely used for slow neuromodulation.

Blockade of the classic neurotransmitter receptors such as AMPA, NMDA, and GABAergic receptors inhibits miniature and evoked excitatory and inhibitory postsynaptic currents. This is the primary basis for the understanding that these receptors, and classic neurotransmission, is the dominant form of neuronal communication. In addition, neurotrophic and peptide signaling mechanisms can modulate neurotransmission. For example, brain-derived

neurotrophic factor (BDNF) can modulate the magnitude and type of LTP, though the exact role for and magnitude of this modulation is debated(Lu, Christian, and Lu 2008; Mei et al. 2011). These are largely considered to be in the class of neurotrophic factors, many of which modulate neurotransmitter release or function in unique circuits and perform particular functions. Other such factors include nerve growth factor (NGF), Ephrins, Insulin growth factor-1 (IGF-1), and many others(Bergado et al. 1997; Bozdagi, Tavassoli, and Buxbaum 2013; Ivanov et al. 2015). Many of these factors play important roles in the development of the nervous system, learning and memory, and molecular mechanisms underlying LTP and LTD. In addition to neurotrophic factors, a large class of neuromodulatory factors called neuropeptides are expressed in unique circuits to modulate behavior and circuit function. A classic example of a neuropeptide is Enkephalin, a 30 amino acid neuropeptide that largely regulates pain sensing. Another well-studied neuropeptide is oxytocin, which regulates a variety of social behaviors. Finally, there are classes of neuropeptides that regulate feeding and thirst, such as Gastrin, Ghrelin, and Agouti-related peptide (AGRP)(Nestler et al. 2015). Finally, small molecules are also capable of modulating neurotransmission. The most well studied and rigorous example of this is through endocannabinoids, which are released from the postsynaptic site and act at the presynaptic terminal to modulate neurotransmitter release. All of these types of atypical neurotransmitters, neuropeptides, and neuromodulators are derived from specific gene transcripts. This propeptides or prohormones are extensively post-translationally modified and cleaved to generate the active form, which are then released. There are exceptions to these rules, for molecules such as gasotransmitters such as nitric oxide, carbon monoxide, and hydrogen sulfide. Each of these can individually modify LTP, LTD, and a host of intracellular signaling pathways(Nestler et al. 2015). In addition, the endocannabinoids are also synthesized through regulated metabolic pathways and eventually released. The classic examples are the eicosanoids anandamide and 2-arachidonoylgycerol (2-AG). These lipids are released from the postsynaptic terminal and act as a

retrograde signal to modulate presynaptic synaptic release and overall neuronal excitability(Nestler et al. 2015).

All of these systems rely on transcriptional responses, cleavage of particular proproteins, or metabolic signaling mechanisms to generate functional neuropeptides and neuromodulators. However, inhibition of certain pathways that do not affect either of these canonical neuronal communication mechanisms can lead to changes in neuronal function and neuronal firing. The biochemical mechanisms that generate proteins and peptides within cells have extraordinary capacity to influence neuronal function. These mechanisms constitutively generate an enormous amount of proteins and peptides, and are necessary for the overall protein homeostasis of the cell. However, separating the contributions of these biochemical mechanisms to just protein homeostasis versus signaling remains to be clearly elucidated. This needs to be elaborated in light of data demonstrating that inhibition of these pathways can very rapidly modulate neuronal signaling. Therefore, the goal of my thesis work was to determine what the roles of protein synthesis and protein degradation were in rapid neuronal signaling. By investigating these mechanisms, I revealed a coordination between protein synthesis and degradation through a neuronal-specific plasma membrane 20S proteasome complex. This coordination and degradation generates a class of extracellular peptides that rapidly modulate neuronal calcium signaling.

**Table 3.1 Proteasome subunits in cytosolic and membrane proteasomes purifications**

| GENE | MW (kDa) | Exp 1 (MEM) | Exp 2 (MEM) | Exp 1 (CYTO) | Exp 2 (CYTO) | Protein identification probability (MEM) | Percentage sequence coverage Exp1 (MEM) | Percentage sequence coverage Exp2 (MEM) | Percentage sequence coverage Exp1 (CYTO) | Percentage sequence coverage Exp2 (CYTO) |
|---|---|---|---|---|---|---|---|---|---|---|
| PRS10 | 44 | 0 | 0 | 11 | 22 | 0 | 0 | 0 | 44.00% | 27.80% |
| PRS4 | 49 | 0 | 0 | 6 | 16 | 0 | 0 | 0 | 31.80% | 13.90% |
| PRS6A | 50 | 0 | 0 | 10 | 16 | 0 | 0 | 0 | 30.80% | 23.05% |
| PRS6B | 47 | 0 | 0 | 18 | 27 | 0 | 0 | 0 | 58.40% | 33.80% |
| PRS7 | 49 | 0 | 0 | 15 | 20 | 0 | 0 | 0 | 36.70% | 25.80% |
| PRS8 | 46 | 0 | 0 | 9 | 21 | 0 | 0 | 0 | 51.00% | 20.90% |
| PSMD1 | 106 | 0 | 0 | 20 | 48 | 0 | 0 | 0 | 29.98% | 18.60% |
| PSD11 | 47 | 22 | 6 | 14 | 19 | 0 | 48.81% | 11.85% | 43.10% | 31.80% |
| PSD12 | 53 | 0 | 0 | 8 | 24 | 0 | 0 | 0 | 52.19% | 15.57% |
| PSD13 | 43 | 0 | 0 | 7 | 21 | 0 | 0 | 0 | 40.20% | 16.00% |

| | | | | | | | | | | |
|---|---|---|---|---|---|---|---|---|---|---|
| PSDE | 35 | 0 | 0 | 2 | 11 | 0 | 0 | 0 | 28.40% | 4.52% |
| PSMD2 | 100 | 85 | 8 | 27 | 61 | 0 | 44.63% | 7.71% | 39.00% | 24.64% |
| PSMD3 | 61 | 0 | 0 | 11 | 35 | 0 | 0 | 0 | 54.38% | 18.88% |
| PSMD4 | 41 | 0 | 0 | 3 | 5 | 0 | 0 | 0 | 12.76% | 6.91% |
| PSMD5 | 56 | 0 | 0 | 2 | 4 | 0 | 0 | 0 | 6.15% | 3.77% |
| PSMD6 | 46 | 0 | 0 | 12 | 22 | 0 | 0 | 0 | 42.20% | 29.00% |
| PSMD7 | 37 | 0 | 0 | 8 | 14 | 0 | 0 | 0 | 32.70% | 19.90% |
| PSME4 | 211 | 0 | 0 | 16 | 3 | 0 | 0 | 0 | 17.30% | 1.84% |
| PSMG1 | 33 | 0 | 0 | 4 | 4 | 0 | 0 | 0 | 13.50% | 14.50% |
| PSMG2 | 30 | 0 | 0 | 4 | 7 | 0 | 0 | 0 | 15.20% | 20.80% |
| PSA1 | 30 | 13 | 13 | 30 | 39 | 100.00% | 42.22% | 39.20% | 51.69% | 77.23% |
| PSA2 | 26 | 10 | 6 | 36 | 29 | 100.00% | 45.70% | 41.50% | 58.70% | 58.10% |
| PSA3 | 28 | 16 | 9 | 35 | 37 | 100.00% | 57.64% | 27.04% | 54.80% | 52.00% |

| | | | | | | | | | | |
|---|---|---|---|---|---|---|---|---|---|---|
| PSA4 | 29 | 9 | 9 | 29 | 24 | 100.00% | 27.95% | 19.50% | 82.40% | 67.81% |
| PSA5 | 26 | 11 | 7 | 22 | 17 | 100.00% | 56.04% | 38.60% | 55.80% | 74.70% |
| PSA6 | 27 | 13 | 6 | 36 | 29 | 100.00% | 58.70% | 27.65% | 71.20% | 66.40% |
| PSA7 | 28 | 7 | 3 | 34 | 20 | 100.00% | 25.80% | 14.10% | 57.56% | 60.90% |
| PSB1 | 26 | 8 | 4 | 27 | 17 | 100.00% | 30.80% | 13.75% | 64.60% | 55.80% |
| PSB2 | 23 | 17 | 6 | 33 | 26 | 100.00% | 48.26% | 29.90% | 52.06% | 63.10% |
| PSB3 | 23 | 7 | 3 | 26 | 19 | 100.00% | 34.10% | 20.00% | 50.80% | 68.80% |
| PSB4 | 29 | 5 | 8 | 15 | 16 | 100.00% | 14.40% | 33.30% | 37.88% | 53.00% |
| PSB5 | 29 | 23 | 20 | 39 | 31 | 100.00% | 54.74% | 52.70% | 64.80% | 43.70% |
| PSB6 | 25 | 5 | 7 | 12 | 14 | 100.00% | 16.80% | 32.30% | 44.90% | 51.00% |
| PSB7 | 30 | 3 | 5 | 28 | 15 | 100.00% | 15.20% | 25.70% | 39.70% | 35.79% |
| PSB8 | 30 | 3 | 5 | | | 100.00% | 9.42% | 18.48% | 0 | 0 |

**Table 3.2 Membrane proteins associated with the NMP**

| GENE | MW | Exp 1 (MEM) | Exp 2 (MEM) | Exp 1 (CYTO) | Exp 2 (CYTO) | Protein identification probability (MEM) | Percentage sequence coverage Exp1 | Percentage sequence coverage Exp2 | Percentage sequence | Percentage sequence |
|---|---|---|---|---|---|---|---|---|---|---|
| AT1A3 | 112 | 201 | 186 | 0 | 0 | 100.00% | 38.42% | 31.37% | 0 | 0 |
| CMC1 | 75 | 93 | 57 | 0 | 0 | 100.00% | 36.67% | 49.70% | 0 | 0 |
| AT1A1 | 113 | 73 | 76 | 0 | 0 | 100.00% | 62.00% | 49.30% | 0 | 0 |
| AT1A2 | 112 | 41 | 63 | 0 | 0 | 98.40% | 34.00% | 38.10% | 0 | 0 |
| PLXA1 | 211 | 38 | 37 | 0 | 0 | 100.00% | 18.88% | 16.74% | 0 | 0 |
| PLXA4 | 213 | 29 | 42 | 0 | 0 | 100.00% | 14.31% | 18.68% | 0 | 0 |
| AT1B1 | 35 | 21 | 43 | 0 | 0 | 99.80% | 54.26% | 77.60% | 0 | 0 |
| GPM6A | 31 | 16 | 13 | 0 | 0 | 100.00% | 18.30% | 32.05% | 0 | 0 |
| 4F2 | 58 | 14 | 10 | 0 | 0 | 100.00% | 22.95% | 18.10% | 0 | 0 |
| EAA1 | 60 | 12 | 7 | 0 | 0 | 99.10% | 19.51% | 10.50% | 0 | 0 |
| SFXN3 | 35 | 11 | 20 | 0 | 0 | 99.80% | 35.80% | 53.30% | 0 | 0 |
| VDAC1 | 32 | 11 | 12 | 0 | 0 | 100.00% | 34.29% | 36.13% | 0 | 0 |

| | | | | | | | | | | |
|---|---|---|---|---|---|---|---|---|---|---|
| LPP3 | 35 | 9 | 10 | 0 | 0 | 99.20% | 31.70% | 25.30% | 0 | 0 |
| RTN1 | 84 | 8 | 8 | 0 | 0 | 97.00% | 7.94% | 5.64% | 0 | 0 |
| GRIA3 | 101 | 7 | 14 | 0 | 0 | 100.00% | 6.98% | 11.90% | 0 | 0 |
| PLTP | 54 | 7 | 5 | 0 | 0 | 100.00% | 15.66% | 10.34% | 0 | 0 |
| VDAC2 | 32 | 6 | 9 | 0 | 0 | 100.00% | 16.95% | 31.19% | 0 | 0 |
| RTN3 | 104 | 4 | 8 | 0 | 0 | 97.60% | 2.80% | 3.01% | 0 | 0 |

**Table 4.1 NMP substrates with p<.01**

| Gene Symbol | # Peptides | emPAI (rel. abundance) | Coverage | Molecular Weight (kDa) | Log Fold change | P values - bayes moderated | Q values - bayes moderated |
|---|---|---|---|---|---|---|---|
| Rgs4 | 10.000 | 3.924 | 46.829 | 23.200 | 1.102 | 0.000 | 0.001 |
| Npas4 | 3.000 | 0.501 | 4.988 | 87.200 | 0.809 | 0.000 | 0.002 |
| 1190005I06 Rik | 2.000 | 2.162 | 26.126 | 11.900 | 0.801 | 0.002 | 0.083 |
| Wbscr22 | 3.000 | 0.995 | 15.302 | 31.600 | 0.779 | 0.002 | 0.086 |
| Snurf | 1.000 | 0.778 | 19.718 | 8.400 | 0.731 | 0.000 | 0.015 |
| Hnrnpd | 22.000 | 204.353 | 51.961 | 32.700 | 0.664 | 0.005 | 0.104 |
| Bex2 | 3.000 | 0.874 | 27.907 | 15.400 | 0.623 | 0.000 | 0.006 |
| Fos | 5.000 | 3.329 | 15.000 | 40.800 | 0.619 | 0.000 | 0.010 |
| Myo6 | 59.000 | 6.743 | 49.268 | 149.500 | 0.596 | 0.007 | 0.121 |
| Fosl2 | 2.000 | 0.425 | 7.362 | 35.300 | 0.510 | 0.000 | 0.048 |
| Anxa5 | 24.000 | 12.183 | 82.759 | 35.700 | 0.486 | 0.007 | 0.115 |
| Lix1 | 3.000 | 0.638 | 13.830 | 31.900 | 0.474 | 0.006 | 0.112 |
| Mgme1 | 1.000 | 0.145 | 3.254 | 38.400 | 0.435 | 0.005 | 0.110 |
| Odc1 | 4.000 | 0.492 | 9.544 | 51.100 | 0.402 | 0.000 | 0.013 |
| Fosb | 4.000 | 1.783 | 15.385 | 36.000 | 0.402 | 0.000 | 0.048 |

| | | | | | | | |
|---|---|---|---|---|---|---|---|
| Creg2 | 2.000 | 0.292 | 9.028 | 31.700 | 0.363 | 0.001 | 0.064 |
| Slc39a9 | 1.000 | 0.389 | 2.540 | 33.200 | 0.360 | 0.005 | 0.105 |
| Ubc | 15.000 | 0.988 | 92.234 | 82.500 | 0.351 | 0.000 | 0.027 |
| Egr1 | 7.000 | 2.831 | 14.447 | 56.600 | 0.328 | 0.001 | 0.068 |
| Plk2 | 6.000 | 0.431 | 10.411 | 77.800 | 0.326 | 0.007 | 0.121 |
| Svs1 | 2.000 | 0.101 | 2.195 | 93.500 | 0.313 | 0.003 | 0.097 |
| Smpd4 | 13.000 | 1.228 | 21.219 | 96.700 | 0.313 | 0.000 | 0.048 |
| Rbm18 | 3.000 | 0.778 | 20.526 | 21.600 | 0.309 | 0.006 | 0.114 |
| Sox4 | 2.000 | 0.359 | 5.682 | 45.000 | 0.306 | 0.000 | 0.044 |
| Slc18b1 | 1.000 | 0.212 | 2.407 | 48.800 | 0.300 | 0.000 | 0.053 |
| Tmem130 | 3.000 | 0.350 | 10.979 | 46.600 | 0.288 | 0.001 | 0.083 |
| Rexo1 | 6.000 | 0.215 | 7.573 | 132.400 | 0.287 | 0.004 | 0.100 |
| 6330403K07Rik | 2.000 | 3.642 | 33.058 | 13.400 | 0.283 | 0.000 | 0.013 |
| Enc1 | 18.000 | 2.252 | 33.277 | 66.100 | 0.279 | 0.000 | 0.001 |
| Casd1 | 8.000 | 0.490 | 11.987 | 101.300 | 0.270 | 0.006 | 0.112 |
| Jund | 1.000 | 0.292 | 4.106 | 34.900 | 0.264 | 0.004 | 0.100 |
| Ggcx | 6.000 | 0.711 | 9.775 | 87.100 | 0.260 | 0.001 | 0.083 |
| Supt20 | 4.000 | 0.301 | 7.755 | 94.200 | 0.253 | 0.005 | 0.105 |
| Hmgcr | 15.000 | 1.268 | 18.952 | 98.100 | 0.250 | 0.000 | 0.013 |
| Tmem117 | 2.000 | 0.202 | 4.475 | 60.300 | 0.248 | 0.002 | 0.086 |
| Cic | 17.000 | 0.607 | 11.425 | 258.200 | 0.246 | 0.000 | 0.039 |

| | | | | | | | |
|---|---|---|---|---|---|---|---|
| Gnl3l | 12.000 | 1.581 | 25.650 | 65.200 | 0.246 | 0.001 | 0.083 |
| Ahctf1 | 16.000 | 0.382 | 10.194 | 254.600 | 0.242 | 0.000 | 0.048 |
| Tcof1 | 27.000 | 1.414 | 24.926 | 138.500 | 0.242 | 0.003 | 0.096 |
| Tpm1 | 22.000 | 17.233 | 54.577 | 32.800 | 0.241 | 0.005 | 0.110 |
| Nfx1 | 8.000 | 0.362 | 7.899 | 123.700 | 0.241 | 0.001 | 0.072 |
| Soat1 | 6.000 | 0.905 | 11.481 | 63.800 | 0.235 | 0.001 | 0.068 |
| Trpc4ap | 14.000 | 1.121 | 24.216 | 90.700 | 0.235 | 0.000 | 0.039 |
| COX2 | 7.000 | 25.827 | 30.837 | 25.900 | 0.233 | 0.003 | 0.097 |
| Junb | 7.000 | 2.728 | 34.884 | 35.700 | 0.232 | 0.001 | 0.083 |
| Sft2d3 | 2.000 | 0.425 | 13.208 | 21.900 | 0.231 | 0.004 | 0.099 |
| Fads1 | 9.000 | 2.981 | 22.595 | 52.300 | 0.228 | 0.001 | 0.066 |
| Ccnd1 | 8.000 | 1.818 | 38.486 | 35.900 | 0.226 | 0.001 | 0.083 |
| Wnt7b | 13.000 | 3.062 | 39.943 | 39.300 | 0.224 | 0.001 | 0.068 |
| Zfp871 | 3.000 | 0.218 | 4.228 | 71.500 | 0.223 | 0.004 | 0.100 |
| Prodh | 11.000 | 0.983 | 21.202 | 68.000 | 0.222 | 0.008 | 0.126 |
| Mbtps2 | 1.000 | 0.179 | 1.748 | 56.900 | 0.218 | 0.000 | 0.061 |
| 4930433I11 Rik | 2.000 | 0.129 | 1.108 | 69.800 | 0.216 | 0.006 | 0.114 |
| Mpnd | 2.000 | 0.334 | 7.828 | 55.900 | 0.215 | 0.005 | 0.106 |
| Clcc1 | 7.000 | 0.630 | 19.669 | 61.200 | 0.214 | 0.001 | 0.080 |
| Ndn | 11.000 | 2.675 | 38.769 | 36.800 | 0.213 | 0.000 | 0.013 |
| Tmem246 | 6.000 | 0.931 | 21.588 | 46.600 | 0.212 | 0.002 | 0.083 |

| | | | | | | | |
|---|---|---|---|---|---|---|---|
| Cox7c | 3.000 | 9.000 | 38.095 | 7.300 | 0.212 | 0.003 | 0.090 |
| Fads2 | 12.000 | 2.481 | 25.225 | 52.400 | 0.211 | 0.002 | 0.083 |
| Cadps | 54.000 | 8.412 | 50.300 | 150.800 | 0.211 | 0.002 | 0.088 |
| Atp2b4 | 50.000 | 11.969 | 40.355 | 136.900 | 0.209 | 0.005 | 0.104 |
| Sil1 | 12.000 | 2.775 | 37.634 | 52.400 | 0.208 | 0.002 | 0.086 |
| Ccdc91 | 12.000 | 2.311 | 28.054 | 50.000 | 0.204 | 0.000 | 0.044 |
| Olig1 | 7.000 | 3.394 | 40.385 | 27.100 | 0.203 | 0.003 | 0.099 |
| Galnt18 | 6.000 | 0.682 | 13.023 | 71.100 | 0.203 | 0.006 | 0.114 |
| Nog | 2.000 | 0.668 | 11.638 | 25.800 | 0.203 | 0.000 | 0.059 |
| Tm9sf1 | 4.000 | 0.468 | 9.241 | 68.900 | 0.202 | 0.005 | 0.106 |
| Prkcd | 10.000 | 0.778 | 15.000 | 80.200 | 0.199 | 0.000 | 0.059 |
| Tmem135 | 3.000 | 0.269 | 6.332 | 52.300 | 0.197 | 0.001 | 0.064 |
| Gas2l1 | 2.000 | 0.110 | 3.097 | 72.400 | 0.197 | 0.006 | 0.110 |
| Fzd2 | 3.000 | 0.318 | 7.193 | 64.000 | 0.197 | 0.001 | 0.083 |
| Ppp1r37 | 16.000 | 3.299 | 29.073 | 77.500 | 0.196 | 0.001 | 0.064 |
| Tmem209 | 8.000 | 0.848 | 21.228 | 64.000 | 0.196 | 0.000 | 0.031 |
| Apitd1 | 1.000 | 0.233 | 7.042 | 16.300 | 0.196 | 0.009 | 0.127 |
| Gbp6 | 4.000 | 0.266 | 3.857 | 80.300 | 0.192 | 0.008 | 0.126 |
| Scn1b | 5.000 | 1.848 | 33.028 | 24.600 | 0.189 | 0.001 | 0.066 |
| Gm21949 | 3.000 | 0.292 | 9.302 | 61.900 | 0.189 | 0.004 | 0.100 |
| Smim14 | 2.000 | 2.162 | 19.192 | 10.700 | 0.187 | 0.000 | 0.032 |
| Ntn1 | 11.000 | 1.412 | 22.351 | 67.800 | 0.186 | 0.007 | 0.121 |

| | | | | | | | |
|---|---|---|---|---|---|---|---|
| Mzt2 | 2.000 | 1.154 | 22.013 | 16.500 | 0.186 | 0.006 | 0.114 |
| Csrp2 | 5.000 | 1.424 | 32.642 | 20.900 | 0.185 | 0.009 | 0.127 |
| Polr3a | 15.000 | 0.486 | 17.254 | 158.600 | 0.184 | 0.001 | 0.066 |
| Tmem109 | 2.000 | 0.585 | 8.642 | 26.300 | 0.181 | 0.001 | 0.068 |
| Virma | 24.000 | 0.769 | 20.097 | 207.000 | 0.181 | 0.002 | 0.088 |
| Pcmtd2 | 9.000 | 2.162 | 25.627 | 40.700 | 0.181 | 0.001 | 0.080 |
| 0610009B22Rik | 6.000 | 6.743 | 43.571 | 16.400 | 0.180 | 0.002 | 0.086 |
| Mxra7 | 4.000 | 5.813 | 23.179 | 16.200 | 0.178 | 0.005 | 0.105 |
| Sqle | 13.000 | 1.955 | 25.874 | 63.700 | 0.178 | 0.009 | 0.128 |
| Cdkn2c | 5.000 | 2.511 | 45.238 | 18.100 | 0.177 | 0.006 | 0.110 |
| Rab13 | 8.000 | 2.981 | 44.059 | 22.800 | 0.177 | 0.007 | 0.121 |
| Utp15 | 13.000 | 1.297 | 26.705 | 59.300 | 0.176 | 0.002 | 0.086 |
| Jam2 | 9.000 | 3.160 | 34.808 | 37.500 | 0.176 | 0.003 | 0.099 |
| Abcb10 | 10.000 | 0.805 | 17.343 | 77.100 | 0.176 | 0.002 | 0.083 |
| Scd2 | 5.000 | 1.371 | 11.732 | 40.900 | 0.175 | 0.008 | 0.121 |
| Cspg4 | 35.000 | 1.783 | 23.034 | 252.200 | 0.175 | 0.001 | 0.083 |
| Pomt1 | 5.000 | 0.389 | 8.981 | 85.200 | 0.175 | 0.001 | 0.064 |
| Gtf2e2 | 10.000 | 1.610 | 41.017 | 33.400 | 0.174 | 0.000 | 0.059 |
| Dtx1 | 4.000 | 0.359 | 6.973 | 68.500 | 0.172 | 0.000 | 0.048 |
| Slco1c1 | 8.000 | 0.748 | 15.105 | 78.300 | 0.170 | 0.004 | 0.102 |
| Slc25a3 | 18.000 | 11.328 | 47.899 | 39.600 | 0.169 | 0.008 | 0.127 |

| | | | | | | | |
|---|---|---|---|---|---|---|---|
| Nat14 | 6.000 | 6.499 | 31.068 | 21.800 | 0.169 | 0.001 | 0.080 |
| Cyp20a1 | 10.000 | 1.712 | 27.489 | 52.100 | 0.168 | 0.004 | 0.100 |
| Capn1 | 8.000 | 0.492 | 16.690 | 82.100 | 0.167 | 0.002 | 0.086 |
| Amfr | 13.000 | 3.047 | 33.177 | 72.700 | 0.165 | 0.006 | 0.112 |
| Far1 | 15.000 | 2.652 | 34.563 | 59.400 | 0.165 | 0.008 | 0.121 |
| Lage3 | 4.000 | 1.783 | 24.324 | 15.800 | 0.165 | 0.009 | 0.128 |
| Klhl7 | 9.000 | 0.833 | 23.720 | 65.900 | 0.165 | 0.007 | 0.121 |
| Bnip3l | 4.000 | 1.512 | 16.972 | 23.800 | 0.164 | 0.001 | 0.083 |
| Mrpl20 | 5.000 | 2.511 | 38.255 | 17.600 | 0.164 | 0.010 | 0.130 |
| Srebf2 | 13.000 | 0.759 | 15.310 | 122.800 | 0.162 | 0.009 | 0.127 |
| Fam69a | 7.000 | 0.957 | 25.701 | 48.900 | 0.162 | 0.001 | 0.080 |
| Kat8 | 7.000 | 0.978 | 18.341 | 52.500 | 0.161 | 0.001 | 0.066 |
| Akap11 | 14.000 | 0.474 | 9.024 | 208.700 | 0.160 | 0.000 | 0.048 |
| B230219D22Rik | 5.000 | 2.162 | 38.298 | 20.100 | 0.160 | 0.009 | 0.128 |
| Alg9 | 10.000 | 1.395 | 17.349 | 69.500 | 0.159 | 0.001 | 0.068 |
| Rabac1 | 5.000 | 14.849 | 27.568 | 20.600 | 0.159 | 0.009 | 0.128 |
| Ppp4r3b | 14.000 | 1.485 | 21.341 | 93.900 | 0.159 | 0.000 | 0.061 |
| Fmo1 | 3.000 | 0.218 | 6.579 | 59.900 | 0.159 | 0.008 | 0.126 |
| Chd4 | 86.000 | 9.228 | 49.103 | 221.400 | 0.158 | 0.001 | 0.082 |
| Lman1 | 20.000 | 5.529 | 46.422 | 57.800 | 0.158 | 0.003 | 0.098 |
| Bloc1s6 | 3.000 | 2.981 | 27.326 | 19.700 | 0.157 | 0.009 | 0.128 |

| | | | | | | | |
|---|---|---|---|---|---|---|---|
| Saraf | 10.000 | 3.281 | 33.884 | 38.700 | 0.157 | 0.001 | 0.083 |
| Abcf1 | 35.000 | 7.577 | 51.732 | 94.900 | 0.156 | 0.004 | 0.100 |
| Pxmp2 | 5.000 | 1.610 | 21.762 | 22.100 | 0.155 | 0.002 | 0.086 |
| Agap2 | 28.000 | 1.832 | 23.845 | 142.200 | 0.154 | 0.002 | 0.085 |
| Syne2 | 80.000 | 0.546 | 14.984 | 782.200 | 0.154 | 0.000 | 0.055 |
| Fbxl20 | 16.000 | 2.857 | 43.578 | 48.400 | 0.153 | 0.004 | 0.102 |
| Tnk2 | 5.000 | 0.318 | 6.919 | 116.900 | 0.153 | 0.005 | 0.110 |
| Gamt | 8.000 | 11.328 | 46.825 | 27.900 | 0.152 | 0.009 | 0.128 |
| Ephx1 | 25.000 | 9.000 | 60.659 | 52.500 | 0.152 | 0.008 | 0.122 |
| Tmem55a | 7.000 | 2.875 | 36.576 | 28.000 | 0.151 | 0.002 | 0.083 |
| Lyst | 28.000 | 0.431 | 9.977 | 430.500 | 0.151 | 0.002 | 0.086 |
| Hira | 19.000 | 1.399 | 27.087 | 113.100 | 0.150 | 0.001 | 0.083 |
| Cpt1a | 20.000 | 2.675 | 28.947 | 90.600 | 0.150 | 0.005 | 0.107 |
| Pgap1 | 25.000 | 4.289 | 28.416 | 104.500 | 0.149 | 0.006 | 0.111 |
| Mettl7a1 | 5.000 | 1.929 | 27.459 | 28.100 | 0.148 | 0.010 | 0.129 |
| Ptpn13 | 21.000 | 0.420 | 11.016 | 270.100 | 0.148 | 0.004 | 0.100 |
| Nol3 | 6.000 | 4.995 | 38.182 | 24.600 | 0.147 | 0.007 | 0.121 |
| Gpc1 | 21.000 | 7.620 | 53.479 | 55.500 | 0.146 | 0.007 | 0.121 |
| Utp6 | 8.000 | 0.567 | 14.573 | 70.400 | 0.145 | 0.002 | 0.088 |
| Dlx2 | 2.000 | 1.683 | 7.229 | 34.700 | 0.145 | 0.009 | 0.128 |
| Gpc6 | 18.000 | 3.748 | 45.664 | 64.300 | 0.145 | 0.009 | 0.127 |
| Nme3 | 7.000 | 3.642 | 28.994 | 19.100 | 0.142 | 0.001 | 0.066 |

| | | | | | | | |
|---|---|---|---|---|---|---|---|
| Tmem100 | 2.000 | 1.512 | 11.940 | 14.500 | 0.142 | 0.001 | 0.083 |
| Rbm15b | 13.000 | 0.647 | 19.842 | 97.000 | 0.141 | 0.003 | 0.094 |
| Kctd18 | 7.000 | 0.905 | 14.219 | 46.900 | 0.140 | 0.000 | 0.061 |
| Nek6 | 6.000 | 1.081 | 12.570 | 40.800 | 0.140 | 0.007 | 0.120 |
| Iqgap1 | 54.000 | 3.827 | 43.486 | 191.300 | 0.140 | 0.009 | 0.127 |
| Tspyl4 | 15.000 | 3.924 | 46.059 | 44.800 | 0.140 | 0.002 | 0.083 |
| Cbx4 | 8.000 | 0.995 | 17.604 | 60.500 | 0.139 | 0.004 | 0.100 |
| Maged1 | 22.000 | 4.179 | 29.419 | 85.600 | 0.139 | 0.005 | 0.104 |
| Pes1 | 17.000 | 2.490 | 24.829 | 67.800 | 0.139 | 0.002 | 0.086 |
| Timp3 | 5.000 | 2.162 | 27.962 | 24.200 | 0.137 | 0.010 | 0.131 |
| Pomp | 4.000 | 2.511 | 43.972 | 15.800 | 0.137 | 0.002 | 0.086 |
| Top2b | 95.000 | 15.596 | 59.739 | 181.800 | 0.137 | 0.003 | 0.095 |
| Tmem56 | 3.000 | 0.701 | 11.957 | 31.200 | 0.136 | 0.002 | 0.088 |
| Fdft1 | 21.000 | 13.125 | 50.481 | 48.100 | 0.136 | 0.000 | 0.059 |
| Atp13a1 | 35.000 | 3.823 | 34.505 | 135.000 | 0.135 | 0.003 | 0.095 |
| Abcb7 | 18.000 | 3.072 | 29.787 | 82.500 | 0.134 | 0.001 | 0.083 |
| Tmpo | 14.000 | 5.422 | 42.920 | 50.300 | 0.134 | 0.001 | 0.066 |
| Abcb8 | 22.000 | 2.814 | 36.541 | 78.000 | 0.133 | 0.010 | 0.131 |
| Mrfap1 | 5.000 | 14.849 | 47.200 | 14.200 | 0.132 | 0.006 | 0.111 |
| Rab33b | 10.000 | 6.356 | 38.428 | 25.800 | 0.131 | 0.003 | 0.094 |
| Kdm5b | 25.000 | 1.233 | 20.013 | 175.400 | 0.131 | 0.002 | 0.083 |
| Kcnj3 | 4.000 | 0.688 | 13.772 | 56.500 | 0.130 | 0.001 | 0.066 |

| | | | | | | | |
|---|---|---|---|---|---|---|---|
| Ppfibp1 | 13.000 | 0.647 | 16.667 | 115.900 | 0.130 | 0.007 | 0.115 |
| Lemd3 | 22.000 | 1.619 | 33.660 | 100.100 | 0.127 | 0.007 | 0.121 |
| Gtf3c1 | 53.000 | 2.162 | 33.079 | 237.300 | 0.127 | 0.002 | 0.083 |
| Serac1 | 13.000 | 1.154 | 26.603 | 70.600 | 0.127 | 0.007 | 0.121 |
| Alg11 | 8.000 | 1.565 | 21.341 | 55.200 | 0.126 | 0.004 | 0.100 |
| Rnf114 | 7.000 | 2.384 | 41.921 | 25.700 | 0.122 | 0.003 | 0.093 |
| Tst | 10.000 | 3.281 | 36.364 | 33.400 | 0.122 | 0.007 | 0.121 |
| Mospd1 | 4.000 | 1.031 | 16.929 | 28.800 | 0.122 | 0.009 | 0.127 |
| Galnt2 | 25.000 | 6.326 | 48.070 | 64.500 | 0.122 | 0.006 | 0.112 |
| Lemd2 | 14.000 | 2.282 | 29.550 | 57.500 | 0.121 | 0.004 | 0.100 |
| Abca1 | 47.000 | 1.903 | 26.823 | 253.800 | 0.121 | 0.003 | 0.096 |
| Utp14a | 10.000 | 0.802 | 18.905 | 87.200 | 0.120 | 0.009 | 0.127 |
| Pnpla6 | 19.000 | 0.947 | 17.734 | 149.900 | 0.120 | 0.007 | 0.121 |
| Rbbp5 | 18.000 | 4.179 | 42.600 | 55.000 | 0.120 | 0.008 | 0.126 |
| Tnks | 8.000 | 0.311 | 6.894 | 140.900 | 0.120 | 0.000 | 0.053 |
| 4933434E20Rik | 8.000 | 2.162 | 36.364 | 28.700 | 0.120 | 0.009 | 0.127 |
| Tmem214 | 17.000 | 1.818 | 27.365 | 76.400 | 0.119 | 0.005 | 0.105 |
| Rab24 | 9.000 | 4.412 | 45.320 | 23.100 | 0.118 | 0.001 | 0.068 |
| 2310022B05Rik | 17.000 | 9.000 | 63.354 | 35.300 | 0.118 | 0.006 | 0.110 |
| Alg10b | 8.000 | 1.310 | 14.557 | 55.400 | 0.117 | 0.002 | 0.086 |

| | | | | | | | |
|---|---|---|---|---|---|---|---|
| Nsdhl | 15.000 | 9.000 | 55.525 | 40.700 | 0.117 | 0.009 | 0.127 |
| Pip5k1a | 8.000 | 1.096 | 16.636 | 60.500 | 0.116 | 0.006 | 0.110 |
| Lrrc59 | 17.000 | 30.623 | 57.003 | 34.900 | 0.116 | 0.005 | 0.104 |
| Vangl2 | 13.000 | 2.433 | 26.679 | 59.700 | 0.116 | 0.004 | 0.100 |
| Nup205 | 59.000 | 3.239 | 36.164 | 232.100 | 0.115 | 0.005 | 0.110 |
| Wipi1 | 6.000 | 1.637 | 22.646 | 48.700 | 0.115 | 0.010 | 0.130 |
| Rlbp1 | 10.000 | 3.833 | 42.271 | 36.400 | 0.114 | 0.009 | 0.128 |
| Prpf8 | 111.000 | 8.237 | 54.133 | 273.400 | 0.114 | 0.002 | 0.083 |
| Tpbg | 5.000 | 1.154 | 14.789 | 46.400 | 0.114 | 0.004 | 0.100 |
| Ncln | 16.000 | 4.109 | 28.826 | 62.700 | 0.113 | 0.008 | 0.126 |
| Ccdc177 | 12.000 | 1.254 | 18.130 | 79.800 | 0.113 | 0.004 | 0.100 |
| Tmem43 | 16.000 | 6.197 | 43.750 | 44.800 | 0.113 | 0.006 | 0.111 |
| Smpd2 | 11.000 | 1.894 | 32.697 | 47.400 | 0.113 | 0.004 | 0.100 |
| Lactb2 | 10.000 | 5.310 | 46.528 | 32.700 | 0.112 | 0.002 | 0.086 |
| Atp2a2 | 54.000 | 41.622 | 53.161 | 114.800 | 0.112 | 0.005 | 0.108 |
| Acbd5 | 15.000 | 4.179 | 29.615 | 58.000 | 0.112 | 0.004 | 0.100 |
| Ints8 | 11.000 | 0.628 | 12.663 | 113.300 | 0.111 | 0.008 | 0.127 |
| Pcdhga12 | 9.000 | 1.106 | 12.554 | 100.800 | 0.111 | 0.008 | 0.126 |
| Abhd16a | 20.000 | 6.880 | 42.473 | 63.000 | 0.110 | 0.001 | 0.068 |
| Pqlc1 | 2.000 | 1.371 | 7.380 | 30.600 | 0.110 | 0.005 | 0.108 |
| Rims4 | 7.000 | 4.878 | 38.662 | 29.300 | 0.110 | 0.003 | 0.094 |
| Opa3 | 5.000 | 2.162 | 25.140 | 20.100 | 0.109 | 0.007 | 0.121 |

| | | | | | | | |
|---|---|---|---|---|---|---|---|
| "March2" | 18.000 | 9.000 | 42.899 | 38.200 | 0.109 | 0.009 | 0.128 |
| Cxx1c | 5.000 | 4.623 | 55.357 | 13.600 | 0.109 | 0.002 | 0.086 |
| Gprin3 | 14.000 | 1.434 | 22.850 | 89.700 | 0.108 | 0.000 | 0.057 |
| Pisd | 9.000 | 1.276 | 20.690 | 45.900 | 0.107 | 0.007 | 0.121 |
| Bri3bp | 5.000 | 2.831 | 19.763 | 28.200 | 0.107 | 0.002 | 0.086 |
| Sbk1 | 2.000 | 0.334 | 5.036 | 45.700 | 0.106 | 0.006 | 0.110 |
| Alkbh5 | 5.000 | 0.874 | 18.987 | 44.400 | 0.105 | 0.005 | 0.104 |
| Glg1 | 54.000 | 9.680 | 46.809 | 133.600 | 0.105 | 0.003 | 0.095 |
| Fam69b | 10.000 | 3.642 | 29.930 | 48.800 | 0.105 | 0.001 | 0.080 |
| Commd4 | 7.000 | 3.642 | 36.181 | 21.800 | 0.104 | 0.004 | 0.102 |
| Trmt10c | 14.000 | 2.728 | 43.478 | 48.400 | 0.104 | 0.010 | 0.131 |
| Kif1b | 57.000 | 3.453 | 42.126 | 204.000 | 0.104 | 0.004 | 0.100 |
| Mettl9 | 7.000 | 2.162 | 34.906 | 36.400 | 0.103 | 0.006 | 0.110 |
| Cyb5r4 | 14.000 | 1.322 | 31.439 | 59.700 | 0.102 | 0.004 | 0.100 |
| Wdr36 | 14.000 | 1.260 | 20.912 | 99.700 | 0.102 | 0.009 | 0.127 |
| Rhot2 | 16.000 | 5.210 | 37.742 | 69.000 | 0.100 | 0.001 | 0.080 |
| Gpaa1 | 11.000 | 2.162 | 18.035 | 67.900 | 0.096 | 0.007 | 0.121 |
| Lbr | 10.000 | 1.395 | 18.211 | 71.400 | 0.095 | 0.002 | 0.083 |
| Cpt1c | 17.000 | 2.162 | 24.656 | 90.100 | 0.094 | 0.003 | 0.098 |
| Ubtf | 27.000 | 2.802 | 35.094 | 93.000 | 0.093 | 0.002 | 0.086 |
| Nlgn3 | 20.000 | 8.211 | 38.061 | 91.100 | 0.092 | 0.006 | 0.110 |
| Trim35 | 16.000 | 2.384 | 38.372 | 58.700 | 0.092 | 0.003 | 0.095 |

| | | | | | | | |
|---|---|---|---|---|---|---|---|
| Stk3 | 17.000 | 4.298 | 44.064 | 56.800 | 0.091 | 0.004 | 0.100 |
| Exosc10 | 23.000 | 1.404 | 31.960 | 102.000 | 0.090 | 0.001 | 0.083 |
| Spg7 | 22.000 | 1.894 | 33.803 | 85.900 | 0.087 | 0.009 | 0.128 |
| Atp8a2 | 31.000 | 2.325 | 28.451 | 133.500 | 0.086 | 0.006 | 0.110 |
| Surf4 | 4.000 | 1.848 | 14.870 | 30.400 | 0.086 | 0.007 | 0.121 |
| Slc30a9 | 13.000 | 2.162 | 23.810 | 62.800 | 0.085 | 0.005 | 0.108 |
| Casc4 | 17.000 | 4.754 | 37.931 | 49.400 | 0.083 | 0.002 | 0.083 |
| Sec62 | 9.000 | 1.818 | 13.819 | 45.600 | 0.082 | 0.006 | 0.110 |
| Chd8 | 29.000 | 0.733 | 13.822 | 291.600 | 0.080 | 0.010 | 0.130 |
| Ktn1 | 69.000 | 7.799 | 51.380 | 149.700 | 0.080 | 0.009 | 0.128 |
| Use1 | 6.000 | 1.081 | 19.298 | 32.300 | 0.077 | 0.004 | 0.102 |
| Pbrm1 | 43.000 | 1.591 | 29.884 | 197.400 | 0.076 | 0.007 | 0.121 |
| Jmy | 25.000 | 3.642 | 29.400 | 110.500 | 0.076 | 0.007 | 0.121 |
| Mrps30 | 20.000 | 11.115 | 58.824 | 49.900 | 0.076 | 0.008 | 0.126 |
| Abi2 | 11.000 | 4.012 | 22.509 | 58.800 | -0.072 | 0.009 | 0.127 |
| Ptprd | 65.000 | 6.909 | 45.336 | 215.100 | -0.073 | 0.004 | 0.100 |
| Rpp25l | 4.000 | 1.610 | 22.321 | 24.300 | -0.073 | 0.009 | 0.128 |
| Matr3 | 49.000 | 29.858 | 55.674 | 94.600 | -0.078 | 0.006 | 0.110 |
| Erc2 | 51.000 | 6.068 | 45.089 | 123.100 | -0.078 | 0.003 | 0.097 |
| Hnrnpa3 | 25.000 | 88.125 | 53.826 | 39.600 | -0.078 | 0.008 | 0.123 |
| Csnk1e | 18.000 | 14.199 | 51.202 | 47.300 | -0.078 | 0.006 | 0.113 |
| Add2 | 40.000 | 22.556 | 65.379 | 80.600 | -0.079 | 0.009 | 0.127 |

| | | | | | | | |
|---|---|---|---|---|---|---|---|
| Epn2 | 17.000 | 9.000 | 36.875 | 68.300 | -0.079 | 0.005 | 0.110 |
| Gdap1l1 | 14.000 | 6.848 | 38.692 | 41.900 | -0.079 | 0.009 | 0.128 |
| Ap2a2 | 49.000 | 15.103 | 56.397 | 104.000 | -0.080 | 0.007 | 0.121 |
| Psmc6 | 23.000 | 15.681 | 66.067 | 44.100 | -0.080 | 0.003 | 0.099 |
| Vat1l | 19.000 | 17.233 | 59.952 | 45.800 | -0.081 | 0.005 | 0.105 |
| Tcerg1 | 37.000 | 5.367 | 29.742 | 126.500 | -0.084 | 0.010 | 0.129 |
| Ctsd | 16.000 | 38.811 | 48.537 | 44.900 | -0.085 | 0.006 | 0.110 |
| Dbn1 | 30.000 | 77.137 | 47.808 | 77.400 | -0.085 | 0.008 | 0.123 |
| Raph1 | 38.000 | 4.125 | 36.950 | 142.500 | -0.086 | 0.010 | 0.130 |
| Ap3d1 | 63.000 | 25.827 | 52.294 | 135.000 | -0.086 | 0.009 | 0.128 |
| Atp6v1d | 20.000 | 162.789 | 59.919 | 28.400 | -0.090 | 0.003 | 0.095 |
| Shank1 | 41.000 | 2.442 | 25.336 | 225.200 | -0.090 | 0.006 | 0.110 |
| Add1 | 39.000 | 39.842 | 57.107 | 87.100 | -0.090 | 0.008 | 0.123 |
| Tollip | 11.000 | 7.577 | 57.299 | 30.300 | -0.090 | 0.004 | 0.102 |
| Tubb3 | 30.000 | 2564.021 | 73.556 | 50.400 | -0.091 | 0.009 | 0.127 |
| Tfg | 14.000 | 48.239 | 46.348 | 43.000 | -0.091 | 0.004 | 0.100 |
| Nsf | 54.000 | 27.368 | 69.220 | 82.600 | -0.093 | 0.009 | 0.128 |
| Stx1a | 22.000 | 76.426 | 63.194 | 33.000 | -0.093 | 0.005 | 0.107 |
| Ppp5c | 32.000 | 24.929 | 58.717 | 56.800 | -0.093 | 0.005 | 0.104 |
| Purb | 14.000 | 17.957 | 56.481 | 33.900 | -0.094 | 0.009 | 0.127 |
| Mtfr1l | 7.000 | 4.179 | 24.913 | 31.700 | -0.094 | 0.003 | 0.097 |

| | | | | | | | |
|---|---|---|---|---|---|---|---|
| Ran | 11.000 | 27.480 | 51.852 | 24.400 | -0.095 | 0.008 | 0.124 |
| Calb2 | 19.000 | 25.367 | 69.004 | 31.400 | -0.096 | 0.005 | 0.108 |
| Mpped2 | 8.000 | 6.197 | 45.238 | 33.400 | -0.097 | 0.004 | 0.102 |
| Syn1 | 35.000 | 43.367 | 70.963 | 74.100 | -0.097 | 0.003 | 0.095 |
| Edil3 | 24.000 | 15.681 | 51.458 | 53.700 | -0.098 | 0.006 | 0.112 |
| Slc7a14 | 8.000 | 1.424 | 16.602 | 83.900 | -0.098 | 0.004 | 0.100 |
| Crmp1 | 40.000 | 126.427 | 74.490 | 74.200 | -0.098 | 0.002 | 0.086 |
| Psmb5 | 17.000 | 55.234 | 64.015 | 28.500 | -0.098 | 0.002 | 0.088 |
| Syp | 7.000 | 5.105 | 27.707 | 34.000 | -0.099 | 0.005 | 0.110 |
| Atxn2l | 30.000 | 9.000 | 34.033 | 115.200 | -0.100 | 0.009 | 0.128 |
| Pde1b | 17.000 | 4.520 | 36.075 | 61.200 | -0.100 | 0.004 | 0.100 |
| Wbp11 | 19.000 | 4.736 | 30.577 | 69.800 | -0.101 | 0.004 | 0.100 |
| Htra1 | 26.000 | 22.101 | 58.542 | 51.200 | -0.101 | 0.006 | 0.110 |
| Metap1 | 19.000 | 11.217 | 64.767 | 43.200 | -0.101 | 0.009 | 0.127 |
| Eef1d | 34.000 | 16.508 | 51.105 | 74.800 | -0.102 | 0.006 | 0.113 |
| Ppp2r1a | 36.000 | 40.246 | 66.044 | 65.300 | -0.104 | 0.008 | 0.127 |
| Rbm8a | 9.000 | 73.989 | 61.494 | 19.900 | -0.104 | 0.002 | 0.086 |
| Lysmd1 | 9.000 | 3.394 | 39.823 | 24.800 | -0.106 | 0.003 | 0.097 |
| Ash2l | 17.000 | 2.371 | 33.068 | 68.700 | -0.106 | 0.003 | 0.090 |
| Homer2 | 19.000 | 8.006 | 48.588 | 40.500 | -0.107 | 0.005 | 0.106 |
| Zkscan3 | 5.000 | 0.417 | 13.743 | 62.600 | -0.107 | 0.006 | 0.110 |
| Baiap2 | 37.000 | 17.548 | 76.820 | 57.600 | -0.107 | 0.003 | 0.094 |

| | | | | | | | |
|---|---|---|---|---|---|---|---|
| Rtn3 | 36.000 | 12.503 | 47.822 | 103.800 | -0.107 | 0.006 | 0.110 |
| Map2 | 134.000 | 110.706 | 66.434 | 202.300 | -0.109 | 0.008 | 0.126 |
| Rps3 | 27.000 | 111.884 | 79.424 | 26.700 | -0.110 | 0.008 | 0.126 |
| Pclo | 154.000 | 5.039 | 39.740 | 550.500 | -0.110 | 0.007 | 0.121 |
| Lrrn1 | 16.000 | 2.924 | 29.749 | 80.500 | -0.112 | 0.009 | 0.127 |
| Actr3b | 22.000 | 27.480 | 62.679 | 47.500 | -0.112 | 0.004 | 0.100 |
| Irf2bpl | 20.000 | 3.833 | 32.774 | 80.500 | -0.112 | 0.004 | 0.099 |
| Cpeb2 | 21.000 | 4.532 | 27.317 | 108.700 | -0.113 | 0.001 | 0.066 |
| Camk2a | 26.000 | 42.940 | 53.556 | 54.100 | -0.114 | 0.010 | 0.130 |
| Sirpa | 15.000 | 6.356 | 44.401 | 56.000 | -0.115 | 0.003 | 0.093 |
| Wasf1 | 21.000 | 58.948 | 41.503 | 61.500 | -0.117 | 0.006 | 0.110 |
| Pcyt2 | 18.000 | 6.743 | 56.218 | 43.400 | -0.117 | 0.009 | 0.127 |
| Ubap2l | 25.000 | 13.030 | 32.863 | 119.900 | -0.117 | 0.008 | 0.127 |
| Camkk2 | 26.000 | 7.209 | 56.633 | 64.600 | -0.118 | 0.001 | 0.083 |
| Ahsa1 | 22.000 | 12.335 | 73.077 | 38.100 | -0.118 | 0.003 | 0.094 |
| Snx27 | 26.000 | 9.000 | 57.699 | 61.000 | -0.119 | 0.002 | 0.086 |
| Rpl38 | 5.000 | 214.443 | 47.143 | 8.200 | -0.119 | 0.001 | 0.080 |
| Lamtor5 | 4.000 | 6.499 | 51.034 | 15.300 | -0.119 | 0.002 | 0.086 |
| Ywhag | 20.000 | 128.155 | 81.377 | 28.300 | -0.119 | 0.004 | 0.100 |
| Ube2z | 12.000 | 7.577 | 31.180 | 38.300 | -0.120 | 0.009 | 0.128 |
| Nt5c | 11.000 | 16.783 | 55.500 | 23.100 | -0.120 | 0.005 | 0.110 |
| Hgs | 22.000 | 7.577 | 27.081 | 89.200 | -0.121 | 0.006 | 0.112 |

| | | | | | | | |
|---|---|---|---|---|---|---|---|
| Cplx1 | 10.000 | 99.000 | 69.403 | 15.100 | -0.122 | 0.003 | 0.097 |
| Adprh | 16.000 | 10.159 | 53.591 | 40.000 | -0.123 | 0.002 | 0.083 |
| Dgkg | 22.000 | 2.008 | 34.532 | 93.900 | -0.123 | 0.006 | 0.112 |
| Aak1 | 47.000 | 26.977 | 65.240 | 103.200 | -0.125 | 0.001 | 0.083 |
| Bag4 | 8.000 | 5.105 | 19.475 | 49.100 | -0.125 | 0.001 | 0.066 |
| Nectin1 | 19.000 | 9.000 | 50.097 | 57.000 | -0.127 | 0.006 | 0.113 |
| Wasf3 | 14.000 | 9.000 | 37.325 | 55.200 | -0.127 | 0.005 | 0.108 |
| Rap1gap | 27.000 | 8.397 | 41.265 | 80.500 | -0.127 | 0.004 | 0.100 |
| Kctd12 | 17.000 | 15.681 | 47.706 | 35.900 | -0.127 | 0.001 | 0.066 |
| Eif4a1 | 33.000 | 145.780 | 68.473 | 46.100 | -0.128 | 0.006 | 0.112 |
| Pcp4l1 | 3.000 | 5.310 | 58.824 | 7.500 | -0.128 | 0.004 | 0.101 |
| Sf3a1 | 34.000 | 14.849 | 50.695 | 88.500 | -0.129 | 0.002 | 0.083 |
| R3hdm2 | 13.000 | 2.054 | 17.337 | 114.500 | -0.129 | 0.008 | 0.126 |
| Cyb5a | 4.000 | 2.162 | 38.060 | 15.200 | -0.131 | 0.001 | 0.071 |
| Itsn2 | 27.000 | 1.038 | 21.246 | 191.600 | -0.131 | 0.002 | 0.088 |
| Nova2 | 17.000 | 12.895 | 42.886 | 49.000 | -0.132 | 0.006 | 0.112 |
| Ppp4r2 | 16.000 | 5.422 | 49.880 | 46.400 | -0.133 | 0.004 | 0.100 |
| Calb1 | 15.000 | 19.535 | 57.471 | 30.000 | -0.134 | 0.007 | 0.115 |
| Camk2b | 29.000 | 27.804 | 47.376 | 72.900 | -0.134 | 0.008 | 0.126 |
| Gpd1 | 26.000 | 14.317 | 77.077 | 37.500 | -0.141 | 0.005 | 0.110 |
| Eloc | 7.000 | 11.915 | 55.224 | 14.900 | -0.142 | 0.002 | 0.086 |
| Lgi2 | 15.000 | 1.848 | 28.364 | 63.000 | -0.142 | 0.002 | 0.083 |

| | | | | | | | |
|---|---|---|---|---|---|---|---|
| Mrpl55 | 4.000 | 3.217 | 35.075 | 15.800 | -0.142 | 0.008 | 0.127 |
| Sez6 | 12.000 | 1.246 | 18.567 | 107.400 | -0.145 | 0.006 | 0.110 |
| Atxn2 | 29.000 | 5.190 | 26.594 | 136.400 | -0.146 | 0.001 | 0.080 |
| Fam49a | 17.000 | 18.953 | 65.944 | 37.300 | -0.149 | 0.004 | 0.100 |
| Mrps21 | 6.000 | 6.197 | 63.218 | 10.600 | -0.153 | 0.009 | 0.128 |
| Traf3 | 20.000 | 2.758 | 41.799 | 64.300 | -0.153 | 0.001 | 0.083 |
| Smap2 | 16.000 | 18.684 | 39.019 | 46.500 | -0.154 | 0.006 | 0.110 |
| Ctsl | 9.000 | 6.356 | 41.317 | 37.500 | -0.156 | 0.002 | 0.088 |
| Wipi2 | 14.000 | 6.197 | 49.213 | 48.400 | -0.157 | 0.000 | 0.061 |
| Lsm8 | 4.000 | 6.197 | 68.750 | 10.400 | -0.157 | 0.006 | 0.112 |
| Tra2a | 11.000 | 4.817 | 40.129 | 35.500 | -0.163 | 0.004 | 0.103 |
| Klc1 | 40.000 | 50.795 | 61.887 | 62.700 | -0.164 | 0.008 | 0.127 |
| Limd2 | 5.000 | 2.594 | 28.906 | 14.200 | -0.166 | 0.009 | 0.127 |
| Polr2k | 2.000 | 0.931 | 8.081 | 11.700 | -0.166 | 0.002 | 0.083 |
| Mapre2 | 19.000 | 68.519 | 73.620 | 36.900 | -0.169 | 0.002 | 0.083 |
| Mrps18b | 4.000 | 1.610 | 21.654 | 28.700 | -0.171 | 0.007 | 0.121 |
| Pla2g7 | 15.000 | 4.623 | 36.136 | 49.200 | -0.174 | 0.002 | 0.083 |
| Eif6 | 9.000 | 17.738 | 54.286 | 26.500 | -0.175 | 0.004 | 0.099 |
| Tnc | 52.000 | 5.310 | 48.338 | 172.100 | -0.177 | 0.005 | 0.108 |
| Mfge8 | 24.000 | 45.416 | 56.371 | 51.200 | -0.186 | 0.000 | 0.048 |
| Hp1bp3 | 25.000 | 6.197 | 37.005 | 63.800 | -0.189 | 0.000 | 0.044 |
| Sf3b5 | 3.000 | 3.642 | 40.698 | 10.100 | -0.190 | 0.001 | 0.080 |

| | | | | | | | |
|---|---|---|---|---|---|---|---|
| Arpp19 | 6.000 | 4.995 | 41.379 | 16.100 | -0.192 | 0.002 | 0.085 |
| Acbd7 | 3.000 | 2.162 | 29.545 | 10.000 | -0.196 | 0.002 | 0.083 |
| Mug2 | 3.000 | 0.113 | 1.678 | 166.400 | -0.203 | 0.005 | 0.110 |
| Mdk | 8.000 | 11.915 | 47.143 | 15.400 | -0.214 | 0.001 | 0.066 |
| Ppil3 | 8.000 | 3.125 | 60.248 | 18.100 | -0.219 | 0.002 | 0.085 |
| Rps27 | 4.000 | 14.849 | 39.286 | 9.500 | -0.222 | 0.000 | 0.032 |
| Gemin4 | 12.000 | 0.842 | 13.800 | 120.100 | -0.225 | 0.009 | 0.127 |
| Mapre3 | 15.000 | 14.013 | 59.774 | 30.300 | -0.226 | 0.009 | 0.127 |
| Clstn3 | 23.000 | 4.012 | 30.021 | 105.800 | -0.233 | 0.004 | 0.100 |
| Fam135a | 6.000 | 0.222 | 4.427 | 170.000 | -0.234 | 0.002 | 0.083 |
| Ss18l1 | 4.000 | 9.000 | 16.667 | 43.700 | -0.246 | 0.008 | 0.121 |
| Cnbp | 6.000 | 1.929 | 41.808 | 19.500 | -0.249 | 0.002 | 0.084 |
| Kdelr1 | 3.000 | 1.154 | 20.755 | 24.500 | -0.256 | 0.007 | 0.121 |
| Cadm1 | 11.000 | 20.544 | 44.136 | 35.500 | -0.258 | 0.009 | 0.127 |
| Ank2 | 217.000 | 23.302 | 65.394 | 434.500 | -0.261 | 0.004 | 0.100 |
| Aplp1 | 19.000 | 2.793 | 33.333 | 72.800 | -0.262 | 0.010 | 0.131 |
| Sparcl1 | 26.000 | 8.345 | 45.846 | 72.200 | -0.267 | 0.007 | 0.121 |
| Serpind1 | 2.000 | 0.172 | 3.975 | 54.500 | -0.284 | 0.001 | 0.066 |
| Aox1 | 14.000 | 0.585 | 14.254 | 146.600 | -0.290 | 0.009 | 0.127 |
| Cyb5b | 5.000 | 2.594 | 45.205 | 16.300 | -0.295 | 0.008 | 0.121 |
| Ccdc92b | 5.000 | 0.896 | 18.395 | 33.300 | -0.317 | 0.000 | 0.012 |
| Smarcc2 | 54.000 | 19.962 | 40.595 | 135.800 | -0.327 | 0.000 | 0.053 |

| | | | | | | | |
|---|---|---|---|---|---|---|---|
| A2m | 15.000 | 0.742 | 12.687 | 164.200 | -0.329 | 0.003 | 0.099 |
| Nell2 | 20.000 | 2.639 | 32.967 | 91.400 | -0.341 | 0.003 | 0.095 |
| Clstn1 | 25.000 | 4.854 | 33.504 | 108.800 | -0.350 | 0.004 | 0.099 |
| Cst3 | 8.000 | 18.953 | 62.857 | 15.500 | -0.359 | 0.003 | 0.091 |
| Cwf19l1 | 7.000 | 1.783 | 35.959 | 33.200 | -0.361 | 0.003 | 0.094 |
| Pzp | 4.000 | 0.222 | 3.144 | 165.700 | -0.363 | 0.003 | 0.096 |
| Timp2 | 11.000 | 12.895 | 57.727 | 24.300 | -0.367 | 0.001 | 0.066 |
| Cycs | 13.000 | 315.228 | 69.524 | 11.600 | -0.373 | 0.003 | 0.095 |
| Ecm1 | 2.000 | 0.136 | 2.773 | 64.600 | -0.375 | 0.002 | 0.083 |
| | 14.000 | 1.728 | 19.309 | 85.600 | -0.396 | 0.005 | 0.109 |
| Itih1 | 3.000 | 0.170 | 2.744 | 101.600 | -0.396 | 0.004 | 0.100 |
| Igfbp2 | 9.000 | 4.275 | 41.967 | 32.800 | -0.409 | 0.001 | 0.080 |
| Ambp | 2.000 | 0.413 | 5.444 | 39.000 | -0.415 | 0.001 | 0.083 |
| Usp27x | 2.000 | 0.202 | 5.708 | 49.600 | -0.415 | 0.006 | 0.110 |
| Serpinc1 | 15.000 | 2.924 | 29.892 | 52.000 | -0.416 | 0.004 | 0.102 |
| C3 | 13.000 | 0.418 | 8.118 | 186.400 | -0.431 | 0.003 | 0.099 |
| Csnk1a1 | 18.000 | 11.452 | 62.769 | 37.500 | -0.435 | 0.002 | 0.083 |
| | 18.000 | 4.412 | 28.448 | 52.600 | -0.442 | 0.003 | 0.094 |
| | 45.000 | 41.453 | 64.900 | 77.000 | -0.474 | 0.004 | 0.100 |
| Sncaip | 3.000 | 0.148 | 3.316 | 105.900 | -0.476 | 0.002 | 0.083 |
| | 3.000 | 0.778 | 19.608 | 15.800 | -0.478 | 0.003 | 0.097 |
| Krt4 | 5.000 | 0.450 | 6.476 | 56.200 | -0.524 | 0.005 | 0.108 |

| | | | | | | | |
|---|---|---|---|---|---|---|---|
| Ces1g | 1.000 | 0.202 | 2.124 | 62.600 | -0.533 | 0.002 | 0.086 |
| Hp | 3.000 | 0.551 | 8.357 | 38.700 | -0.598 | 0.004 | 0.100 |
| | 2.000 | 0.155 | 2.958 | 78.100 | -0.630 | 0.000 | 0.058 |

**Table 4.2 NMP substrates with q<.1**

| Gene Symbol | # Peptides | emPAI (rel. abundance) | Coverage | Molecular Weight (kDa) | Log Fold change | P values - bayes moderated | Q values - bayes moderated |
|---|---|---|---|---|---|---|---|
| Rgs4 | 10.000 | 3.924 | 46.829 | 23.200 | 1.102 | 0.000 | 0.001 |
| Npas4 | 3.000 | 0.501 | 4.988 | 87.200 | 0.809 | 0.000 | 0.002 |
| 1190005I06Rik | 2.000 | 2.162 | 26.126 | 11.900 | 0.801 | 0.002 | 0.083 |
| Wbscr22 | 3.000 | 0.995 | 15.302 | 31.600 | 0.779 | 0.002 | 0.086 |
| Snurf | 1.000 | 0.778 | 19.718 | 8.400 | 0.731 | 0.000 | 0.015 |
| Bex2 | 3.000 | 0.874 | 27.907 | 15.400 | 0.623 | 0.000 | 0.006 |
| Fos | 5.000 | 3.329 | 15.000 | 40.800 | 0.619 | 0.000 | 0.010 |
| Fosl2 | 2.000 | 0.425 | 7.362 | 35.300 | 0.510 | 0.000 | 0.048 |
| Odc1 | 4.000 | 0.492 | 9.544 | 51.100 | 0.402 | 0.000 | 0.013 |
| Fosb | 4.000 | 1.783 | 15.385 | 36.000 | 0.402 | 0.000 | 0.048 |
| Creg2 | 2.000 | 0.292 | 9.028 | 31.700 | 0.363 | 0.001 | 0.064 |
| Ubc | 15.000 | 0.988 | 92.234 | 82.500 | 0.351 | 0.000 | 0.027 |
| Egr1 | 7.000 | 2.831 | 14.447 | 56.600 | 0.328 | 0.001 | 0.068 |
| Svs1 | 2.000 | 0.101 | 2.195 | 93.500 | 0.313 | 0.003 | 0.097 |
| Smpd4 | 13.000 | 1.228 | 21.219 | 96.700 | 0.313 | 0.000 | 0.048 |
| Sox4 | 2.000 | 0.359 | 5.682 | 45.000 | 0.306 | 0.000 | 0.044 |
| Slc18b1 | 1.000 | 0.212 | 2.407 | 48.800 | 0.300 | 0.000 | 0.053 |
| Tmem130 | 3.000 | 0.350 | 10.979 | 46.600 | 0.288 | 0.001 | 0.083 |
| 6330403K07Rik | 2.000 | 3.642 | 33.058 | 13.400 | 0.283 | 0.000 | 0.013 |
| Enc1 | 18.000 | 2.252 | 33.277 | 66.100 | 0.279 | 0.000 | 0.001 |
| Ggcx | 6.000 | 0.711 | 9.775 | 87.100 | 0.260 | 0.001 | 0.083 |
| Hmgcr | 15.000 | 1.268 | 18.952 | 98.100 | 0.250 | 0.000 | 0.013 |
| Tmem117 | 2.000 | 0.202 | 4.475 | 60.300 | 0.248 | 0.002 | 0.086 |
| Cic | 17.000 | 0.607 | 11.425 | 258.200 | 0.246 | 0.000 | 0.039 |
| Gnl3l | 12.000 | 1.581 | 25.650 | 65.200 | 0.246 | 0.001 | 0.083 |
| Ahctf1 | 16.000 | 0.382 | 10.194 | 254.600 | 0.242 | 0.000 | 0.048 |
| Tcof1 | 27.000 | 1.414 | 24.926 | 138.500 | 0.242 | 0.003 | 0.096 |
| Nfx1 | 8.000 | 0.362 | 7.899 | 123.700 | 0.241 | 0.001 | 0.072 |
| Soat1 | 6.000 | 0.905 | 11.481 | 63.800 | 0.235 | 0.001 | 0.068 |
| Trpc4ap | 14.000 | 1.121 | 24.216 | 90.700 | 0.235 | 0.000 | 0.039 |

| | | | | | | | |
|---|---|---|---|---|---|---|---|
| COX2 | 7.000 | 25.827 | 30.837 | 25.900 | 0.233 | 0.003 | 0.097 |
| Junb | 7.000 | 2.728 | 34.884 | 35.700 | 0.232 | 0.001 | 0.083 |
| Sft2d3 | 2.000 | 0.425 | 13.208 | 21.900 | 0.231 | 0.004 | 0.099 |
| Fads1 | 9.000 | 2.981 | 22.595 | 52.300 | 0.228 | 0.001 | 0.066 |
| Ccnd1 | 8.000 | 1.818 | 38.486 | 35.900 | 0.226 | 0.001 | 0.083 |
| Wnt7b | 13.000 | 3.062 | 39.943 | 39.300 | 0.224 | 0.001 | 0.068 |
| Mbtps2 | 1.000 | 0.179 | 1.748 | 56.900 | 0.218 | 0.000 | 0.061 |
| Clcc1 | 7.000 | 0.630 | 19.669 | 61.200 | 0.214 | 0.001 | 0.080 |
| Ndn | 11.000 | 2.675 | 38.769 | 36.800 | 0.213 | 0.000 | 0.013 |
| Tmem246 | 6.000 | 0.931 | 21.588 | 46.600 | 0.212 | 0.002 | 0.083 |
| Cox7c | 3.000 | 9.000 | 38.095 | 7.300 | 0.212 | 0.003 | 0.090 |
| Fads2 | 12.000 | 2.481 | 25.225 | 52.400 | 0.211 | 0.002 | 0.083 |
| Cadps | 54.000 | 8.412 | 50.300 | 150.800 | 0.211 | 0.002 | 0.088 |
| Sil1 | 12.000 | 2.775 | 37.634 | 52.400 | 0.208 | 0.002 | 0.086 |
| Ccdc91 | 12.000 | 2.311 | 28.054 | 50.000 | 0.204 | 0.000 | 0.044 |
| Olig1 | 7.000 | 3.394 | 40.385 | 27.100 | 0.203 | 0.003 | 0.099 |
| Nog | 2.000 | 0.668 | 11.638 | 25.800 | 0.203 | 0.000 | 0.059 |
| Prkcd | 10.000 | 0.778 | 15.000 | 80.200 | 0.199 | 0.000 | 0.059 |
| Tmem135 | 3.000 | 0.269 | 6.332 | 52.300 | 0.197 | 0.001 | 0.064 |
| Fzd2 | 3.000 | 0.318 | 7.193 | 64.000 | 0.197 | 0.001 | 0.083 |
| Ppp1r37 | 16.000 | 3.299 | 29.073 | 77.500 | 0.196 | 0.001 | 0.064 |
| Tmem209 | 8.000 | 0.848 | 21.228 | 64.000 | 0.196 | 0.000 | 0.031 |
| Scn1b | 5.000 | 1.848 | 33.028 | 24.600 | 0.189 | 0.001 | 0.066 |
| Smim14 | 2.000 | 2.162 | 19.192 | 10.700 | 0.187 | 0.000 | 0.032 |
| Polr3a | 15.000 | 0.486 | 17.254 | 158.600 | 0.184 | 0.001 | 0.066 |
| Tmem109 | 2.000 | 0.585 | 8.642 | 26.300 | 0.181 | 0.001 | 0.068 |
| Virma | 24.000 | 0.769 | 20.097 | 207.000 | 0.181 | 0.002 | 0.088 |
| Pcmtd2 | 9.000 | 2.162 | 25.627 | 40.700 | 0.181 | 0.001 | 0.080 |
| 0610009B22Rik | 6.000 | 6.743 | 43.571 | 16.400 | 0.180 | 0.002 | 0.086 |
| Utp15 | 13.000 | 1.297 | 26.705 | 59.300 | 0.176 | 0.002 | 0.086 |
| Jam2 | 9.000 | 3.160 | 34.808 | 37.500 | 0.176 | 0.003 | 0.099 |
| Abcb10 | 10.000 | 0.805 | 17.343 | 77.100 | 0.176 | 0.002 | 0.083 |
| Cspg4 | 35.000 | 1.783 | 23.034 | 252.200 | 0.175 | 0.001 | 0.083 |
| Pomt1 | 5.000 | 0.389 | 8.981 | 85.200 | 0.175 | 0.001 | 0.064 |
| Gtf2e2 | 10.000 | 1.610 | 41.017 | 33.400 | 0.174 | 0.000 | 0.059 |
| Dtx1 | 4.000 | 0.359 | 6.973 | 68.500 | 0.172 | 0.000 | 0.048 |
| Nat14 | 6.000 | 6.499 | 31.068 | 21.800 | 0.169 | 0.001 | 0.080 |
| Capn1 | 8.000 | 0.492 | 16.690 | 82.100 | 0.167 | 0.002 | 0.086 |

| | | | | | | | |
|---|---|---|---|---|---|---|---|
| Bnip3l | 4.000 | 1.512 | 16.972 | 23.800 | 0.164 | 0.001 | 0.083 |
| Fam69a | 7.000 | 0.957 | 25.701 | 48.900 | 0.162 | 0.001 | 0.080 |
| Kat8 | 7.000 | 0.978 | 18.341 | 52.500 | 0.161 | 0.001 | 0.066 |
| Akap11 | 14.000 | 0.474 | 9.024 | 208.700 | 0.160 | 0.000 | 0.048 |
| Alg9 | 10.000 | 1.395 | 17.349 | 69.500 | 0.159 | 0.001 | 0.068 |
| Ppp4r3b | 14.000 | 1.485 | 21.341 | 93.900 | 0.159 | 0.000 | 0.061 |
| Chd4 | 86.000 | 9.228 | 49.103 | 221.400 | 0.158 | 0.001 | 0.082 |
| Lman1 | 20.000 | 5.529 | 46.422 | 57.800 | 0.158 | 0.003 | 0.098 |
| Saraf | 10.000 | 3.281 | 33.884 | 38.700 | 0.157 | 0.001 | 0.083 |
| Pxmp2 | 5.000 | 1.610 | 21.762 | 22.100 | 0.155 | 0.002 | 0.086 |
| Agap2 | 28.000 | 1.832 | 23.845 | 142.200 | 0.154 | 0.002 | 0.085 |
| Syne2 | 80.000 | 0.546 | 14.984 | 782.200 | 0.154 | 0.000 | 0.055 |
| Tmem55a | 7.000 | 2.875 | 36.576 | 28.000 | 0.151 | 0.002 | 0.083 |
| Lyst | 28.000 | 0.431 | 9.977 | 430.500 | 0.151 | 0.002 | 0.086 |
| Hira | 19.000 | 1.399 | 27.087 | 113.100 | 0.150 | 0.001 | 0.083 |
| Utp6 | 8.000 | 0.567 | 14.573 | 70.400 | 0.145 | 0.002 | 0.088 |
| Nme3 | 7.000 | 3.642 | 28.994 | 19.100 | 0.142 | 0.001 | 0.066 |
| Tmem100 | 2.000 | 1.512 | 11.940 | 14.500 | 0.142 | 0.001 | 0.083 |
| Rbm15b | 13.000 | 0.647 | 19.842 | 97.000 | 0.141 | 0.003 | 0.094 |
| Kctd18 | 7.000 | 0.905 | 14.219 | 46.900 | 0.140 | 0.000 | 0.061 |
| Tspyl4 | 15.000 | 3.924 | 46.059 | 44.800 | 0.140 | 0.002 | 0.083 |
| Pes1 | 17.000 | 2.490 | 24.829 | 67.800 | 0.139 | 0.002 | 0.086 |
| Pomp | 4.000 | 2.511 | 43.972 | 15.800 | 0.137 | 0.002 | 0.086 |
| Top2b | 95.000 | 15.596 | 59.739 | 181.800 | 0.137 | 0.003 | 0.095 |
| Tmem56 | 3.000 | 0.701 | 11.957 | 31.200 | 0.136 | 0.002 | 0.088 |
| Fdft1 | 21.000 | 13.125 | 50.481 | 48.100 | 0.136 | 0.000 | 0.059 |
| Atp13a1 | 35.000 | 3.823 | 34.505 | 135.000 | 0.135 | 0.003 | 0.095 |
| Abcb7 | 18.000 | 3.072 | 29.787 | 82.500 | 0.134 | 0.001 | 0.083 |
| Tmpo | 14.000 | 5.422 | 42.920 | 50.300 | 0.134 | 0.001 | 0.066 |
| Rab33b | 10.000 | 6.356 | 38.428 | 25.800 | 0.131 | 0.003 | 0.094 |
| Kdm5b | 25.000 | 1.233 | 20.013 | 175.400 | 0.131 | 0.002 | 0.083 |
| Kcnj3 | 4.000 | 0.688 | 13.772 | 56.500 | 0.130 | 0.001 | 0.066 |
| Gtf3c1 | 53.000 | 2.162 | 33.079 | 237.300 | 0.127 | 0.002 | 0.083 |
| Rnf114 | 7.000 | 2.384 | 41.921 | 25.700 | 0.122 | 0.003 | 0.093 |
| Abca1 | 47.000 | 1.903 | 26.823 | 253.800 | 0.121 | 0.003 | 0.096 |
| Tnks | 8.000 | 0.311 | 6.894 | 140.900 | 0.120 | 0.000 | 0.053 |
| Rab24 | 9.000 | 4.412 | 45.320 | 23.100 | 0.118 | 0.001 | 0.068 |
| Alg10b | 8.000 | 1.310 | 14.557 | 55.400 | 0.117 | 0.002 | 0.086 |
| Prpf8 | 111.000 | 8.237 | 54.133 | 273.400 | 0.114 | 0.002 | 0.083 |

| | | | | | | | |
|---|---|---|---|---|---|---|---|
| Lactb2 | 10.000 | 5.310 | 46.528 | 32.700 | 0.112 | 0.002 | 0.086 |
| Abhd16a | 20.000 | 6.880 | 42.473 | 63.000 | 0.110 | 0.001 | 0.068 |
| Rims4 | 7.000 | 4.878 | 38.662 | 29.300 | 0.110 | 0.003 | 0.094 |
| Cxx1c | 5.000 | 4.623 | 55.357 | 13.600 | 0.109 | 0.002 | 0.086 |
| Gprin3 | 14.000 | 1.434 | 22.850 | 89.700 | 0.108 | 0.000 | 0.057 |
| Bri3bp | 5.000 | 2.831 | 19.763 | 28.200 | 0.107 | 0.002 | 0.086 |
| Glg1 | 54.000 | 9.680 | 46.809 | 133.600 | 0.105 | 0.003 | 0.095 |
| Fam69b | 10.000 | 3.642 | 29.930 | 48.800 | 0.105 | 0.001 | 0.080 |
| Rhot2 | 16.000 | 5.210 | 37.742 | 69.000 | 0.100 | 0.001 | 0.080 |
| Lbr | 10.000 | 1.395 | 18.211 | 71.400 | 0.095 | 0.002 | 0.083 |
| Cpt1c | 17.000 | 2.162 | 24.656 | 90.100 | 0.094 | 0.003 | 0.098 |
| Ubtf | 27.000 | 2.802 | 35.094 | 93.000 | 0.093 | 0.002 | 0.086 |
| Trim35 | 16.000 | 2.384 | 38.372 | 58.700 | 0.092 | 0.003 | 0.095 |
| Exosc10 | 23.000 | 1.404 | 31.960 | 102.000 | 0.090 | 0.001 | 0.083 |
| Casc4 | 17.000 | 4.754 | 37.931 | 49.400 | 0.083 | 0.002 | 0.083 |

# Chapter 2

Materials and Methods

## 2.1 Mice

All animal procedures were performed under protocols compliant and approved by the Institutional Animal Care and Use Committees of The Johns Hopkins University School of Medicine. No difference was observed in experiments performed distinguishing between sexes. As such, both male and female mice were considered for analyses for this study. For all experiments, we use wild-type C57BL/6 mice (stock number 027 from Charles River Laboratories). These are general-use animals that are used by many laboratories in the field. The specific age of animal used is listed in the experimental procedure sections. For the majority of experiments, mice were euthanized with carbon dioxide-induced anoxia and decapitated as a secondary method of euthanasia. For in vivo experiments, animals were anesthetized with Isofluorane and then decapitated.

## 2.2 Antibodies

***Chapter 3***: The following were used according to manufacturer's and/or published suggestions for western blotting and immunocytochemistry: anti-α1-7 proteasome subunit (Enzo), anti-α2 proteasome subunit (Cell Signaling), anti-α5 proteasome subunit (Santa Cruz), anti-β1 proteasome subunit (Santa Cruz), anti-β2 proteasome subunit (Santa Cruz), anti-β2 proteasome subunit (Enzo), anti-β2 proteasome subunit (Novus), anti-β2 proteasome subunit (Santa Cruz), anti-β5 proteasome subunit (Santa Cruz), anti-β5 proteasome subunit (Enzo), anti-Rpt5 proteasome subunit (Enzo), anti-calregulin (Santa Cruz), anti-β-Actin (Abcam), anti-Biotin (Cell Signaling), Streptavidin-AF647 (Invitrogen), anti-Tubulin (Milipore), anti-GluR1 (Cell Signaling), anti-Myc (Abcam), anti-Transferrin (Invitrogen), anti-EphB2 (M. Greenberg)(Margolis et al. 2010), anti-NGluR1 (R. Huganir), cleaved Caspase-3 (Cell Signaling), anti-Kv1.3 (NeuroMab), anti-S2 (Milipore), anti-PA200 (Novus), anti-11Sα (Cell Signaling), anti-11Sβ (Cell Signaling). Antibodies obtained from commercial vendors were verified for specificity using western blotting, immunofluorescence, or immunoprecipitation. We prioritize

those antibodies with a continued record of use in multiple independent studies (Supplementary Table 2). For proteasome antibodies, many antibodies used recognize a single band or set of bands at the known molecular weight. Genetic validation of these antibodies is impossible as all proteasome subunits are essential and no knockout controls can be obtained.

***Chapter 4***: The following were used according to manufacturer's and/or published suggestions for immunoblotting: anti-β-Actin (Abcam), anti-Biotin (Cell Signaling), Streptavidin-AF647 (Invitrogen), anti-Arc (Gift from P. Worley, Johns Hopkins, verified against knockout), anti-Fos (Cell Signaling), anti-Npas4 (Gift from Y. Lin, MIT, verified against knockout), anti-PSD-95 (Pierce), anti-Ube3A (Sigma, verified against knockout), anti-Ubiquitin (FK2, Enzo), anti-S6 ribosomal subunit (Cell Signaling), standard secondary antibodies were purchased. We attempted to use antibodies that were verified by knockout controls in either our study, or by other groups. We only used antibodies that provided a signal at the appropriate molecular weight, and where minimal nonspecific bands were observed.

**2.3 Mice**

All animal procedures were performed under protocols compliant and approved by the Institutional Animal Care and Use Committees of The Johns Hopkins University School of Medicine. No difference was observed in experiments performed distinguishing between sexes. As such, both male and female mice were considered for analyses for this study. For all experiments, we use wild-type C57BL/6 mice (stock number 027 from Charles River Laboratories). These are general-use animals that are used by many laboratories in the field. The specific age of animal used is listed in the experimental procedure sections. For the majority of experiments, mice were euthanized with carbon dioxide-induced anoxia and decapitated as a secondary method of euthanasia. For in vivo experiments, animals were anesthetized with Isofluorane and then decapitated.

### 2.4 Perfusion

P30 WT C57Bl/6 Mice were anesthetized with Isoflourane and rapidly perfused with phosphate buffer and 0.5% paraformaldehyde/1.0% glutaraldehyde and brains were thin-sectioned for Immuno-EM analysis.

### 2.5 Immuno-electron microscopy analysis

Brain slices from perfused mice and neuronal cultures were fixed and processed for Electron Microscopy. EM Grids were incubated in the primary antibody overnight at 4 °C followed by secondary antibodies for 2 hours at room temperature. All grids were viewed with a Phillips CM 120 TEM operating at 80 Kv and images were captured with an XR 80-8 Megapixel CCD camera by AMT. Neuronal cultures were fixed in 1.5% glutaraldehyde (EM grade, Pella) buffered with 70 mM sodium cacodylate containing 3 mM $MgCl_2$ (356 mOsmols pH 7.2), for 1 hour at room temperature. Thin-sectioned fixed brain slices and neuronal cultures were processed using the following protocol. Following a 30 minute buffer rinse (100 mM cacodylate, 3% sucrose, 3 mM $MgCl_2$, 316 mOsmols, pH 7.2), samples were post-fixed in 1.5% potassium ferrocyanide reduced 1% osmium tetroxide in 100 mM cacodylate containing 3 mM $MgCl_2$, for 1 hr in the dark at 4C. After en-bloc staining with filtered 0.5% uranyl acetate (aq.), neurons were dehydrated through graded series of ethanols and embedded/cured with Eponate 12 (Pella). LR-white procedural staining was used for HEK293 cells as well as neuronal cultures (Supplementary Fig. 4C). A metal hole punch was used to remove 5 mm discs from the polymerized plates. Discs were mounted onto epon blanks and trimmed. Sections were cut on a Reichert Ultra cut E with a Diatome diamond knife. 80 nm sections were picked up on formvar coated 200 mesh nickel grids and treated for antigen removal followed by on grid immunolabelling. Grids were floated on 95 °C citrate buffer pH 6.0 in a porcelain staining dish for 25 minutes, and then allowed to cool on the same solution for 20 min. After a brief series of 50 mM TBS rinses, grids were floated on 50 mM $NH_4Cl$ in TBS, blocked with 2% horse serum in TBS (no tween) for 20 minutes. Grids were

incubated in primary antibody diluted in blocking solution (1-50 Goat, mouse, rabbit antibody). Grids incubated on blocking solutions served as negative controls. Sections were allowed to come to room temperature (1 hour) on antibody solutions and placed on appropriated blocking solutions for 10 min. After further TBS rinses, grids were floated upon 12 nm Au conjugated donkey anti-goat, 12 nm Au conjugated goat anti-rabbit, 12 nm Au conjugated donkey anti-mouse, or Au conjugated streptavidin (Jackson Immunoresearch) at 1-40 dilutions in TBS for 2 hours at room temperature. Grids were then rinsed in TBS, floated upon 1% glutaraldehyde for 5min, rinsed again and stained with 2% filtered uranyl acetate. All grids were viewed with a Phillips CM 120 TEM operating at 80 Kv and images were captured with an XR 80-8 Megapixel CCD camera by AMT.

**2.6 Cell Lines**

For primary mouse neuronal cultures, pregnant wild-type C57/B6 mice were obtained from Charles River Laboratories, and sacrificed at E17.5. Whole cortices were dissected, processed into a single cell suspension, and plated as previously described[58]. Primary cell lines isolated in our laboratory from mouse brains are identified by surface markers that are unique to neuronal cells. These approaches have high sensitivity to accurately identify specific cells. Alternatively, for biochemical studies analysis of primary cell lines can be done using western blotting with well-validated antibodies to neuronal specific markers. Human Embryonic Kidney (HEK293) and Neuro-2A neuroblastoma cells were obtained from ATCC and maintained and expanded and frozen down in a series of aliquots. These aliquots are cultured for a limited number of passages (<10). They are regularly tested for any infection. The lab maintains strict guidelines for cell culture and monitoring of cell health in order to minimize biological variability and to prevent cell line cross-contamination during culture. Each cell line is maintained in its own culture medium.

### 2.7 Cell Culture and Transfections

***Chapter 3***: HEK293 and Neuro2A cells were cultured in DMEM supplemented with 10% fetal bovine serum, 2 mM glutamine (Sigma), and penicillin/streptomycin (100 U/mL and 100 µg/mL, respectively; Sigma). Mouse cortical neurons were prepared from E17.5 C57Bl/6 mouse embryos as previously described (Margolis et al. 2010). Neurons were maintained in Neurobasal Medium (Invitrogen) supplemented with 2% B-27 (Invitrogen), penicillin/streptomycin (100 U/mL and 100 µg/mL, respectively), and 2 mM glutamine. Dissociated neurons were transfected using the Lipofectamine method (Invitrogen) according to the manufacturer's suggestions.

***Chapter 4***: For primary mouse neuronal cultures, pregnant wild-type C57/B6 mice were obtained from Charles River Laboratories (stock number 027 from Charles River Laboratories), and sacrificed at E17.5. Whole cortices were dissected, processed into a single cell suspension, and plated as previously described(Ramachandran and Margolis 2017). Human Embryonic Kidney (HEK293) cells were maintained as previously described. Each cell line is maintained in its own culture medium. Neurons were maintained in Neurobasal Medium (Invitrogen) supplemented with 2% B-27 (Invitrogen), penicillin/streptomycin (100 U/mL and 100 µg/mL, respectively), and 2 mM glutamine. HEK293 cells were cultured in DMEM supplemented with 10% fetal bovine serum, 2 mM glutamine (Sigma), and penicillin/streptomycin (100 U/mL and 100 µg/mL, respectively; Sigma).

For analyzing the expression of immediate-early gene products, unique care was taken to ensure that neurons had reduced activity at baseline as measured by the expression of immediate early genes. After switching 500K neurons/well in 12 well format of cultured cortical neurons into 1mL Neurobasal/B27 at DIV3, neurons were maintained in that medium, with only one 100ul media exchange at DIV9. At DIV15, neurons were treated with pharmacological agents as indicated. Great caution was taken to minimize physical perturbation of these cultures so as not to induce any activation of IEG proteins. For example, drugs were resuspended in a small volume of

growth media (media in which neurons were growing in) before addition, so cultures did not have to be shaken to treat neurons.

### 2.8 Antibody feeding and immunocytochemistry

Cultured cortical neurons were plated on glass coverslips coated with poly-L lysine overnight. Neurons were allowed to mature to DIV 14 for feeding experiments. DIV 14 cortical neurons were slowly washed twice with cold PBS supplemented with 1 mM $CaCl_2$ and 2 mM $MgCl_2$ to slow recycling and internalization. Care was taken not to shear cell bodies from the neuron, and to maintain neuronal morphology. Cold neurons, while alive, were treated with Chicken anti-MAP2 antibodies (1:100), Goat anti-β5 proteasome subunit antibodies (1:50), and Rabbit anti-GluR1 (1:100) in PBS supplemented with 1mM $CaCl_2$ and 2 mM $MgCl_2$ for 30 minutes at 4°C. Antibodies were washed off, and neurons were rinsed twice in cold PBS, 1 minute each. Neurons with bound antibodies were fixed in 4% paraformaldehyde/4% sucrose in PBS for 75 seconds, so not to destroy the antibody itself but to maintain neuronal morphology. Samples were visualized using donkey anti-goat AF-488, donkey anti-chicken AF-555, and donkey anti-rabbit AF-647 (1:250 each) in 1× non-permeabilizing GDB (30 mM phosphate buffer pH 7.4 containing 0.2% gelatin, and 0.8 M NaCl) for 1 hour at 25 °C. Samples on coverslips were mounted on glass slides using Fluoromount-G (Southern Biotech). Neurons were imaged using a laser scanning Zeiss LSM780 FCS microscope. Images are representative maximal Z projections of multiple optical sections.

### 2.9 Protease protection assay

Cortical neuronal cultures were treated for the indicated times with 1 µg/mL of Proteinase K (NEB) in HBSSM (Hank's Balanced Salt Solution without $CaCl_2$ or phenol red, supplemented with 1 mM $MgCl_2$). Excess Proteinase K was quickly washed away three times in HBSSM, and Proteinase K activity was quenched twice for 3 minutes with 10 µM PMSF in HBSSM at 4 °C.

Neurons were then fractionated into cytosolic and membrane fractions as described above, and samples were prepared for SDS-PAGE and western analysis.

**2.10 Surface biotinylation, cell lysis, streptavidin pulldown, western blots**

***Chapter 3***: Surface biotin-labeling was performed as previously described (Lin et al. 2009). Whole mouse brains, cultured cells or whole animal tissue were obtained where indicated and each sample was labeled using Sulfo-NHS-LC-Biotin (ThermoFisher). Cultured cells were washed in pH 8.0 PBS (Gibco) with 1 mM $CaCl_2$ and 2 mM $MgCl_2$ (PBSCM) and treated with 1 mg/mL Sulfo-NHS-LC-Biotin dissolved in PBSCM for 20 minutes at 4 °C before the reaction was quenched for 10 minutes in 50 mM glycine in PBSCM. Intact tissue was quickly and manually chopped, following biotinylation for only 10 minutes at 4 °C in 0.5 mg/mL Sulfo-NHS-LC-Biotin prior to quenching the reaction. Whole mouse tissues and cultured neurons were collected and homogenized in RIPA buffer (50 mM Tris pH 8.0, 150 mM NaCl, 1% Triton X-100, 0.5% Sodium Deoxycholate, 0.1% SDS, 5 mM EDTA, complete protease inhibitor cocktail tablet (Roche), 1 mM β-glycerophosphate). Where indicated, the salt concentration in our RIPA lysis buffer was increased up to 300mM NaCl. Primary, human central nervous system (CNS) tissue, gestational weeks 19–21, were obtained under surgical written consent following protocols approved by the Johns Hopkins Institutional Review Board, based on its designation as biological waste. Tissue was mechanically chopped at 4°C, and immediately processed for surface biotinylation. For streptavidin pulldown experiments, lysed cells were incubated with high-capacity streptavidin agarose beads (ThermoFisher) overnight and then washed thrice with RIPA buffer before elution in SDS sample buffer. Western blots were performed using conventional approaches. Gels were run either on 4-15% SDS-PAGE gradient gels (Bio-Rad) or on 10% gels made in the laboratory. Proteins were transferred to nitrocellulose membranes at 100V for 1.5 hours in 20% methanol containing transfer buffer. All antibodies were made up in 5% BSA in 0.1% TBST. Western blots were incubated with appropriate secondary antibodies coupled to

Horseradish Peroxidase, extensively washed, and incubated with ECL. Images were exposed on film, and were scanned in and quantified using ImageJ by standard densitometry analysis.

***Chapter 4***: Immunoblots were performed using conventional approaches. Tris/Glycine gels were run on either 10% or 12% gels made in the laboratory. Proteins were transferred to nitrocellulose membranes at 100V for 2 hours in 20% methanol containing transfer buffer. All antibodies were made up in 5% BSA in 0.1% TBST, except for Arc antibody which was made up in 5% Milk in 0.1% TBST. Immunoblots were incubated with appropriate secondary antibodies coupled to Horseradish Peroxidase, extensively washed, and incubated with ECL. Blots were exposed on film, and were scanned in and quantified using ImageJ by standard densitometry analysis.

### 2.11 Cellular fractionation and integral membrane protein determination

For cellular fractionation experiments to determine the membrane attachment of the proteasome, cultured neurons were lysed in either a sucrose buffer (0.32 M sucrose, 5 mM HEPES, 0.1 mM EDTA, 0.25 mM DTT) or hypotonic lysis buffer (5 mM HEPES, 2 mM ATP, 1 mM $MgCl_2$) collected. Nuclei were pelleted at 800 RPM for 5 minutes, and the supernatant containing membranes was pelleted at 55000 RPM for 1 hour. Pelleted membranes were washed twice by homogenizing in lysis buffer and re-pelleted. Following two washes, membranes were processed for appropriate application. Supernatants containing the cytosolic extracts were concentrated down to the same volume that membranes were eventually resuspended in. Membrane association was determined by classic methods of sodium carbonate extraction. Briefly, purified neuronal membranes were resuspended in 50 mM sodium carbonate, pH 11 and incubated for 10 minutes at 4C to strip away membrane-associated proteins. Membranes, along with tightly-associated membrane proteins, were pelleted at 55000 RPM for 1 hour. Samples were subsequently prepared for SDS-PAGE analysis. For Digitonin fractionation, samples were lysed in sucrose buffer. Once the supernatant (cytosolic fraction) was set aside, the pellet was washed 2x with sucrose buffer, and then resuspended in sucrose buffer with indicated concentrations of digitonin. Following a 30

minute incubation in the buffer, samples were spun down at 55000 RPM for 1 hour. This was repeated for all indicated concentrations of detergent. For Fig. 3A, based on our fractionation protocol, we calculated that the input was about 60% cytosol and 40% membrane. We only collected the non-nuclei, non-mitochondria membrane (i.e. 20% of remaining membranes). For our westerns in Fig. 3A we used 10 µl of input and ~3x-purified cytosol and ~5x-purified membrane. Combining the data from the cytosol and membrane fractions and considering error in our experimental approach proteasome signal from our input is likely coming from both the cytosol and a larger fraction from the membrane preparations. Because our input includes all the cellular material and the fractionation removes the nuclei and mitochondria we believe, if any, a very small amount of proteasome signal in our input can account for that which is coming from these organelles.

**2.12 TX-114 phase extraction**

Protocol was adapted from (Park et al. 2013). Briefly, primary neuronal cultures were treated with 1% precondensed TX-114. Samples were dounce homogenized, spun at 4°C, and incubated at 30°C. Samples were centrifuged for 3 minutes at room temperature. Supernatant was retained as the DT-free fraction and resulting pellet was kept as the DT-rich fraction.

**2.13 Concanavalin-A plama membrane isolation**

Protocol was adapted from (Lee et al. 2012). Briefly, 0.25 mg biotinylated Concanavalin-A (ConA) was first coupled to 1 mL of streptavidin-coated agarose beads. Nuclei were pelleted from hypotonically lysed DIV 16 cultured cortical neurons, as described above, and the supernatant containing plasma membranes and cytosol were applied to 150ul of ConA beads. After thorough washing in lysis buffer containing 0.025% Nonidet-P40, samples were prepared for SDS-PAGE and western analysis.

### 2.14 DNA constructs

The full-length mouse tagged GPM6A, tagged GPM6B, tagged β5 constructs were acquired from Origene. All vectors obtained from commercial sources are verified and tested for the appropriate expression of the inserts using primary antibodies or epitope-tag antibodies against the expressed proteins. While we keep stocks of each validated plasmid, we periodically sequence these plasmids to confirm their authenticity. All plasmids used in this study are amplified and purified using standard kits from commercial vendors.

### 2.15 shRNA knockdown

Four unique shRNA constructs were obtained each against GPM6A, GPM6B, and PLP from Origene. These were validated HuSH 29mer shRNA constructs expressing GFP. Each construct was transfected into neurons using previously described and standard protocols. Each construct was transfected at 100 ng and 500 ng/well. In addition, the constructs were co-transfected in combination to knockdown either two, or all three genes.

### 2.16 Human subjects

Fetal brain tissue was obtained at Johns Hopkins University. Primary cultures of fetal cortical tissues were prepared. The use of fetal brain tissue was approved by the Johns Hopkins University institutional review board (IRB). Informed consent was obtained from all subjects. The authors did not have access to any identifying personal information.

### 2.17 Co-immunoprecipitations

Transfected HEK293 cells were collected and homogenized in IP Buffer (1% NP-40, 2mM MgCl2, 300mM NaCl, 2mM CaCl2, 50mM HEPES, 10% Glycerol) buffer. For immunoprecipitations, lysates were incubated with FLAG-M2 agarose beads (Sigma-Aldrich). Precipitated samples were washed and prepared for SDS-PAGE and immunoblot analysis.

### 2.18 Proteasome purification and assessment of catalytic activity

For proteasome purification, cells were treated and then immediately put on ice before purifications were performed as previously described (Besche and Goldberg 2012). Briefly, proteasomes were purified out of neuronal cytosol and detergent-extracted neuronal plasma membranes using the 20S proteasome purification kit (Enzo Life Sciences) or the 26S proteasome purification kit (UBPBio). For western blots, samples were denatured at 65 °C for 5 minutes in SDS sample buffer, resolved by SDS PAGE, transferred to nitrocellulose, and immunoblotted. For catalytic activity assays, 1/6th of the bead volume following proteasome purification was resuspended in activity assay buffer (20 mM Tris-HCl, pH8.0, 5 mM ATP, 5 mM $MgCl_2$, 1 mM DTT). 26S Proteasomal activity was assessed by the addition of 10 μM of SUC-LLVY-AMC (Enzo Life Sciences). The contribution of 20S proteasomal activity was assessed by the comparison of 26S proteasome activity to that of total proteasome activity (26S+20S), measured by the activity of samples containing SDS at a final concentration of 0.05%.

### 2.19 Cell culture radiolabeling

***Chapter 3***: Cortical neurons were cultured for 12 days in vitro. Radioactive labeling was done in Neurobasal growth media with B-27 supplement and without methionine or cysteine (Life Technologies, special order). $^{35}S$ methionine/cysteine (EasyTag PerkinElmer) was incorporated during indicated times at 55 mCi in the met/cys free growth medium. Where indicated, MG-132 (25 μM, Cell Signaling) and ATPγS (1 mM, Sigma) was added during the radioactive labeling window. For all labeling experiments, normal growth media on neurons was switched into labeling media supplemented with radioactive label for 10 minutes. Lysates were prepared in RIPA buffer (50 mM Tris pH 8.0, 150 mM NaCl, 1% Triton X-100, 0.5% Sodium Deoxycholate, 0.1% SDS, 5 mM EDTA, complete protease inhibitor cocktail tablet (Roche), 1 mM sodium orthovanadate, 1 mM β-glycerophosphate). SDS sample buffer was added and samples were boiled for 5 minutes prior to loading onto SDS-PAGE gels. Autoradiographs were done by

loading samples onto large SDS-PAGE gels, coomassie stained to verify equal loading, and then gels were dried down on a large gel drier onto Whatman filter paper. Dried gels were exposed to phosphorimager screens and scanned with a Typhoon FLA5500 imager.

***Chapter 4***: Cortical neurons were cultured for 12-16 days in vitro. Radioactive labeling was done in Neurobasal growth media with B-27 supplement and without methionine or cysteine (Life Technologies, special order). $^{35}$S-methionine/cysteine (EasyTag PerkinElmer) was incorporated during indicated times at 55 mCi in the met/cys free growth medium. Where indicated, MG-132 (20 μM, Cell Signaling) was added during the radioactive labeling window. For all labeling experiments, normal growth media on neurons was switched into labeling media supplemented with radioactive label for 10 minutes. For stimulation experiments, neurons were membrane depolarized with 55 mM extracellular KCl by addition of prewarmed depolarization buffer (55 mM KCl, 0.2 mM $CaCl_2$, 1 mM $MgCl_2$, 10 mM HEPES pH7.5) or a control buffer (Depolarization buffer, substituting 55mM NaCl for 55mM KCl) in fresh neuronal growth media as previously described (Lin et al. 2008). Lysates were prepared directly in RIPA buffer (50 mM Tris pH 8.0, 150 mM NaCl, 1% Triton X-100, 0.5% Sodium Deoxycholate, 0.1% SDS, 5 mM EDTA, complete protease inhibitor cocktail tablet (Roche), 1 mM sodium orthovanadate, 1 mM β-glycerophosphate) with SDS sample buffer added. This was done to prevent any enzymatic activity as soon as possible. Samples were heated at 70 °C for 5 minutes prior to loading onto SDS-PAGE gels. Autoradiographs were done by loading samples onto large SDS-PAGE gels, coomassie stained to verify equal loading, and then gels were dried down on a large gel drier onto Whatman filter paper. Dried gels were exposed to phosphorimager screens and scanned with a Typhoon FLA5500 imager. A variety of other manipulations and pharmacological agents were used during the pulse-chase protocol as indicated in supplementary figure 1. Synaptic activity was blocked by the addition of Tetrodotoxin (1 □M, Tocris), CNQX(1 □M, Tocris), and AP5 (1 □M, Tocris). Alternative stimuli to KCl depolarization included previously reported Glutamate (100

□M), and chemical LTP (125 mM NaCl, 2.5 mM KCl, 2 mM $CaCl_2$, 5 mM Hepes, 33 mM Glucose , 0.2 mM Glycine, 0.02 mM Bicuculline, and 0.003 mM Strychnine) protocols. Neurons were treated with ACSF, chemical LTP buffer, or glutamate for 10 minutes during radiolabeling. 5% FES was added for 30 minutes prior to radiolabeling and during radiolabeling. Media exchange was done by simply replacing growth media with fresh neurobasal-b27 to account for the stress of replacing media.

**2.20 Peptide collection and quantification**

***Chapter 3***: Following incorporation of radioactive $^{35}S$ methionine/cysteine, neurons were rapidly washed in PBS and fresh Neurobasal media without phenol red and with 2x B-27 supplement was added. At the two-minute time point, all of the media was collected and then spun through a 10 kDa Amicon filter (Millipore) and the flow through was then spun through a 3 kDa Amicon filter (Millipore). The flow-through from this sequential filtering was then dialyzed using dialysis tubing with a 100-500 Da cutoff (Spectrum Labs) into either 1x PBS (Gibco) or 20 mM Ammonium Bicarbonate (Sigma). Following four days of dialysis, samples were lyophilized and resuspended in MilliQ water for downstream calcium imaging. Quantification of peptides was done by counting the amount of radioactivity in each sample by liquid scintillation (Wallac 1410). Proteinase K control experiments were done by treating the media with 100 µg/mL proteinase K overnight in 2M Urea and 10mM BME, prior to re-dialyzing the proteolyzed media into 2M Urea for two days, and then gradually reducing the Urea concentration down into NaCl and then into Ammonium Bicarbonate. Resuspended peptides were quantified prior to applications using LavaPep Fluorescent Peptide Quantification Kit (LP022010, Gel Company).

***Chapter 4***: Radiolabelled peptide collections were done as previously described (Ramachandran and Margolis 2017). Briefly, neurons growing in their endogenous medium were treated with either a control or stimulation buffer. This was removed and replaced with pre-warmed Neurobasal/B27 minus met/cys and supplemented with radiolabeled $^{35}S$ methionine/cysteine,

with either control or stimulation buffers. Following 10 minutes of radiolabeling and stimulation, neurons were quickly washed with pre-warmed PBS and then 10mL of fresh Neurobasal/B27 was added. 50□l samples were immediately taken from the extracellular space. Samples were then quantified by liquid scintillation.

### 2.21 Biotin-epoxomicin

Biotin-epoxomicin is de-novo synthesized and purchased from Leiden University Institute of Chemistry. They are fully equipped with synthetic capabilities in organic chemistry. Mass spectrometry and NMR verify all batches produced by his lab for quality and purity. All batches used have had >99% purity. To further minimize batch variation, we test all batches in biological experiments (dose-titration for peptide release, NMP inhibition and cell viability responses).

Biotin-epoxomicin was added to neuronal cultures at 25 μM immediately after labeling. Following peptide release assays, treated cells were lysed in a sucrose homogenization buffer (0.32 M sucrose, 5 mM HEPES, 0.1 mM EDTA, 0.25 mM DTT). Membranes were separated from the cytosol by high-speed centrifugation at 55,000 RPM for 1 hour. Fractions were solubilized in SDS sample buffer prior to loading on SDS-PAGE gels for western analysis. EM processing was done after 5 minutes of treatment with Biotin-Epoxomicin.

### 2.22 Calcium imaging

Calcium imaging was performed as previously described (Kim et al. 2014). Briefly, for the Biotin-Epoxomicin experiments, cultured embryonic cortical neurons were transfected with 1 μg of a mammalian expression construct encoding GCaMP3 at DIV10 and imaged at DIV 12-14. Bicuculline treatment was administered as a 1 μM stimulation in calcium imaging buffer in a perfusion setup. Once the bicuculline stimulation was washed out, biotin-epoxomicin (25 μM) was co-administered with 1 μM Bicuculline in calcium imaging buffer. Each treatment was monitored for three minutes prior to washout. Coverslips were not imaged twice due to Biotin-Epoxomicin being a covalent inhibitor. Cells were ensured to be healthy at the end of the imaging

process by stimulating with 55 mM KCl and washing out and assessing for a proper calcium signal. Quantification was done by picking multiple regions of interests in primary and secondary dendrites across multiple coverslips over different imaging days. Data was analyzed using the Time Series Analyzer V3.0 ImageJ plugin and the ROI manager. Data were pooled for all the ROIs to generate a single N value. Brains from P0-P3 mouse pups (Cre-GCaMP3; Nestin-Cre ER) were dissected and plated in Neurobasal-A with B-27 supplement for two weeks. At DIV7, 4-hydroxytamoxifen (4-HT, concentration) was added to induce GCaMP expression. Neurons were imaged in a calcium-imaging buffer (130 mM NaCl, 3 mM KCl, 2.5 mM $CaCl_2$, 0.6 mM $MgCl_2$, 10 mM Hepes, 10 mM glucose, 1.2 mM $NaHCO_3$ pH 7.45). Peptides were collected, filtered, and dialyzed and then lyophilized prior to resuspension in 1 mL of MilliQ water and addition onto GCaMP-encoding neurons. 5 µl of resuspended peptides were sufficient to induce the described calcium-induced effects. Peptides treated with Proteinase K were spun through a 10 kDa MW cutoff filter prior to addition onto neurons in order to remove Proteinase K. Pharmacological inhibitors were perfused in at the indicated times at the following concentrations: BAPTA (2 µM), Thapsigargin (5 µM), Tetrodotoxin (1 µM), Nifedipine (1 µM), APV (2 µM).

### 2.23 Mass Spectrometry

***Chapter 3***: Mass spectrometry for proteasomes isolated from cytosolic and membrane fractions was performed at MS Bioworks, LLC.

***Chapter 4***: The fractionated peptides were analyzed on an Orbitrap Fusion Lumos Tribrid Mass Spectrometer coupled with the UltiMate™ RSLCnano nano-flow liquid chromatography system (Thermo Fisher Scientific). The peptides from each fraction were reconstituted in 0.1% formic acid and loaded on a Acclaim PepMap100 Nano-Trap Column (100 µm × 2 cm, Thermo Fisher Scientific) packed with 5 µm C18 particles at a flow rate of 5 µl per minute. Peptides were resolved at 250-nl/min flow rate using a linear gradient of 10% to 35% solvent B (0.1% formic

acid in 95% acetonitrile) over 95 minutes on an EASY-Spray column (50 cm x 75 µm ID, Thermo Fisher Scientific)packed with 2 µm C18 particles, which was fitted with an EASY-Spray ion source that was operated at a voltage of 2.0 kV.

Mass spectrometry analysis was carried out in a data-dependent manner with a full scan in the mass-to-charge ratio (m/z) range of 350 to 1550 in the "Top Speed" setting, three seconds per cycle. MS1 and MS2 were acquired for the precursor ion detection and peptide fragmentation ion detection, respectively. MS1 scans were measured at a resolution of 120,000 at an *m/z* of 200. MS2 scan were acquired by fragmenting precursor ions using the higher-energy collisional dissociation (HCD) method and detected at a mass resolution of 50,000, at an *m/z* of 200. Automatic gain control for MS1 was set to one million ions and for MS2 was set to 0.05 million ions. A maximum ion injection time was set to 50 ms for MS1 and 100 ms for MS2. MS1 was acquired in profile mode and MS2 was acquired in centroid mode. Higher-energy collisional dissociation was set to 35 for MS2. Dynamic exclusion was set to 30 seconds, and singly-charged ions were rejected. Internal calibration was carried out using the lock mass option (m/z 445.1200025) from ambient air.

**2.24 Statistics**

No statistical methods were used to predetermine sample size. The experiments were not randomized. All statistical analyses were performed using Origin Prism and Graphpad software, accounting for appropriate distribution and variance to ensure proper statistical parameters were applied. Experimental sample sizes were chosen according to norms within the field. The observed magnitude of differences, together with the low replicate variance, permits high power of analysis based on the sample size chosen. For quantification of proteasomal localization by EM analysis, images were acquired by an independent assistant in the Johns Hopkins imaging core not involved in the experimentation and counts were then objectively tallied by a second assistant without knowledge of the experimental groups. Statistical methods used are described in

figure legends for the respective EM experiments. For remaining experiments investigators were not blinded to allocation during experiments and outcome assessment.

Statistical analysis using Student's *t* tests, 1-way ANOVAs and the appropriate post hoc tests were performed as described in each figure legend. *P* values $\leq 0.05$ were considered significant

**2.25 Ribosome pelleting**

Ribosome-nascent chain complexes were isolated according to well established protocols(Brandman et al. 2012; Duttler, Pechmann, and Frydman 2013). Following various treatments and radiolabelling, neurons were lysed in a buffer containing either 100ug/mL Cycloheximide or Puromycin (25 mM HEPES pH7.5, 10mM MgCl2, 20mM KCl, 50mM NaCl, 2mM ATP, 10u SuperASE-In, 20uM MG-132, 1.5% Triton X-100, protease inhibitors). Lysates were cleared by centrifugation at 10,000 RPM for 10 minutes, and the supernatant was layered onto a 1M sucrose cushion. Ribosome-nascent chain complexes or empty ribosomes (following puromycin treatment) were pelleted via centrifugation at 70,000 RPM in a Ti 70.3 rotor. Supernatants were discarded and ribosomal pellets were washed three times with lysis buffer. 1/10 of the ribosomes were counted by liquid scintillation and the remainder was prepared in SDS loading buffer.

**2.26 Two-dimensional gels for nascent chain analysis**

2-dimensional gels to analyze the ribosome-nascent chain complex were performed as previously described(Ito et al. 2011). Briefly, following 30 seconds of radiolabel incorporation at room temperature, neurons were lysed in buffers containing either Cycloheximide or Puromycin. Following lysis, RNCs were isolated as described above. Isolated RNC complexes were resuspended in SDS loading buffer, and then loaded onto neutral pH SDS-PAGE gels to minimize in-gel tRNA hydrolysis. Each samples was run with a few microliters of prestained ladder to delineate the lanes. After running in a single dimension, lanes were cut out of the gel and then incubated with 1N NaOH at 80°C to degraded any RNA in the sample. This treatment

hydrolyzes the ester bond linking the tRNA to its nascent polypeptide, generating a population of radiolabeled proteins whose mass is reduced by the weight of the tRNA (~25 kDa). Following RNA hydrolysis, samples were run in a second dimension, and then transferred onto nitrocellulose membranes. After exposure for autoradiography, membranes were blocked in BSA and immunoblotted using anti-ubiquitin antibodies.

**2.27 Protein extraction, digestion, and labeling**

After indicated treatments, the cells were lysed by adding in 6 M urea and 2 M thiourea buffer with protease inhibitor cocktail. The lysates were sonicated with 35% amplitude for 1 min. Protein lysates were centrifuged at 16,000 g at 4 °C to exclude cell debris (pelleting at the bottom), and protein concentration was estimated using a SDS-PAGE method. Briefly, protein lysate was loaded with BSA standard ranging from 0.33 µg to 9 µg on a 3-12% NuPAGE gradient gel and separated for about 0.5 cm. The gel was stained with Colloidal Coomassie G-250 followed by destaining with water. The band intensities were measured by ImageJ software. A total of 200 µg of each sample was reduced with 10 mM dithiothreitol at room temperature for one hour and alkylated with 30 mM iodoacetamide for 20 minutes in the dark. The protein samples were digested using endoproteinase LysC (1:100) at 37 °C for 3 hours followed by sequencing-grade trypsin (1:50) at 37 °C overnight. After the digestion, the peptide samples were subjected to desalting and labeling with 10-plex TMT reagents according to the manufacturer's instructions (Thermo Fisher Scientific) and the 9/10 channels (126, 127N, 127C, 128N, 128C, 129N, 129C, 130N, 130C) were used for labeling. The labeling reaction was performed for one hour at room temperature, followed by quenching with 100 mM Tris-HCl (pH 8.0). The digested and labeled peptides from all 10 channels were pooled.

The peptides were fractionated by basic pH reversed-phase liquid chromatography (bRPLC) into 96 fractions, followed by concatenation into 24 fractions by combining every 24$^{th}$ fractions. Briefly, Agilent 1260 offline LC system was used for bRPLC fractionation, which includes a

binary pump, VWD detector, an autosampler, and an automatic fraction collector. In brief, lyophilized samples were reconstituted in solvent A (10 mM triethylammonium bicarbonate, pH 8.5) and loaded onto XBridge $C_{18}$, 5 µm 250 × 4.6 mm column (Waters, Milford, MA). Peptides were resolved using a gradient of 3 to 50% solvent B (10 mM triethylammonium bicarbonate in acetonitrile, pH 8.5) at a flow rate of 1 ml per min over 50 min collecting 96 fractions. Subsequently, the fractions were concatenated into 24 fractions followed by vacuum drying using SpeedVac. The dried peptides were suspended in 0.1% formic acid.

**2.28 Proteasome purification and activity assays**

Proteasomes were purified from either neuronal plasma membranes or out of the cytosol as previously described (Ramachandran and Margolis 2017). Briefly, neurons treated with either control or depolarization buffer were separated into membrane and cytosolic fractions using ultracentrifugation as previously described. Proteasomes were subsequently immunoprecipitated using resin conjugated to an antibody against the β2 proteasome subunit (Enzo). Immunoprecipitated proteasomes were then incubated with Suc-LLVY-AMC (Enzo) to test for activity. 20S activity was monitored as previously described.

**2.29 Data analysis, Mass Spectrometry – Chapter 4**

Proteome Discoverer (v 2.1; Thermo Scientific) suite was used for quantitation and identification. During the preprocessing of MS/MS spectra, the top 10 peaks in each window of 100 *m/z* were selected for database search. The tandem mass spectrometry data were then searched using SEQUEST algorithms against mouse RefSeq protein database (version 84) with common contaminant proteins. The search parameters used were as follows: a) trypsin as a proteolytic enzyme (with up to two missed cleavages); b) peptide mass error tolerance of 10 ppm; c) fragment mass error tolerance of 0.02 Da; and d) carbamidomethylation of cysteine (+57.02146 Da) and TMT tags (+229.162932 Da) on lysine residues and peptide N-termini as a fixed modification and oxidation of methionine (+15.99492 Da) as a variable modification. The

minimum peptide length was set to 6 amino acids. Peptides and proteins were filtered at a 1 % false-discovery rate (FDR) at the PSM level using percolator node and at the protein level using protein FDR validator node, respectively.

The protein quantification was performed with following parameters and methods. The most confident centroid option was used for the integration mode while the reporter ion tolerance was set to 20 ppm. The MS order was set to MS2 and the activation type was set to HCD. Unique and razor peptides both were used for peptide quantification while protein groups were considered for peptide uniqueness. Reporter ion abundance was computed based on signal-to-noise ratio and the missing intensity values were replaced with the minimum value. The quantification value corrections for isobaric tags and data normalization were disabled while the co-isolation threshold was set to 50%. The highest signal-to-noise ratio value from PSMs for a peptide was used to generate a peptide level abundance followed by averaging peptide level signal-to-noise ratio values for a protein to generate a protein level abundance.

Protein grouping was performed with strict parsimony principle to generate the final protein groups. All proteins sharing the same set or subset of identified peptides were grouped while protein groups with no unique peptides were filtered out. The Proteome Discoverer iterated through all spectra and selected PSM with the highest number of unambiguous and unique peptides.

### 2.30 TMT Differential Expression

The list of quantified proteins exported from Proteome Discoverer 2.1 was utilized as the input for our differential expression analysis. The raw values were organized in a matrix where each column represented a sample and each row a protein. To normalize the raw expression values, we began by $\log_2$ transforming the matrix with a +1 for computation. Then we median polished the log-transformed values by subtracting the row median from each row, followed by the subtraction

of the column median from each column. The resulting normalized expression values for each sample appeared normally distributed and was comparable across samples.

For the detection of differential regulation, we followed the recommendation outline in (Kammers et al. 2015). An empirical Bayes method was employed on the normalized matrix to detect differences between the 3 samples of the biotin-epoxomicin treated group compared to the 6 samples of the control and cycloheximide groups. The empirical Bayes method shrinks individual protein's sample variance towards a pooled estimate, and creates a more stable and powerful inference in differential protein abundance detection.

The output of the differential abundance analysis detected 1340 and 408 proteins to be differentially abundant at the 0.05 and 0.01 level respectively. However, due to the large number of proteins tested, we were more interested in q-values that adjust for multiple comparisons. Using a cutoff of $q < 0.1$, which corresponds to a false discovery rate of 10%, we detect 190 proteins to be differentially abundant in the 2 groups that we defined. Of those 190 proteins, 122 were up-regulated.

For the selection of the colors in the heatmap, we carried out feature-scaling of the normalized expression values on a gene-by-gene basis. For each gene, this process assigns the largest expression a value of 1, and the smallest expression a value of 0. The remaining values are scaled between 0 and 1 based on where they are relative to the largest and smallest expression values. For instance, a feature-scaled value of 0.5 represents an expression level that is halfway between the lowest expression and the highest expression observed for a gene. In other words, this sample's expression is 50% of the maximum fold change away from the lowest and the highest expression values at this gene.

### 2.31 Markov Chains to Model Radioisotope Release

To model the radioisotope release curves that were experimentally observed, we employed Markov chain simulations. A given Markov chain simulates the location of a single radioisotope

in 1-second increments, starting at the moment of washout until 1800 seconds (30 minutes) after. The transition process and probabilities between states is given in figure 2E. Each radioisotope is assumed to begin as a free isotope within the cell.

A free isotope has at each second interval a pBackground chance of diffusing across the cell membrane to become a free isotope extracellularly. In that same second interval, that isotope also has a pLoading chance of coming in contact with a ribosome and becoming a part of a nascent polypeptide. This leaves that for each interval, a free isotope has a 1-pLoading-pBackground chance of remaining as a free isotope.

Once a radioisotope has progressed to the state of a nascent polypeptide, it has some probability pCTD of being released co-translationally. If entering that release path, the time it takes for the release to be realized extracellularly requires a time that is distributed N(8, sd=2)/2.5. The N(8, sd=2) represents that on average cleave sites are every 8 or so amino acids, while 2.5 is the well established rate which degradation occurs. If not entering this pathway, the nascent chain becomes a folding intermediate. The time required for this is dependent upon the length of the protein that this isotope is being incorporated into, the location at which it is being incorporated, and the rate of translation. To determine the length of the protein, we sampled a protein at random from the list of detected intracellular proteins under full protein degradation inhibited conditions. The probability of sampling each protein is proportional to their relative abundance. Once the protein has been selected, we simulated the point of incorporation of the radioisotope to be uniform along the length of the full protein. The time to progress from a nascent polypeptide to the folding intermediate is determined as the (# of AA in the protein after the incorporation point/5), with 5AA/s being the established rate translation.

Upon becoming a folding intermediate, the radioisotope has a chance pFID of being degraded and released extracellularly. If entering this degradation path, the time before the radioisotope is realized extracelluarly is calculated as the #AA in the protein before the incorporation point (recorded from the previous step) divided by the well-established rate of degradation of

2.5AA/second. If at this point, the radioisotope does not enter the degradation path, it will initiate the process towards a folded protein.

The time it takes for a folding intermediate to become a folded protein is based upon the power law (Lane and Pande 2013)and is calculated as a random variable following exp(5*log(#AA)-27.7+Norm(0, sd=3)). This corresponds to a folding time of approximately 30 seconds for a 50 kDa protein. Once the protein is folded, it has a probability pFD of entering degradation in any 1-second interval. If it does enter the pathway, we assume the time it takes for the isotope to be released extracellularly is determined mostly by the unfolding time, which we assumed conservatively to be equal to the folding time distribution. Otherwise, the protein remains folded with a probability of 1-pFD. We chose a pFD of 1e-5 for our model because it corresponded to a conservative representation that the half-life of a folded protein existing in a folded state is approximately 20 hours.

### 2.32 Monte Carlo Inference for Model Parameters

With this formulation of the Markov chain, there remains 4 variables that are not based upon previously established results: pLoading, pBackground, pCTD, and pFID. We employed Monte Carlo simulations in a 2-stage process to optimize those parameters to most closely mirror the experimental observed release curves. Experimental release curves were estimated as follows. For each experimental condition, we have observations of released radioisotope at times 0, 60, 120, 300, 600, and 1800 seconds after washout. The value of each time point was divided by the total amount of radioisotope within the cell at 0 seconds after washout to rescale the observations as a proportion. For any point in time between the 5 observed time points, the released proportion was assumed to follow a linear relationship.

We first exploited the assumption that the dominant isotope release pathway should be diffusion (between 0-600 seconds) in an experimental condition where all degradation of proteins is inhibited. We inferred the optimal values of pLoading and pBackground by exploring the

parameter space of all pairwise combinations of pLoading between 0.0035 and 0.0075 in 0.0001 increments and pBackground between 0.00001 and 0.0004 in 0.00001 increments. For each of combination of pLoading and pBackground we used Monte Carlo simulations of 2500 Markov chains, each one starting as a free isotope and having transition probabilities given by the pairwise combination of pLoading and pBackground. The proportion of the 2500 initial radioisotopes that is released extracellularly at each second in time was recorded as the simulated release curve. The simulated release curves were compared to the experimental release curve when all protein degradation was inhibited to determine the optimal combination of pLoading and pBackground. The penalty measure is the sum of the squared distance between observed and simulated at each time point between 1 and 600 seconds. We chose not to evaluate the curves beyond 600 seconds because it appeared reasonable that diffusion was the dominant form of isotope release prior to 600 seconds. For the time range between 600-1800 seconds, other release mechanisms like autophagy might confound our efforts. This process revealed pLoading and pBackground to be optimized at 0.0056 and 0.00017 respectively.

After having optimized pLoading and pBackground, we continue on to find the pair of pCTD and pFID that best matches the experimental release curves under control conditions. We used a similar Monte Carlo simulation approach looking at all pairwise combinations of pCTD and pFID both between 0 and 0.7 in 0.001 increments. Using experimental data, we calculated that at the moment of washout, the ratio of free radioisotopes to isotopes in folded protein to isotopes in nascent polypeptides to be 300:20:1. As such, for each pairwise simulation, we initiated the initial state of the Markov chains to reflect that ratio. For each pairwise simulation, we simulated between 15,000 – 20,000 Markov chains, and tracked the progression of the isotopes for 1800 seconds. The simulated proportion of radioisotopes at any point of time that is extracellular was calculated as our simulated release curve. We searched for the pair of pCTD and pFID that produced the minimum total squared error at each time point from 1-1800 seconds between the

simulated curve and the observed control release curve. The optimal values for pCTD and pFID were observed to be 0.047 and 0.0 respectively.

We conducted the same optimization process of pCTD and pFID under KCI stimulation to in a manner that mirrored the above approach. We evaluated a parameter space for pCTD and pFID both between 0 and 0.2 in 0.05 increments. We searched for the pair that produced the minimum total squared error at each time point from 1-600 seconds between the simulated curve and the observed KCI release curve. The optimal values for pCTD and pFID were 0.165 and 0 respectively.

# Chapter 3

## Identification of a neuronal-specific plasma membrane 20S proteasome complex that generates extracellular signaling peptides

Modified from:

**Kapil V. Ramachandran** & Seth S. Margolis. A mammalian nervous-system-specific plasma membrane proteasome complex that modulates neuronal function. Nature Structural and Molecular Biology. 2017; 24, 419–430

Proteasomes are heterogeneous multisubunit catalytic complexes that consist of a core 20S stacked ring of α and β subunits with a $\alpha_7 \beta_7 \beta_7 \alpha_7$ architecture, and can be associated with 19S regulatory cap-particles to form a 26S proteasome(Coux, Tanaka, and Goldberg 1996). Among the other 20S-containing proteasomes are 20S proteasomes capped with 11S or PA200(Coux, Tanaka, and Goldberg 1996). While capped 26S proteasomes mediate ATP-dependent degradation of ubiquitinated proteins, uncapped 20S proteasomes do not require ubiquitin or ATP for their catalytic function(Ciechanover 1998; Ciechanover and Schwartz 1998; Ben-Nissan and Sharon 2014). Recent studies have shown that 20S proteasomes may have key biological functions separate from the canonical 26S ubiquitin-proteasome, particularly in clearing unstructured proteins and in degrading proteins during cellular stress(Ben-Nissan and Sharon 2014).

20S proteasomes are absolutely essential in mammalian cells. In lieu of genetic perturbation, proteasome function has been studied through the use of many different inhibitors such as MG-132, Lactacystin, Epoxomicin, and peptide boronates(Kisselev, van der Linden, and Overkleeft 2012). The use of these inhibitors has revealed diverse roles for the proteasome in many different tissues and contexts, driven by protein homeostasis through ubiquitin-dependent proteasomal degradation. Typically, these processes require proteasome function over hours to days (long-term). Indeed, proteasomes do play such long-term roles in important aspects of neuronal function such as synaptic remodeling and cell migration(Ehlers 2003; Wang et al. 2003). However, proteasome function is also required for activity-dependent neuronal processes over very short timescales (seconds to minutes), such as regulating the speed and intensity of neuronal transmission or the maintenance of long-term potentiation, a molecular underpinning of learning and memory(Karpova et al. 2006; Dong et al. 2008; Djakovic et al. 2009; Ehlers 2003; Bingol and Schuman 2006; Cai et al. 2010; Rinetti and Schweizer 2010). Presumably, short-term inhibition of the proteasome should not be able to meaningfully change the overall protein

landscape, so it was unclear how proteasomes could rapidly alter neuronal function. Thus, we reasoned that an unidentified function for proteasomes in the nervous system must exist.

Changes in calcium dynamics and transients underlie many of these neuronal processes that occur over short timescales. Indeed, perturbation of proteasome activity has been shown to affect calcium dynamics in neurons(Rinetti and Schweizer 2010; Wu, Hyrc, et al. 2009). Consistent with these findings, we observed that acute addition of the pan-proteasome inhibitor MG-132 onto neurons suppressed neuronal activity-induced calcium signaling (Figure 3.1). The effect on calcium dynamics that we observed occurred within seconds of MG-132 addition, indicative of a signaling role for proteasomes independent of their proteostatic role. Studies addressing the role for proteasomes in the nervous system have used pan-proteasome inhibitors such as MG-132 or lactacystin or have focused on the 26S proteasome through altering the ubiquitination pathway(Bingol and Schuman 2006; Fonseca et al. 2006; Rinetti and Schweizer 2010). These approaches do not distinguish between uncapped 20S or capped-20S proteasomes. We considered that evaluating proteasomes in the nervous system, without bias for 20S or 20S-containing proteasomes, would provide a means to identify unique proteasomes that could have acute signaling functions.

20S proteasome subunits are localized to neuronal plasma membranes

Previous studies have identified localization as a key feature in determining proteasome function(Pines and Lindon 2005). Distribution of the 26S proteasome in the nervous system has been measured using fluorescently-tagged 19S cap subunits or electron cryotomography (Cryo-ET)(Asano et al. 2015; Patrick et al. 2003; Djakovic et al. 2009). While cryo-ET approaches are theoretically unbiased, the processing methods inherently select for analysis of larger complexes, and therefore are more likely to identify singly- and doubly-capped proteasomes. In order to take a high resolution and unbiased approach to evaluate localization of all proteasomes (20S and

20S-containing) in the nervous system, we performed an immunogold electron microscopy (Immuno-EM) analysis of hippocampal slice preparations using antibodies raised against either the proteasome β2, β5 or β2 subunits (hence forth referred to as anti-β2, anti-β5, anti-β2). These are core 20S proteasome subunits common to all catalytically active proteasomes(Coux, Tanaka, and Goldberg 1996; Blomen et al. 2015).

We first performed western blot analysis of mouse brain lysates to assess the antibodies used for our immuno-EM studies. Brains from P30 mice were lysed and prepared for SDS-PAGE, and then immunoblotted with anti-β2, anti-β5, or anti-β2. Each antibody recognized a single band by western analysis at the appropriate molecular weight (Figure 3.2a-e). We proceeded to perform immuno-EM from mouse hippocampal sections using these antibodies and appropriate gold-conjugated secondary antibodies. We did not detect any significant staining using secondary gold-conjugated antibodies alone (Figure 3.3a-c). We observed diverse subcellular and cytosolic distribution of gold particles corresponding to proteasome subunits, as previously reported(Coux, Tanaka, and Goldberg 1996) (Figure 3.2a-e and Figure 3.4a-c). Unexpectedly, we observed ~40% of all gold particles localized to neuronal plasma membranes (PM). Similar results were obtained using two additional antibodies raised against □2 and □5 subunits, but directed against different epitopes (Figure 3.2b, d and Figure 3.4a, b). In contrast, we did not observe PM localization of gold particles when using antibodies raised against 19S cap proteins Rpt5 or S2 subunit (Figure 3.2f and Figure 3.4d). Immunostaining using these 19S antibodies show diffuse cytosolic localization, consistent with prior studies(Djakovic et al. 2009).

Extending these findings, we performed immuno-EM analysis from mouse primary neuronal cultures, as these preparations are largely devoid of non-neuronal cell types and can provide higher resolution analysis(van Weering et al. 2010; Chen et al. 2015). No immunogold label was observed in samples treated with secondary gold-conjugated antibodies alone (Figure

3.6a). For these experiments, using anti□β2 or anti□□5 we observed ~40% of immunogold signal at neuronal PMs (Figure 3.5a and Figure 3.6b). Of those particles observed at neuronal PMs, 43 ± 1% overlaid PMs, 39 ± 0.9% were located at the intracellular face, and 18 ± 0.9% were at the extracellular face (Figure 3.5a). Using similar immuno-EM approaches, we did not observe PM localization of proteasomes in cultured non-neuronal HEK293 cells, which had particles localized to the cytoplasm (Figure 3.6c). Because conjugation of a primary antibody to a gold-particle tagged secondary antibody can result in the gold particle being localized up to ~20 nm from the target antigen, we quantified the fine localization of gold particles near neuronal PMs and plotted each particle in relation to its distance from the PM. This was a linear measurement taken from the center of the PM to the centroid of the gold particle. A majority of particles overlaid the PM, with the particle density diminishing as a function of distance from the membrane (Figure 3.5b). Thus, the signal observed at plasma membranes corresponds to a unique pool of membrane-localized proteasome subunits rather than a reflection of intracellular proteasome subunits. Since core proteasome subunits are not known to be present in the cell separate from the macromolecular proteasome complex, these data likely reflected the membrane localization of intact proteasomes(Coux, Tanaka, and Goldberg 1996).

Neuronal membrane proteasomes are exposed to the extracellular space

Immuno-EM staining with a previously validated antibody raised against the cytoplasmic domain of the voltage-gated potassium channel, Kv1.3, only showed cytosolic labeling and labeling on the intracellular face of the PM as previously described(Gazula et al. 2010) (Figure 3.7a). By immuno-EM analysis we see 20S proteasome staining on the extracellular face of the PM, which raises the possibility that proteasomes may be exposed to the extracellular space (Figure 3.2a-e, 3.5a and Figures 3.4a-c, 3.6b). We decided to use three additional approaches to substantiate these findings: one specifically detecting proteasome subunits (antibody feeding) and two unbiased approaches to detect surface exposed proteins

(surface biotinylation & protease protection) (Figure 3.5c). First, we used antibody feeding onto live neuronal cultures(Kim et al. 2005; Hanley et al. 2002). No staining was observed using secondary alone controls (Figure 3.7b). Feeding a primary antibody against an N-terminal extracellular epitope of the GluR1 (N-GluR1) ionotropic receptor showed punctal staining as previously reported(Peebles et al. 2010). We did not observe staining feeding an antibody against intracellular protein MAP2 (Figure 3.5d). Consistent with proteasomes subunits being exposed to the extracellular space, feeding anti□□5 we observed punctal localization of which 20% overlapped with GluR1 (Figure 3.5d). Pretreatment of anti□□5 with the □5 blocking peptide eliminated 84% of the signal (Figure 3.5d).

To biochemically determine whether proteasomes were surface-exposed, we turned to previously described surface-biotinylation/purification approaches(Lin et al. 2009; Ehlers 2000) followed by immunoblotting with antibodies against 20S proteasome subunits, Rpt5, Actin, and GluR1. As expected, in our streptavidin pulldown samples from surface-biotinylated neurons we did not detect cytosolic Actin and did detect GluR1 (Figure 3.5e). Consistent with proteasomes being extracellularly accessible, we detected core 20S proteasome subunits in our streptavidin pulldown (Figure 3.5e). We did not detect significant pulldown of Rpt5. Several measurements were taken to assure our results were not due to poor cell health or enhanced cell permeability (Figure 3.7c and 3.7d).

As an orthogonal method of identifying surface exposed proteins, we used a protease protection assay, which relies on the proteolysis of extracellularly exposed epitopes of proteins upon treatment of live cells with an extracellular protease(Caterina, Hereld, and Devreotes 1995; Zhu et al. 2003). Cultured cortical neurons were treated with Proteinase K (PK) for varying times and then fractionated into either cytosolic or membrane fractions. By immunoblot analysis, we found that proteasome subunits fractionated to the membrane, similar to N-GluR1, and were susceptible to proteolysis by extracellular PK (Figure 3.5f). In contrast, proteasome subunits

from the cytosolic fraction, similar to Tubulin, were protected from protease cleavage(Wunder, Lippincott-Schwartz, and Lorenz 2010) (Figure 3.5f). Because PK, when added to live cells can only degrade proteins exposed to the extracellular space, we interpreted this observation to mean that proteasomes were surface-exposed and that the majority of proteasomes in our membrane preparations are from plasma membranes and not from other membrane organelles. This result was corroborated using Concanavalin-A (ConA), a lectin binding protein that binds glycosylated molecules, and has been used to enrich for plasma membranes(Lee et al. 2012) (Figure 3.7e). Taken together, these data support the existence of a surface exposed proteasome complex at the neuronal PM. For convenience, we will henceforth refer to the proteasome localized to the neuronal plasma membrane as the neuronal membrane proteasome, or NMP.

Neuronal membrane proteasomes are tightly associated with plasma membranes

We wanted to further enhance our biochemical understanding of how proteasomes, as largely hydrophilic complexes, could be localized to the hydrophobic PM. Neuronal membranes were isolated and sequentially extracted with increasing concentrations of digitonin to pull out increasingly hydrophobic proteins. Samples were prepared for western analysis (Figure 3.10a). Quantification of these immunoblots revealed that a significant percentage of alpha and beta subunits co-fractionated with cytosolic proteins (Tubulin) and hydrophobic membrane proteins (GluR1). These data are consistent with proteasomes fractionating in two different modes, one that is cytosolic and another that is membrane-bound, providing additional evidence for a unique pool of membrane-localized proteasomes in contrast to cytosolic proteasomes (Figure 3.10a). To determine whether NMPs were tightly or peripherally associated with plasma membranes, we used sodium carbonate extraction. Neuronal cultures were separated into cytosolic, peripherally-associated (carbonate-soluble) and tightly-associated (carbonate-insoluble) membrane proteins fractions(Zhu et al. 2003). Calregulin(Smith and Koch 1989) was used as a marker of peripherally-associated membrane proteins, whereas GluR1 was used as a marker of tightly-

associated membrane proteins. Immunoblotting these fractions showed that core 20S proteasome components were tightly-associated (carbonate-insoluble), while Rpt5 was peripherally-associated (carbonate-soluble) (Figure 3.10b).

We considered there were two primary ways this could be possible: (1) the proteasome itself was hydrophobic in some way or (2) the proteasome was tightly associating with integral membrane proteins. In an attempt to distinguish between these possibilities, we performed Triton X-114 phase partitioning of cultured neurons to separate hydrophilic and hydrophobic proteins(Park et al. 2013). Immunoblotting the Triton-rich and Triton-free fractions, we observed Actin fractionated into the Triton-free phase, multi-pass transmembrane protein GluR1 fractionated into the Triton-rich phase, and EphB2, a single-pass transmembrane protein fractionated into both phases (Figure 3.10c). Proteasome subunits fractionated in both phases, with only ~15-25% of proteasome subunits fractionating in the Triton-rich phase (Figure 3.10c). Based on our immuno-EM, surface biotinylation and membrane fractionation data up to 40% of proteasome subunits were plasma membrane localized. We reasoned that the discrepancy between these analyses might be due to the fact that proteasomes were not sufficiently hydrophobic to exist in the plasma membrane independent of auxiliary membrane proteins.

Neuronal membrane proteasomes are largely a 20S proteasome and in complex with GPM6 family glycoproteins

To identify potential auxiliary membrane proteins associated with the NMP we purified proteasomes out of neurons using two different affinity methods(Besche et al. 2009). Cytosolic and membrane-extracted fractions from neuronal cultures were incubated with 20S-purification matrix (purifies any 20S-containing proteasome complex) or 26S purification matrix (only purifies cap containing proteasome complex). Immunoblot analysis revealed that both 20S and 26S affinity purification matrices isolated cytosolic proteasomes, but only the 20S purification

matrix was able to purify proteasomes out of the membrane (Figure 3.11a), suggesting to us that this is an approach for purifying the NMP.

Using the 20S-purification matrix, we purified 20S proteasomes from the cytosol and membrane of neurons for in-depth mass spectrometry (MS) analysis. As expected, we identified all of the core 20S proteasome subunits in the purification from both membranes and cytosol (Table 1a). While we identified a variety of regulatory cap proteins to co-purify with the cytosolic proteasome, we identified very few to co-purify with the proteasome purified from membranes (Table 1a). These findings were validated by extensive western analysis (Figure 3.8a-c).

We sought to identify auxiliary membrane proteins in our MS data sets that may be capable of mediating proteasome association with the plasma membrane. We postulated that such a protein would specifically associate with the NMP compared to the cytosolic proteasome, be highly expressed in the nervous system, and be transmembrane (Table 1b). Based on these criteria, we focused our efforts on the neuronal membrane glycoprotein GPM6A, a known member of the Proteolipid Protein family of multi-pass transmembrane glycoproteins(Werner et al. 2001; Fuchsova et al. 2009). To validate these mass spectrometry data, we turned to HEK293 cells as a non-neuronal heterologous system that does not express the NMP (Figure 3.9a). Lysates from HEK293 cells previously transfected with expression plasmids encoding myc-/FLAG-tagged GPM6A and GPM6B (myc/FLAG-GPM6A/B) were immunoprecipitated using an anti-FLAG antibody. Immunoblotting using antibodies against myc and 20S proteasome subunits, we found that endogenous proteasome subunits from HEK293s co-immunoprecipitate with myc/FLAG-GPM6A/B (Figure 3.11b). While we interpret these data to mean that proteasomes can associate with GPM6 proteins, as demonstrated from our MS data from neurons, we wanted to know whether the GPM6 proteins could induce the proteasome to become membrane-bound and surface-exposed. Using the surface biotinylation assay, we determined

that expression of GPM6A and GPM6B in HEK293s was sufficient to induce surface expression of the endogenous HEK293 proteasome at the PM (Figure 3.11c). These results are not seen upon overexpressing GFP, single-pass transmembrane protein EphB2, or multi-pass transmembrane protein Channelrhodopsin 2 (Figure 3.11c). As a control for our surface biotinylation assay, we uniformly detected the plasma membrane protein, Transferrin, verifying equal pulldown efficiency (Figure 3.11c). Additionally, overexpression of myc-tagged □5 proteasome subunit together with myc/FLAG-GPM6A/B led to both myc-□5 and the endogenous subunits to become surface exposed (Figure 3.11c). These findings phenocopy the phenomenon we observe in primary cultured neurons, and indicate the GPM6A/B proteins are sufficient to expose proteasomes to the extracellular space. Attempts to determine whether GPM6 family proteins were required for NMP expression were unsuccessful as shRNA mediated knockdown of GPM6A in neuronal cultures induced cell death suggesting GPM6 proteins may be essential for viability (data not shown).

GPM6A and GPM6B are primarily expressed in the nervous system(Zhang et al. 2014). Consistent with these data, using our surface biotinylation assay in whole mouse tissues, we determined that NMP expression was restricted to mouse neuronal tissues (Figure 3.11d). Similar results were observed using human brain tissue (Figure 3.9b). These were the first set of data to indicate some specific role for NMP in neuronal function and prompted us to determine whether NMP expression was regulated and changed over neuronal development. Using our surface biotinylation assay in slice preparations from mouse brain, we determined that NMP expression paralleled *in vivo* expression patterns of GluR1, whose expression functionally correlates with critical stages in neuronal development(Lin et al. 2009) (Figure 3.11e). Performing the same experiments in neuronal cultures, we observed that the NMP was expressed in neurons at DIV8, but not prior (Figure 3.9c, d) in contrast to relatively constant total proteasome expression.

Neuronal membrane proteasomes degrade intracellular proteins into extracellular peptides

To test whether the NMP was catalytically active, we purified proteasomes from both the cytosol and neuronal plasma membranes using a 20S purification matrix and incubated them with a substrate that fluoresces upon proteasomal chymotrypsin-like cleavage(Vilchez et al. 2012). Addition of a low concentration of SDS to the reaction relieves the gating mechanism of the 20S proteasome without denaturing the 20S or 26S proteasome holocomplex(Ben-Nissan and Sharon 2014). Addition of SDS greatly stimulated the catalytic activity of membrane proteasomes and had little effect on cytosolic proteasome activity (Figure 3.12a and Figure 3.13a), consistent with a large fraction of NMPs being 20S and catalytically active.

Since the core 20S complex alone is ~11x15 nm, any orientation of the NMP at the neuronal PM, which is 6-10 nm across, would provide it access to both the intracellular and extracellular space. We hypothesized that in intact cells, a catalytically active NMP in such an orientation would be able to promote proteasome-dependent degradation of intracellular proteins into the extracellular space. To test this hypothesis, we used $^{35}$S-methionine/cysteine-radiolabelling approaches to trace the fate of newly synthesized intracellular proteins(Schubert et al. 2000) (Figure 3.12b). After 10 minutes of radiolabel incorporation (Figure 3.12c), free radioactivity was washed away, and media was collected over a timecourse and analyzed by liquid scintillation to detect radiolabeled proteins. We observed rapid release of radioactivity into the culture medium under baseline conditions (Figure 3.12d). We observed a significant decrease in radioactive flux following addition of MG-132, without affecting radiolabelling efficiency (Figure 3.12c, d). Addition of ATP□S, a non-hydrolyzable ATP analog, had no effect on release of radioactive material (Figure 3.12d). This was consistent with the release of radioactivity being due to an uncapped 20S proteasome, which does not require ATP. To determine whether the released radiolabel was incorporated into protein peptides, different fractions from the media were treated with PK to breakdown peptidergic material into single

amino acids and dipeptides. Of the released radioactive material at the 2-minute collection time, 82 ± 11% was made up of PK-sensitive molecules that ranged between 500 and 3000 Daltons in size (Figure 3.12e). Similar results were observed at a 30-minute collection time (Figure 3.13b). Since proteasome cleavage products are peptides between 500 and 3000 Da in size we conclude that a large fraction of radioactivity in the media was composed of protein peptides derived from a proteasome(Kisselev, Akopian, and Goldberg 1998) and not individual amino acids or small molecules. To discriminate between cytosolic and membrane proteasomes in mediating the efflux of extracellular peptides, we took advantage of the temporal switch in NMP expression between DIV7 and DIV8, where both DIV7 and DIV8 neurons express cytosolic proteasomes but only DIV8 neurons express the NMP (Figure 3.9c, d). We observed that proteasome-dependent release of radiolabeled peptides into the media was observed at DIV8, but not at DIV7(Figure 3.12f). Consistent with this being an NMP-mediated neuronal phenomenon, we did not observe proteasome-dependent release of radiolabeled peptides in heterologous HEK293 cells that do not express the NMP (Figure 3.13c). Taken together, these data support our hypothesis that the NMP degrades intracellular proteins into extracellular peptides.

Neuronal membrane proteasomes are required for release of extracellular peptides and modulate neuronal activity

To specifically determine the contribution of the NMP in the generation of these extracellular peptides, separately from that of the cytosolic proteasome, we identified a chemical tool that was selective to the NMP. We found that biotinylation of the non-reactive portion of epoxomicin, a highly potent and specific proteasome inhibitor, generates a cell-impermeable compound (biotin-epoxomicin) that maintains target specificity(Li et al. 2013). The epoxomicin of biotin-epoxomicin covalently attaches to the catalytic proteasome □ subunits thus permanently tagginging □ subunits with biotin. To test this, cultured neurons acutely treated with biotin-epoxomicin were separated into cytosolic and membranes fractions, and probed with

fluorescent streptavidin. Biotin signal was only observed as two distinct bands in membranes from neurons treated with biotin-epoxomicin, denoting the covalent modification of the membrane proteasome □ subunits (Figure 3.14a).

Furthermore, Immuno-EM analysis of neuronal cultures treated with biotin-epoxomicin showed 91 ± 5% of biotin at plasma membranes (Figure 3.14b and Figure 3.15a). Any cytosolic labeling was likely due to the streptavidin-Au binding of endogenously biotinylated proteins, as we detected low-abundance cytosolic labeling in cultures not treated with biotin-epoxomicin (Figure 3.15a, b). Since biotin was directly labeled using streptavidin-Au, this analysis reduces the distance between the gold particle and the target antigen compared to conventional antibody-based immuno-EM. These data show that NMPs overlay neuronal plasma membranes and are exposed to the extracellular space and provide further evidence that the NMP is catalytically active, since epoxomicin requires proteasome activity in order to bind to and inhibit the catalytic subunits(Meng et al. 1999b). Using this inhibitor, we sought to separate the role of the NMP from the role of the cytosolic proteasome in regulating extracellular peptide production. Acute application of biotin-epoxomicin to radiolabeled neurons inhibited radioactive peptide release into the extracellular space (Figure 3.14c). Using biotin-epoxomicin, we wanted to test our initial hypothesis that the NMP could mediate rapid neuronal signaling.

To test whether the NMP was relevant to aspects of neuronal signaling, changes in intracellular calcium were measured since calcium serves as a rapid readout for many types of neuronal signaling(Patel et al. 2015). Calcium imaging was performed using GCaMP3-transfected cultured neurons treated with perfusate containing GABAergic receptor antagonist bicuculline which, by relieving inhibition on neuronal circuits, induces regular firing of action potentials and calcium transients(Patel et al. 2015). Following 2 minutes of bicuculline stimulation, perfusate was switched to buffer containing both bicuculline and 25 □M biotin-epoxomicin. Within 10-30 seconds of biotin-epoxomicin addition, we observed a rapid and

robust attenuation of the amplitude of bicuculline-induced calcium transients, similar to that which we observed upon acute addition of MG-132 (Figure 3.14d and e). Addition of biotin-epoxomicin induced a large variability in the frequency of calcium transients: 47% of neurons displayed an increase in frequency, while the same treatment induced a potent abrogation of bicuculline-induced calcium signals in 38% of neurons (Figure 3.14f). Based on these data, an endogenous function of the NMP is to modulate the strength and speed of activity-dependent neuronal signaling through its proteolytic activity, possibly through the actions of the resulting extracellular peptides.

Neuronal membrane proteasome-derived peptides are sufficient to induce neuronal signaling

To systematically test the effects of proteasome-directed peptide signaling, peptides were purified and then perfused onto GCaMP3-encoding neurons under various conditions. Neurons were ensured to be healthy at the end of every experiment by stimulating with 55 mM KCl, which consistently induced strong calcium signaling. The proteasome-directed peptides were purified and resuspended in calcium imaging buffer. Peptide concentration was determined to be ~50 ng/mL and was added back at that concentration. Alone, purified peptides induced a robust degree of calcium signaling in naïve neurons (Figure 3.16a). This peptide-induced stimulation was eliminated if the peptide purification was done in the presence of PK (Figure 3.16b). These data suggest that the observed calcium-signaling effects were due to the actions of extracellular protein peptides, and not small molecules or excitatory amino acids. Moreover, media collected in the presence of MG-132 did not possess the capacity to stimulate naïve neuronal cultures (Figure 3.16c), indicating that the relevant bioactive peptides were derived from the proteasome. Moreover, in similar experiments, addition of random peptides to GCaMP3-encoding neurons did not possess the capacity to stimulate naïve neuronal cultures (Figure 3.17). We then determined that these peptides were inducing calcium flux from the outside of the cell in, rather than promoting release from intracellular calcium stores. Addition of cell-impermeable calcium

chelator BAPTA to the perfusate abrogated the peptide-induced calcium signal (Figure 3.16d), whereas depletion of ER calcium stores using thapsigargin did not reduce the maximum amplitude of the peptide-induced calcium signal (Figure 3.16e).

To identify which channels were relevant to peptide-induced calcium activity, we used different ion channel inhibitors to pharmacologically identify relevant pathways. Blocking fast voltage-gated sodium channels using Tetrodotoxin did not block the peptide-induced calcium signal, revealing that the influx of calcium was probably not due to action potential-induced signaling, and more likely directly due to effects on calcium channels (Figure 3.16f). Blockade of L-type calcium channel dependent influx using Nifedipine also did not modulate the peptide-induced calcium signal (Figure 3.16g). However, inhibiting N-methyl-D-aspartate receptors (NMDARs) using 2-amino-5-phosphonopentanoic acid (APV) reduced the maximum amplitude of the peptide-induced calcium influx (Figure 3.16h). Together, these data suggest that the peptides derived from the neuronal membrane proteasome can modulate neuronal activity, at least in part by driving calcium influx through NMDARs (Figure 3.16i).

We report on an unusual finding of a 20S proteasome that is tightly associated with the neuronal plasma membrane and exposed to the extracellular space. In this capacity, it can degrade intracellular proteins into bioactive extracellular peptides that induce calcium signaling through NMDA receptors. The model we prefer (discussed further below) based on these data are that a 20S proteasome complex is coupled to the plasma membrane by GPM6 glycoproteins, and that the extracellular peptides generated are the means by which the NMP acutely regulates neuronal function.

Proteasome association with neuronal plasma membranes and surface-exposure by GPM6 family glycoproteins

Identification of the GPM6 glycoprotein family as proteins that interact with proteasomes and are sufficient to induce the expression of proteasomes at the plasma membrane provides some insight into how proteasomes, as hydrophilic protein complexes, could interact so tightly with the hydrophobic plasma membrane. However, we noticed that the magnitude to which GPM6-induced membrane proteasome expression in heterologous cells did not match the magnitude of endogenous membrane proteasome expression in neurons. This suggests that there may in fact be other proteins that mediate the interaction of the NMP with the membrane, an area being actively investigated.

We postulate that the GPM6 glycoproteins may form a protein pore, perhaps through oligomeric interactions, which have been proposed previously(Werner et al. 2001; Sato et al. 2011). In the right conformation, proteasomes binding to pore-containing membrane proteins could give proteasomes a hydrophilic binding surface to the hydrophobic plasma membrane, allowing the proteasome to gain access to the extracellular space. We propose a few models for how GPM6 proteins, or other membrane tethers may localize the proteasome to the plasma membrane (Figure 3.18). In each case, we posited that 1) proteasomes must be located at plasma membranes, 2) proteasomes were in some fashion bound to auxiliary membrane proteins such as

GPM6, and 3) proteasomes must be able to degrade proteins from the intracellular to the extracellular space. Model 1 – Cytoplasmic docking: In this model, a proteasome located at the plasma membrane would be docked on or tethered to auxiliary membrane proteins on the cytoplasmic side of the membrane. Degraded proteins would be shed through a peptide pore formed by the auxiliary proteins. Model 2 – Extracellular docking: In this model, a proteasome located at the plasma membrane would be docked on or tethered to auxiliary membrane proteins on the extracellular side of the membrane. Proteins would be delivered through a protein pore formed by the auxiliary proteins. Model 3 – Intramembrane docking: In this model, a proteasome located at the plasma membrane would be tethered or anchored to auxiliary membrane proteins within the lipid bilayer. The cell biological conundrum of how a proteasome can interact with the plasma membrane may be the most significant question to address in order to gain a deeper understanding of NMP function. Because antibody feeding and protease protection require that large molecules gain access to the proteasome, we posit that model 1 is less likely, and either model 2 or model 3 will prevail. While we find these models most consistent with our data, we certainly do not preclude other potential models. Ultimately, the nature of this seemingly transmembrane complex can only be validated by a structural approach.

NMP composition and regulation

We made significant attempts to identify NMP interacting partners in an effort to determine whether the NMP was capped by the 19S, 11S, or PA200 subunits. Our data likely preclude the presence of the canonical 19S proteasome cap, or regulatory caps such as 11S or PA200(Besche and Goldberg 2012; Ben-Nissan and Sharon 2014; Tai and Schuman 2008a). While we identified a few 19S subunits co-fractionating with the NMP by mass spectrometry, we could not identify significant amount of key 19S subunits Rpt5 or S2. We also made the intriguing observation that immunoproteasome subunit PSMB8 uniquely co-fractionated with the NMP. Our finding that the NMP is likely a 20S core proteasome lacking the 19S cap is significant

for two primary reasons. First, while a few functions for 20S proteasomes have been ascribed, their function independent of the 19S cap largely remains a mystery, especially in the nervous system(Tai and Schuman 2008a). Second, significant implications come from the idea that 20S proteasomes are primarily tasked with clearing misfolded or unstructured proteins(Ben-Nissan and Sharon 2014; Tsvetkov et al. 2008; Tsvetkov et al. 2009). A large source of disordered or unfolded proteins is derived from failed products of protein translation and misfolded or improperly folded proteins. These end-products of proteotoxic stress are hallmarks of many neurodegenerative disorders(Schmidt and Finley 2014; Tai and Schuman 2008b), a fact which places the NMP at the heart of various disease states.

NMP-directed peptide signaling modulates neuronal function

Unconventional secretion pathways have been implicated in release of cellular protein cargos(Jiang et al. 2013; Lee et al. 2016). Moreover, many groups have demonstrated that inhibition of ubiquitin-dependent proteasome function affects synaptic signaling and transmission. Our data support a role for the existence of a specialized neuronal membrane proteasome that mediates neuronal function by "inside-out" signaling through the production of extracellular proteasome-derived peptides. While it remains possible, we have not detected any role for secretion pathways or ubiquitin in the release of these peptides (Ramachandran and Margolis, unpublished data).

Proteasome-derived peptides, which when purified, rapidly and robustly stimulate neurons. Pharmacological dissection of the downstream pathways of peptide signaling revealed that NMP-derived peptides act in part by modulating NMDARs. The signaling through NMDARs only makes up ~50% of the total activity of the peptides. Other possible targets include: 1) Peptides interact with major histocompatibility immune complexes (MHC) that have recently been shown to play key roles in developmental and experience-dependent mechanisms in the nervous system(Huh et al. 2000; Shatz 2009); 2) peptides modulate metabotropic ion

channels, thereby altering calcium-mediated signaling; and/or 3) peptides signal to neuronal or non-neuronal cells such as glial cells through yet to be identified receptors.

It is well-established that NMDARs are critical for neuronal activity-dependent signaling relevant to learning and memory(Xia et al. 1996; Nicoll and Roche 2013; Malenka and Nicoll 1999). Given that cytosolic proteasomes have been shown to be regulated by neuronal activity, it will be intriguing to better understand whether the NMP and the resulting extracellular peptides are also modulated by changes in neuronal activity. It is also unclear how this signaling is specified within the brain, but we postulate that it relies on how the NMP recognizes and targets proteins for degradation. Therefore, it will be critical to identify not only the sequences of the peptides, but also the substrates from which they are derived. These insights into substrate identity and targeting will reveal how the NMP functions, but may begin to link proteostatic failure under pathological conditions to NMP dysfunction.

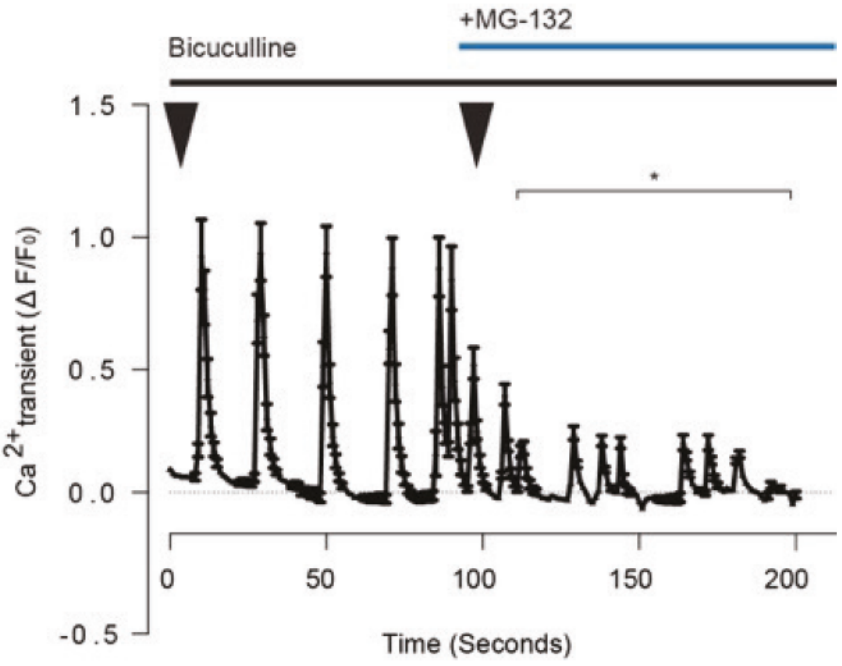


**Figure 3.1. Proteasomes rapidly regulate neuronal calcium signaling**

Cortical neuronal cultures at 14 days in vitro were transfected using a plasmid that encodes for GCaMP3, a genetically encoded calcium indicator. Bicuculline, a GABA receptor antagonist that relieves inhibition on neuronal circuits and induces regular firing of action potentials, was added to naïve GCaMP3-encoding neurons. Calcium imaging was performed on transfected cultures. Traces of Bicuculline response before and after MG-132 addition are plotted. First black arrowhead indicates when Bicuculline is perfused onto neurons, second arrowhead indicates when MG-132 is spiked into perfusion. Lines above graph (Bicuculline – black, MG-132 – Blue) indicate time window when drug is applied. Quantification of normalized fluorescence intensity ($\Delta F/F_0$) measurements of calcium signals over imaging timecourse is presented. Trace is accumulated data from representative neuron over 18 ROIs (regions of interest). Two independent neuronal cultures. 15 neurons quantified per culture. *$P$<0.01 (two-tailed Student's $t$-test). Data are presented as mean ± SEM.

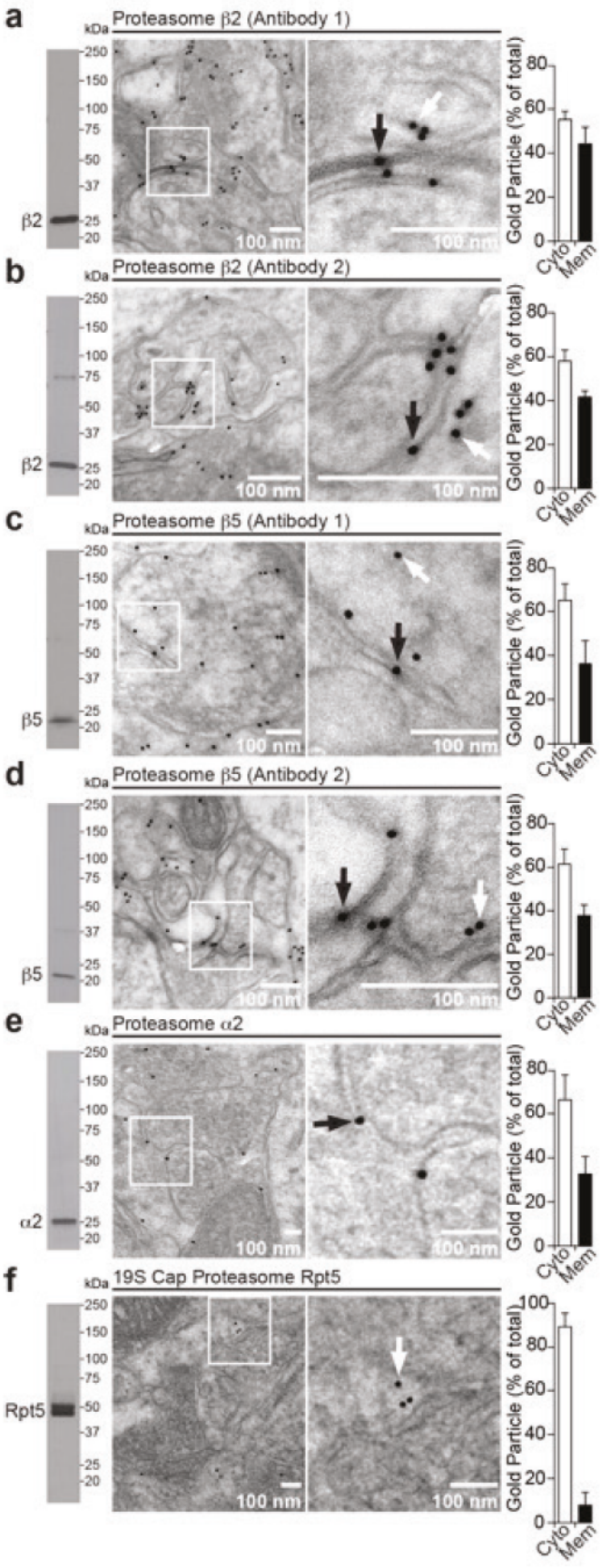
a
Proteasome β2 (Antibody 1)
kDa
250
150
100
75
50
37
25
20
β2
100 nm
100 nm
Gold Particle (% of total)
80
60
40
20
0
Cyto
Mem
b
Proteasome β2 (Antibody 2)
β2
c
Proteasome β5 (Antibody 1)
β5
d
Proteasome β5 (Antibody 2)
β5
e
Proteasome α2
α2
f
19S Cap Proteasome Rpt5
Rpt5
100

**Figure 4.1. Ephexin5 is upregulated in AS mouse hippocampal tissue and removal of Ephexin5 modulates Figure 3.2. 20S proteasome subunits are localized to neuronal plasma membranes**

(**a**-**f**) (left) Western blots of neuronal lysates probed using indicated antibodies. (**a**-**f**) (center) Electron micrographs of immunogold labeling (12 nm gold particles) from hippocampal slice preparations using antibodies raised against core catalytic β2 (**a, b**), β5 (**c, d**), □2 (**e**) proteasomal subunits and 19S cap proteasome subunit Rpt5 (**f**). Representative images shown. White boxes on EM show magnified region (displayed to the right). Several arrows shown corresponding to immunogold label; cytosolic (white); membrane (black). (**a**-**f**) (Right) Quantification of gold particles from stated number of micrographs to get at least 300 gold particles: **a**) N=49; **b**) N=47; **c**) N=43; **d**) N=54; **e**) N=54; **f**) N=82. >300 gold-particles per antibody were counted. Slices were made from two separate 3-month old mice, >20 slices were generated for immuno-EM analysis. Data are presented as mean ± SEM.

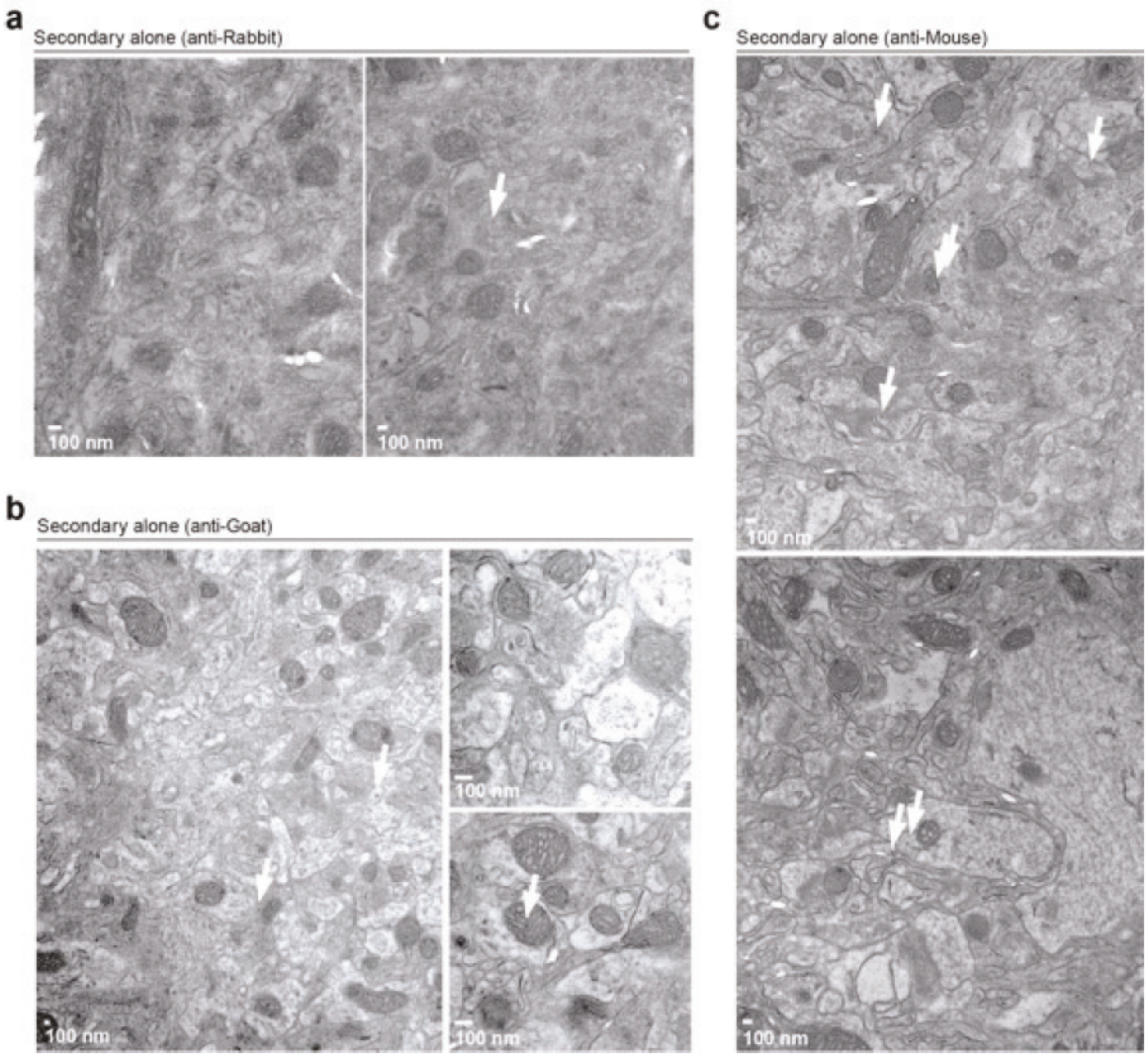


**Figure 3.3. Secondary-alone antibody controls do not detect signal by Immuno-EM**

(**a**) Immuno-EM analysis of hippocampal slice preparations using only a secondary gold-conjugated anti-rabbit antibody in the absence of the primary antibody to detect non-specific background staining. Secondary alone controls for anti-goat (**b**) and anti-mouse (**c**) are shown. White arrows indicate low background immuno-Gold particle staining observed, note low magnification (11000X). Slices were made from two separate 3 month old mice, >20 slices were generated for immuno-EM analysis, same metrics were used for secondary controls as for slices incubated with primary.

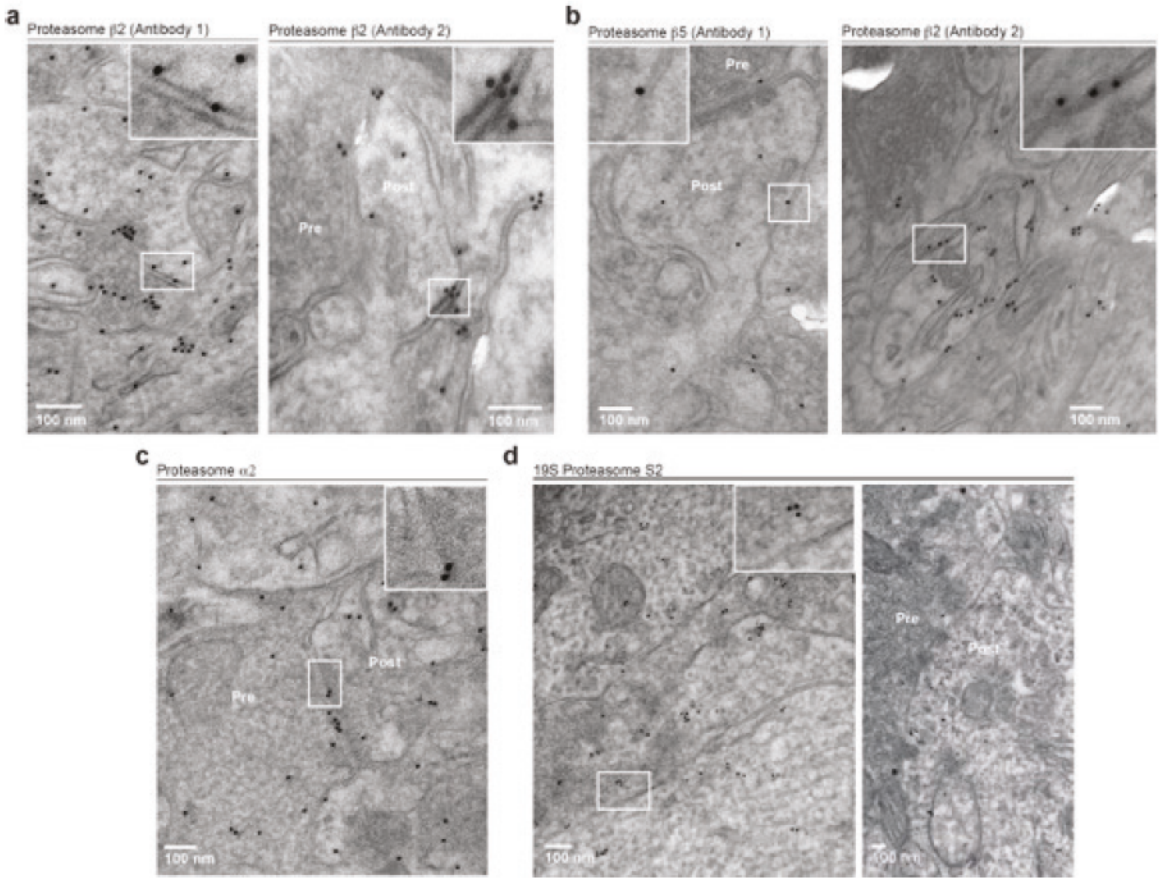


**Figure 3.4. 20S proteasome subunits are localized to neuronal plasma membranes.** Low magnification (63000X) image of immuno-electron micrographs performed using antibodies against β2 (**a**), β5 (**b**), α2 (**c**), and 19S cap proteasome subunit S2 (**d**). Labeled ultrastructures: Presynaptic regions (Pre), Postsynaptic regions (Post). Insets shown at higher magnification. Slices were made from two separate 3-month-old mice, >20 slices were generated for immuno-EM analysis.

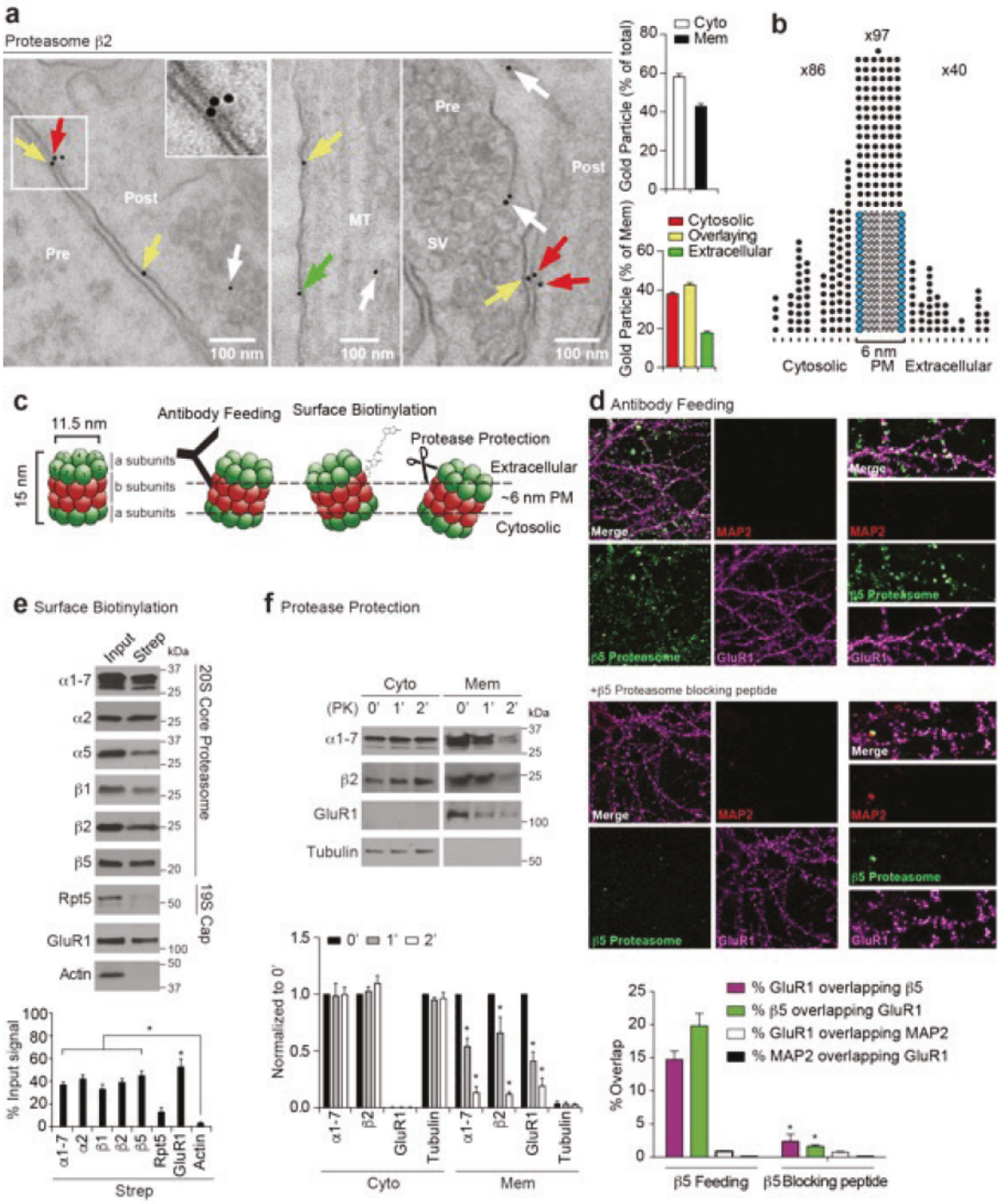


**Figure 3.5. Neuronal membrane proteasomes are exposed to the extracellular space**

(**a**) Electron micrographs of immunogold labeling (12 nm gold particles) from from DIV14 primary mouse cortical cultures using anti-β2. Representative images shown. Inset shows magnified region. Ultrastructures: Presynaptic (Pre); Postsynaptic (Post); Microtubules (MT);

Synaptic vesicles (SV). Arrows corresponding to immunogold label; cytosolic (white); membrane (red-cytosolic face), (yellow-directly overlaying), (green-extracellular face). (N=84 images, >300 gold-particles counted. Multiple punches from single DIV14 culture, >20 slices generated). (**b**) Quantification depicted for a subset of gold particles near membranes, with every tick mark representing 2 nm from the PM. Each dot represents a single gold particle. Numbers above dots represent the number of dots counted. (**c**) Schematic showing three different approaches taken to determine whether proteasomes were surface-exposed. (**d**) Antibody Feeding: Live primary mouse cortical neuronal cultures at DIV14 were incubated with antibodies against MAP2, N terminus of GluR1 (GluR1), or β5 proteasome subunits. Representative images shown. β5 proteasome antibody pre-incubated with the blocking peptide shown below. Quantification of percentage overlap between the signal from each antibody shown (N=2 independent neuronal cultures, n=15 neurons/culture). Significance is calculated between □5 staining alone and □5 antibody pre-incubated with blocking peptide. *$P$<0.01 (two-tailed Student's $t$-test). (**e**) Surface biotinylation: Proteins from surface biotinylated DIV14 cortical neurons were precipitated on streptavidin affinity beads and subjected to immunoblotting. Inputs (~3.5% of total) are shown to left of streptavidin pulldown (Strep) (~11% of total). Quantification is of streptavidin signal normalized to input signal (N=4 independent neuronal cultures). *$P$<0.01 (one-way ANOVA). (**f**) Protease Protection: PK was applied onto cultured cortical neurons at DIV14 for the indicated minutes. Cytosolic and membrane fractions were immunoblotted with anti-GluR1 (GluR1), anti-α1-7, anti-β2, and anti-Tubulin. Quantification is below. Significance for each timepoint against the zero minute timepoint is calculated (N=3 independent neuronal cultures). *$P$<0.01 (two-tailed Student's $t$-test). All data are presented as mean ± SEM. Uncropped blots are shown in Supplementary Data Set 1.

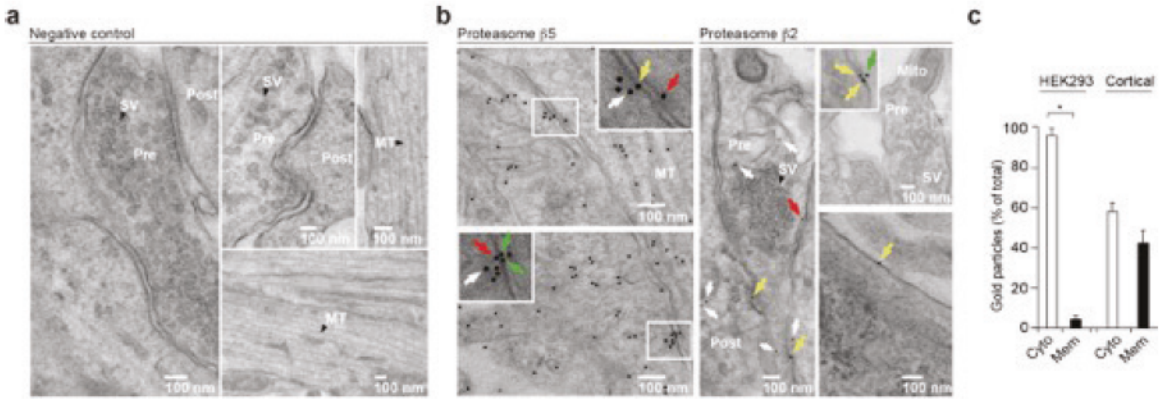


**Figure 3.6. 20S proteasome subunits are localized to neuronal plasma membranes.** (**a**) Immuno-EM analysis using only a secondary gold-conjugated anti-goat antibody in the absence of the primary antibody to detect non-specific background staining (63000X). Labeled ultrastructures: Presynaptic regions (Pre), Postsynaptic regions (Post), Microtubules (MT – black arrowheads), and synaptic vesicles (SV - black arrowheads). Single DIV14 culture, >20 slices generated. Same metrics were used for secondary controls as for slices incubated with primary.(**b**) Low magnification (63000X) image of Immuno-EM performed using antibodies against the β5 and β2 proteasomal subunits. Arrows correspond to immunogold label distinguished as cytosolic (white) or on membranes (cytosolic face - red, directly on - yellow, extracellular face- green). Labeled ultrastructures: Presynaptic regions (Pre), Postsynaptic regions (Post), Microtubules (MT – black arrowheads), Mitochondria (Mito) and synaptic vesicles (SV - black arrowheads). Multiple punches from single DIV14 culture, >20 slices generated. (**c**) Quantification of Immuno-EM analysis of HEK293 (HEK293) cells and cortical (Cortical) neurons for the β2 proteasome subunit. Percentage of gold particles in the cytosol (Cyto) and at plasma membranes (Mem) was quantified. *$P$<0.01 (two-tailed Student's $t$-test). Data are presented as mean ± SEM. >300 gold-particles counted, multiple punches from single DIV14 culture and single HEK 293 culture, >20 slices generated.

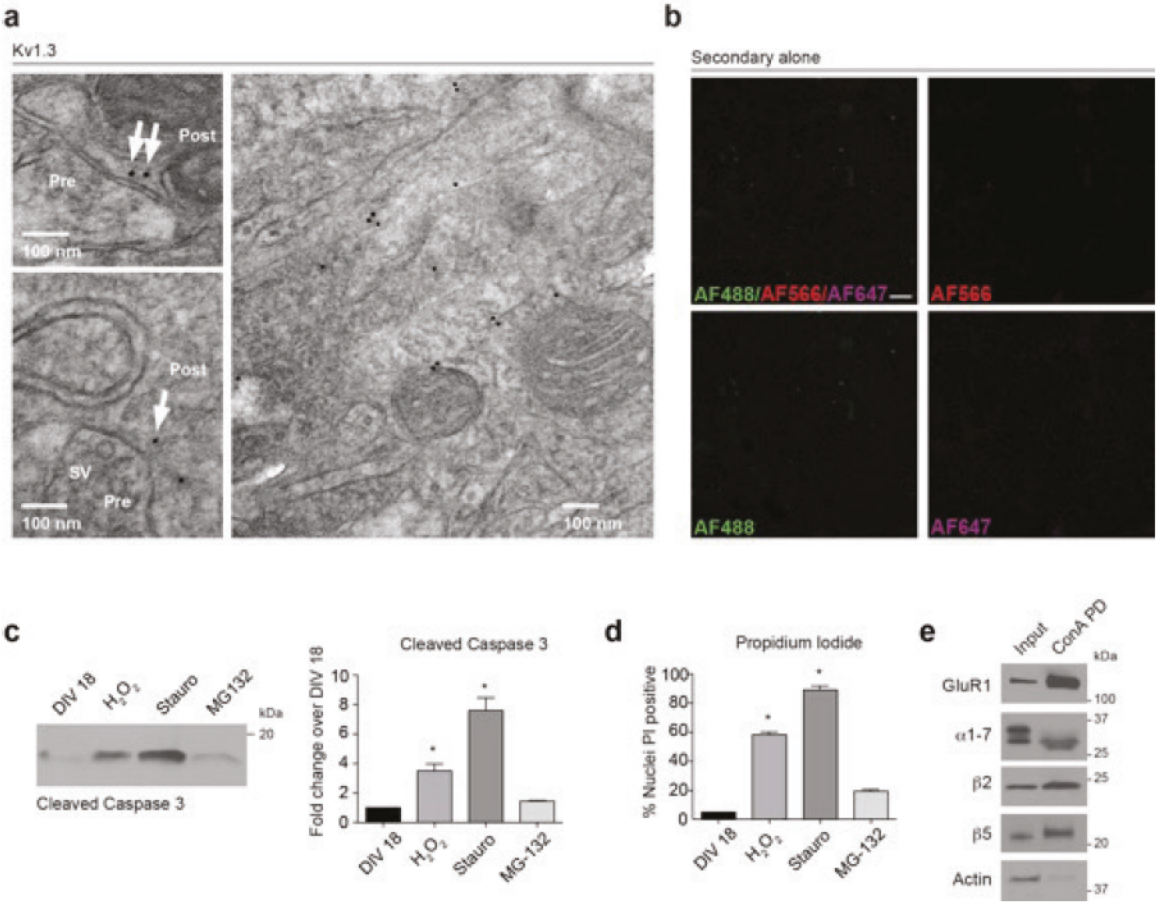


**Figure 3.7. Neuronal membrane proteasomes are exposed to the extracellular space.** (**a**) Immuno-electron micrographs performed using antibodies against the intracellular domain of Ion Channel Kv1.3 (63000X (left) and 43000X (right)). Arrows correspond to immunogold label distinguished as cytosolic (white). Note close proximity of gold particles to membranes. Similar results were observed and extensively quantified by Gazula et al, 2010. No membrane or extracellular staining was observed using this the antibody raised against Kv1.3. Slices were made from two separate 3 month old mice, >20 slices were generated for immuno-EM analysis. (**b**) The antibody feeding protocol (Figure 2D) was performed on primary neuronal cultures at DIV14 without primary antibodies, and stained using indicated secondary antibodies alone. Scale bar = 10 □M. Same metrics were used for secondary controls as for slices incubated with primary. N=2 neuronal cultures, >15 neurons/culture. (**c, d**) Primary neuronal cultures at DIV 18

were either untreated (DIV 18), or treated with hydrogen peroxide ($H_2O_2$ - 1 mM), Staurosporine (Stauro - 1 μM), or MG-132 (10 μM) . Neurons were collected in sample buffer and immunoblotted for caspase-3 cleavage to measure cell death. Quantification shown to the right (E). A separate batch of neurons were treated and incubated with propidium iodide (PI), an intercalating agent that can get into neurons undergoing cellular death. Following PI addition, neurons were immediately imaged to determine whether treatments affected cell death. The percentage of nuclei that were PI positive were counted, compared to the total number of cell bodies, and quantification is shown (E). Note, in both cases our neuronal cultures are not dying. *$P$<0.01 (two-tailed Student's $t$-test). Data are presented as mean ± SEM. (**e**) Neuronal cultures were lysed and plasma membranes were pulled down on Concanavalin A-coupled agarose beads (ConA PD). Samples were subjected to immunoblotting using antibodies against indicated proteins.

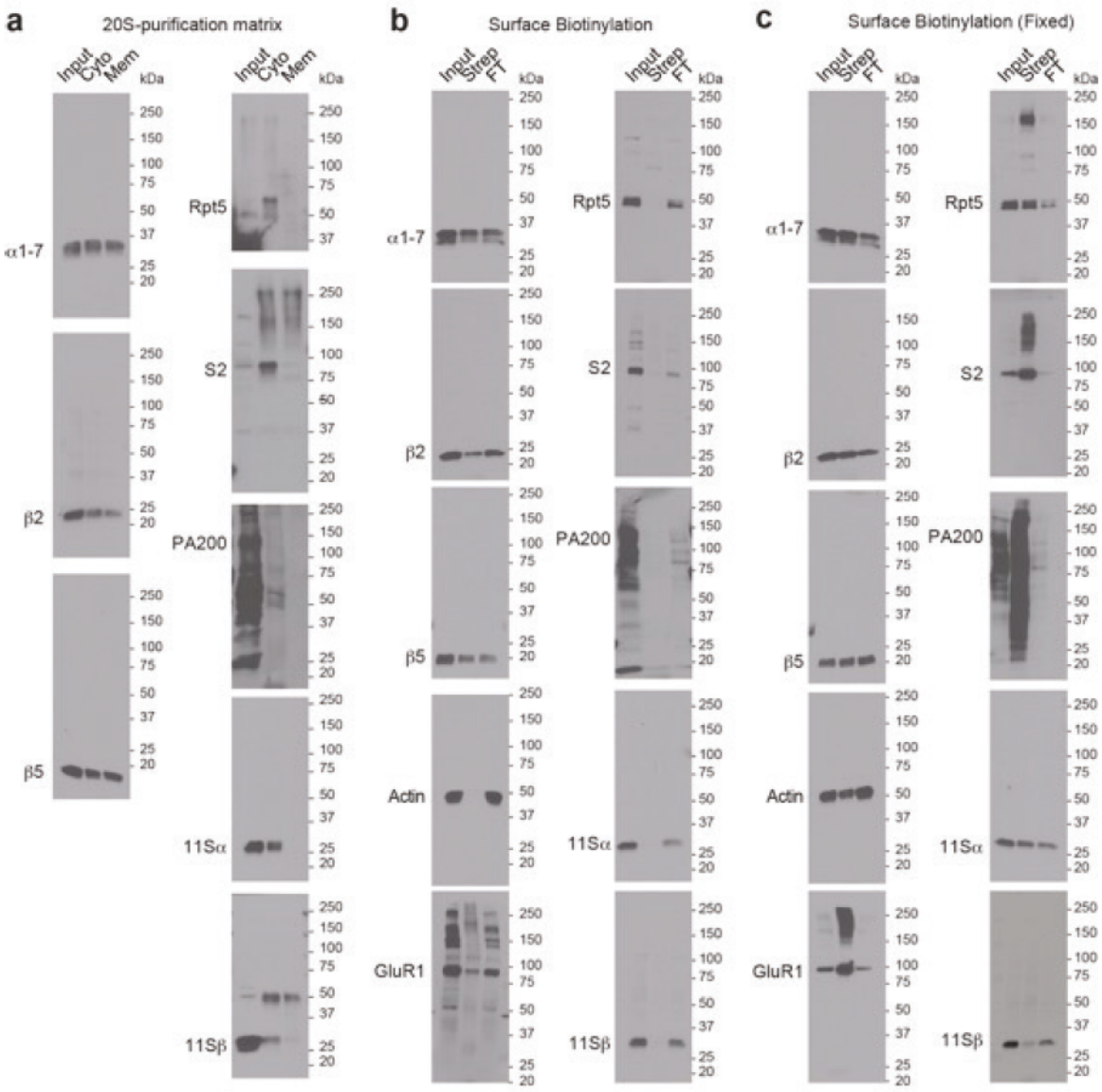


**Figure 3.8. Neuronal membrane proteasomes are largely made of 20S core proteasome subunits.** (**a**) Representative western blots of proteasomes purified out of DIV16 neuronal cultures using 20S purification matrices. Purification was done out of either neuronal cytosol (Cyto) or detergent-extracted neuronal plasma membranes (Mem). Inputs (5%) shown to the left. (**b,c**) Surface biotinylation: Biotinylated proteins from surface biotinylated DIV12 cortical neurons were precipitated on streptavidin affinity beads and subjected to immunoblotting using indicated antibodies. Inputs (10%) are shown to left of streptavidin pulldown (Strep).

Flowthrough (FT) that did not bind to streptavidin beads was loaded to the right of Streptavidin pulldown. Note that the combined FT and Strep lanes are roughly equivalent to the Input. This is consistent with the proteasomes being both in the membrane and cytosol. Additionally, surface biotinylation experiments were performed on neurons that had been treated with 1% Formaldehyde to covalently fix protein-protein interactions. Performing identical precipitation and preparation to (b), samples were immunoblotted with indicated antibodies (c). Note that actin is pulled down following fixation, unlike conditions without fixation, indicating that surface biotinylation of fixed samples may introduce artifacts of proteins that associate with membrane proteins but are not truly surface exposed. The precipitation of 19S cap proteins with our surface biotinylation under these conditions may indicate an artificial result or the existence of true interactions that are very weak (i.e. they do not occur in non-fixed conditions).

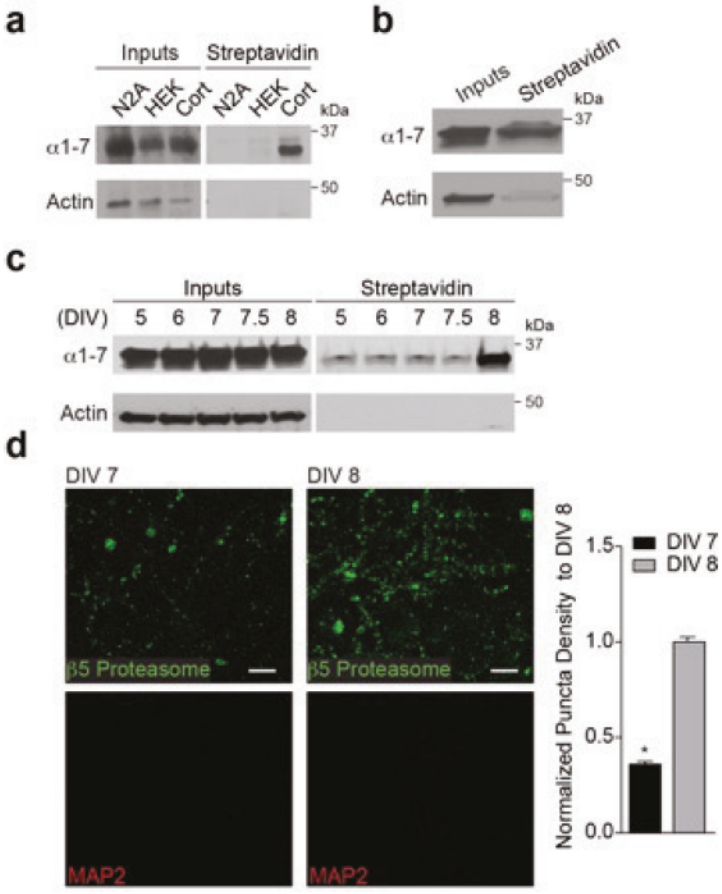


**Figure 3.9. Neuronal membrane proteasomes do not exist in heterologous cells and are developmentally regulated in neuronal cultures.** (**a**) Neuroblastoma-2A cells (N2A), HEK293 cells (HEK), and primary cortical neuronal cultures at DIV 14 (Cort) were surface biotinylated. HEK293 cells were used as a heterologous system with non-neural origins and N2A cells were used as a heterologous system with neural origins. Biotinylated proteins were precipitated using streptavidin affinity beads and immunoblotted using indicated antibodies. (**b**) Human brain tissue was obtained according to IRB protocol, and surface biotinylated. Proteins were purified on streptavidin-agarose beads and subsequently immunoblotted using indicated antibodies. (**c**) Primary neuronal cultures from DIV 5 to DIV 8 were surface biotinylated. Biotinylated proteins were precipitated using streptavidin affinity beads and immunoblotted using indicated antibodies. (**d**) Live primary mouse cortical neuronal cultures at DIV 7 or DIV 8 were incubated with

antibodies against MAP2 or β5 proteasome subunits. Representative images shown. Scale bar = 10 □M. Quantification of immunocytochemistry is shown to the right for the total amount of proteasome signal observed at DIV 7 and DIV 8 (N=2 independent cultures, n=11 neurons quantified per age). *P<0.01 (two-tailed Student's t-test). Data are presented as mean ± SEM.

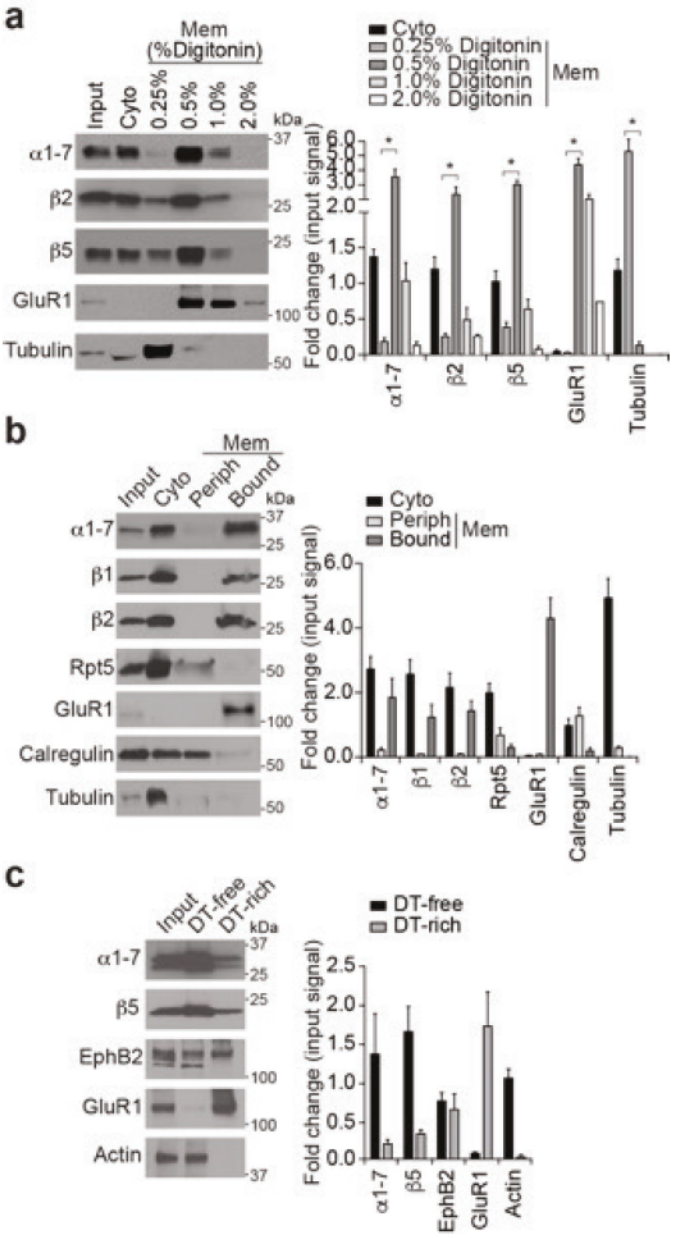


**Figure 3.10. Neuronal membrane proteasomes are tightly associated with plasma membranes**

(**a**) Primary mouse cortical neuronal cultures at DIV 14 were fractionated into cytosolic (Cyto) and membrane (Mem) components. Membranes were extracted with indicated sequentially increasing concentrations of Digitonin. Samples were analyzed by immunoblotting using antibodies against indicated proteins. Quantification to the right is normalized to input signal

levels for each antibody. While 0.25% digitonin extracted cytosolic protein Tubulin, higher concentrations (0.5%, 1.0%) of digitonin were required to extract known hydrophobic proteins such as GluR1. An explanation of percentages loaded on gel is explained in materials and methods. Significance is calculated by comparing signal from the 0.5% digitonin fraction to the 0.25% digitonin fraction for each antibody (N=3 independent neuronal cultures quantified). *$P$<0.01 (one-way ANOVA). Data are presented as mean ± SEM. (**b**) Proteasome subunits are tightly bound to membranes. Neuronal cultures at DIV14 were fractionated into cytosolic, peripherally-associated (Periph), and tightly-bound (Bound) proteins. Immunoblots of each fraction using indicated antibodies are shown. Quantification to right, data are presented as mean ± range (N=2 independent neuronal cultures). (**c**) Cultured neurons at DIV14 where phase separated with TX-114. Immunoblots shown using indicated antibodies. DT-free indicates aqueous phase, and DT-rich contains the TX-114 phase. Quantification to the right, data are presented as as mean ± range (N=2 independent neuronal cultures). Uncropped blots are shown in Supplementary Data Set 1.

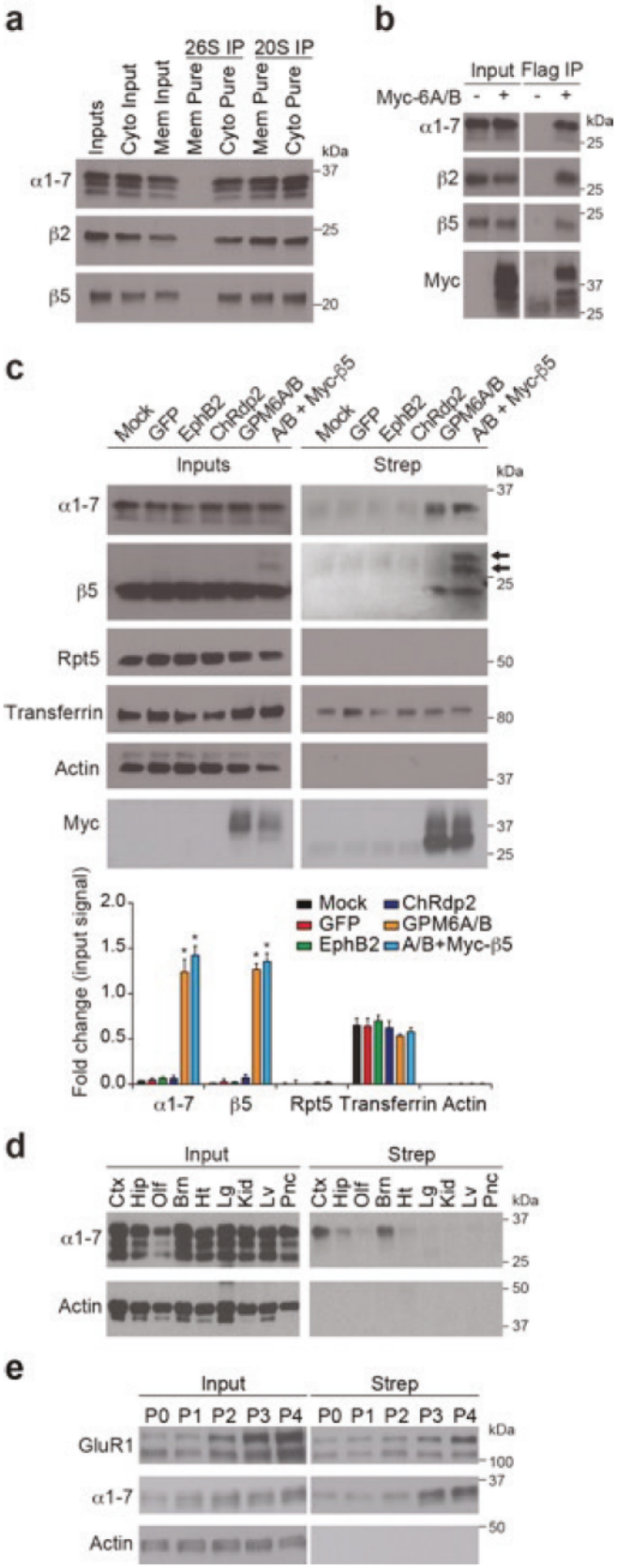
a
26S IP
20S IP
Inputs
Cyto Input
Mem Input
Mem Pure
Cyto Pure
Mem Pure
Cyto Pure
kDa
α1-7
β2
β5
37
25
20
b
Input
Flag IP
Myc-6A/B - + - +
α1-7
β2
β5
Myc
kDa
25
25
25
37
25
c
Mock
GFP
EphB2
ChRdp2
GPM6A/B
A/B + Myc-β5
Inputs
Strep
kDa
α1-7
β5
Rpt5
Transferrin
Actin
Myc
37
25
50
80
37
37
25
Fold change (input signal)
2.0
1.5
1.0
0.5
0.0
Mock
GFP
EphB2
ChRdp2
GPM6A/B
A/B+Myc-β5
α1-7
β5
Rpt5
Transferrin
Actin
d
Input
Strep
Ctx
Hip
Olf
Brn
Ht
Lg
Kid
Lv
Pnc
kDa
α1-7
Actin
37
25
50
37
e
Input
Strep
P0 P1 P2 P3 P4
P0 P1 P2 P3 P4
kDa
GluR1
α1-7
Actin
100
37
50

**Figure 3.11. Neuronal membrane proteasomes are largely a 20S proteasome and in complex with GPM6 family glycoproteins**

(**a**) Representative western blots of proteasomes purified out of neuronal cultures using capped-26S (26S IP) or 20S purification matrices (20S IP). Purification was done out of either neuronal cytosol (Cyto Pure) or detergent-extracted neuronal plasma membranes (Mem Pure). (**b**) Immunoprecipitation with anti-Flag from HEK293 cell lysates previously transfected with plasmids containing Myc/Flag tagged GPM6A and GPM6B, followed by immunoblotting with Myc or proteasome antibodies (α1-7, β2, β5). Inputs (10% of total, left) and immunoprecipitated samples (75% of total, right) are shown. (**c**) Exogenous expression of GPM6A/B is sufficient to induce surface expression of endogenous proteasomes in HEK293 cells. HEK293 cells were mock transfected (Blank) or transfected with plasmids containing GFP, EphB2, Channelrhodopsin-2 (ChRdp2), GPM6A/B, and GPM6A/B + Myc-tagged β5 (A/B +Myc-β5). Following transfection, cells were biotinylated and lysates prepared for streptavidin pulldown and western analysis. Western blots for indicated proteins are shown at left (4% of total) and right (streptavidin pulldowns, 32% of total). Quantification shown below is normalized to input signal. β5 western is overexposed in order to see Myc-tagged bands (two arrows, right of immunoblot). Significance is calculated between A/B transfected samples, and all others (N=3 independent cell cultures and transfections quantified). *$P$<0.01, one way ANOVA. Data are presented as mean ± SEM. (**d**) Surface-exposed proteasome expression is unique to nervous system tissues. Representative western blot of input (2% of total) lysates (left) and streptavidin pulldown (4% of total, right) of biotinylated proteins following surface biotinylation of dissected tissues from a P3 mouse. Cortex (Ctx), Hippocampus (Hip), Olfactory bulb (Olf), Hind Brain (Brn), Heart (Ht), Lung (Lg), Kidney (Kid), Liver (Lv), Pancreas (Pnc). Immunoblots were performed using antibodies against indicated proteins. (**e**) Representative western blots of input (2.5% of total) lysates (left) and streptavidin pulldown (7.5% of total,

right) of biotinylated proteins following surface biotinylation of mouse cortex tissue dissected from indicated postnatal ages. Uncropped blots are shown in Supplementary Data Set 1.

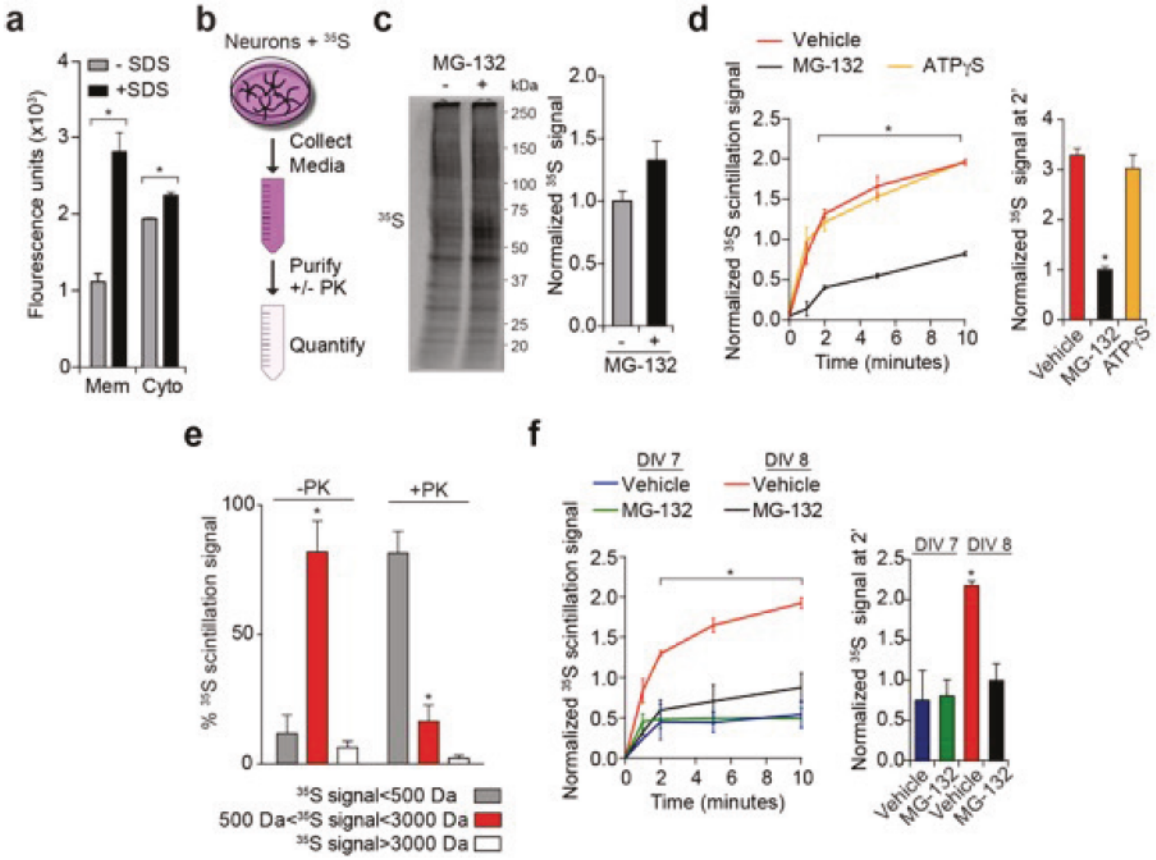


**Figure 3.12. Neuronal membrane proteasomes degrade intracellular proteins into extracellular peptides**

(**a**) Purified 20S proteasomes from neuronal cytosol (Cyto) or membrane (Mem) were incubated with the fluorogenic proteasome peptide substrate SUC-LLVY-AMC. Fluorescence is released upon cleavage, endpoint fluorescence with and without incubation with SDS is quantified. Significance is shown between SDS-treated and untreated samples (N=3 replicate proteasome purifications from independent neuronal cultures quantified). (**b**) Schematic for collection and purification of extracellular peptides. Media from radiolabeled mouse cortical neuronal cultures is collected and purified. Media collected from neurons following radiolabeling was subjected to size exclusion purification, with or without Proteinase K (PK). (**c**) Representative autoradiograph of lysates from cortical neurons previously radiolabeled with $^{35}$S methionine/cysteine for 10 minutes in the presence or absence of MG-132. Quantification of signal normalized to vehicle-

treated neurons is shown at right. (**d**) Rapid efflux of radioactive material out of neuronal cultures into media depends upon proteasome function. Media collected from neurons following radiolabeling with or without MG-132 or ATPγS. Liquid scintillation quantification of media at indicated timepoints is shown normalized to control at the 10-minute timepoint; 2 minute timepoint shown separately on bar graph (right) (Media from N=3 independent cell cultures). Significance in line graph is shown for MG-132 treated neurons compared to vehicle alone at each time point. (**e**) Media collected from neurons following radiolabeling was subjected to size exclusion purification, with or without Proteinase K (PK). The percentage of total radioactivity eluting at different sizes is shown (N=3 independent cell cultures and purifications quantified). (**e**) Release of proteasome-derived peptides in the extracellular space correlates with NMP expression. Experiment performed as described in (**d**); media collected from either DIV 7 or DIV 8 neurons, with MG-132 (MG-132) or without (Vehicle). (Media of N=3 independent cell cultures) *$P$<0.01 ((**a**, **e**) two-tailed Student's $t$-test, (**e**) significance of 500<$^{35}$S Signal<3000Da compared to <500Da and >3000Da; (**d**, **f**) One-way ANOVA). Data are mean ± SEM.

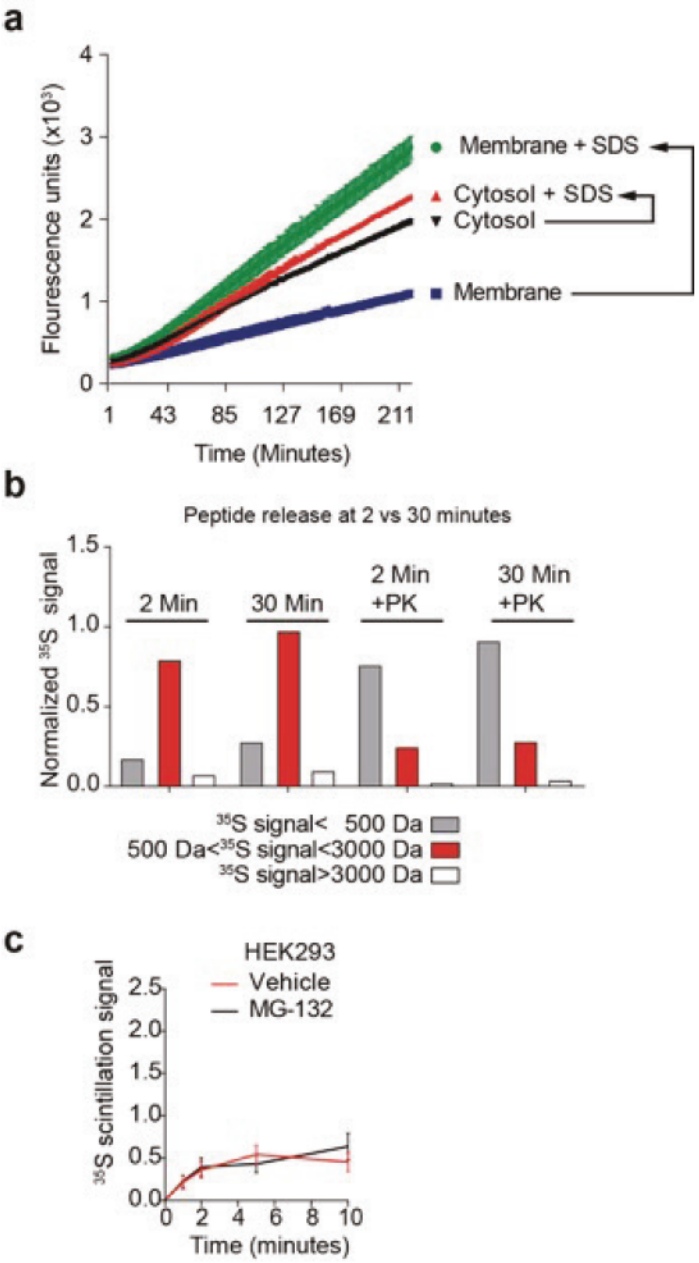


**Figure 3.13. Neuronal membrane proteasomes are catalytically active and degrade intracellular proteins into extracellular peptides.** (**a**) Quantification of the 60-minute timecourse of the endpoint proteasome activity assay shown in Figure 4e. Note difference in activity from membrane proteasomes when SDS is added compared to cytosolic proteasomes. *P<0.01 (two-tailed Student's t-test). Data are presented as mean ± SEM (Data from N=3 independent proteasome purifications quantified). (**b**) Following 10 minutes of radiolabel

incorporation, media was washed out and replaced with Neurobasal growth media. Media was collected at either the two-minute or 30 minute timepoint following washout. Collected medium was then run through a size-exclusion protocol. An aliquot from each fraction was taken and quantified by liquid scintillation. Samples are normalized to the total amount of radioactivity present in the input sample taken at the two-minute timepoint, following subtraction of the zero-minute timepoint. We observed an increase in the fraction of radioactivity eluting below 500 Da and between 500 and 3000 Da at the 30 minute timepoint compared to the 2 minute timepoint, consistent with a sustained turnover of the intracellular pool of short-lived proteins into amino acids and short peptides. (**c**) Media from radiolabeled HEK293 cells is collected and purified, as described in Figure 4d, following vehicle treatment or MG-132 treatment. Data are presented as mean ± SEM (Media from N=3 independent replicate cell cultures quantified).

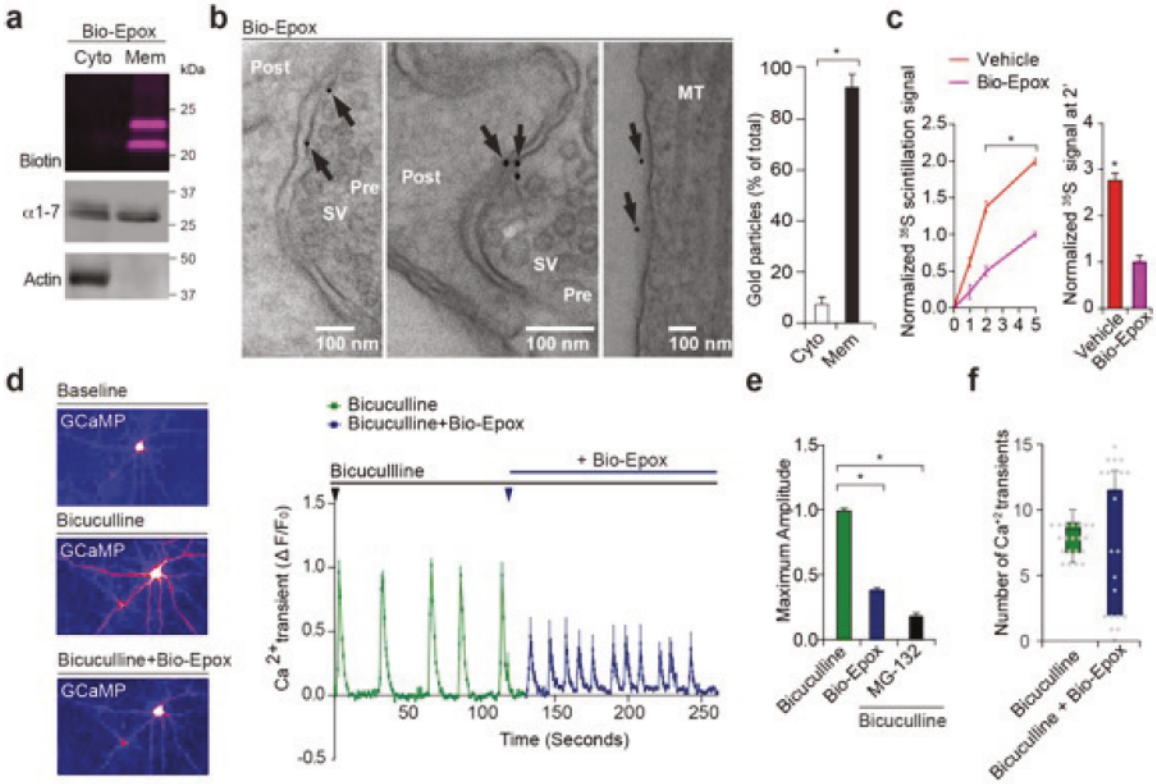


**Figure 3.14. Neuronal membrane proteasomes are required for release of extracellular peptides and modulate neuronal activity**

(**a,b**) Biotin-epoxomicin does not cross neuronal membranes and covalently binds proteasome subunits. (**a**) Neurons treated with biotin-epoxomicin (Bio-Epox) were separated into cytosolic (Cyto) and membrane (Mem) fractions and analyzed by western using streptavidin conjugated to a fluorophore. Immunoblots using indicated antibodies shown below. (**b**) Immunogold labeling against biotin using streptavidin-Au (black arrows) from neuronal cultures treated with Bio-Epox, with representative images shown (N=54, obtained from multiple punches of a single neuronal culture, >20 slices generated. Labeled ultrastructures: Presynaptic regions (Pre), Postsynaptic regions (Post), Microtubules (MT), and synaptic vesicles (SV). Quantification of particles in cytosol and on membrane (right); *$P$<0.01 (two-tailed Student's $t$-test). (**c**) Media collected from radiolabelled neurons treated with Bio-Epox (Bio-Epox) or without (Vehicle). Liquid scintillation quantification of media at indicated timepoints is shown normalized to control at the 5 minute

timepoint; 2 minute timepoint shown separately on bar graph. Significance in line graph is shown for Bio-Epox treated neurons compared to vehicle alone at each time point. (N=3 independent neuronal cultures quantified, *$P$<0.01, two-tailed Student's $t$-test). (**d**) NMP inhibition modulates speed and intensity of neuronal calcium transients. Bicuculline added (downward black arrowhead) to naïve GCaMP3-encoding neurons. Downward dark blue arrowhead indicates timing of Bio-Epox addition. Representative images (left) and traces of Bicuculline response before and after Bio-Epox addition are plotted (right). Quantification of normalized fluorescence intensity ($\Delta F/F_0$) measurements of calcium signals over imaging timecourse are shown. (**e**) Average maximum amplitudes are plotted, and include analysis of calcium signaling after treatment with MG-132. Significance compared to Bicuculline stimulation alone. (**f**) Box-and-whisker plot of all frequencies observed. *$P$<0.01, one-way ANOVA (E), two-tailed Student's $t$-test (**f**), All data are presented as mean ± SEM (D-F, N=2 independent replicate cultures, n=24 neurons per culture, with 18 ROIs (regions of interest) analyzed per neuron). Uncropped blots are shown in Supplementary Data Set 1.

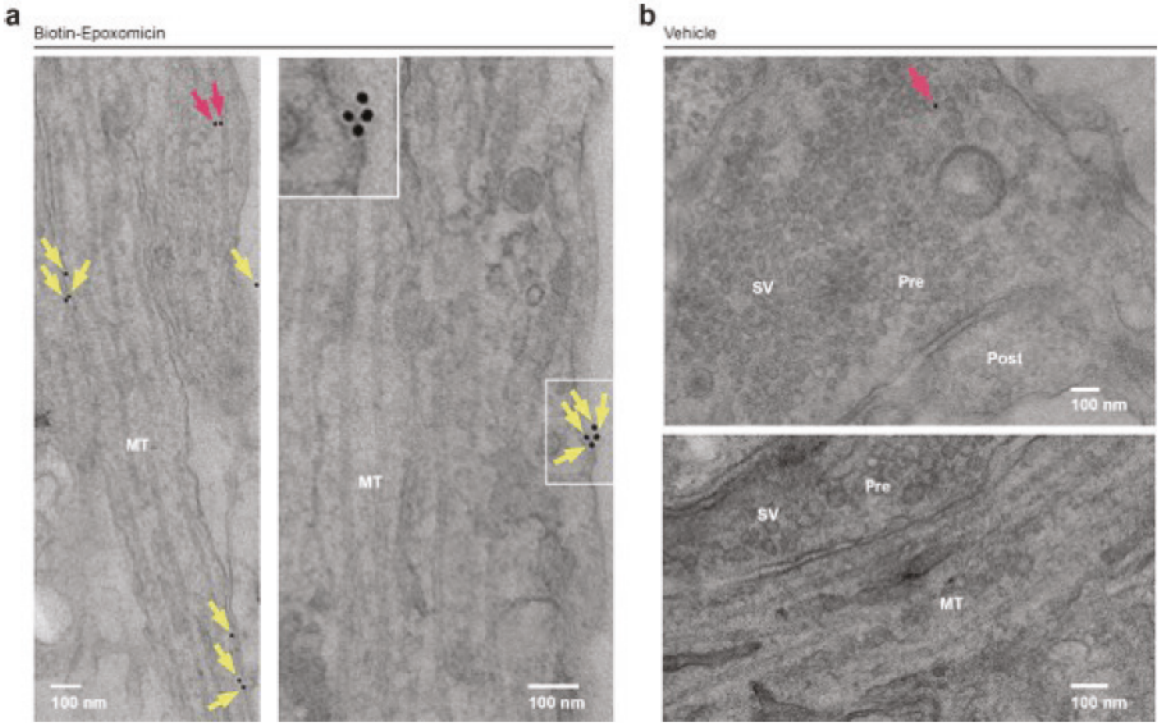


**Figure 3.15. Neuronal membrane proteasomes are required for release of extracellular peptides and modulate neuronal activity.** (**a**) Low magnification image of immuno-electron micrographs performed using streptavidin conjugated to gold particles in cortical neurons treated with Biotin-Epoxomicin. Immunogold label shown by arrows in cytosol (red) and on membrane (yellow). Labeled ultrastructures: Presynaptic regions (Pre), Postsynaptic regions (Post), Microtubules (MT). Obtained from multiple punches of a single neuronal culture, >20 slices generated. (**b**) Immuno-EM analysis using streptavidin conjugated to gold particles in the absence (Vehicle) of the Biotin-Epoxomicin to detect non-specific background staining. Cytosol labeling (red). Same metrics were used for secondary controls as for slices incubated with Biotin-Epoxomicin.

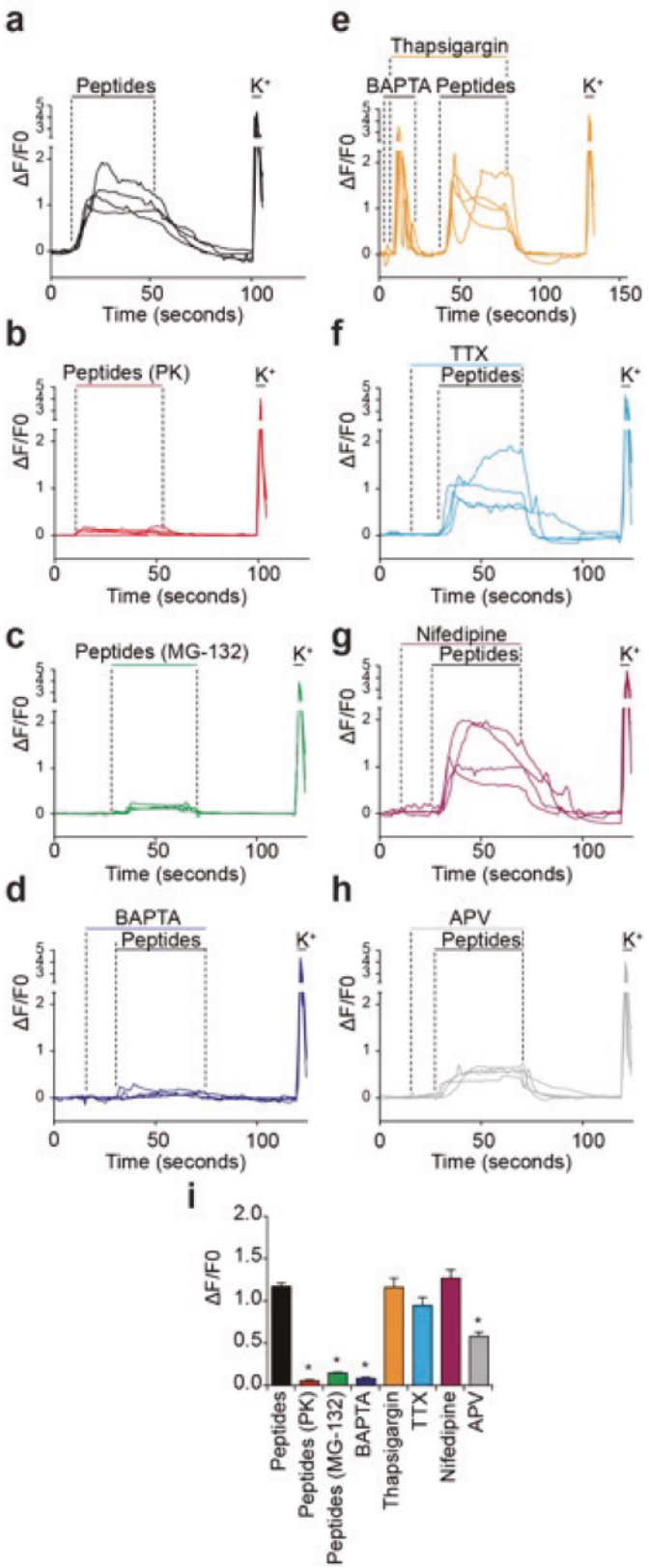
a
Peptides
K+
ΔF/F0
Time (seconds)
b
Peptides (PK)
c
Peptides (MG-132)
d
BAPTA
Peptides
e
Thapsigargin
BAPTA Peptides
f
TTX
Peptides
g
Nifedipine
Peptides
h
APV
Peptides
i
Peptides
Peptides (PK)
Peptides (MG-132)
BAPTA
Thapsigargin
TTX
Nifedipine
APV

**Figure 3.16. Neuronal membrane proteasome-derived peptides are sufficient to induce neuronal signaling**

(**a**) Purified peptides were perfused onto GCaMP3-encoding mouse cortical cultured neurons. Dotted lines indicate time of peptide addition and washout. $K^+$ indicates the timing of 55 mM KCl addition to neurons to determine that they still respond properly at the end of the experiment. Line graph shows increase in fluorescence over baseline during time of peptide addition, a decrease following washout and robust increase with KCl addition. Four sample traces from different neurons are plotted. (**b, c**) Similar to part (**a**), cultured neurons were incubated with either Peptides (PK) (peptides were pretreated with P K, PK was removed, and then samples dialyzed to remove small molecules) or with Peptides (MG-132) (peptides purified from cells treated with MG-132). (**d-h**) Indicated drugs were perfused onto neuronal cultures during the times depicted by the dashed lines. Peptides were subsequently added as indicated and described in (**a**). Concentrations of drugs: BAPTA (2 □M), Thapsigargin (5 □M), Tetrodotoxin (1 □M), Nifedipine (1 □M), APV (2 □M). (**i**) Quantification of maximum intensity of change from each condition is plotted. *$P$<0.01 one-way ANOVA. Data are presented as mean ± SEM (N=3 independent replicate cultures, n>15 neurons per treatment, with at least 10 ROIs analyzed per neuron, per condition).

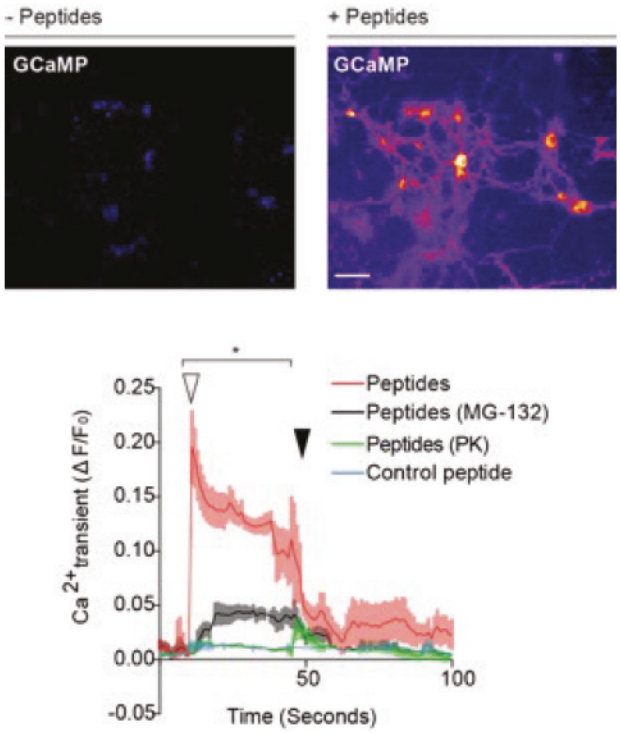


**Figure 3.17. Neuronal membrane proteasome-derived peptides are sufficient to induce neuronal signaling.** Purified extracellular peptides were added to naïve GCaMP3-encoding neurons. Representative images (top), quantification of normalized fluorescence intensity measurements of calcium signals over imaging timecourse (bottom). Scale bar = 40 □M. Arrowheads depict peptide addition (white arrowhead) and peptide washout (black arrowhead). Peptides (PK): Peptides pretreated with Proteinase K; Peptides (MG-132): purified media from neurons radiolabeled in the presence of MG-132; Control peptide: random peptides. *P<0.01 (one-way ANOVA). Data represent mean ± SEM (N=3 independent biological replicate cultures, n=8 neurons/culture, total fluorescence in field of view quantified).

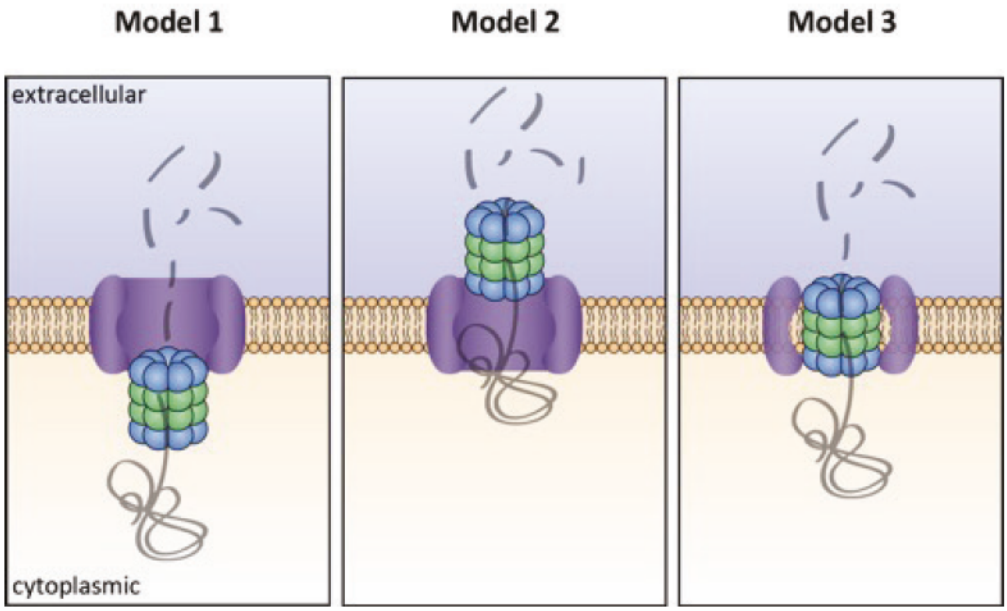


**Figure 3.18. Proposed theoretical models of NMP association with the plasma membrane**

Three models of how proteasomes can associate with plasma membranes are shown above. Extracellular and cytoplasmic sides of the plasma membrane are indicated. Symbol key shown to left.

# Chapter 4

## Activity-dependent degradation of the immediate-early nascentome by the neuronal membrane proteasome

Modified from:

**Kapil V. Ramachandran**, Jack M. Fu, Thomas B. Schaffer, Chan-Hyun Na, and Seth S. Margolis. "Activity-dependent degradation of the nascentome by the neuronal membrane proteasome" *(Manuscript in review)*

Neuronal activity-dependent processes have been shown by many laboratories to be dependent upon new protein synthesis and proteasome-dependent protein degradation (Schratt et al. 2004; Djakovic et al. 2009; Fonseca, Nagerl, and Bonhoeffer 2006; Fonseca et al. 2006; Kelleher, Govindarajan, and Tonegawa 2004). Inhibition of either of these pathways impairs neuronal signaling in a host of systems and paradigms. Consistent with a role for neural activity in regulating protein synthesis and degradation, the ribosome and proteasome independently localize to sites of synaptic activity and are important for activity-mediated synaptic remodeling (Ehlers 2003; Ostroff et al. 2017; Ostroff et al. 2002; Bingol and Schuman 2006; Tai et al. 2010; Tcherkezian et al. 2010). Additionally, these two complexes are hypothesized to coordinate their functions to modulate neuronal signaling (Fonseca et al. 2006; Klein, Castillo, and Jordan 2015; Deglincerti et al. 2015; Schwanhausser et al. 2013). However, the biochemical evidence for the existence and mechanism of this coordination remains to be elucidated.

We considered that such a mechanism might simultaneously engage the actions of both the ribosome and proteasome in neurons, emulating a protein quality control mechanism to maintain neuronal protein homeostasis. This would manifest as co-translational degradation, which is the direct proteasome-mediated degradation of a nascent polypeptide while still associated with the ribosome(Inada 2017; Duttler, Pechmann, and Frydman 2013; Kramer et al. 2009; Wheatley, Grisolia, and Hernandez-Yago 1982). Co-translational degradation remains an elusive phenomenon. In the 1970s and 80s, classic experiments in monitoring protein fate reported a significant portion of proteins underwent rapid degradation either during or immediately following their synthesis (Robertson and Wheatley 1979; Wheatley, Giddings, and Inglis 1980; Wheatley, Grisolia, and Hernandez-Yago 1982; Wheatley and Inglis 1980). Over the next 30 years, further investigation of these observations in yeast and *in vitro* revealed that some proteins undergoing synthesis are degraded co-translationally (Benoist and Grand-Perret 1997; Turner and Varshavsky 2000; Anton and Yewdell 2014; Schubert et al. 2000; Vabulas and Hartl

2005). However, how these events are regulated remains unknown, the extent to which these events occur is debated, and have never been monitored in neurons. In contrast, significant evidence has emerged for co-translational ubiquitylation, a process where a nascent chain is ubiquitylated while still ribosome-associated, but then is removed from the ribosome and subsequently degraded by proteasomes. A plethora of evidence for such quality control mechanisms in yeast and heterologous cells has emerged over the past 40 years (Anton and Yewdell 2014; Brandman et al. 2012; Comyn, Chan, and Mayor 2014; Dimitrova et al. 2009; Duttler, Pechmann, and Frydman 2013; Fletcher et al. 2014; Ha et al. 2016; Ha, Ju, and Xie 2014; Inada 2017; Kirstein-Miles et al. 2013; Turner and Varshavsky 2000; von der Malsburg, Shao, and Hegde 2015; Yonashiro et al. 2016; Shao, von der Malsburg, and Hegde 2013). Most notably, there is a significant body of literature on co-translational ubiquitylation mechanisms through Listerin1 (Ltn1, an E3 ubiquitin-ligase) and the ribosome quality-control complex (Brandman et al. 2012; Yonashiro et al. 2016; Shao, von der Malsburg, and Hegde 2013; von der Malsburg, Shao, and Hegde 2015; Duttler, Pechmann, and Frydman 2013; Wang, Durfee, and Huibregtse 2013). These ubiquitylated nascent chains are subsequently removed and sent to the proteasome for degradation. However, despite Ltn1's involvement in neurodegeneration, the vast majority of these biochemical experiments have been done in yeast or non-neuronal cells (Bengtson and Joazeiro 2010; Chu et al. 2009; Yonashiro et al. 2016; Brandman et al. 2012; von der Malsburg, Shao, and Hegde 2015). The contribution of co-translational protein homeostasis mechanisms in neurons, which must maintain a delicately balanced proteome, remains largely unexplored.

Many of these mechanisms, especially co-translational ubiquitylation, rely on the concerted actions of the ubiquitin-proteasome system (Ben-Nissan and Sharon 2014; Ciechanover 1998; Collins and Goldberg 2017; Coux, Tanaka, and Goldberg 1996). In this paradigm, ubiquitylated proteins are delivered to and degraded by the 26S proteasome, a large multisubunit protease with two major functional holoenzymes. The first is the 20S core complex, a chamber with $\square_7\square_7\square_7\square_7$

stacked subunit configuration that contains the catalytic domains required to cleave protein substrates (Ciechanover 1998). The other is the 19S cap complex, containing multiple subunits which recognize ubiquitylated substrates and ATPases which unfold proteins (de Poot, Tian, and Finley 2017; Finley, Ciechanover, and Varshavsky 2004; Schmidt and Finley 2014). These 19S ATPases are generally required since the 20S core proteasome can only degrade already unfolded proteins, or those with large unstructured domains such as intrinsically disordered proteins (Tsvetkov et al. 2008; Tsvetkov, Reuven, and Shaul 2009; Ben-Nissan and Sharon 2014; Coux, Tanaka, and Goldberg 1996). While the majority of studies on proteasome-dependent degradation have been attributed to the actions of the 26S, roles for the 20S proteasome are emerging.

Recently, we discovered an uncapped 20S proteasome complex tightly associated with the neuronal plasma membrane, where it degrades intracellular proteins into extracellular peptides (Ramachandran and Margolis 2017). The mechanisms for substrate delivery to this neuronal membrane proteasome (NMP) remained unknown, but we presumed they must be unfolded to some extent since the NMP is a 20S proteasome (Ramachandran and Margolis 2017). Protein synthesis produces a significant source of unfolded proteins, initially as nascent polypeptides and then as folding intermediates (Duttler, Pechmann, and Frydman 2013; Balchin, Hayer-Hartl, and Hartl 2016; Pechmann, Willmund, and Frydman 2013; Sontag, Samant, and Frydman 2017). We hypothesized that coordination between translation and degradation in the nervous system was manifested through the NMP, possibly mediated by neuronal activity. We began by asking whether neuronal activity modulates NMP function, initially testing whether it was required for NMP-dependent production of extracellular peptides (Ramachandran and Margolis 2017). We added tetrodotoxin (TTX) to our neuronal culture, which binds voltage-gated sodium channels and blocks firing of spontaneous action potentials within our cultures. We found that TTX strongly abrogated extracellular peptide release, previously defined as being NMP-dependent (Figure 4.1)(Ramachandran and Margolis 2017). These data generated the impetus to further

study activity-dependent mechanisms of NMP function in detail.

In this manuscript, we made the observation that that elevated neuronal activity leads to an increase in NMP-dependent peptide production, coincident with a ~40% decrease in newly synthesized proteins. We then used Monte Carlo simulations of Markov models to monitor the fates of proteins inside the cell and trace their fate as they were being degraded into the extracellular space. This predicted that nascent polypeptides, and not full-length proteins or folding intermediates, provided the substrates for NMP to generate extracellular peptides. We experimentally validated these *in silico* findings and found that tRNA-bound nascent polypeptides were direct co-translational targets of the NMP. In an effort to identify specific NMP substrates, we found that neuronal activity controlled the NMP-mediated degradation of a large class of substrates including the immediate-early gene products. These data define an activity-dependent mechanism of neuronal co-translational degradation and identify the very first set of substrates targeted by this process through the NMP.

Neuronal stimulation induces NMP-dependent degradation of newly synthesized proteins into extracellular peptides

To extend our observed findings in Figure 4.1 and determine whether neuronal activity induces NMP function, we monitored NMP-dependent production of extracellular peptides under states of neuronal stimulation. We first used KCl-induced membrane depolarization as a classic and effective tool to induce elevated activity of the majority of neurons in culture (Lin et al. 2008; West et al. 2001; Xia et al. 1996). Primary mouse cortical neuronal cultures at days *in vitro* (DIV) 10-14 were treated with either a stimulation buffer (KCl) or a control buffer (NaCl). These neurons were concomitantly radiolabelled with $^{35}$S-methionine/cysteine for 10 minutes, without any prior metabolic deprivation (Vabulas and Hartl 2005; Ramachandran and Margolis 2017). Following concomitant radiolabeling and neuronal stimulation, we washed away both free isotope and stimulation buffer. This media was replaced with fresh conditioned media containing either a pan-proteasome inhibitor (MG-132), an NMP-specific inhibitor (biotin-epoxomicin), or control (DMSO) (Meng et al. 1999b; Li et al. 2013; Meng et al. 1999a; Sin et al. 1999; Ramachandran and Margolis 2017). Immediately following washout, samples were taken from the extracellular medium over time and analyzed by liquid scintillation. We have previously shown that this method preferentially monitors the release of extracellular NMP-derived peptides over small molecules or free isotope (Ramachandran and Margolis 2017). We observed a significant MG-132 and biotin-epoxomicin-sensitive increase in radiolabelled extracellular peptides released from neurons that had been stimulated, compared to controls (Figure 4.2). These data were consistent with the released material being comprised of protein peptides derived from the NMP (Ramachandran and Margolis 2017).

Our working hypothesis was that the observed stimulation-induced NMP-dependent increase in extracellular peptide production would be reflected in enhanced NMP-mediated degradation of a pool of intracellular protein substrates. To test this, we measured the intracellular

pool of proteins made during elevated neuronal activity using SDS-PAGE and autoradiography. Neurons were treated with the radiolabeling protocols described above. All samples were coomassie stained after SDS-PAGE to ensure equal sample loading (Figure 4.3A). By densitometry analysis of these autoradiographs, we noticed a decrease in radioactive intracellular protein signal from neurons that had been radiolabelled during stimulation (Figure 4.2B). This effect was induced by a variety of well-characterized stimulation protocols that give rise to activity-dependent neuronal signaling, but not by serum containing growth factors (Figure 4.3B-D)(Lin et al. 2008; Scheetz, Nairn, and Constantine-Paton 2000; Marin et al. 1997; Fortin et al. 2010). Treating these neurons with MG-132 or biotin-epoxomicin during radiolabelling blocked the stimulation-induced loss of radiolabelled protein signal (Figure 4.2B). We interpret this to mean that neuronal activity enhances NMP-mediated degradation of intracellular proteins made during stimulation. This enhanced degradation of intracellular substrates was not due to increased intrinsic catalytic activity of the NMP (Figure 4.3E).

Our experiments thus far monitored the NMP-mediated and activity-dependent turnover of proteins made *during* stimulation. Given that certain protein populations have been shown to be more susceptible to degradation than others (Wheatley, Giddings, and Inglis 1980; McShane et al. 2016; Ha et al. 2016), we asked whether the degradation kinetics for proteins synthesized *during* stimulation were different than those for proteins made *prior to* or *following* stimulation. Surprisingly, by changing our radiolabeling protocols, we did not observe the same magnitude of stimulation-induced degradation of proteins from neurons that had been radiolabelled *prior to* the onset of stimulation, even after sustained stimulation (Figure 4.2C). Consistent with this, we also did not detect a stimulation-induced increase in extracellular radioactive peptide efflux when neurons were radiolabeled *prior to*, instead of *during* stimulation (Figure 4.2D). Additionally, we observed no change in intracellular radiolabelled protein signal from neurons that had been radiolabelled immediately *following* stimulation (Figure 4.3F). These data illustrate that neuronal

stimulation does not simply promote the turnover of all proteins, but specifically enhances the NMP-mediated turnover of newly synthesized proteins made *during* neuronal stimulation. These observations raised a fundamental question – why were proteins made during stimulation, as compared to all other proteins, being turned over by the NMP? We hypothesized that the answer to this was linked to the properties of the substrates it was targeting.

Monte Carlo simulation of Markov chains favors degradation of nascent polypeptides as the source for NMP-derived extracellular peptides

Our understanding of NMP function was that it directly degrades intracellular proteins into peptides in the extracellular space (Ramachandran and Margolis 2017). This predicts that degradation kinetics of intracellular NMP substrates are directly coupled to the release kinetics of the extracellular peptides (Ramachandran and Margolis 2017). The data thus far relied on $^{35}$S-methionine/cysteine addition to neuronal cultures and tracing the fates of the proteins in which radioactive isotopes were incorporated. Following charging onto a tRNA, isotopes go through two major steps on their way to being incorporated into a folded protein: First, they must be incorporated into the growing nascent polypeptide which is associated with the ribosome during protein synthesis. Subsequently, this polypeptide must go through the complex task of folding before achieving its proper folded conformation, some of which is achieved while still ribosome-associated (Gloge et al. 2014; Kramer et al. 2009; Hartl, Bracher, and Hayer-Hartl 2011; Pechmann, Willmund, and Frydman 2013). Very generally, polypeptides progressing from one stage to the next adopt increasing conformational stability with a corresponding increase in their half-lives (Alberts B 2002). We sought to understand whether our data revealed any selectivity by which population of polypeptides (i.e. nascent polypeptide, folding intermediate, or folded protein) were being targeted for degradation by the NMP.

To achieve this goal, we constructed a simplified Markov chain model to track the fate of

radioisotopes over a time course that mirrors our experimental peptide release data. Each Markov chain follows the trajectory of a single radioisotope that begins as a free radioisotope inside the cell, following 10 minutes of simulated isotope incorporation (Figure 4.4A). The radioisotope can progress from the initial free state to become incorporated into a nascent polypeptide, and then into a folding intermediate, and finally into a folded protein. In each of these four possible states of incorporation, the radioisotope has some probability of extracellular release (Figure 4.4A). The transition probabilities from one state into the next and the release mechanisms at each state are modeled after well-established kinetic parameters (e.g. rates of protein translation, degradation, and protein folding) and take into account the distribution of protein sizes in neurons (Figure 4.4C and 4.5A)(Lane and Pande 2013; Pande 2014; Balchin, Hayer-Hartl, and Hartl 2016; Hartl, Bracher, and Hayer-Hartl 2011; Wu et al. 2016). By representing a single experiment as a collection of Markov chains, we could model the proportion of radioisotopes that are either inside or outside of the cell at any point in time. These simulated values for extracellular radioisotope release were evaluated against our experimentally observed release curve. We took the diffusion of free isotope into account by optimizing our model against radioisotope release when all proteasomes are inhibited by MG-132 (Figure 4.5B). The precise methods used to generate the model parameters are described in detail in materials and methods.

While our model was simple, we attempted to account for as many factors as reasonable using biologically determined parameters. When the model was biased towards turnover of nascent polypeptides, we observed that the shape of the *in silico* release curve closely mirrors the shape of the experimental release curves (Figure 4.4B). The direct degradation of nascent polypeptides by a proteasome is the operational definition of co-translational degradation(Inada 2017; Duttler, Pechmann, and Frydman 2013; Kramer et al. 2009; Wheatley, Grisolia, and Hernandez-Yago 1982), which is how we will refer to this process. In contrast, by shifting the bias towards turnover of folding intermediates, the simulated release curves followed a sigmoidal

shape. Although this curve can match the experimental release curve at 5 minutes and beyond, these data considerably underestimate values for any time span less than 5 minutes (Figure 4.4C). More dramatically, biasing the model towards turnover of folded proteins generated a continually gradual and linear release curve. This indicated a rate far too slow to account for the rapid release and subsequent taper of experimentally released radioisotopes (Figure 4.4D).

The shapes of the release curves for co-translational degradation and folding intermediate degradation more closely approximated our experimental data than those for folded protein degradation. To further refine our analysis, we used Monte Carlo simulations to optimize which combinations of the probabilities for co-translational and for folding intermediate degradation best give rise to the observed release data (Figure 4.6A). We sampled a large parameter space of possible pairwise probabilities, and for each combination of co-translational and folding-intermediate degradation probability, we simulated a large number of Markov chains and calculated each predicted release curve. By minimizing the error of the predicted curves against the experimental data, we could identify a set of probabilities that most closely mirrored our experimental data. We began performing calculations using the release data from control-treated neurons. In this condition, the error between the simulated and observed data was minimized at values corresponding to 0% folding intermediate degradation probability, and a probability of 4.7% that a nascent polypeptide would be targeted to co-translational degradation in a one second time window (Figure 4.6A, 4.5A). These values favoring degradation of nascent polypeptides give rise to a simulated release curve that exhibits the rapid logarithmic rise and gradual taper of released radioisotopes with minimal discrepancy to the experimental release curve (Figure 4.6B). By increasing the co-translational degradation probability from 4.7% to 16.5%, we minimized error against the experimental KCl stimulation data more efficiently than by modifying the probability of folding intermediate degradation (Figure 4.6B, 4.7). This also simulated decreased intracellular protein to a similar magnitude to what we observed in our experimental data (Figure

4.2B, 4.4E). We conclude from these models that the most likely explanation for our experimental release data is that neuronal stimulation enhances the rate of co-translational degradation. We next sought to experimentally test this prediction made by the Markov model.

Co-translational degradation requires translation elongation (Inada 2017; Duttler, Pechmann, and Frydman 2013; Kramer et al. 2009; Wheatley, Grisolia, and Hernandez-Yago 1982). One of the hallmarks of co-translational degradation is its sensitivity to the translation elongation inhibitor puromycin (Nathans 1964). Puromycin is an aminoacyl-tRNA structural analog that engages into the peptidyl transferase center of the ribosome and covalently modifies the growing polypeptide (Figure 4.6C)(Nathans 1964; Nathans and Neidle 1963; Wang, Durfee, and Huibregtse 2013; Shao, von der Malsburg, and Hegde 2013). This specifically disrupts translation elongation by dissociating the growing nascent polypeptide from the ribosome. Treatment of neurons with puromycin following concomitant radiolabeling and neuronal stimulation resulted in a significant reduction of NMP peptide release from both KCl-stimulated and control neurons (Figure 4.6D). These data support the prediction made by our modeling data that translation elongation was required for the production of NMP-derived extracellular peptides. Collectively, these data provide evidence that nascent polypeptides were co-translationally degraded by the NMP into extracellular peptides.

Neuronal stimulation induces NMP-mediated co-translational degradation of ribosome-associated nascent polypeptides

During translation elongation, nascent polypeptides are bound to a tRNA within the ribosome. This complex is collectively referred to as a ribosome-nascent chain complex (RNC)(Duttler, Pechmann, and Frydman 2013). However, multiple groups have reported conditions where nascent polypeptides are separated from the RNC prior to their completion and are subsequently degraded (Shao, von der Malsburg, and Hegde 2013; Wang, Durfee, and

Huibregtse 2013; Duttler, Pechmann, and Frydman 2013). To determine whether the NMP was targeting nascent polypeptides while still associated with the RNC, we performed ribosome pelleting assays to isolate RNCs (Brandman et al. 2012). Briefly, $^{35}$S-cysteine/methionine radiolabel was added to neuronal cultures in the presence of proteasome inhibitors for only 30 seconds. This shortened protocol preferentially labels nascent polypeptides before they finish synthesis into full-length proteins (Duttler, Pechmann, and Frydman 2013; Ito et al. 2011). Immediately following radiolabelling, neurons were lysed either in the presence of cycloheximide (CHX) and proteasome inhibitors to freeze translation and degradation, or with puromycin and proteasome inhibitors to release the nascent polypeptide from the ribosome and freeze degradation (Figure 4.8A - model). RNCs were subsequently pelleted as previously described, with equal ribosome loading across samples (Figure 4.9A). By liquid scintillation analysis of CHX-treated samples, we noticed a decrease in radioactive signal in RNC pellets from neurons that had been radiolabelled during stimulation compared to controls (Figure 4.9A). Consistent with the radioactivity solely coming from the nascent polypeptide, treatment with puromycin resulted in a complete loss of radioactivity in the RNC pellet (Figure 4.9A). Treating neurons with MG-132 or biotin-epoxomicin during radiolabelling blocked the stimulation-induced reduction in radioactive signal in the RNC pellet (Figure 4.9A). We believed that this proteasome-mediated turnover of nascent polypeptides was neuronal-specific, as we did not observe an increase in radiolabelled signal from RNCs isolated from MG-132 treated HEK293 cells (which do not express the NMP (Ramachandran and Margolis 2017)) (Figure 4.9B). Notably, we observed a ~20% increase in radiolabeled signal in RNCs isolated from neurons that had been treated with proteasome inhibitors (Figure 4.8A).

To extend these analyses and specifically monitor nascent polypeptides separately from the RNC complex, we leveraged previously described two-dimensional gel electrophoresis (2D-gel) approaches that separate the nascent polypeptides in the form of peptidyl-tRNA from full-

length proteins (Ito et al. 2011). Briefly, pelleted RNCs from neurons radiolabeled for 30 seconds were separated in the first dimension by SDS-PAGE (Figure 4.8B). Next, individual gel lanes were treated with base to hydrolyze tRNAs from their bound nascent polypeptides, and subsequently separated by SDS-PAGE in the second dimension (Figure 4.8B). Separating nascent polypeptides from their tRNAs shifts their molecular weight, changing the migration of pattern of these nascent polypeptides in the second dimension. Nascent polypeptides hydrolyzed from their tRNAs ran as a fast-migrating band, in stark contrast to a slow-migrating band consisting of polypeptides that were not bound to tRNA in the first dimension. This tRNA-free population was comprised of full-length proteins (e.g. ribosomal proteins) and nascent polypeptides separated from their tRNAs during processing in the first dimension (Figure 4.8B). In our analysis, we found puromycin-sensitive radiolabelled signal in both the fast- and slow-migrating bands, consistent with the entire radioactive signal associated with the RNC complex being derived from the nascent polypeptide (Figure 4.8C).

Using this approach, we analyzed isolated RNCs from radiolabelled neurons following KCl stimulation. We observed approximately a 40% reduction in radiolabel signal intensity of both the fast- (tRNA-hydrolyzed polypeptide) and slow-migrating bands from KCl-stimulated versus control samples (Figure 4.8C). Consistent with our quantification of scintillation counts in RNCs, the stimulation-induced loss of radiolabel signal was entirely recovered by treating neurons with MG-132 or biotin-epoxomicin as described above (Figure 4.8C, 4.9C). Immunoblotting these samples using an antibody against ubiquitin revealed detectable signal in the slower migrating band of the 2D-gel which was undetectable in the faster migrating nascent polypeptide band (Figure 4.8D). Importantly, we detected ubiquitin immunoblot signal from puromycin-treated samples in the slower migrating band (Figure 4.8D). Therefore, based on these data, we suggest that the nascent chain is not ubiquitylated at sufficient levels to explain the stimulation-induced turnover we observed. However, nascent chains bound to tRNA and most

likely RNC-associated, are targeted for degradation. We concluded from these data that neuronal stimulation induces NMP-mediated co-translational degradation of ribosome-associated nascent polypeptides in a ubiquitin-independent manner. These data were consistent with the NMP operating as a 20S proteasome, which degrades unfolded polypeptides in an ubiquitin-independent manner (Ben-Nissan and Sharon 2014; Coux, Tanaka, and Goldberg 1996).

Identification of activity-dependent nascent NMP substrates

During neuronal stimulation, were all nascent polypeptides similarly susceptible to co-translational degradation or was there some selectivity in which nascent polypeptides were being targeted? To specify these principles of co-translational degradation through the NMP in an unbiased manner, we turned to global proteomic analysis. A variety of methods have been developed to analyze newly synthesized polypeptides, typically by introducing chemically modifiable noncanonical or unnatural amino acids (Aakalu et al. 2001; Dieterich et al. 2010; Dieterich et al. 2006; Landgraf et al. 2015). These are typically methionine analogs that are incorporated into newly synthesized polypeptides, and serve as a handle to isolate the polypeptides they modify (Aakalu et al. 2001; Dieterich et al. 2010; Dieterich et al. 2006; Landgraf et al. 2015). While these are powerful tools, two issues confounded our use of such approaches. First, decades of work into the stability of nascent chains and newly synthesized polypeptides has shown that proteins made with non-natural amino acids have a higher propensity to be turned over by the proteasome during or immediately following their synthesis [(Benaroudj et al. 2001; Rock et al. 2014; Rock et al. 1994; Wheatley, Giddings, and Inglis 1980; Wheatley 2011; Wheatley, Grisolia, and Hernandez-Yago 1982; Prouty and Goldberg 1972; Goldberg and Dice 1974; Prouty, Karnovsky, and Goldberg 1975; Etlinger and Goldberg 1977)]. This method would likely bias our analysis of newly synthesized proteasome substrates, and provide an artificial overestimate of this population. Second, the met-tRNA that charges these amino acids prefers endogenous methionine. Therefore, to induce the incorporation of noncanonical amino

acids, cells must be incubated in methionine-free media. Additionally, the charging of noncanonical amino acids on met-tRNA is slower, and the efficiency of chemical modification and purifications are imperfect (Hartman, Josephson, and Szostak 2006). To overcome these limitations, studies utilizing these techniques usually incubated cells for at least one hour in media containing noncanonical amino acids to maximize labeling. These timescales were incongruent with the timescales at which we were conducting our experiments.

Because of the combination of these variables, we chose not to use noncanonical or unnatural amino acids to identify co-translationally degraded substrates of the NMP. Instead, we leveraged unbiased and high-coverage mass spectrometry-based quantitative proteomic analysis using tandem mass tag (TMT) technology (Figure 4.10A). Primary mouse cortical neuronal cultures were incubated with bicuculline for one hour and treated with vehicle (DMSO), biotin-epoxomicin, or biotin-epoxomicin+ Cycloheximide (CHX) in the last 10 minutes of the 1-hour stimulation. We chose bicuculline for our activity-inducing paradigm for these experiments since it provided us with more dynamic control of the timing of our experiments. Importantly, bicuculline stimulation recapitulates the earlier observations made using KCl-stimulation (Figure S2D). Following these treatments in biological triplicates, proteins were extracted from the samples and derivatized using TMT tags following enzymatic digestion (Figure 5A). In order to increase protein coverage, reduce artifacts from ratio compression, and increase our signal/noise ratio, peptides from all treatment groups fractionated offline before mass spectrometry (MS) analysis. We performed MS/MS analysis on each of the 24 fractions, with 2-hour runs per fraction in an Orbitrap Fusion Lumos mass spectrometer (Figure 4.10A). An additional fragmentation event with high-energy collisional detection was used for quantification, which increases the accuracy of estimates of protein levels. Protein identification and TMT-based quantitation was conducted using Proteome Discoverer 2.1, applying a false discovery rate of 1% at the protein and peptide levels. Statistical normalization and analysis using inferential Bayes

normalization to account for the population variance was performed as described in materials and methods. Statistically significant differences were determined after taking multiple comparisons testing into account. Overall, the combined analysis of the replicates across treatment groups yielded 141,295 peptides that were mapped to 8,223 proteins (Figure 4.10B). The reproducibility across biological replicates was robust, with coefficients of variation of <10% observed for >99% of the proteins. We defined a co-translationally degraded substrate of the NMP as one with higher protein levels in bicuculline/biotin-epoxomicin-treated neurons as compared to both bicuculline and bicuculline/biotin-epoxomicin/CHX. Statistically significant differences between biotin-epoxomicin treated samples compared to the other groups were observed for 1,339 proteins at $p<0.05$, and 408 for $p<0.01$ (Table 4.1). However, we found it necessary to take multiple comparisons testing into account, increasing the stringency and robustness of this data set. This analysis yielded a list of 191 differentially expressed proteins, of which 122 were up-regulated, and therefore considered co-translationally degraded NMP substrates (Figure 4.10B,C, Table 4.2).

In our MS data, we identified NMP substrates that were previously described as ubiquitin-proteasome system (UPS) targets, such as Odc1 and Rgs4 (Figure 4.10D)(Hoyt, Zhang, and Coffino 2003; Zhang, Pickart, and Coffino 2003; Asher et al. 2005; Davydov and Varshavsky 2000; Lee et al. 2005; Bodenstein, Sunahara, and Neubig 2007). Further analysis of our MS data also revealed a set of substrates not previously shown to be turned over by proteasomes, such as Bex2, Ubc, and Snurf (Figure 4.10D). However, by and large, the levels of many previously characterized UPS targets such as Shank, GKAP, PSD95, Ube3A and ApoER2 did not change in this assay (Figure 4.10D) (Ehlers 2003; Gao et al. 2017; Colledge et al. 2003; Lee et al. 2008; Hung et al. 2010; Shin et al. 2012). Further analysis of this dataset revealed an unusual enrichment of the immediate-early gene (IEG) products in our MS data as NMP substrates. These IEG proteins have all been shown to be activity-dependent targets of the UPS(Tsurumi et al.

1995; Ito et al. 2005; Carle et al. 2007; Adler et al. 2010; Bae et al. 2002; Mabb et al. 2014; Speckmann et al. 2016; Peebles et al. 2010). Specifically, we found that c-Fos, Fosb, Npas4, and Egr1 were significantly upregulated in response to biotin-epoxomicin treatment (Figure 4.10D). These IEG proteins have characteristically low expression in unstimulated neurons and are induced by prolonged neuronal stimulation We initially attributed the upregulation observed in our MS data to canonical activity-induced mechanisms of IEG expression. However, by immunoblot analysis, bicuculline stimulation for one hour does not lead to significant increase in IEG protein expression (Figure 4.12A). In contrast, following two hours of bicuculline stimulation, we observed the canonical induction of IEG protein expression that was dependent on neuronal activity, transcription, and translation (Figure 4.12A) Based on these data, we suspected that our MS data revealed a unique mechanism of IEG protein regulation through the NMP, temporally distinct and prior to the canonical activity-dependent mechanisms of IEG protein expression.

To independently validate our MS data, we used similar treatment conditions as in our MS analysis and analyzed IEG protein levels by immunoblot analysis. Neurons were stimulated with bicuculline for one hour, and treated with either MG-132 or biotin-epoxomicin for the final 10 minutes. The addition of either MG-132 or biotin-epoxomicin in the presence of bicuculline led to an accumulation of IEG proteins, but no change in the protein levels of UPS targets such as PSD95 or Ube3A (Figure 4.11A). This increase in IEG protein levels was blocked by co-incubation with Cycloheximide, but transcriptional inhibitor actinomycin D had no effect (Figure 4.11A). While we did not detect a change in Arc levels in the MS analysis, we did observe significant changes by immunoblot. This likely reflects the differences in detection sensitivity between the two methods. Notably, in the absence of bicuculline stimulation, MG-132 and biotin-epoxomicin treatment also led to a small, but reproducible increase in IEG products (Figure 4.11A and 4.12B). Addition of CHX or TTX blocked this inhibitor-mediated increase, suggesting

that the effect depends on translation and baseline activity present in neuronal cultures (Figure 4.12B). In all of these experiments, the effects on IEG protein expression due to treatment with MG-132 and biotin-epoxomicin were nearly identical, suggesting that the majority of changes we observe are due to the NMP, and not the cytosolic proteasome (Figures 4.11A and 4.12A). Together, we interpreted these data to mean that neuronal activity was required for and induces NMP-mediated degradation of IEG proteins.

Taking these experimental data together with the Markov modeling and validation, we hypothesized that the NMP exclusively mediates co-translational degradation of IEGs, and not full-length proteins. The data above demonstrating NMP-mediated IEG protein turnover do not distinguish between co-translational degradation and full-length protein degradation. To monitor turnover only of the full-length protein population, we took advantage of the robust induction of IEG protein expression following two hours of bicuculline stimulation (Figure 4.12A). Following stimulation, we washed out the bicuculline to monitor the turnover of these IEG proteins for one hour. Neurons were incubated with Cycloheximide after the washout to prevent any further protein expression, allowing us to monitor the fate of these IEG protein products that had completed synthesis. As expected, we observed robust induction of immediate-early gene products following two hours of bicuculline stimulation that was largely turned over in one hour in the absence of sustained translation (Figure 4.11B).This turnover was inhibited by the addition of MG-132, consistent with data from many groups demonstrating that IEG proteins are targeted by the ubiquitin-proteasome pathway (Figure 4.11B) (Adler et al., 2010; Bae et al., 2002; Carle et al., 2007; Ito et al., 2005; Mabb et al., 2014; Peebles et al., 2010; Speckmann et al., 2016; Tsurumi et al., 1995). In contrast, biotin-epoxomicin does not prevent the turnover of these full-length IEG products (Figure 4.11B). These data were the clearest demonstration that the NMP co-translationally degrades nascent polypeptides during states of activity, but is not capable of degrading a substrate once it is fully synthesized (Figure 4.11B).

During elevated states of neural activity, protein synthesis and protein degradation are independently essential for regulating the expression level of proteins important for promoting, enhancing and maintaining neuronal activity-dependent processes . Our experiments unify these observations and elucidate an activity-dependent coordination of protein synthesis and protein degradation through the NMP. This resulted in NMP-dependent degradation of nascent polypeptides being synthesized during neuronal stimulation. We identified immediate-early gene products as among the many activity-dependent substrates of the NMP. Taken together, our studies define a protein homeostasis program that involves the coordination of protein synthesis and NMP-mediated degradation in the nervous system.

Ubiquitin-independent co-translational degradation

Protein turnover and degradation kinetics have been studied extensively over the past few decades (Prouty and Goldberg 1972; Prouty, Karnovsky, and Goldberg 1975; Duttler, Pechmann, and Frydman 2013; Schubert et al. 2000; Vabulas and Hartl 2005; Zhao, Garcia, and Goldberg 2016; Schwanhausser et al. 2013; McShane et al. 2016; Wheatley, Giddings, and Inglis 1980; Wheatley, Grisolia, and Hernandez-Yago 1982). The majority of these studies have used isotope pulse labeling of proteins made over at least one hour, and then have monitored the fate of those synthesized proteins. Cumulatively, they have concluded that protein turnover is most well-explained by two-state degradation kinetics, which predicts that some proteins degrade at the same rate over many hours, while others have both fast (within 2 hours) and slow (>8 hour) kinetics(McShane et al. 2016). These radioisotope pulse labeling approaches use long labeling times that are more biased towards monitoring folded full-length proteins. Short labeling times have been shown to preferentially monitor polypeptides on the ribosome or folding intermediates. Indeed, by reducing the radiolabel pulse time to within a few minutes (timeframes much more similar to our analysis), other classic studies on protein turnover have shown that immediately newly synthesized proteins are quickly turned over (Goldberg and Dice 1974; Prouty, Karnovsky,

and Goldberg 1975; Wheatley, Giddings, and Inglis 1980; Wheatley, Grisolia, and Hernandez-Yago 1982). Whether these studies define co-translational degradation has not been fully elucidated and certainly, such mechanistic studies have not been carried out in the nervous system. Our use of short radiolabeling protocols allowed us to capture a coordination of protein synthesis and protein degradation. This led to the preferential NMP-dependent degradation of polypeptides being synthesized during neuronal stimulation (i.e. the activity-dependent nascentome).

The NMP has previously been described to be a 20S proteasome complex and despite extensive effort, no cap to recognize a ubiquitylated substrate has yet been identified on the NMP (Ramachandran and Margolis 2017). Given that the 20S requires an unfolded substrate, it is logical that this NMP-dependent program of co-translational degradation would be ubiquitin-independent. Consistent with NMP degradation mechanisms operating independently of ubiquitylation pathways, we do not detect in our MS analysis changes in the levels of previously well-characterized ubiquitylated substrates (Shank, GKAP, and AKAP79/150) of the UPS. These proteins are likely primarily degraded by the UPS pathways as full-length proteins and not nascent polypeptides by the NMP. The mechanisms that discriminate substrate selectivity to the UPS pathway versus NMP degradation are unknown and critical to identify. In addition, the kinetics of our Markov modeling analysis, which predicted that the NMP degrades unfolded nascent polypeptides and not full-length proteins, are also consistent with this NMP-dependent program being ubiquitin-independent. If nascent polypeptides were being ubiquitylated, our model would predict a delay in release curves corresponding to ubiqutiylation and deubiquitylation prior to degradation. The experimental release curves we observe are far too rapid to incorporate these additional steps.

Based on our Markov modeling, we predicted that a nascent polypeptide has a probability of 4.7% that it will be co-translationally degraded in neurons at baseline. This evaluation was

consistent with experimentally observations made in Figure 1C, comparing the intracellular radiolabeled proteins in the input (taken immediately after radiolabeling) with the 30 minute chase under baseline conditions. The biochemical approaches we used in Figures 4.2, 4.4, and 4.8 are similar to those used in other systems analyzing nascent polypeptides – for example, nascent chains in yeast have been shown to be co-translationally ubiquitylated and degraded. The fraction of nascent polypeptides being targeted for degradation in these experiments were estimated to comprise about 1-5% of the total translated proteome at any given time(Duttler, Pechmann, and Frydman 2013). Though these are two different modes of protein degradation (i.e. ubiquitin-independent vs ubiquitin-dependent) they do suggest consistent instability of the nascentome across species and systems. How robust this process is across other cell systems, and whether they are handled by 20S or 26S proteasomes, remains to be determined.

While our model predicted an increase in nascent chain degradation (16.5%) under stimulation conditions, this data is much more challenging to properly model, as evidenced by the larger uncertainty between the predicted and experimental release data. The predicted 16.5% intracellular degradation also underestimates what we observe in the experimental data (Figure 4.2B). These discrepancies are likely due to an inability to accurately model how synthesis and degradation change under stimulation conditions. Multiple groups have now shown changing translation dynamics during neuronal stimulation, and further work will be required to integrate these data into NMP biology and our analyses. Mechanistic insight into activity-dependent co-translational degradation will be critical for understanding the roles and function for NMP-mediated degradation.

Nascent polypeptides, including the immediate-early gene products, as NMP substrates

The concept that proteasome-mediated protein degradation responds to neuronal activity is not new – multiple groups have reported enhanced proteasomal degradation in response to

neuronal activity. However, these studies relied on pan-proteasome inhibitors over the course of hours to days, typically focused on homeostatic plasticity. Such sustained proteasome inhibition leads to induction of stress pathways and initiation of the ER stress response, which includes a global shutdown of translation(Ding et al. 2006; Wu, Volta, et al. 2009; Obeng et al. 2006). This likely explains why groups have not observed the phenomena we report in this manuscript. By using short windows of inhibition and narrowing in on a specific pool of proteins (e.g. those made during neuronal stimulation), we have unveiled an unconventional modality of activity-dependent degradation of many substrates including IEG products.

Over the past 30 years, many groups have focused their efforts on studying the role of immediate-early genes (IEGs) in experience-induced changes in neuronal activity. Several groups have gone on to show that proteasome inhibition using MG-132 can lead to an elevated expression of 2-3 fold of the products of IEGs in neurons, such as Arc, c-Fos, and Npas4 (Adler et al., 2010; Bae et al., 2002; Carle et al., 2007; Ito et al., 2005; Mabb et al., 2014; Peebles et al., 2010; Speckmann et al., 2016; Tsurumi et al., 1995). However, these studies have not explicitly discriminated between those IEGs being synthesized and those which have already been synthesized. In fact, the vast majority focus on those already synthesized and monitor their turnover through the UPS pathway, typically by focusing on the E3 ubiquitin ligases that target these IEGs. Our finding that MG-132 blocks the degradation of full-length IEG products (Figure 4.11B) is consistent with previous data that full-length IEGs are degraded by the cytosolic proteasome. Since biotin-epoxomicin has no effect on the turnover of these full-length IEG products (Figure 4.11B), we do not believe the NMP targets these full-length products. This is consistent with the notion that the NMP does not degrade proteins made prior to stimulation (Figure 4.2C) and with the Markov modeling that the NMP does not target full-length and folded proteins (Figures 4.4 and 4.6). In contrast, by adding biotin-epoxomicin during stimulation instead of following stimulation, we made the remarkable observation that IEG proteins in the

process of being synthesized are degraded by the NMP (Figure 4.11A). This is also consistent with the phenomenon observed in Figure 1B and with the predictions made by the Markov modeling. We find it interesting to mention that IEGs and other NMP substrates (such as Rgs4) contain intrinsically disordered domains. Whether these properties contribute to their susceptibility to co-translational degradation by the NMP remains to be explored.

For decades immediate early genes have been defined by their rapid response to neuronal activity at the level of gene transcription. While this is known to eventually lead to translation and expression of a IEG proteins product, the relationship between gene expression and timing of protein production has not indicated a direct 1:1 correlation (Haider and Pal 2013; Maier, Guell, and Serrano 2009). Our study indicates that transcription is not required for the NMP mediated turnover of IEG protein products. These data suggested to us that mRNA for several IEGs must be available for IEG products to be continuously targeted by the NMP. It is well known that induced mRNAs can remain in the cell for hours to days(Schwanhausser et al. 2013; Schwanhausser et al. 2011). Many studies monitoring the impact of neuronal activity on IEG gene transcription use a strategy of quieting the neurons with activity blockers, largely to remove any residually expressed mRNA. This condition does not mimic the in vivo environment which expresses mRNA for many IEGs at appreciable levels. Our studies do not quiet neurons prior to stimulation. Based on our data that inhibiting the NMP of neurons at baselines induces activity-dependent increases in IEG protein products, we believe that our cultures do exhibit substantial neuronal activity at baselines. This change in IEG protein levels likely reflects the translation of a small but available pool of IEG mRNAs that in response to stimulation, are rapidly co-translationally degraded by the NMP. We speculate that transcriptional induction serves to overwhelm the co-translational degradation system, and leads to the generation of full-length IEGs that go on to carry out specific functions. The observed transcription-independent coupling of translation and degradation in response to neuronal activity raises the fundamental question of

whether this mechanism gives rise to the discrepancy between the transcriptome and the proteome. In summary, our data codify the principles of co-translational degradation through the NMP into changes in particular substrates known to be critical for neuronal function.

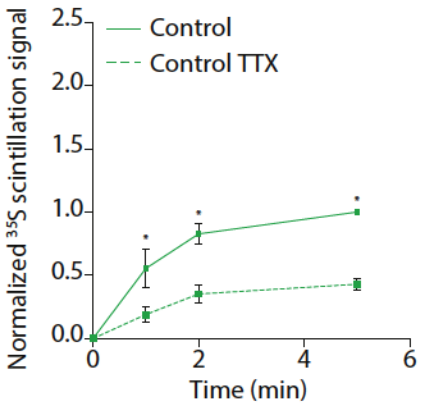


Supplemental Figure 1. Ramachandran et al.

**Figure 4.1: Suppression of neuronal activity reduces peptide efflux.** Cultured cortical neurons at days in vitro (DIV) 14 were incubated with Tetrodotoxin (TTX - dashed lines, 1hr) or without (Control - solid line). $^{35}$S-methionine/cysteine radiolabel was incorporated for 10 minutes. Radiolabel was washed out, and fresh media +/- TTX was added. Samples were taken at indicated timepoints over a 10 minute timecourse and counted by liquid scintillation. Data are mean and s.e.m. of $n = 3$ experiments from independent neuronal cultures. Line graph, *$p < 0.01$ (Students t-test) for control compared to TTX treatment at each time point.

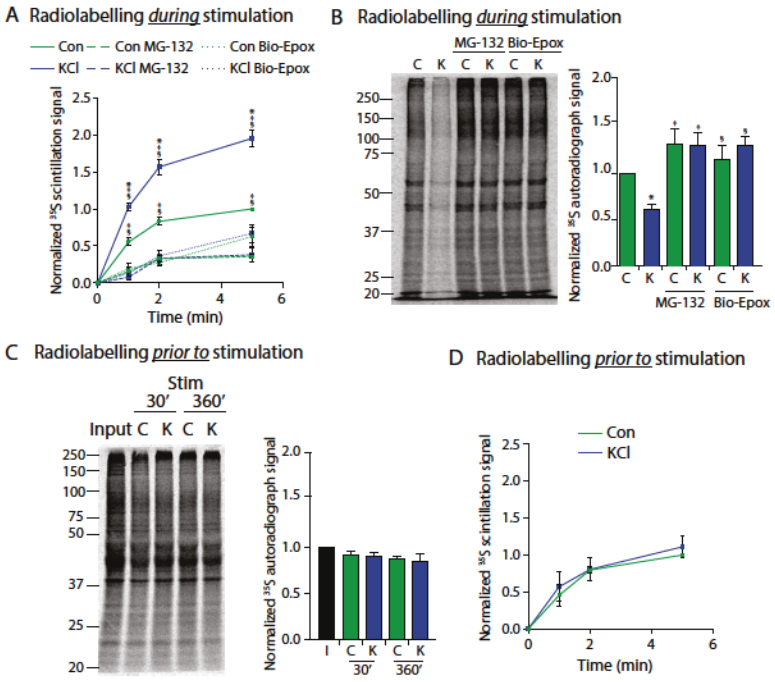


Figure 1. Ramachandran et al.

**Figure 4.2. Neuronal stimulation induces NMP-dependent degradation of newly synthesized proteins into extracellular peptides.**

(**A**) Concomitant radiolabelling *during* neuronal stimulation induces NMP-mediated radiolabeled peptide release. Media collected from neurons concomitantly radiolabeled and treated with control (Con) or KCl stimulation buffer with or without MG-132 or biotin-epoxomicin (Bio-Epox). Liquid scintillation data for media at the indicated time points are shown normalized to control at the 5-minute time point. Data are mean and s.e.m. of $n = 3$ experiments from independent neuronal cultures. Line graph, *$p < 0.01$ (two-way ANOVA) for Control compared to KCl treatment at each time point. Line graph, $^{‡}p < 0.01$ (two-way ANOVA) for Untreated compared to MG-132 treatment at each time point. Line graph, $^{§}p < 0.01$ (two-way ANOVA) for Untreated compared to Bio-Epox treatment at each time point.

(**B**) Neuronal stimulation induces NMP-mediated degradation of intracellular proteins made

*during* stimulation. Left, representative autoradiograph of lysates from cortical neurons radiolabelled with $^{35}$S-methionine/cysteine *during* either control (C) or KCl (K) stimulation and treated with MG-132 or biotin-epoxomicin (Bio-Epox). Right, quantification of densitometry signal normalized to control alone. Data are mean and s.e.m. of $n = 3$ experiments from independent neuronal cultures. Bar graph, *$p < 0.01$ (two-way ANOVA) compared to control, $^{\ddagger}p < 0.01$ (one-way ANOVA) for Untreated compared to MG-132 treatment, $^{\S}p < 0.01$ (two-way ANOVA) for Untreated compared to Bio-Epox treatment.

(**C**) Neuronal stimulation does not induce NMP-mediated degradation of proteins made *prior to* stimulation. Left, Representative autoradiograph of lysates from cortical neurons previously radiolabelled and then chased into either control (C) or KCl (K) stimulation buffers for indicated times. Input shows sample collected immediately following labeling. Right, quantification of densitometry signal normalized to control alone. Data are mean and s.e.m. of $n = 3$ experiments from independent neuronal cultures. Statistically significant differences between samples was not observed (two-way ANOVA).

(**D**) Radiolabelling immediately *prior to* neuronal stimulation does not induce NMP-mediated radiolabeled peptide release. Experiments done as described in (**A**), note neurons were radiolabelled *prior to* instead of *during* stimulation as in (**A**). Data are mean and s.e.m. of $n = 3$ experiments from independent neuronal cultures. Statistically significant differences between samples was not observed (two-way ANOVA).

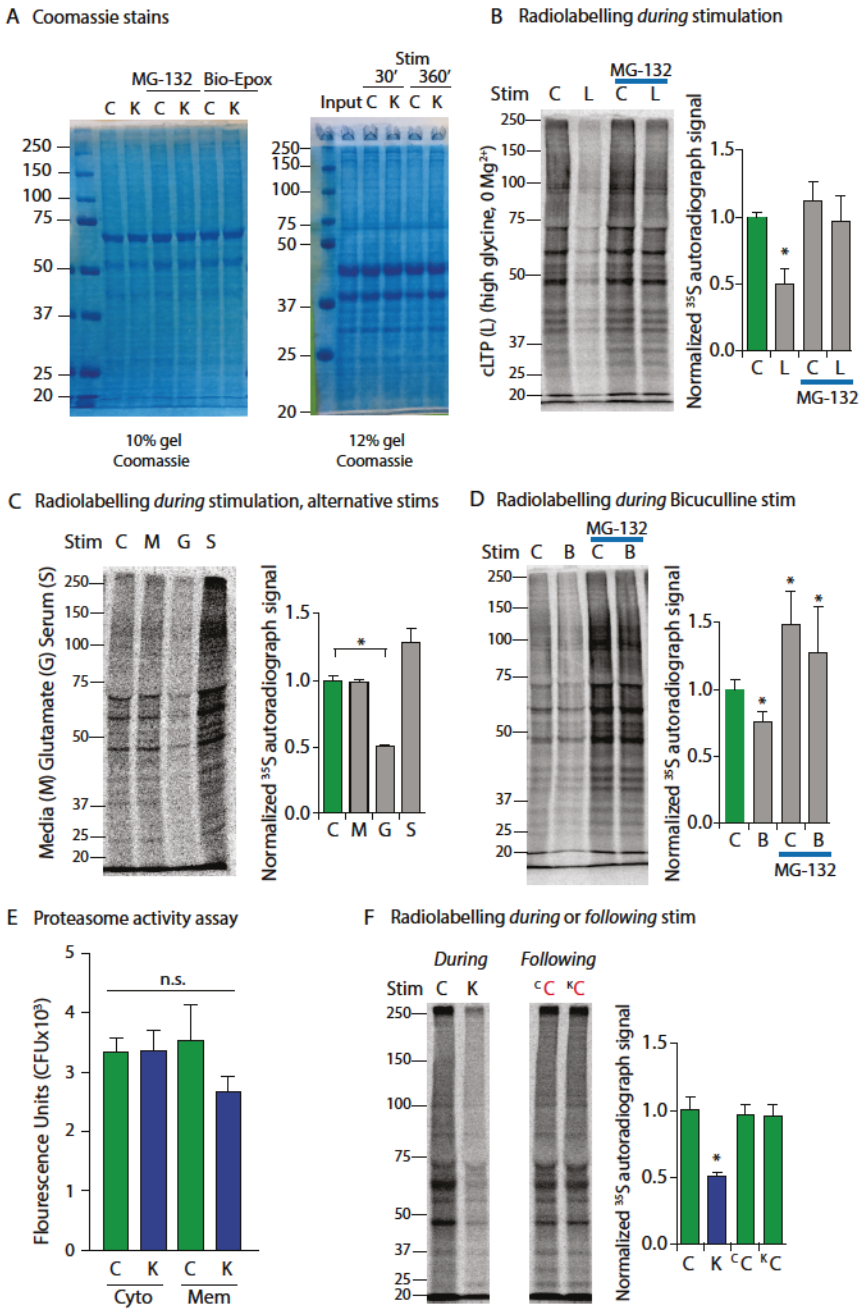


Supplemental Figure 2. Ramachandran et al.

**Figure 4.3: Neuronal stimulation reduces radiolabel incorporation into proteins in a proteasome dependent manner.**

(**A**) Gels for Figures 1B and 1C were stained with coomassie dye and dried down onto whatman filter paper. Note equal loading across conditions.

(**B**) Cortical neurons at Days *in vito* 15 were radiolabelled during either ACSF treatment (C) or chemical LTP induction (L) (as described in Materials and methods). MG-132 was added to indicated neurons during stimulation. Autoradiographs quantified by densitometry shown to right. Data are mean and s.e.m. of $n = 2$ experiments from independent neuronal cultures. Bar graph, *p < 0.01 (two-way ANOVA) for treatments compared to controls.

(**C**) Neurons were treated with either a Media exchange (M), Glutamate (G), or 5% Fetal Equine Serum (S) and radiolabelled for 10 minutes. Autoradiographs quantified by densitometry shown to right. Data are mean and s.e.m. of $n = 2$ experiments from independent neuronal cultures. Bar graph, *p < 0.01 (two-way ANOVA) for treatments compared to controls.

(**D**) Neurons were treated with bicuculline (B) or water (C) for one hour. MG-132 and radiolabel were added during the final 10 minutes of bicuculline stimulation. Autoradiographs quantified by densitometry shown to right. Data are mean and s.e.m. of $n = 2$ experiments from independent neuronal cultures. Bar graph, *p < 0.01 (two-way ANOVA) for treatments compared to controls.

(**E**) Neurons stimulated with Control (C) or KCl (K) buffers were separated into Cytosolic (Cyto) and Membrane (Mem) fractions. Proteasomes were purified from each of these samples. Purified proteasomes were incubated for 30 minutes with Suc-LLVY-AMC, a small-molecule proteasome substrate that releases fluorescence when cleaved. Raw fluorescence units are shown. Data are mean and s.e.m. of $n = 2$ experiments from independent neuronal cultures. Bar graph, data were not statistically significantly different across samples (two-way ANOVA).

(**F**) Neurons stimulated with either Control (C) or KCl (K) buffers were incubated with $^{35}S$ methionine/cysteine radiolabel. Radiolabel was either incorporated at the same time as the stimulation (during), or as soon as the stimulation was washed out into media (following). For following experiment, superscript denotes stimulation condition, red lettering indicates treatment

during radiolabelling. Data are mean and s.e.m. of $n = 3$ experiments from independent neuronal cultures. Bar graph, *$p < 0.01$ (two-way ANOVA) for treatments compared to controls.

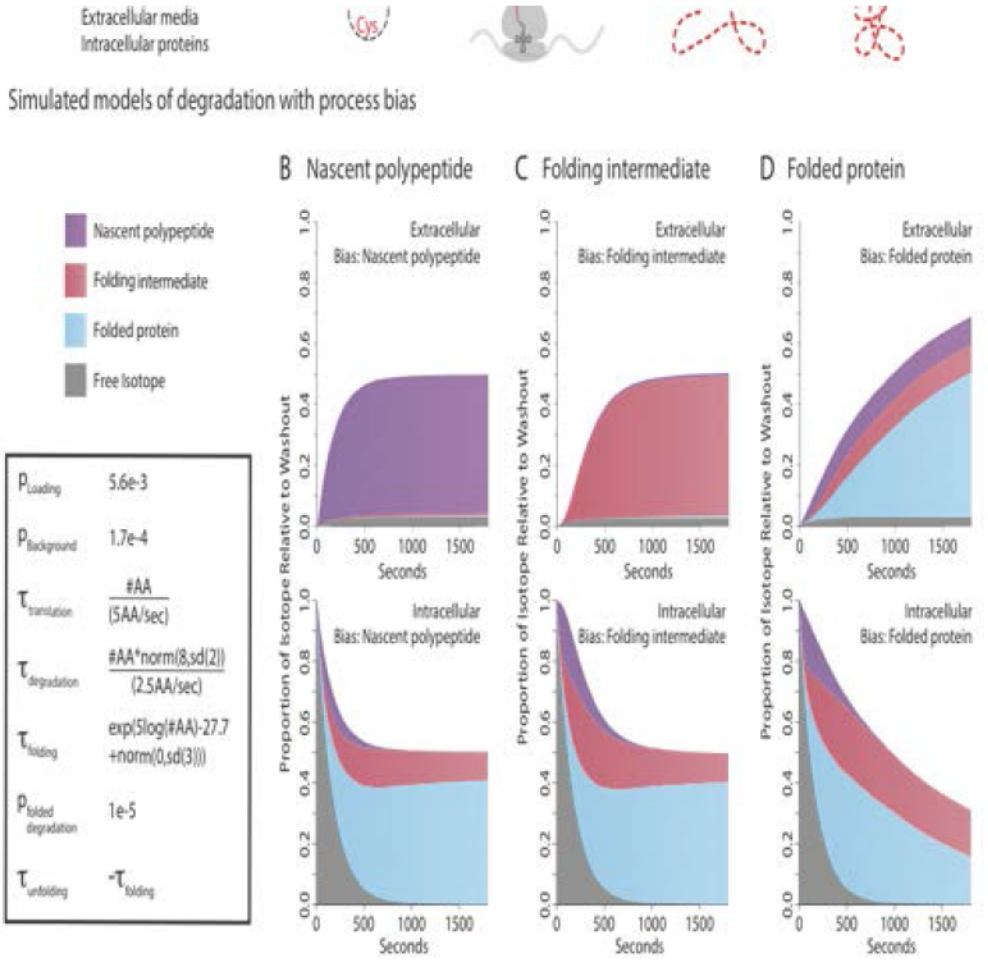


**Figure 4.4. Establishment of Markov chain processes to model degradation of nascent chains, folding intermediates, and folded proteins**

(**A**) Overview of model converting protein translation, degradation, and arising fates into Markov decision nodes using experimentally determined radioisotope fate tracing. Experimental timeline to build the Markov chain is shown to the left. Each Markov node is indicated in the top row, as either a free isotope (Met/Cys), Nascent Polypeptide, Folding intermediate, or Folded protein. Probabilities of transitioning between different Markov nodes is indicated by p. Bottom row depicts those paths which can give rise to extracellular isotope release indicated by dashed lines (denoting degradation). Time between steps is shown by □.

(**B,C,D**) Simulated release curves generated by weighting parameters to bias outcomes. Values

for different kinetic parameters based on either calculated or well-established data are shown to the left. Simulated Markov chains (50,000 simulations) to analyze intracellular and extracellular radioisotope composition. The probability for each plot is shown artificially biased towards either Nascent polypeptide (**B**), Folding intermediate (**C**), or Folded protein (**D**). Top, the simulated graphs illustrate the resulting shapes of isotope release curves for a given bias. Each graph represents the proportion of total isotopes at any given second resulting from degradation of nascent polypeptides (Purple), Folding intermediates (Red), or Folded proteins (Blue). Diffusion of free isotope (Grey) was taken into account and constant across conditions. Bottom, the simulated graphs illustrate the resulting shapes of isotope changes inside the cell for a given bias.

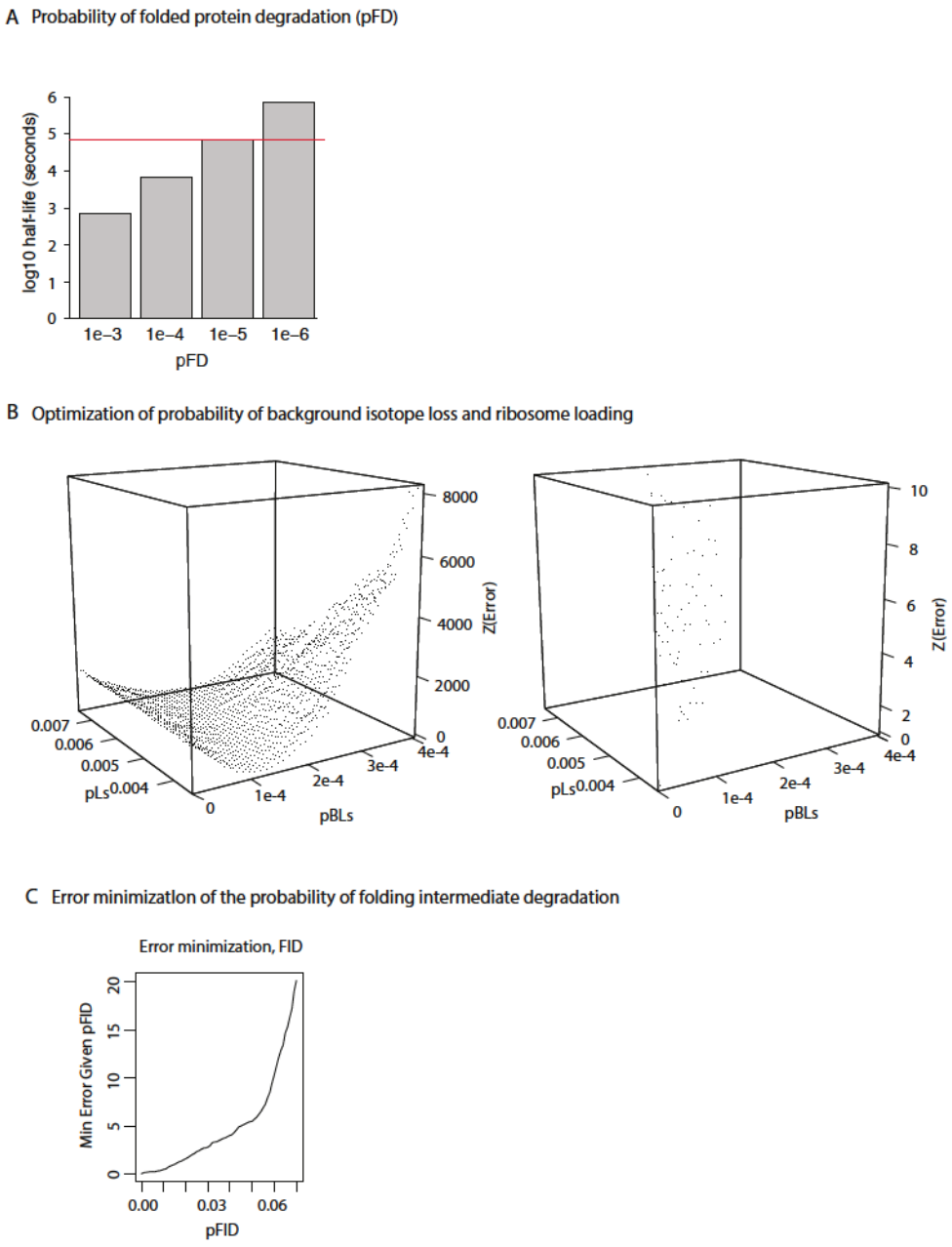


Supplemental Figure 3. Ramachandran et al.

**Figure 4.5: Optimization of parameters for Markov chain modeling**

(**A**) Probabilities of unfolding were optimized based on previous work calculating average half lives of protein substrates (McShane et al. 2016). Certain protein substrates are much more likely to unfold than others, and while this is highly substrate-dependent, our analyses rely on aggregate

data. We first calculated protein half lives based on different values of probability of unfolding and subsequent degradation, plotted above. We then took the approximate half lives of proteins as determined by previous studies that rigorously determine protein half life (McShane et al. 2016). To be on the extremely conservative end of protein half life estimation, we assumed an average and aggregate half life of 20 hours, as indicated by the red line. This was despite an aggregate average of 40-50 hours based on prior work.

(**B**) The error of our predicted *in silico* Markov chains across the 2D parameter space of probability of background release of radioisotopes (pBackground) versus the probability of loading onto a ribosome (pLoading). This optimization was done under degradation inhibition, to ensure that the observed release is theoretically dominated by the diffusion of radioisotope. The red dot denotes the location of the minimum. The figure on the right is a zoomed in view of the region around the minimum that has up to 10x the error, and indicates that the minimum is very dramatic. The optimal pBackground and pLoading are 0.00017 and 0.0056 respectively.

(**C**) Parameter space of probabilities of co-translational degradation and folding intermediate degradation to optimize values against experimental data. Error minimization for folding intermediate degradation probability (pFID) as a 2-dimensional zoomed in representation shown.

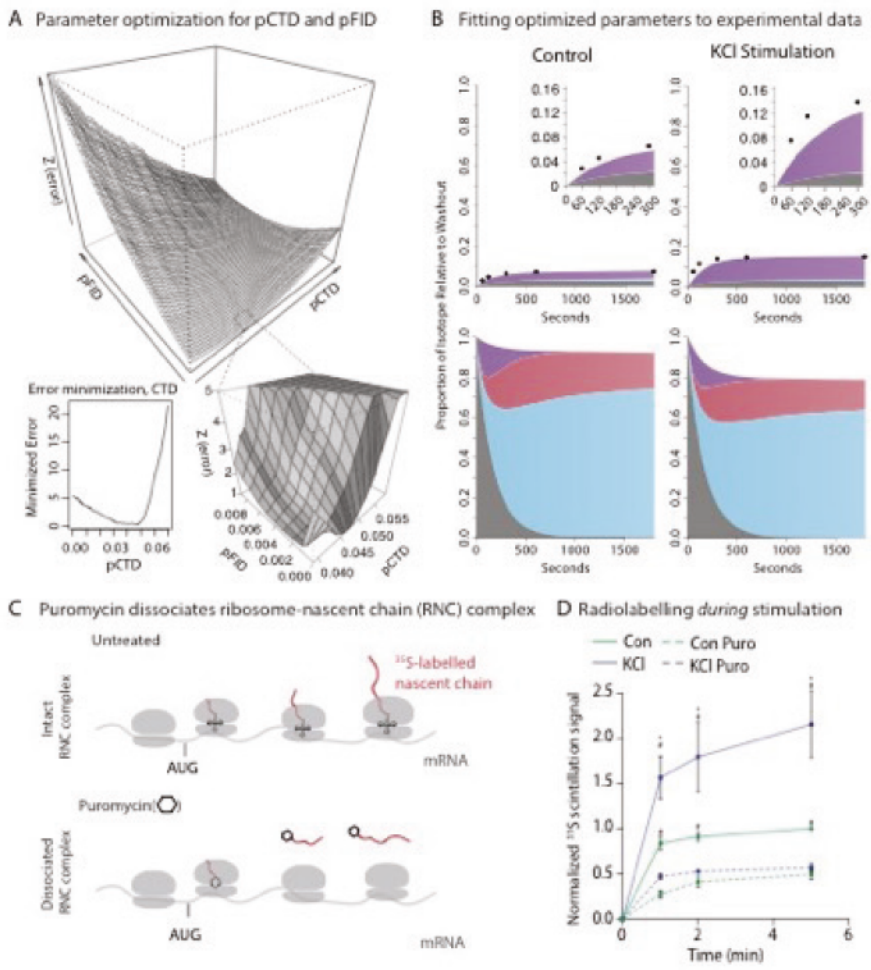


Figure 3. Ramachandran et al.

**Figure 4.6. Nascent polypeptides are likely the source for NMP-derived extracellular peptides.**

(**A**) Parameter space of probabilities of co-translational degradation and folding intermediate degradation to optimize values against experimental data. Optimized values in the indicated parameter space are shown zoomed in to the bottom right. Error minimization for co-translational degradation probability as a 2-dimensional zoomed in representation shown to the bottom left. Note the minimized error for pCTD (probability co-translational degradation) is non-zero and a funnel, compared to pFID (probability folding intermediate degradation).

(**B**) Graph of *in silico* release data using parameters optimized by minimizing error of probabilities against experimental isotope release data. Calculated release data for untreated (Control) is shown to the left. Calculated release data for neurons stimulated with KCl is shown to right. Insets show zoomed in time-course for the first 300 seconds, similar to experimental release data shown in Figure 1. Experimental data are shown in black dots, overlaid with simulated release curves.

(**C**) Schematic of experiments with Puromycin. Translating ribosomes shown in grey on mRNA. AUG start site shown just prior to tRNA (small structure with codon recognition loops, in ribosome P site) and growing radioactive polypeptide (growing red line out of translating ribosomes). Puromycin (hexagon) modifies and releases the nascent polypeptide (red) from actively translating ribosomes.

(**D**) Concomitant radiolabelling *during* neuronal stimulation induces NMP-mediated radiolabeled peptide release that is sensitive to Puromycin treatment. Media collected from neurons concomitantly radiolabeled and treated with control (Con) or KCl stimulation buffer. Puromycin (Puro) or Vehicle added following washout of stimulation and radiolabel. Liquid scintillation data for media at the indicated time points are shown normalized to control at the 5-minute time point. Data are mean and s.e.m. of $n = 3$ experiments from independent neuronal cultures. Line graph, $^{*}p < 0.01$ (two-way ANOVA) compared to control, $^{\#}p < 0.01$ (two-way ANOVA) for Untreated compared to Puromycin treatment.

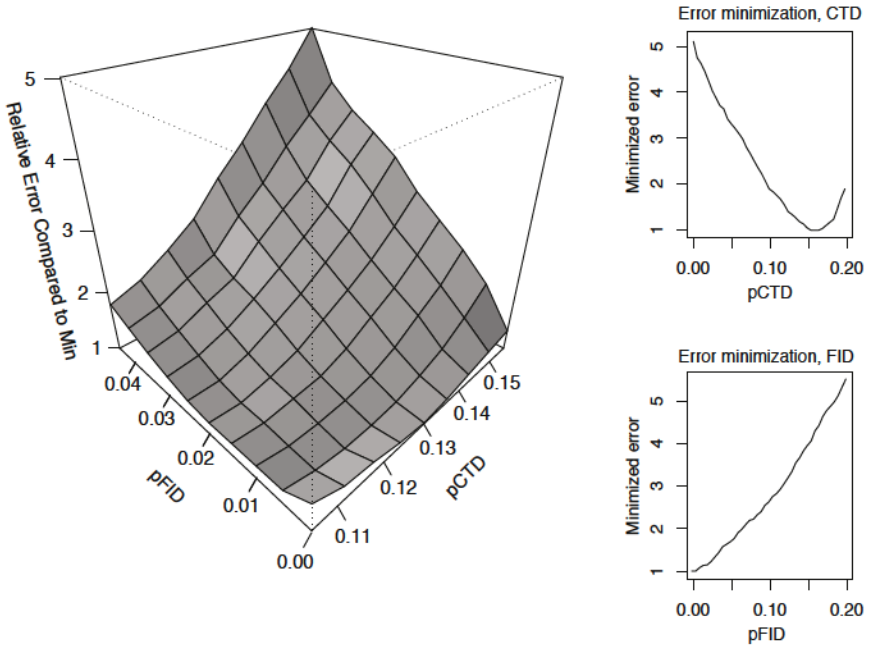


Supplemental Figure 4. Ramachandran et al.

**Figure 4.7: Parameter space of probabilities of co-translational degradation and folding intermediate degradation to optimize values against experimental KCl stimulation data**

The error of our predicted *in silico* Markov chains across the 2D parameter space of probability of co-translational degradation pCTD versus the probability of folding intermediate degradation pFID. This optimization was carried out under KCI stimulation, and the optimal values of pCTD and pFID were estimated as 0.165 and 0 respectively. The plot on the top right depict the minimum (relative) error achievable given different values of pCTD – indicating a sharp rise in error as pCTD deviates in either direction from the optimized value of 0.165. Similarly, the plot on the bottom right depicts the minimum error achievable given different values of pFID – indicating that the errors steadily increase as pFID deviates from 0.

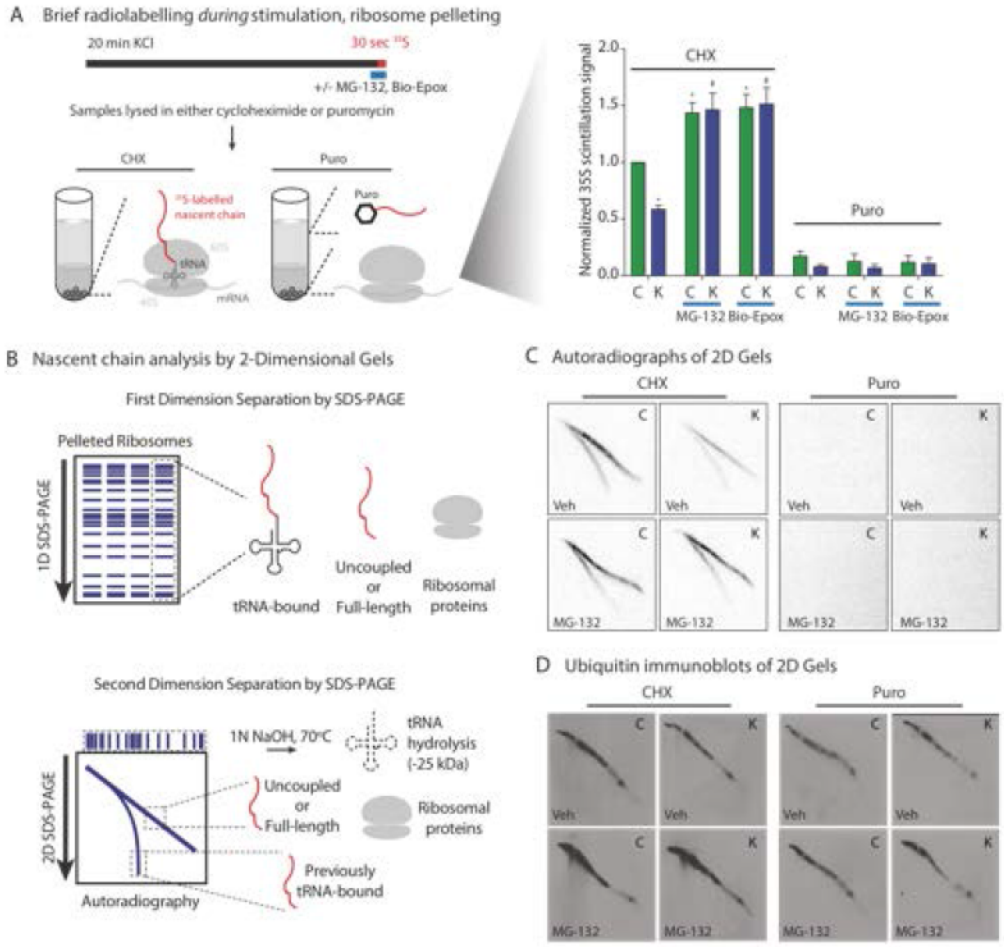


Figure 4. Ramachandran et al.

**Figure 4.8. Neuronal stimulation induces NMP-mediated co-translational degradation of ribosome-associated nascent polypeptides.**

(**A**) Neuronal stimulation induces NMP-mediated degradation of ribosome-associated polypeptides. Left, top, black line shows timeline over which neurons were treated with either Control (C) or KCl (K) stimulation buffers. Red line shows timeline for radiolabeling, blue line for when pharmacological treatments were introduced. MG-132 and biotin-epoxomicin (Bio-Epox) were added 30 seconds prior to, and for the 30 seconds during radiolabelling. Neurons were lysed in either cycloheximide (CHX) or puromycin (Puro). Left, below, strategy to

discriminate ribosome-associated nascent chains. Lysates were layered over a sucrose cushion, and ribosome-nascent chain complexes (RNCs) were pelleted. CHX induces ribosome stalling with tRNA-bound nascent chains (red) still associated with the Ribosome, while Puro dissociates the nascent chain from the Ribosome. Released Puromycylated nascent chains found in supernatant. Right, RNC complexes quantified by liquid scintillation. Graph shows quantification of ribosome scintillation counts, normalized against control alone. Data are mean and s.e.m. of $n = 3$ experiments from independent neuronal cultures. Bar graph, $^{*}p < 0.01$ (two-way ANOVA) for samples compared to controls, $^{\#}p < 0.01$ (two-way ANOVA) for samples compared to KCl treatment at each time point. All puromycin treatments were statistically significantly lower than controls, but not significant amongst each other.

(**B**) Experimental strategy to separate tRNA-bound nascent polypeptides from RNCs and full-length proteins. Uncoupled indicate those nascent chains that hydrolyze during separation in first dimension (1D) SDS-PAGE. Lanes are cut out, treated with base at high temperature to hydrolyze the tRNA (dotted lines), and run in a second dimension (2D). Slower migrating signal contains ribosomal proteins, full-length proteins, and those uncoupled from the tRNA in the first dimension. Faster migrating signal contains those nascent chains hydrolyzed from their tRNAs in the base hydrolysis step after the first dimension of SDS-PAGE.

(**C**) Elongating nascent polypeptides during KCl stimulation are degraded by the NMP. Representative autoradiographs of pelleted RNCs from (A) processed by 2D SDS-PAGE. Stimulation condition - either Control (C) or KCl (K) in top right corner, treatment condition – either Vehicle (Veh) or MG-132 in bottom left. Translation inhibitors – either cycloheximide (CHX) or pruomycin (Puro) added during lysis shown above autoradiographs.

(**D**). Ubiquitin immunoblots shown of the same samples in (**C**).

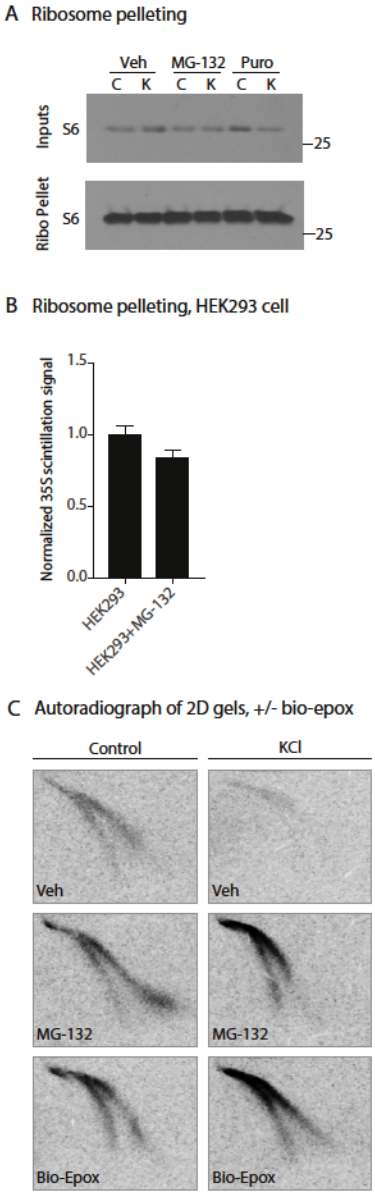


Supplemental Figure 5. Ramachandran et al.

**Figure 4.9: Neuronal stimulation induces NMP-mediated co-translational degradation of ribosome-associated nascent polypeptides.**

(**A**) Ribosome nascent chain (RNC) complexes were pelleted from neurons stimulated with either Control (C) or KCl (K) buffers. MG-132 and Puromycin (Puro) were added to indicated samples.

Samples were immunoblotted using antibodies against Ribosomal S6 protein. Immunoblots of inputs are shown above those for pelleted RNC (Ribo pellet).

(**B**) Pelleted RNCs from HEK293 cells, treated with Vehicle or MG-132. Samples analyzed by liquid scintillation. Scintillation counts normalized to vehicle-treated samples shown, average of $n = 3$ biological replicates plotted as mean and s.e.m.

(**C**) Pelleted RNCs from Control or KCl stimulated neurons treated with or without vehicle, MG-132, or biotin-epoxomicin (Bio-Epox).

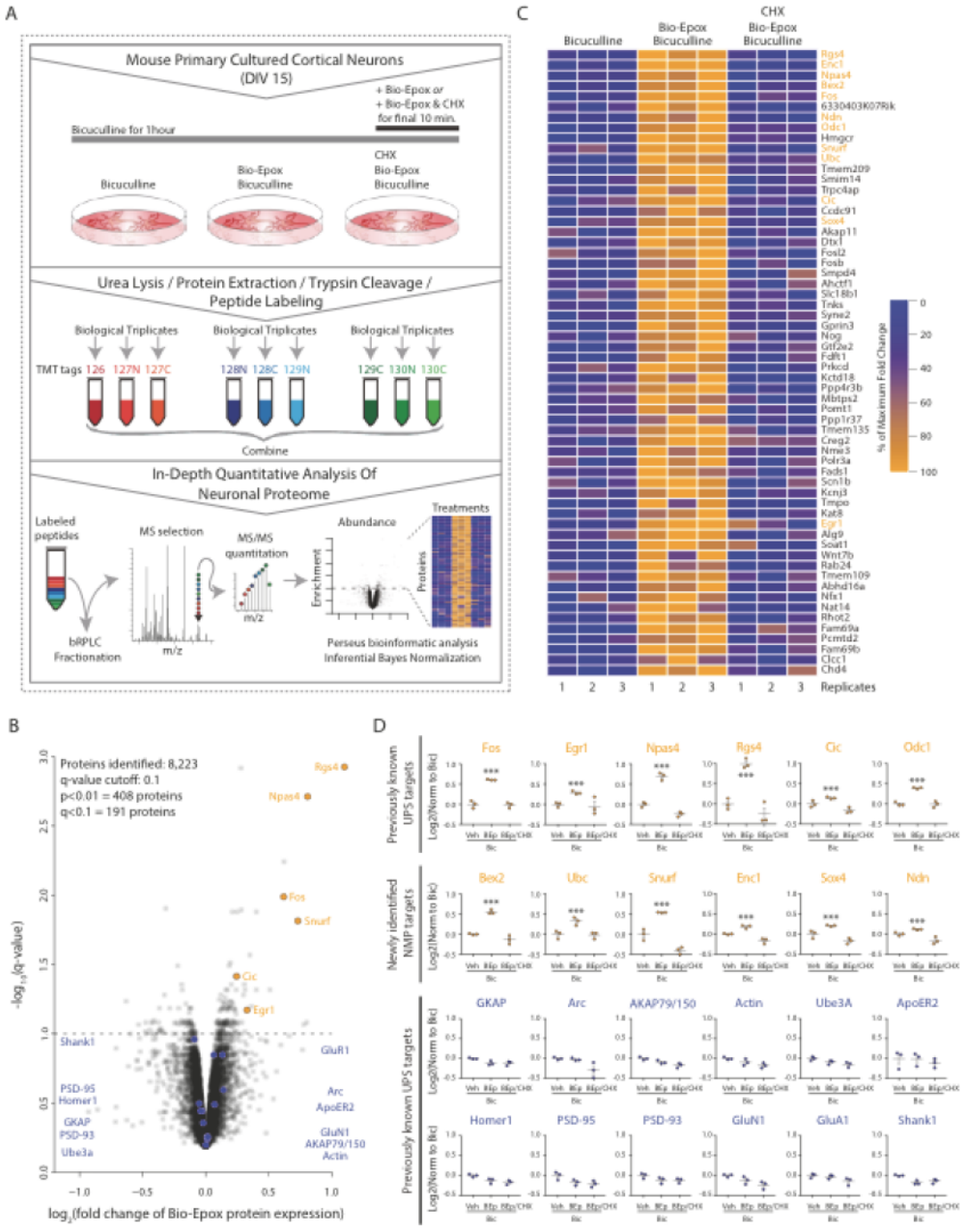


Figure 5. Ramachandran et al.

**Figure 4.10. Quantitative 10-plex mass spectrometry experiment to identify newly synthesized NMP substrates.**

(**A**) Overview of mass spectrometry strategy used to enrich and identify NMP targets. Primary

cortical neurons were treated with indicated drugs over shown timeline. Bicuculline (Bic), biotin-epoxomicin (Bio-Epox), cycloheximide (CHX). Following protein extraction and trypsinization, biological triplicates for each treatment conditions were labeled with tandem mass tags (TMT tags), indicated by the colors. Peptides were pooled together, fractionated offline using basic reverse-phase liquid chromatography (bRPLC), and then analyzed by MS/MS methods.

(**B**) Scatterplot of normalized log2 bicuculline/Bio-Epox treated compared to both bicuculline alone and bicuculline/Bio-Epox/cycloheximide, versus q-values (p-values after multiple comparisons testing). Representative examples of NMP-targets are highlighted in orange, compared to those targets that do not change by MS analysis with biotin-epoxomicin treatment shown in blue.

(**C**) Heat map of proteins differentially expressed in bicuculline/Bio-Epox treated compared to bicuculline and bicuculline/Bio-Epox/cycloheximide. Coloring indicated percentage of maximum fold change, refer to Methods for details on heat map generation. Top 60 statistically significant targets are shown.

(**D**) Individual targets are shown, with replicates in scatterplot format. Mean and s.e.m are graphed for each condition. $^{***}p < 0.001$, $q < 0.1$ (two-way ANOVA (p), adjusted for multiple corrections (q) for biotin-epoxomicin (BEp) treatment compared to other samples). NMP targets previously shown to be UPS targets in top row, orange. NMP targets previously uncharacterized with regards to degradation shown in second row, orange. Lower two rows in blue show previously validated activity-dependent UPS targets.

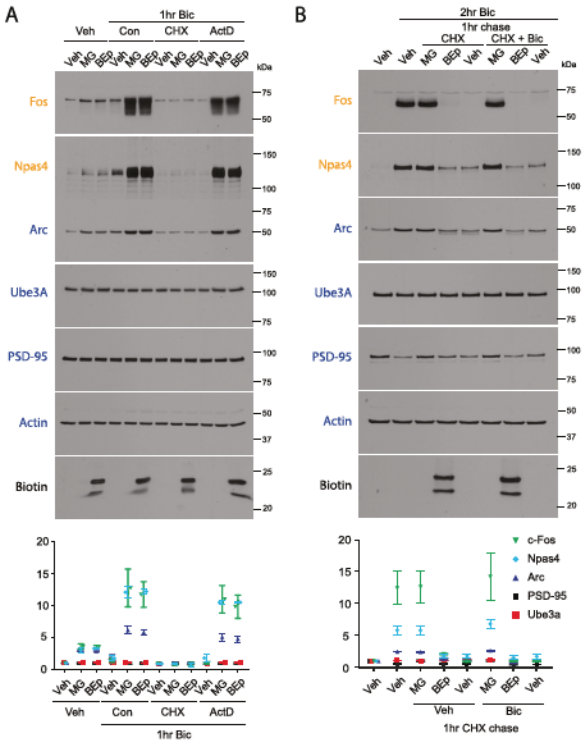


Figure 6. Ramachandran et al.

**Figure 4.11. Nascent, not full length, immediate-early gene products are activity-dependent NMP substrates.**

(**A**) Immediate-early gene (IEG) products are degraded by the NMP during bicuculline stimulation in a translation-dependent and transcription-independent manner. Primary cortical neurons treated with either MG-132 (MG) or biotin-epoxomicin (BEp) for 10 minutes. Indicated neurons were treated with 1 hour (hr) of bicuculline (Bic). Cycloheximide (CHX) applied only during proteasome inhibition, actinomycin D (ActD) and DMSO (Veh) applied during whole Bicuculline timecourse. Neuronal lysates were immunoblotted using antibodies against indicated proteins.

(**B**) Folded IEG protein is not degraded by the NMP, but is turned over by cytosolic proteasomes. Following 2 hours of bicuculline (Bic) treatment compared to DMSO alone (Veh), neurons were chased into cycloheximide (CHX) for one hour. Neurons treated with either DMSO or bicuculline

during CHX Chase. Each set was also treated with either MG-132 (MG), biotin-epoxomicin (BEp), or DMSO (Veh) during chase. Neuronal lysates were immunoblotted using antibodies against indicated proteins. For (A) and (B), protein names in orange classified as NMP targets in mass spectrometry data set (Fig 5), protein names in blue are not NMP targets based on MS data set. Representative immunoblots shown. Data are mean and s.e.m. of $n = 3$ experiments from independent neuronal cultures. Significance table presented in supplement Table S3.

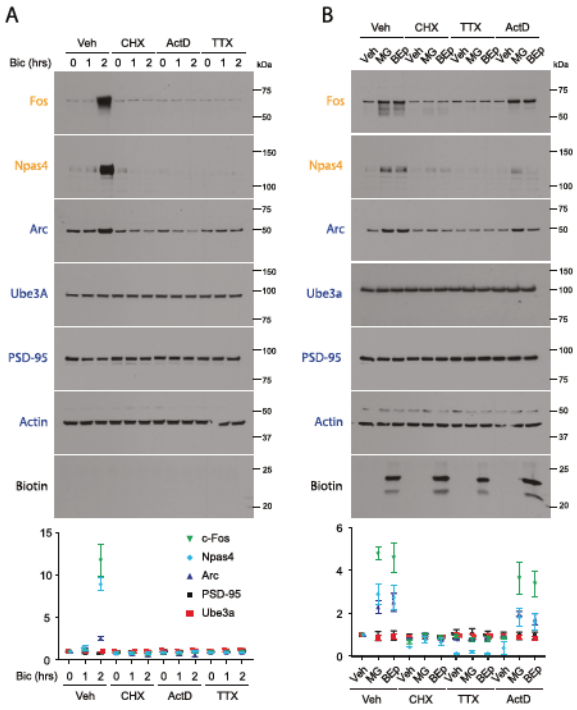


Supplemental Figure 6. Ramachandran et al.

**Figure 4.12: Immediate-early genes products are activity-dependent NMP substrates.**

(**A**) Primary cortical neurons at DIV15 treated with bicuculline (Bic) for indicated times. Treatment conditions above: DMSO (Veh), cycloheximide (CHX), actinomycin D (ActD), Tetrodotoxin (TTX). Treatments applied as indicated. Neuronal lysates were immunoblotted using antibodies against indicated proteins. Protein names in orange classified as NMP targets in mass spectrometry data set (Figure 3), protein names in blue not NMP targets based on MS data set. Representative immunoblots shown. Significance table presented in supplement.

(**B**) Primary cortical neurons at DIV15 treated with bicuculline (Bic) for 1 hour. Treatment conditions above: DMSO (Veh), cycloheximide (CHX), actinomycin D (ActD), Tetrodotoxin (TTX). MG-132 (MG) or biotin-epoxomicin (BEp) applied for final 10 minutes of 1 hour Bicuculline stimulation. Neuronal lysates were immunoblotted using antibodies against indicated

proteins. Protein names in orange classified as NMP targets in mass spectrometry data set (Fig 3), protein names in blue not NMP targets based on MS data set. Representative immunoblots shown. Significance table presented in supplement. For (A) and (B), protein names in orange classified as NMP targets in mass spectrometry data set (Figure 5), protein names in blue are not NMP targets based on MS data set. Representative immunoblots shown. Data are mean and s.e.m. of $n = 3$ experiments from independent neuronal cultures. Significance table presented in supplement Table S3.

# Chapter 5

## Peptides derived from the NMP can interact with activated neurons and may counteract aspects of neurodegenerative disease

NMP-generated peptides interact with stimulated neurons

Over the course of identifying the NMP complex and NMP-dependent peptide communication, we have done a huge number of experiments to try and gain further mechanistic insight into the function for this system. We thought that some of the most important would be to identify where and how the peptides were binding and interacting with neurons. Part of this was addressed using calcium imaging, where we found that NMP-derived peptides induced calcium signaling in both neurons and glial cells. Presumably, this calcium signal originates from cell-surface receptors on neurons and/or glial cells that bound these peptides and led to a secondary effect of opening calcium channels. We considered that in order for this to be true, we should be able to detect peptides bound to the surface of neurons or glial cells.

To test this directly, we first purified the peptides away from the cell culture media and then chemically modified them using biotin. NHS-Biotin selectively modifies exposed amines on peptides, such as N-termini or lysines. Following dialysis to remove the NHS-Biotin tag, we quantified the amount of biotin signal on the peptides and found a significant amount of biotin-modified peptides. This signal was greatly reduced in peptides purified from MG-132 treated neurons or from media that had previously been treated with Proteinase K. Following isolation and modification of these peptides, we applied them onto neurons that had been fixed, and visualized them using streptavidin-AF647 secondaries. We observed very little binding of peptides onto neurons under baseline conditions (Figure 5.1a). However, when we used the same protocol on neurons that had been stimulated with KCl for one minutes, we observed a significant amount of binding (Figure 5.1a). This was reduced back to background levels when we treated the modified peptide mixture with Proteinase K (figure 5.1a). Notably, we did not observe nuclear staining, leading us to propose that the majority of the observed staining was at the cell surface. We observed staining all along axons, dendrites, and at the soma.

Next, we modified our stimulation protocols to refine the role for neuronal activity in determining the interaction of these peptides with neurons. Instead of stimulating neurons en masse with KCl, we chose to use optogenetic methods to only stimulate a small subset of neurons. We transfected channelrhodopsin-2 into cortical neuronal cultures, which only labeled 1-2% of the total neurons in the culture. This sparse labeling and stimulation method would allow us to determine whether the stimulated neuron would be stained by the labeled NMP-mediated peptides, compared to unstimulated but adjacent cells. Following a 7Hz stimulation for one minute, neurons were fixed and stained using biotin-peptides and streptavidin as described before. Intriguingly, we observed biotin-peptide staining of both the ChR2-encoding neurons as well as a small percentage of neurons adjacent to the ChR2+ cells (Figure 5.1b). However, the majority of the cells surrounding the neurons remained unlabeled. We interpret these data to mean that the ChR2+ neuron, as well as the neurons innervated by the ChR2+ neurons, were stimulated and these biotin-peptides served as markers of neuronal stimulation. These data need to substantiated by additional experiments using TTX to inhibit neuronal transmission. This would substantiate the hypothesis that the staining observed in neurons adjacent to the ChR2+ neurons is because these cells are innervated by the ChR2+ cell. Of course, this also raises a fundamental question about how and why these peptides are selectively interacting with stimulated neurons over unstimulated cells. As we gain insight into what the peptides and receptors are, the answers to these questions should begin to be revealed over time.

Dysregulation of the NMP in AD and NMP-generated peptides protect against Abeta-induced toxicity in neurons

As previously discussed, proteasome-mediated protein degradation lies at the crux of a variety of neurodegenerative states. We wanted to distinguish changes in the NMP versus bulk proteasomes in neurodegenerative disease. To determine whether the NMP was dysregulated, separate from the cytosolic proteasome, we turned to the previously described surface

biotinylation assay. We used different models to induce Abeta-mediated effects, including Abeta 1-42 incubation in cultured neurons as well as monitoring the NMP in AD mouse models and in postmortem human brain samples. First, to determine the effects of Aβ on cultured neurons, we treated DIV16 mouse cortical neurons with oligomerized soluble $A\beta_{1-42}$. Following overnight treatment, neurons were surface biotinylated and analyzed for NMP expression. Compared to Abetascrambled controls, we observed a greater than 50% decrease in NMP expression in Abeta1-42 treated neurons (Figure 5.2a). We next decided to move our findings to mouse models of Alzheimer's, where proteasome expression and activity has been shown to be dysregulated. Transgenic mice overexpressing human amyloid precursor protein (hAPP) with familial AD mutations result in high levels of Aβ production in the brain (Cisse et al. 2011; Sell, Schaffer, and Margolis 2017). Consistent with our findings that exogenous addition of Aβ leads to decreased levels of the NMP, we observed a similar magnitude decrease of the NMP from hippocampi of hAPP mice compared to WT littermate controls. Finally, we extended these findings to human patients. We obtained tissue from the cortex of AD patients at advanced Braak stages. When we conducted this analysis, we were blinded to the patient samples. Once again consistent with our previous data, we observed a significant downregulation of the NMP in AD patient samples compared to unaffected individuals (Figure 5.2b). Cumulatively, we believe that these data provide compelling evidence that the NMP is dysregulated in AD.

The consequences of losing the NMP in the membrane could either be 1) an elevation in NMP substrate or set of substrates or 2) a significant reduction in NMP-mediated peptides. We chose to test the peptide hypothesis, simply because it would be far easier to test the peptide hypothesis versus the substrate hypothesis. Considering we could purify NMP-generated peptides, we first tested whether these peptides could relieve the deleterious effects of abeta. In order for abeta to enact its effects, multiple groups have shown that it binds to the cell surface of neurons through particular receptors, such as EphB2 and NMDARs (Cisse et al., 2011; Dalva et

al., 2000). Therefore as a first pass experiment, we incubated neurons with fluorescently labeled abeta, which binds to neurons as an initiating event that cascades into neurodegeneration. We observed punctate staining as previously shown, largely due to interactions with synaptic molecules. We next perfused in peptides in a dose-dependent fashion, with the middle concentration being the endogenous concentration (50ng/mL). We observed a dose-dependent reduction in abeta signal on neurons in response to NMP-derived peptides (Figure 5.3a). Pretreatment of NMP-derived peptides with proteinase K eliminated the capacity to reduce abeta-neuron interactions (Figure 5.3a). These data indicate that NMP-derived peptides either 1) directly compete with Abeta binding at the receptor level or 2) bind Abeta directly, thereby sequestering the Abeta and reducing the interactions with surface receptors on neurons.

While the mechanism by which NMP-derived peptides reduces the interactions between Abeta and neurons remains to be elucidated, we wanted to determine whether this would be sufficient to alleviate molecular aspects of neurodegeneration. A variety of pathways have been shown to be downstream of abeta binding, prior to neuronal death. As an example, Creb has shown to be de-phosphorylated, while c-Jun and Erk1/2 are phosphorylated in response to abeta(Vitolo et al. 2002; Morishima et al. 2001; Chong et al. 2006). This change in Erk1/2 phosphorylation also induces a change in cleaved caspase 3 levels. Finally, the surface levels of EphB2 have been reproducibly downregulated in response to Abeta. We tested all of these effects in our model in the presence of either NMP-derived peptides or those pretreated with Abeta or Abeta scrambled. As a control, we pretreated peptides with proteinase K. In these control experiments, we reproduced the effects of Abeta on CREB, Erk1/2, c-Jun, Caspase-3, and surface EphB2 (Figure 5.3b). By every measure, we observed that the addition of NMP-derived peptides protected against the deleterious effects of Abeta compared to addition of PK-NMP peptides (Figure 5.3b). Taken together with the fluorescent Abeta binding experiments, we believe that these data indicate that NMP-derived peptides can compete against the effects of abeta. Overall, we predict that in healthy individuals, NMP-derived peptides protect against the effects of abeta,

and potentially other disorders of protein aggregation. In pathological states such as in AD, the levels of the NMP are significantly downregulated. This leads to a downregulation of the protective peptides, allowing abeta to enact its deleterious effects. While these data are highly preliminary and only a speculative hypothesis, we believe that delving into the mechanisms of how abeta and the NMP interact will be important to understand the etiology and progression of AD.

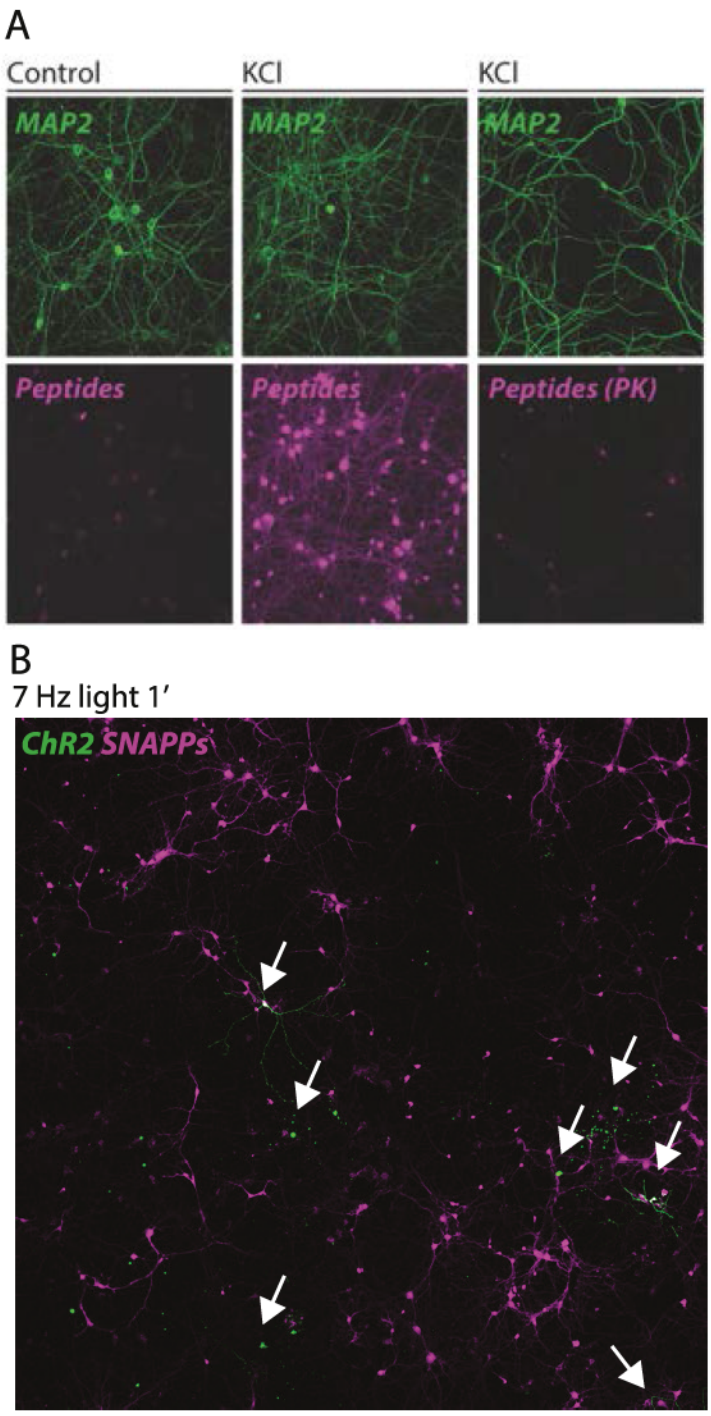


**Figure 5.1. Stimulation-dependent NMP-derived peptides (SNAPPs) label activated neurons**

(**a**) Labeled SNAPPs preferentially bind stimulated neurons. Unstimulated (control) or stimulated (KCl) neurons were fixed and stained with MAP2 (Green) and biotin-labeled SNAPPs (Magenta). Pretreatment of SNAPPs with Proteinase K abolishes their binding capacity.

(**b**) Channelrhodopsin (ChR2) transfected neurons were stimulated at the indicated frequency for one minute, fixed, and stained with an anti-GFP antibody that is reactive against ChR2 protein (Green) and labeled SNAPPs (Magenta). Pretreatment of SNAPPs with Proteinase K abolishes their binding capacity.

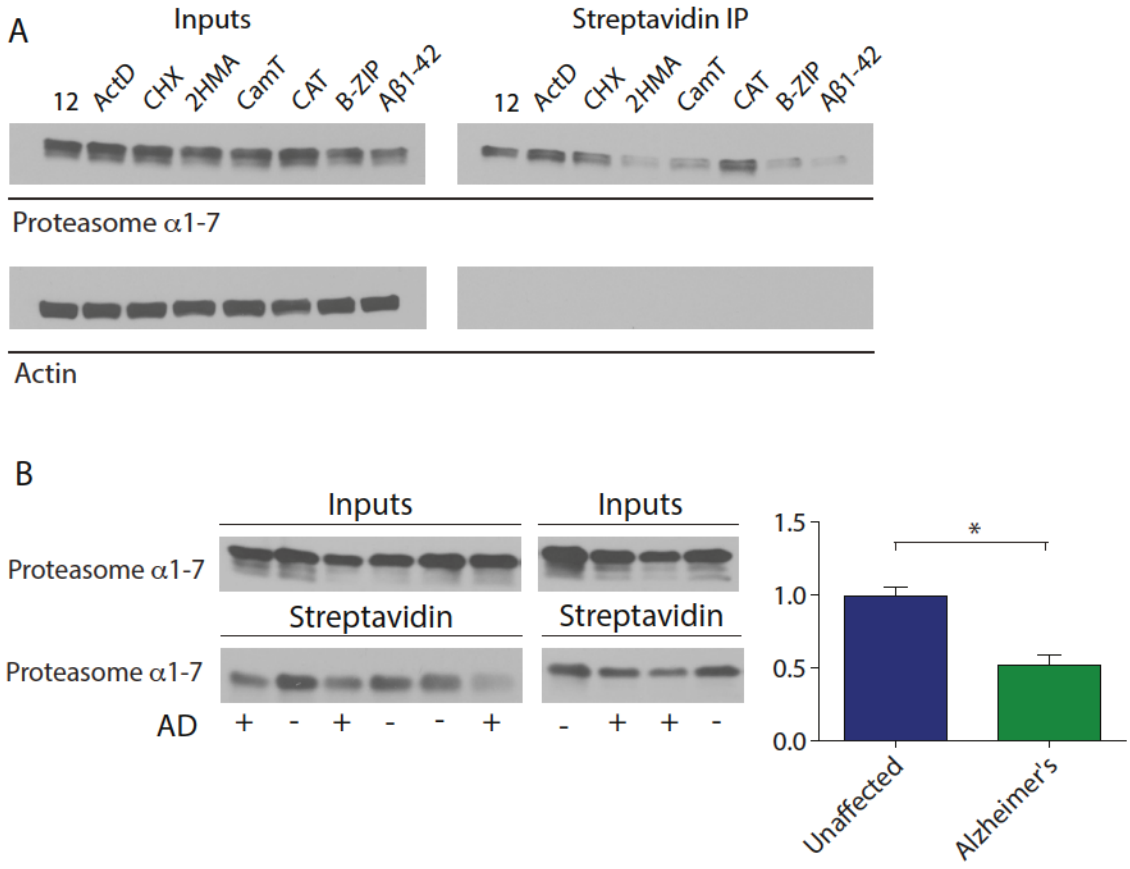


**Figure 5.2. Dysregulation of NMP localization under pathological states such as in AD**

(**a**) A variety of cellular processes are required for expression of the neuronal membrane proteasome. Indicated drugs were added between to DIV12 neurons overnight, and then processed for surface biotinylation. Div 12 (12), Actinomycin D(ActD), Cyclohexamide (CHX), 2 hydroxy-myristic acid (2HMA), Autocamtide (CamT), CNQX/APV/TTX (CAT)., B-ZIP, and Abeta1-42 (Aβ1–42). Inhibitors are discussed further in the methods.

(**b**) Postmortem patient brains were subjected to surface biotinylation and analyzed for NMP expression. Samples were unblinded following analysis and samples obtained from AD patients brains are denoted with (+). Quantificaiton to the right, student's t-test ($p<.01$).

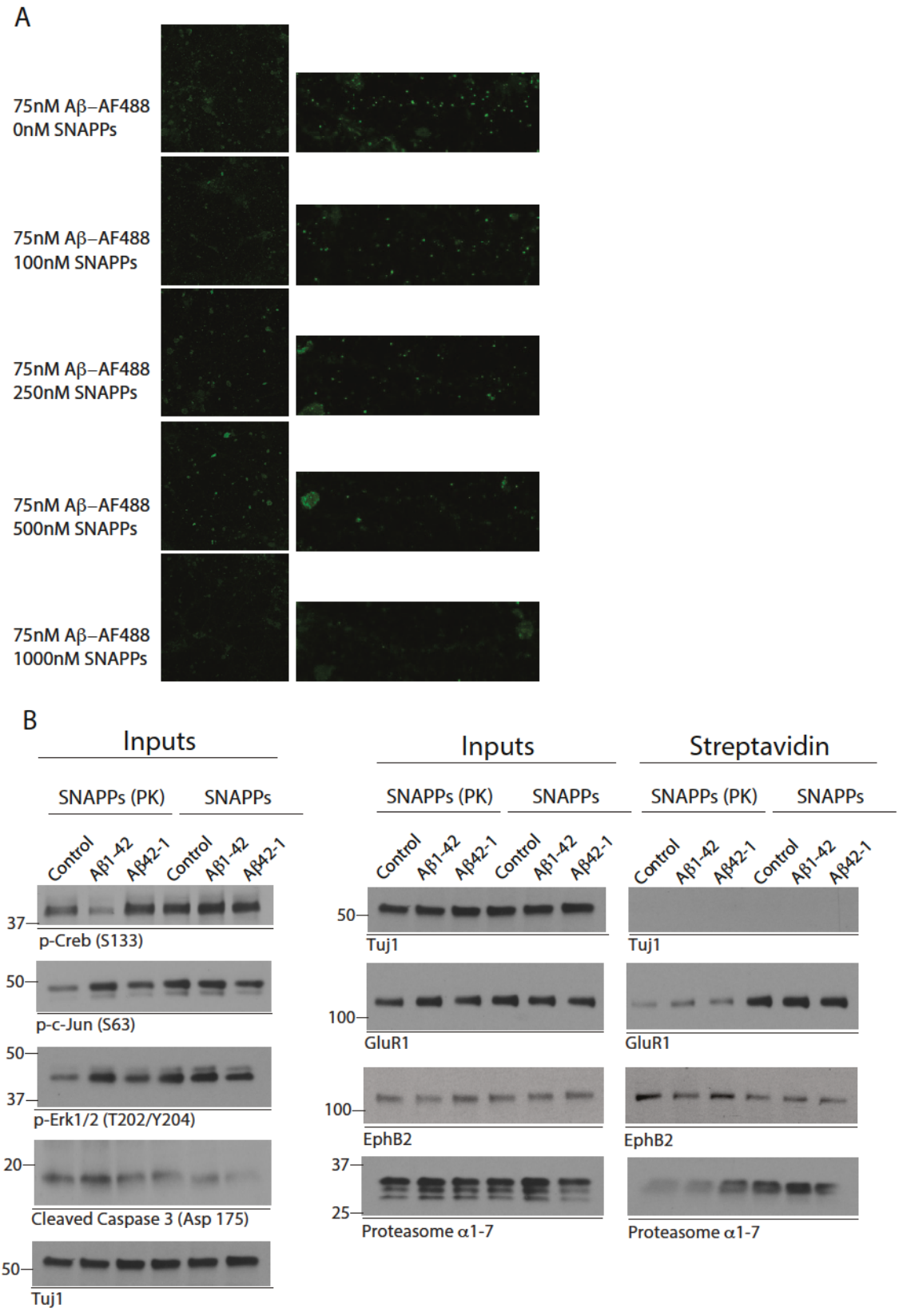
A
75nM Aβ–AF488
0nM SNAPPs
75nM Aβ–AF488
100nM SNAPPs
75nM Aβ–AF488
250nM SNAPPs
75nM Aβ–AF488
500nM SNAPPs
75nM Aβ–AF488
1000nM SNAPPs
B
Inputs
SNAPPs (PK)
SNAPPs
Control
Aβ1-42
Aβ42-1
37
p-Creb (S133)
50
p-c-Jun (S63)
50
37
p-Erk1/2 (T202/Y204)
20
Cleaved Caspase 3 (Asp 175)
50
Tuj1
Inputs
Streptavidin
50
Tuj1
100
GluR1
100
EphB2
37
25
Proteasome α1-7

**Figure 5.3. Stimulation-induced NMP-dependent peptides (SNAPPs) protect against Aβ1-42 binding and downstream molecular cascades**

(**a**) DIV16 primary cortical neurons were treated with indicated concentrations of fluorescently labeled Aβ1–42 for four hours and then indicated concentrations of SNAPPs for an additional two hours. Neurons were washed and then fixed and stained to assess Aβ1–42 binding. Images to right are magnified from zoomed out image to left. Puncta indicate sites of Aβ1–42 binding.

(**b**) Representative western blots from primary cultured neurons treated with 1μM Aβ1–42 or Aβ42-1 for 24 hours, and 250ng SNAPPs for the final four hours. SNAPPs (PK) were pretreated with Proteinase K to remove all peptide material. Inputs and streptavidin pulldowns to the right were done from neurons treated as described and then surface biotinylated and lysed.

# Chapter 6

Discussion

First, we identify a 20S plasma membrane bound proteasome that is unique to neurons in the mammalian nervous system. Based on our studies we conclude that the protein synthesis and NMP protein degradation machinery are cooperating to mediate neuronal activity-induced degradation of newly synthesized proteins. This process subsequently generates signaling peptides important for maintaining and enhancing neuronal activity dependent processes.

**6.1 Implications of 20S membrane proteasomes and ubiquitin-independent degradation**

Since the discovery of the proteasome and ubiquitin-dependent degradation, the vast majority of studies studying this have focused on 26S proteasome-mediated and ubiquitin dependent degradation. There are notable exceptions to this phenomenon. The majority of these studies have focused on specific substrates, largely under the class of intrinsically disordered proteins (IDPs)(Asher et al. 2005; Tsvetkov et al. 2008; Tsvetkov, Reuven, and Shaul 2009). These IDP proteins are characterized by large domains that are difficult to predict structurally or have high regions of disorder. Such proteins have been shown to undergo ubiquitin-independent degradation *in vitro* and to bind to the 20S proteasome(Tsurumi et al. 1995; Benaroudj et al. 2001; Zhang, Pickart, and Coffino 2003). However, the relevance for these mechanisms *in vivo* have been challenging to demonstrate since the role for 20S proteasomes, separately from 26S, has been impossible to test until now.

We have shown that neuronal plasma membrane proteasomes, by all measures, lack 19S subunits or any other cap structure. We believe that this likely indicates that the NMP is a 20S proteasome. Consistent with this, we have shown that treating neurons with the E1 inhibitor MLN-7243 has no effect on the activity-dependent degradation of substrates such as c-Fos or Npas4(Hyer et al. 2018). Therefore, we believe that the mechanism we reveal here of ubiquitin-independent degradation through 20S proteasomes may be a more generalizable phenomenon. While the precise mechanisms may be different, it is entirely possible that 20S proteasomes can degrade substrates in other cells. Whether those mechanisms are co-translational, as the one involved with the NMP, or whether they are post-translational is yet to be determined. Our data

demonstrating that co-translational degradation through 20S proteasomes can be reconstituted in vitro in rabbit reticulocyte lysate might suggest that the phenomenon is more generalizable. The plasma membrane tethering the NMP may simply provide a platform and a docking region for the ribosome to deliver substrates co-translationally. A good analogy to this process is with another membrane, at the endoplasmic reticulum(Brehme et al. 2014). Even more generally, the balance between 20S and 26S proteasomes in vivo needs to be clearly demonstrated in other systems. The NMP system is ideal because the 20S localization is distinct and uniquely separable. Recent studies indicate that the 20S at membranes is where all of the 20S is localized, and almost all of the proteasomes in the cytosol are 26S or capped by other structures(Erokhov et al. 2017).

The question of the whether the NMP is capped by any structures is still an open one. While we have not observed any of the canonical capping structures on the NMP, there are a variety of possibilities of how the NMP can be capped. First, there could be non-canonical caps such as lipid-based caps that have been previously proposed(Newman et al. 1996; Furuike et al. 2003; van Meer, Voelker, and Feigenson 2008). Lipid caps pose an especially interesting possibility since the NMP is localized to the plasma membrane. In vitro, proteasomes have been shown to orient perpendicularly to membranes specifically enriched in phosphatidylinositol (PI), a key signaling phospholipid that is notably enriched in the nervous system over other tissues (Newman et al. 1996; Furuike et al. 2003; van Meer, Voelker, and Feigenson 2008). Other non-canonical caps could include binding partners of the NMP, which actually act as caps. Whether proteins such as GPM6 or other binding partners could serve such a role needs to be clearly demonstrated. Ultimately, rigorous biochemical approaches together with structural approaches will be able to clarify these questions.

In addition to the function of proteasomes and the NMP under normal conditions, the role for proteasomes in pathological states has been under recent and heavy investigation. Certainly, a large amount of evidence has been generated regarding the role for ubiquitin in amyloidogenic diseases(Kazee and Han 1995; Lopez Salon et al. 2000; Wilson et al. 2011; Ben Yehuda et al.

2017; Bence, Sampat, and Kopito 2001; Bennett et al. 2007; Hipp et al. 2012; Iwata et al. 2005). In addition, proteasome dysfunction has also been correlated with a large variety of neurodegenerative and neurodevelopmental diseases. In some cases such as with Angelman Syndrome, mutations in Ube3A (an E3 Ubiquitin ligase) can be causative and central to the etiology of the disease(Albrecht et al. 1997; Sell and Margolis 2015). In the case of mutant huntingtin, polyQ expanded Huntingtin can inhibit the proteasome but also can enact a large variety of other effects(Hipp et al. 2012; Iwata et al. 2005; Bence, Sampat, and Kopito 2001; Ortega, Diaz-Hernandez, and Lucas 2007; Wade et al. 2014). A similar principle to Huntingtin holds for the mechanisms underlying Abeta-induced effects in AD. Of those mechanisms which perturb the proteasome degradation system under pathological states, most are attributed to dysregulation of the ubiquitin-proteasome system. However, our discovery of the 20S NMP necessitates a re-evaluation of these interpretations, and a differentiation of what system is indeed dysregulated. As an example, we show that the NMP is selectively dysregulated in AD, in contrast to the total or cytosolic proteasome. In further support of NMP-dependent mechanisms in disease states, we found that the NMP-derived peptides have unique functions in modulating AD phenotypes in cultured neurons. Not only did the peptides seemingly outcompete Abeta binding to neurons, but they also seemed to alleviate the initiating molecular events characteristic of Abeta-induced neurodegeneration. Further work will be necessary to identify how precisely these peptides compete with Abeta. Specifically, Abeta could either be bound and sequestered by these peptides in its monomeric form, or Abeta could be directly competed for at its binding sites. Finally, more generally, both protein synthesis and protein degradation play critical roles in a variety of disease states. Since NMP-mediated degradation couples these two major systems, any system that perturbs either protein synthesis or protein degradation could affect NMP-mediated co-translational degradation. Therefore, a full evaluation of NMP-dependent effects in many disease states is essential.

### 6.2 Coordination between protein translation and degradation

Based on our studies we conclude that the translation and degradation machinery are cooperating to mediate neuronal activity-induced degradation of newly synthesized proteins. This is, at least in part, mediated through a neuronal membrane proteasome in order to produce signaling peptides important for maintaining and enhancing neuronal activity dependent processes. Several groups have demonstrated stimulation-induced enhancement of proteasomal degradation(Ehlers 2003; Patrick et al. 2003; Bingol and Schuman 2006). Consistent with these findings, we observe that stimulation enhances the rate of proteasomal turnover of proteins labeled under baseline conditions. This previously defined experimental approach assesses the role of proteasomal degradation similar to work previously done in the immune system. We believed that studying the coordination of these two processes would be highly relevant for neuronal function, as this cooperation has recently been demonstrated to underlie various forms of synaptic plasticity. This change in our protocol allowed us to capture a robust coordination of the protein synthesis and degradation machinery and thus provided biochemical evidence for this previously hypothesized coordination. Based on our data we believe that neuronal activity does not simply promote global protein degradation, but rather promotes protein degradation exclusively of newly synthesized proteins. Moreover, our data are consistent with and provide insight into why acute proteasomal inhibition increases the expression level of proteins whose translation is dependent upon neuronal stimulation, i.e. immediate early genes(Mabb et al. 2014; Xia et al. 1996; Lin et al. 2008). Our hypothesis that the NMP degrades newly synthesized proteins was refined by our observations that ribosome-associated tRNA-bound nascent chains were targeted to the NMP in response to neuronal activity. This degradation of nascent chains seemed to occur independent of ubiquitylation. In addition, the degradation was selective for the nascent polypeptides, instead of the fully folded proteins. Substrates were only targeted during stimulation, as nascent chains and not as full-length proteins, all independent of ubiquitylation.

The role for the NMP in mediating neuronal function is likely driven through the production of extracellular proteasome-derived signaling peptides. Addition of purified proteasome-derived peptides had the opposite effect of inhibiting the NMP, driving neuronal stimulation. These data demonstrate that the peptides themselves are capable of inducing neuronal signaling, and likely serve as the means by which the NMP enacts its cellular functions. Our findings reveal that the proteasome does not simply act as a disposal mechanism, but can operate as a direct signaling complex, giving degraded proteins new life in the form of biologically meaningful peptides. Indeed, our studies harken back to seminal studies in the immune system that found tissue-specific proteasomes degrade proteins to make peptides that are essential for immune signaling (Rock et al., 1994; Schubert et al., 2000). These findings add to the growing interest in the molecular overlap between the immune system and nervous system. More broadly, the concept that tissue-specific proteasomes exist as direct signaling complexes may be a principle found in other cellular systems and is likely a new dogma in cellular signaling. Equally intriguing is the possibility that proteasomes are capable of associating with the peptide presentation machinery in the immune system, potentially lending credence to the hypothesis that NMP-derived peptides associate with MHC complexes in the nervous system(Rock et al. 1994; Huh et al. 2000; Shatz 2009; Freudenburg et al. 2013; Anton and Yewdell 2014; Winter et al. 2017). We believe that given the role for the NMP in generating peptides, understanding the mechanisms by which the NMP is expressed at the plasma membrane and the dynamics of this complex at the membrane will be critical for parsing out the role of peptides in neuronal signaling. While the mechanisms in the immune system and nervous system have many similarities, there are already key differences based on our knowledge of the two mechanisms. First, the immune mechanism relies on the loading of immunoproteasome-generated peptides onto functional TAP transporters(Murata, Takahama, and Tanaka 2008; Freudenburg et al. 2013; Basler, Kirk, and Groettrup 2013). These TAPs load the antigenic peptide onto the MHCs in the ER, and this loaded complex is then trafficked to the

plasma membrane. This is a purely constitutive process that by all measures relies on ubiquitylation, like of folded proteins. It is not clear if the mechanism occurs using nascent polypeptides or with folded proteins. In the neuronal mechanism, the proteasome is itself extracellular exposed, generating the polypeptides directly into the extracellular space. TAP-mediated loading is likely not at play in neurons. The process is also entirely regulated by neuronal activity, so not constitutive in the same sense. Finally, the neuronal mechanism degrades specifically and only the nascent chain, and not full length proteins, independent of ubiquitylation.

One fundamental question is where NMP-mediated degradation of nascent chains occurs. The substrates that we have identified are not only transcription factors that are largely expressed at the soma, but also proteins that show synaptic expression. Our immunocytochemistry and immunogold EM data against the NMP are not consistent with somatic localization, but only with dendritic, synaptic, and axonal localization. Therefore, this raises the question about whether the transcripts encoding NMP targets are localized to dendritic and synaptic regions. These questions will be critical to address moving forward. Moreover, there are clear outstanding questions about how activity initiates the translation and degradation of NMP substrates. A few studies have reported that neuronal activity can activate stalled ribosomes in neurons(Graber et al. 2013). An additional mechanism involves the translation of RNAs that are held in ribonucleoprotein granules. Recent evidence suggests that some of the transcripts within these granules are translated upon neuronal activity(Protter and Parker 2016). These different mechanisms may contribute to how certain RNAs are localized to distal compartments and how they are differentially translated and degraded.

On the note of how the coordination and degradation are regulated, additional questions remain on how the ribosome itself, or at least the tRNA-bound nascent chain, is targeted to the NMP. If active translation is occurring and those nascent chains are being fed into the NMP, how

do the ribosomes dock to the NMP? One would predict the presence of an adaptor protein or complex that mediates this process. A good analogy to this process would be signal recognition particle (SRP)-mediated insertion of nascent chains into the ER membrane. This process is established as how membrane proteins are inserted into the ER membrane to insert polytopic membrane proteins. The other possibility is that the ribosome does not directly associate with the NMP, and rather the nascent chain is delivered through chaperones or other indirect mechanisms. In addition, is the ribosome itself targeted or is there some sequence determinant of the RNAs targeted to NMP-mediated co-translational degradation? Based on our data that nascent chains of Fos and other targets can be degraded co-translationally in vitro, we predict that there is some sequence or structural determinants within the RNA itself. There may also be some exposed or disordered domain that drives co-translational degradation through 20S proteasomes. The rabbit reticulocyte translation experiments rely on SDS-activated 20S proteasomes, which is obviously not physiological. Therefore, there must be some other mechanism to open the gates on the 20S proteasome, potentially through the previously discussed alternative capping mechanisms.

**6.3 NMP-mediated peptides and neuronal function**

Multiple studies have posited the coordination of protein synthesis and protein degradation based on inhibitor studies in electrophysiology experiments. In large part, groups have determined that this coordination underlies aspects of synaptic tagging, as well as LTP and LTD. However, this is one of the first to our knowledge that demonstrates a compelling biochemical coordination at the level of the substrates. It will be critical to determine whether activity-dependent coordination of translation and NMP degradation underlies previously observed electrophysiological studies. Perhaps the most interesting question will be whether the NMP-derived peptides or the degradation of nascent substrates is the relevant component for establishing the physiological function of this degradation mechanism. The answer to this question will also reveal why such a mechanism exists - if the peptides are relevant for the physiological function, NMP-mediated degradation is primarily for generating signaling

molecules, whereas if the degradation is the largely relevant component, then NMP-mediated degradation may serve to reduce the biochemical noise of the system. Regardless of the precise mechanism, the function of NMP-mediated degradation will be important to reveal and discriminate from all proteasomes.

We believe that neuronal activity-induced proteasomal degradation of a large fraction of newly synthesized proteins is for the express purpose of generating a new class of extracellular signaling peptides which are important for neuronal activity dependent processes. NMP-derived peptides are a new modality for neuronal communication. While the mechanisms by which NMP-derived peptides enact their signaling capacity are unknown, several possibilities include: 1) NMP-derived peptides interact with major histocompatibility immune complexes (MHC) that have recently been shown to play key roles in developmental and experience-dependent mechanisms in the nervous system; 2) NMP-derived peptides directly modulate ion channels altering calcium-mediated signaling; or 3) NMP-derived peptides signal to surrounding non-neuronal cells such as glial cells through yet to be identified receptors. Probing these possibilities, and others, will likely be an important new area of investigation. Despite this immediate knowledge, the use of labeled NMP-derived peptides to bind to and trace activated neurons within a circuit will likely have utility to neuronal circuit mapping in vivo and in vitro. While it is unclear how NMP-derived peptides mediate their signaling function, our data demonstrate that the mechanism by which they are released is through the NMP. Genetic and biochemical experiments to determine the receptors to which these peptides bind to and interact with will be critical to elucidate the function of this mechanism.

Many groups have demonstrated that acute and rapid inhibition of the proteasome has profound effects on synaptic signaling and transmission. These effects range from changes in transmission at the Drosophila neuromuscular synapse, regulation of activity-dependent spine dynamics, and an essential role in maintenance of LTP and LTD(Campbell and Holt 2001; Rinetti and Schweizer 2010; Ostroff et al. 2002; Fonseca et al. 2006; Fonseca, Nagerl, and Bonhoeffer

2006; Kelleher, Govindarajan, and Tonegawa 2004; Klein, Castillo, and Jordan 2015). We see a similar rapid and acute role for the NMP in mediating peptide release and in modulation of activity-dependent calcium signaling. Neuronal calcium signaling is tightly regulated whereby even small changes in amplitude or frequency result in significant effects on nervous system function. Previous studies indicate that bicuculline-mediated neuronal stimulation synchronizes calcium transients within a neural network(Patel et al. 2015). These alterations in the dynamics of calcium transients have been shown to have an electrophysiological basis. While bicuculline also promotes proteasomal degradation, the role of the proteasome in activity-dependent calcium signaling has not been well studied(Djakovic et al. 2009; Wu, Hyrc, et al. 2009). Our study is the first to identify a critical role for the proteasome in the form of the NMP in mediating Bicuculline-induced changes in calcium signaling. Our data also indicate that resting calcium levels are unaffected by NMP inhibition, suggesting that it is only the activity-dependent aspects of calcium signaling that are altered with inhibition of the NMP. This is consistent with data from prior studies that observe no appreciable rapid effect on calcium levels with inhibition of total proteasomes. Taken together, neuronal stimulation drives proteasomal degradation of newly translated proteins through the NMP. This leads to the production of NMP-derived peptides which, by interacting with nearby activated neurons, promote feedforward regulation of neural network activity. The role and function of the NMP and NMP-derived peptides remain an open and entirely new area of study in neuroscience.

## Bibliography

Aakalu, G., W. B. Smith, N. Nguyen, C. Jiang, and E. M. Schuman. 2001. 'Dynamic visualization of local protein synthesis in hippocampal neurons', *Neuron*, 30: 489-502.

Adler, J., N. Reuven, C. Kahana, and Y. Shaul. 2010. 'c-Fos proteasomal degradation is activated by a default mechanism, and its regulation by NAD(P)H:quinone oxidoreductase 1 determines c-Fos serum response kinetics', *Mol Cell Biol*, 30: 3767-78.

Albanese, V., S. Reissmann, and J. Frydman. 2010. 'A ribosome-anchored chaperone network that facilitates eukaryotic ribosome biogenesis', *J Cell Biol*, 189: 69-81.

Alberts B, Johnson A, Lewis J, et al. 2002. 'The Shape and Structure of Proteins.' in, *Molecular Biology of the Cell* (Garland Science: New York).

Albrecht, U., J. S. Sutcliffe, B. M. Cattanach, C. V. Beechey, D. Armstrong, G. Eichele, and A. L. Beaudet. 1997. 'Imprinted expression of the murine Angelman syndrome gene, Ube3a, in hippocampal and Purkinje neurons', *Nat Genet*, 17: 75-8.

Anton, L. C., and J. W. Yewdell. 2014. 'Translating DRiPs: MHC class I immunosurveillance of pathogens and tumors', *J Leukoc Biol*, 95: 551-62.

Asano, S., Y. Fukuda, F. Beck, A. Aufderheide, F. Forster, R. Danev, and W. Baumeister. 2015. 'Proteasomes. A molecular census of 26S proteasomes in intact neurons', *Science*, 347: 439-42.

Asher, G., Z. Bercovich, P. Tsvetkov, Y. Shaul, and C. Kahana. 2005. '20S proteasomal degradation of ornithine decarboxylase is regulated by NQO1', *Mol Cell*, 17: 645-55.

Bae, M. H., C. H. Jeong, S. H. Kim, M. K. Bae, J. W. Jeong, M. Y. Ahn, S. K. Bae, N. D. Kim, C. W. Kim, K. R. Kim, and K. W. Kim. 2002. 'Regulation of Egr-1 by association with the proteasome component C8', *Biochim Biophys Acta*, 1592: 163-7.

Balchin, D., M. Hayer-Hartl, and F. U. Hartl. 2016. 'In vivo aspects of protein folding and quality control', *Science*, 353: aac4354.

Basler, M., C. J. Kirk, and M. Groettrup. 2013. 'The immunoproteasome in antigen processing and other immunological functions', *Curr Opin Immunol*, 25: 74-80.

Ben Yehuda, A., M. Risheq, O. Novoplansky, K. Bersuker, R. R. Kopito, M. Goldberg, and M. Brandeis. 2017. 'Ubiquitin Accumulation on Disease Associated Protein Aggregates Is Correlated with Nuclear Ubiquitin Depletion, Histone De-Ubiquitination and Impaired DNA Damage Response', *PLoS One*, 12: e0169054.

Ben-Nissan, G., and M. Sharon. 2014. 'Regulating the 20S proteasome ubiquitin-independent degradation pathway', *Biomolecules*, 4: 862-84.

Benaroudj, N., E. Tarcsa, P. Cascio, and A. L. Goldberg. 2001. 'The unfolding of substrates and ubiquitin-independent protein degradation by proteasomes', *Biochimie*, 83: 311-8.

Bence, N. F., R. M. Sampat, and R. R. Kopito. 2001. 'Impairment of the ubiquitin-proteasome system by protein aggregation', *Science*, 292: 1552-5.

Bengtson, M. H., and C. A. Joazeiro. 2010. 'Role of a ribosome-associated E3 ubiquitin ligase in protein quality control', *Nature*, 467: 470-3.

Bennett, E. J., T. A. Shaler, B. Woodman, K. Y. Ryu, T. S. Zaitseva, C. H. Becker, G. P. Bates, H. Schulman, and R. R. Kopito. 2007. 'Global changes to the ubiquitin system in Huntington's disease', *Nature*, 448: 704-8.

Benoist, F., and T. Grand-Perret. 1997. 'Co-translational degradation of apolipoprotein B100 by the proteasome is prevented by microsomal triglyceride transfer protein.

Synchronized translation studies on HepG2 cells treated with an inhibitor of microsomal triglyceride transfer protein', *J Biol Chem*, 272: 20435-42.

Bergado, J. A., C. I. Fernandez, A. Gomez-Soria, and O. Gonzalez. 1997. 'Chronic intraventricular infusion with NGF improves LTP in old cognitively-impaired rats', *Brain Res*, 770: 1-9.

Besche, H. C., and A. L. Goldberg. 2012. 'Affinity purification of mammalian 26S proteasomes using an ubiquitin-like domain', *Methods in molecular biology*, 832: 423-32.

Besche, H. C., W. Haas, S. P. Gygi, and A. L. Goldberg. 2009. 'Isolation of mammalian 26S proteasomes and p97/VCP complexes using the ubiquitin-like domain from HHR23B reveals novel proteasome-associated proteins', *Biochemistry*, 48: 2538-49.

Bingol, B., and E. M. Schuman. 2006. 'Activity-dependent dynamics and sequestration of proteasomes in dendritic spines', *Nature*, 441: 1144-8.

Blomen, V. A., P. Majek, L. T. Jae, J. W. Bigenzahn, J. Nieuwenhuis, J. Staring, R. Sacco, F. R. van Diemen, N. Olk, A. Stukalov, C. Marceau, H. Janssen, J. E. Carette, K. L. Bennett, J. Colinge, G. Superti-Furga, and T. R. Brummelkamp. 2015. 'Gene essentiality and synthetic lethality in haploid human cells', *Science*, 350: 1092-6.

Bodenstein, J., R. K. Sunahara, and R. R. Neubig. 2007. 'N-terminal residues control proteasomal degradation of RGS2, RGS4, and RGS5 in human embryonic kidney 293 cells', *Mol Pharmacol*, 71: 1040-50.

Bozdagi, O., T. Tavassoli, and J. D. Buxbaum. 2013. 'Insulin-like growth factor-1 rescues synaptic and motor deficits in a mouse model of autism and developmental delay', *Mol Autism*, 4: 9.

Brandman, O., J. Stewart-Ornstein, D. Wong, A. Larson, C. C. Williams, G. W. Li, S. Zhou, D. King, P. S. Shen, J. Weibezahn, J. G. Dunn, S. Rouskin, T. Inada, A. Frost, and J. S. Weissman. 2012. 'A ribosome-bound quality control complex triggers degradation of nascent peptides and signals translation stress', *Cell*, 151: 1042-54.

Brehme, M., C. Voisine, T. Rolland, S. Wachi, J. H. Soper, Y. Zhu, K. Orton, A. Villella, D. Garza, M. Vidal, H. Ge, and R. I. Morimoto. 2014. 'A chaperome subnetwork safeguards proteostasis in aging and neurodegenerative disease', *Cell Rep*, 9: 1135-50.

Cai, F., J. U. Frey, P. P. Sanna, and T. Behnisch. 2010. 'Protein degradation by the proteasome is required for synaptic tagging and the heterosynaptic stabilization of hippocampal late-phase long-term potentiation', *Neuroscience*, 169: 1520-6.

Campbell, D. S., and C. E. Holt. 2001. 'Chemotropic responses of retinal growth cones mediated by rapid local protein synthesis and degradation', *Neuron*, 32: 1013-26.

Carle, T. L., Y. N. Ohnishi, Y. H. Ohnishi, I. N. Alibhai, M. B. Wilkinson, A. Kumar, and E. J. Nestler. 2007. 'Proteasome-dependent and -independent mechanisms for FosB destabilization: identification of FosB degron domains and implications for DeltaFosB stability', *Eur J Neurosci*, 25: 3009-19.

Caterina, M. J., D. Hereld, and P. N. Devreotes. 1995. 'Occupancy of the Dictyostelium cAMP receptor, cAR1, induces a reduction in affinity which depends upon COOH-terminal serine residues', *The Journal of biological chemistry*, 270: 4418-23.

Chen, X., J. M. Levy, A. Hou, C. Winters, R. Azzam, A. A. Sousa, R. D. Leapman, R. A. Nicoll, and T. S. Reese. 2015. 'PSD-95 family MAGUKs are essential for anchoring AMPA and NMDA receptor complexes at the postsynaptic density', *Proc Natl Acad Sci U S A*, 112: E6983-92.

Chong, Y. H., Y. J. Shin, E. O. Lee, R. Kayed, C. G. Glabe, and A. J. Tenner. 2006. 'ERK1/2 activation mediates Abeta oligomer-induced neurotoxicity via caspase-3 activation and tau cleavage in rat organotypic hippocampal slice cultures', *J Biol Chem*, 281: 20315-25.

Chu, J., N. A. Hong, C. A. Masuda, B. V. Jenkins, K. A. Nelms, C. C. Goodnow, R. J. Glynne, H. Wu, E. Masliah, C. A. Joazeiro, and S. A. Kay. 2009. 'A mouse forward genetics screen identifies LISTERIN as an E3 ubiquitin ligase involved in neurodegeneration', *Proc Natl Acad Sci U S A*, 106: 2097-103.

Ciechanover, A. 1998. 'The ubiquitin-proteasome pathway: on protein death and cell life', *The EMBO journal*, 17: 7151-60.

Ciechanover, A., and A. L. Schwartz. 1998. 'The ubiquitin-proteasome pathway: the complexity and myriad functions of proteins death', *Proceedings of the National Academy of Sciences of the United States of America*, 95: 2727-30.

Cisse, M., B. Halabisky, J. Harris, N. Devidze, D. B. Dubal, B. Sun, A. Orr, G. Lotz, D. H. Kim, P. Hamto, K. Ho, G. Q. Yu, and L. Mucke. 2011. 'Reversing EphB2 depletion rescues cognitive functions in Alzheimer model', *Nature*, 469: 47-52.

Colledge, M., E. M. Snyder, R. A. Crozier, J. A. Soderling, Y. Jin, L. K. Langeberg, H. Lu, M. F. Bear, and J. D. Scott. 2003. 'Ubiquitination regulates PSD-95 degradation and AMPA receptor surface expression', *Neuron*, 40: 595-607.

Collins, G. A., and A. L. Goldberg. 2017. 'The Logic of the 26S Proteasome', *Cell*, 169: 792-806.

Comyn, S. A., G. T. Chan, and T. Mayor. 2014. 'False start: cotranslational protein ubiquitination and cytosolic protein quality control', *J Proteomics*, 100: 92-101.

Coux, O., K. Tanaka, and A. L. Goldberg. 1996. 'Structure and functions of the 20S and 26S proteasomes', *Annual review of biochemistry*, 65: 801-47.

D'Amours, O., G. Frenette, M. Fortier, P. Leclerc, and R. Sullivan. 2010. 'Proteomic comparison of detergent-extracted sperm proteins from bulls with different fertility indexes', *Reproduction*, 139: 545-56.

Davydov, I. V., and A. Varshavsky. 2000. 'RGS4 is arginylated and degraded by the N-end rule pathway in vitro', *J Biol Chem*, 275: 22931-41.

de Poot, S. A. H., G. Tian, and D. Finley. 2017. 'Meddling with Fate: The Proteasomal Deubiquitinating Enzymes', *J Mol Biol*, 429: 3525-45.

Deglincerti, A., Y. Liu, D. Colak, U. Hengst, G. Xu, and S. R. Jaffrey. 2015. 'Coupled local translation and degradation regulate growth cone collapse', *Nat Commun*, 6: 6888.

Dieterich, D. C., J. J. Hodas, G. Gouzer, I. Y. Shadrin, J. T. Ngo, A. Triller, D. A. Tirrell, and E. M. Schuman. 2010. 'In situ visualization and dynamics of newly synthesized proteins in rat hippocampal neurons', *Nat Neurosci*, 13: 897-905.

Dieterich, D. C., A. J. Link, J. Graumann, D. A. Tirrell, and E. M. Schuman. 2006. 'Selective identification of newly synthesized proteins in mammalian cells using bioorthogonal noncanonical amino acid tagging (BONCAT)', *Proc Natl Acad Sci U S A*, 103: 9482-7.

Dimitrova, L. N., K. Kuroha, T. Tatematsu, and T. Inada. 2009. 'Nascent peptide-dependent translation arrest leads to Not4p-mediated protein degradation by the proteasome', *J Biol Chem*, 284: 10343-52.

Ding, Q., V. Cecarini, and J. N. Keller. 2007. 'Interplay between protein synthesis and degradation in the CNS: physiological and pathological implications', *Trends Neurosci*, 30: 31-6.

Ding, Q., E. Dimayuga, W. R. Markesbery, and J. N. Keller. 2006. 'Proteasome inhibition induces reversible impairments in protein synthesis', *FASEB J*, 20: 1055-63.

Dittmar, K. A., J. M. Goodenbour, and T. Pan. 2006. 'Tissue-specific differences in human transfer RNA expression', *PLoS Genet*, 2: e221.

Djakovic, S. N., L. A. Schwarz, B. Barylko, G. N. DeMartino, and G. N. Patrick. 2009. 'Regulation of the proteasome by neuronal activity and calcium/calmodulin-dependent protein kinase II', *The Journal of biological chemistry*, 284: 26655-65.

Dong, C., S. C. Upadhya, L. Ding, T. K. Smith, and A. N. Hegde. 2008. 'Proteasome inhibition enhances the induction and impairs the maintenance of late-phase long-term potentiation', *Learning & memory*, 15: 335-47.

Doyle, S. M., O. Genest, and S. Wickner. 2013. 'Protein rescue from aggregates by powerful molecular chaperone machines', *Nat Rev Mol Cell Biol*, 14: 617-29.

Duttler, S., S. Pechmann, and J. Frydman. 2013. 'Principles of cotranslational ubiquitination and quality control at the ribosome', *Mol Cell*, 50: 379-93.

Ehlers, M. D. 2000. 'Reinsertion or degradation of AMPA receptors determined by activity-dependent endocytic sorting', *Neuron*, 28: 511-25.

———. 2003. 'Activity level controls postsynaptic composition and signaling via the ubiquitin-proteasome system', *Nature neuroscience*, 6: 231-42.

Erokhov, P. A., Y. V. Lyupina, A. S. Radchenko, A. A. Kolacheva, Y. O. Nikishina, and N. P. Sharova. 2017. 'Detection of active proteasome structures in brain extracts: proteasome features of August rat brain with violations in monoamine metabolism', *Oncotarget*, 8: 70941-57.

Etlinger, J. D., and A. L. Goldberg. 1977. 'A soluble ATP-dependent proteolytic system responsible for the degradation of abnormal proteins in reticulocytes', *Proc Natl Acad Sci U S A*, 74: 54-8.

Ettari, R., M. Zappala, S. Grasso, C. Musolino, V. Innao, and A. Allegra. 2017. 'Immunoproteasome-selective and non-selective inhibitors: A promising approach for the treatment of multiple myeloma', *Pharmacol Ther*.

Finley, D., A. Ciechanover, and A. Varshavsky. 2004. 'Ubiquitin as a central cellular regulator', *Cell*, 116: S29-32, 2 p following S32.

Fletcher, B. R., G. S. Hill, J. M. Long, M. Gallagher, M. L. Shapiro, and P. R. Rapp. 2014. 'A fine balance: Regulation of hippocampal Arc/Arg3.1 transcription, translation and degradation in a rat model of normal cognitive aging', *Neurobiol Learn Mem*, 115: 58-67.

Flexner, J. B., and L. B. Flexner. 1967. 'Restoration of expression of memory lost after treatment with puromycin', *Proc Natl Acad Sci U S A*, 57: 1651-4.

Flexner, J. B., L. B. Flexner, and E. Stellar. 1963. 'Memory in mice as affected by intracerebral puromycin', *Science*, 141: 57-9.

Flexner, J. B., L. B. Flexner, E. Stellar, G. De La Haba, and R. B. Roberts. 1962. 'Inhibition of protein synthesis in brain and learning and memory following puromycin', *J Neurochem*, 9: 595-605.

Flexner, L. B., and J. B. Flexner. 1968. 'Studies on memory: the long survival of peptidyl-puromycin in mouse brain', *Proc Natl Acad Sci U S A*, 60: 923-7.

Flexner, L. B., J. B. Flexner, R. B. Roberts, and G. Delahaba. 1964. 'Loss of Recent Memory in Mice as Related to Regional Inhibition of Cerebral Protein Synthesis', *Proc Natl Acad Sci U S A*, 52: 1165-9.

Flexner, L. B., P. Gambetti, J. B. Flexner, and R. B. Roberts. 1971. 'Studies on memory: distribution of peptidyl-puromycin in subcellular fractions of mouse brain', *Proc Natl Acad Sci U S A*, 68: 26-8.

Fonseca, R., U. V. Nagerl, and T. Bonhoeffer. 2006. 'Neuronal activity determines the protein synthesis dependence of long-term potentiation', *Nat Neurosci*, 9: 478-80.

Fonseca, R., R. M. Vabulas, F. U. Hartl, T. Bonhoeffer, and U. V. Nagerl. 2006. 'A balance of protein synthesis and proteasome-dependent degradation determines the maintenance of LTP', *Neuron*, 52: 239-45.

Fortin, D. A., M. A. Davare, T. Srivastava, J. D. Brady, S. Nygaard, V. A. Derkach, and T. R. Soderling. 2010. 'Long-term potentiation-dependent spine enlargement requires synaptic Ca2+-permeable AMPA receptors recruited by CaM-kinase I', *J Neurosci*, 30: 11565-75.

Freudenburg, W., M. Gautam, P. Chakraborty, J. James, J. Richards, A. S. Salvatori, A. Baldwin, J. Schriewer, R. M. Buller, J. A. Corbett, and D. Skowyra. 2013. 'Immunoproteasome Activation During Early Antiviral Response in Mouse Pancreatic beta-cells: New Insights into Auto-antigen Generation in Type I Diabetes?', *J Clin Cell Immunol*, 4.

Frydman, J., E. Nimmesgern, H. Erdjument-Bromage, J. S. Wall, P. Tempst, and F. U. Hartl. 1992. 'Function in protein folding of TRiC, a cytosolic ring complex containing TCP-1 and structurally related subunits', *EMBO J*, 11: 4767-78.

Frydman, J., E. Nimmesgern, K. Ohtsuka, and F. U. Hartl. 1994. 'Folding of nascent polypeptide chains in a high molecular mass assembly with molecular chaperones', *Nature*, 370: 111-7.

Fuchsova, B., M. E. Fernandez, J. Alfonso, and A. C. Frasch. 2009. 'Cysteine residues in the large extracellular loop (EC2) are essential for the function of the stress-regulated glycoprotein M6a', *J Biol Chem*, 284: 32075-88.

Furuike, S., J. Hirokawa, S. Yamada, and M. Yamazaki. 2003. 'Atomic force microscopy studies of interaction of the 20S proteasome with supported lipid bilayers', *Biochim Biophys Acta*, 1615: 1-6.

Gamerdinger, M., M. A. Hanebuth, T. Frickey, and E. Deuerling. 2015. 'The principle of antagonism ensures protein targeting specificity at the endoplasmic reticulum', *Science*, 348: 201-7.

Gao, J., M. Marosi, J. Choi, J. M. Achiro, S. Kim, S. Li, K. Otis, K. C. Martin, C. Portera-Cailliau, and P. Tontonoz. 2017. 'The E3 ubiquitin ligase IDOL regulates synaptic ApoER2 levels and is important for plasticity and learning', *Elife*, 6.

Gazula, V. R., J. G. Strumbos, X. Mei, H. Chen, C. Rahner, and L. K. Kaczmarek. 2010. 'Localization of Kv1.3 channels in presynaptic terminals of brainstem auditory neurons', *J Comp Neurol*, 518: 3205-20.

Gloge, F., A. H. Becker, G. Kramer, and B. Bukau. 2014. 'Co-translational mechanisms of protein maturation', *Curr Opin Struct Biol*, 24: 24-33.

Goldberg, A. L., and J. F. Dice. 1974. 'Intracellular protein degradation in mammalian and bacterial cells', *Annu Rev Biochem*, 43: 835-69.

Graber, T. E., S. Hebert-Seropian, A. Khoutorsky, A. David, J. W. Yewdell, J. C. Lacaille, and W. S. Sossin. 2013. 'Reactivation of stalled polyribosomes in synaptic plasticity', *Proc Natl Acad Sci U S A*, 110: 16205-10.

Groll, M., M. Bajorek, A. Kohler, L. Moroder, D. M. Rubin, R. Huber, M. H. Glickman, and D. Finley. 2000. 'A gated channel into the proteasome core particle', *Nature structural biology*, 7: 1062-7.

Ha, S. W., D. Ju, W. Hao, and Y. Xie. 2016. 'Rapidly Translated Polypeptides Are Preferred Substrates for Cotranslational Protein Degradation', *J Biol Chem*, 291: 9827-34.

Ha, S. W., D. Ju, and Y. Xie. 2014. 'Nuclear import factor Srp1 and its associated protein Sts1 couple ribosome-bound nascent polypeptides to proteasomes for cotranslational degradation', *J Biol Chem*, 289: 2701-10.

Haider, S., and R. Pal. 2013. 'Integrated analysis of transcriptomic and proteomic data', *Curr Genomics*, 14: 91-110.

Hanley, J. G., L. Khatri, P. I. Hanson, and E. B. Ziff. 2002. 'NSF ATPase and alpha-/beta-SNAPs disassemble the AMPA receptor-PICK1 complex', *Neuron*, 34: 53-67.

Hartl, F. U., A. Bracher, and M. Hayer-Hartl. 2011. 'Molecular chaperones in protein folding and proteostasis', *Nature*, 475: 324-32.

Hartman, M. C., K. Josephson, and J. W. Szostak. 2006. 'Enzymatic aminoacylation of tRNA with unnatural amino acids', *Proc Natl Acad Sci U S A*, 103: 4356-61.

Hipp, M. S., C. N. Patel, K. Bersuker, B. E. Riley, S. E. Kaiser, T. A. Shaler, M. Brandeis, and R. R. Kopito. 2012. 'Indirect inhibition of 26S proteasome activity in a cellular model of Huntington's disease', *J Cell Biol*, 196: 573-87.

Hoyt, M. A., M. Zhang, and P. Coffino. 2003. 'Ubiquitin-independent mechanisms of mouse ornithine decarboxylase degradation are conserved between mammalian and fungal cells', *J Biol Chem*, 278: 12135-43.

Huh, G. S., L. M. Boulanger, H. Du, P. A. Riquelme, T. M. Brotz, and C. J. Shatz. 2000. 'Functional requirement for class I MHC in CNS development and plasticity', *Science*, 290: 2155-9.

Hung, A. Y., C. C. Sung, I. L. Brito, and M. Sheng. 2010. 'Degradation of postsynaptic scaffold GKAP and regulation of dendritic spine morphology by the TRIM3 ubiquitin ligase in rat hippocampal neurons', *PLoS One*, 5: e9842.

Hyer, M. L., M. A. Milhollen, J. Ciavarri, P. Fleming, T. Traore, D. Sappal, J. Huck, J. Shi, J. Gavin, J. Brownell, Y. Yang, B. Stringer, R. Griffin, F. Bruzzese, T. Soucy, J. Duffy, C. Rabino, J. Riceberg, K. Hoar, A. Lublinsky, S. Menon, M. Sintchak, N. Bump, S. M. Pulukuri, S. Langston, S. Tirrell, M. Kuranda, P. Veiby, J. Newcomb, P. Li, J. T. Wu, J. Powe, L. R. Dick, P. Greenspan, K. Galvin, M. Manfredi, C. Claiborne, B. S. Amidon, and N. F. Bence. 2018. 'A small-molecule inhibitor of the ubiquitin activating enzyme for cancer treatment', *Nat Med*, 24: 186-93.

Hyman, S. E. 2005. 'Neurotransmitters', *Curr Biol*, 15: R154-8.

Inada, T. 2017. 'The Ribosome as a Platform for mRNA and Nascent Polypeptide Quality Control', *Trends Biochem Sci*, 42: 5-15.

Ishimura, R., G. Nagy, I. Dotu, H. Zhou, X. L. Yang, P. Schimmel, S. Senju, Y. Nishimura, J. H. Chuang, and S. L. Ackerman. 2014. 'RNA function. Ribosome stalling induced by mutation of a CNS-specific tRNA causes neurodegeneration', *Science*, 345: 455-9.

Ito, K., Y. Chadani, K. Nakamori, S. Chiba, Y. Akiyama, and T. Abo. 2011. 'Nascentome analysis uncovers futile protein synthesis in Escherichia coli', *PLoS One*, 6: e28413.

Ito, Y., D. Inoue, S. Kido, and T. Matsumoto. 2005. 'c-Fos degradation by the ubiquitin-proteasome proteolytic pathway in osteoclast progenitors', *Bone*, 37: 842-9.

Ivanov, A. D., G. R. Tukhbatova, S. V. Salozhin, and V. A. Markevich. 2015. 'NGF but not BDNF overexpression protects hippocampal LTP from beta-amyloid-induced impairment', *Neuroscience*, 289: 114-22.

Iwata, A., J. C. Christianson, M. Bucci, L. M. Ellerby, N. Nukina, L. S. Forno, and R. R. Kopito. 2005. 'Increased susceptibility of cytoplasmic over nuclear polyglutamine aggregates to autophagic degradation', *Proc Natl Acad Sci U S A*, 102: 13135-40.

Jiang, S., N. Dupont, E. F. Castillo, and V. Deretic. 2013. 'Secretory versus degradative autophagy: unconventional secretion of inflammatory mediators', *J Innate Immun*, 5: 471-9.

Johnston-Carey, H. K., L. C. Pomatto, and K. J. Davies. 2015. 'The Immunoproteasome in oxidative stress, aging, and disease', *Crit Rev Biochem Mol Biol*, 51: 268-81.

Kammers, K., R. N. Cole, C. Tiengwe, and I. Ruczinski. 2015. 'Detecting Significant Changes in Protein Abundance', *EuPA Open Proteom*, 7: 11-19.

Karpova, A., M. Mikhaylova, U. Thomas, T. Knopfel, and T. Behnisch. 2006. 'Involvement of protein synthesis and degradation in long-term potentiation of Schaffer collateral CA1 synapses', *The Journal of neuroscience : the official journal of the Society for Neuroscience*, 26: 4949-55.

Kaushik, S., and A. M. Cuervo. 2012. 'Chaperone-mediated autophagy: a unique way to enter the lysosome world', *Trends Cell Biol*, 22: 407-17.

Kazee, A. M., and L. Y. Han. 1995. 'Cortical Lewy bodies in Alzheimer's disease', *Arch Pathol Lab Med*, 119: 448-53.

Kelleher, R. J., 3rd, A. Govindarajan, and S. Tonegawa. 2004. 'Translational regulatory mechanisms in persistent forms of synaptic plasticity', *Neuron*, 44: 59-73.

Kim, M. J., A. W. Dunah, Y. T. Wang, and M. Sheng. 2005. 'Differential roles of NR2A- and NR2B-containing NMDA receptors in Ras-ERK signaling and AMPA receptor trafficking', *Neuron*, 46: 745-60.

Kim, S. Y., E. J. Miller, J. Frydman, and W. E. Moerner. 2010. 'Action of the chaperonin GroEL/ES on a non-native substrate observed with single-molecule FRET', *J Mol Biol*, 401: 553-63.

Kim, Y. S., Y. Chu, L. Han, M. Li, Z. Li, P. C. Lavinka, S. Sun, Z. Tang, K. Park, M. J. Caterina, K. Ren, R. Dubner, F. Wei, and X. Dong. 2014. 'Central terminal sensitization of TRPV1 by descending serotonergic facilitation modulates chronic pain', *Neuron*, 81: 873-87.

Kirstein-Miles, J., A. Scior, E. Deuerling, and R. I. Morimoto. 2013. 'The nascent polypeptide-associated complex is a key regulator of proteostasis', *EMBO J*, 32: 1451-68.

Kisselev, A. F., T. N. Akopian, and A. L. Goldberg. 1998. 'Range of sizes of peptide products generated during degradation of different proteins by archaeal proteasomes', *The Journal of biological chemistry*, 273: 1982-9.

Kisselev, A. F., W. A. van der Linden, and H. S. Overkleeft. 2012. 'Proteasome inhibitors: an expanding army attacking a unique target', *Chem Biol*, 19: 99-115.

Klein, M. E., P. E. Castillo, and B. A. Jordan. 2015. 'Coordination between Translation and Degradation Regulates Inducibility of mGluR-LTD', *Cell Rep*.

Kong, M., E. S. Diaz, and P. Morales. 2009. 'Participation of the human sperm proteasome in the capacitation process and its regulation by protein kinase A and tyrosine kinase', *Biol Reprod*, 80: 1026-35.

Kramer, G., D. Boehringer, N. Ban, and B. Bukau. 2009. 'The ribosome as a platform for co-translational processing, folding and targeting of newly synthesized proteins', *Nat Struct Mol Biol*, 16: 589-97.

Labbadia, J., and R. I. Morimoto. 2015. 'The biology of proteostasis in aging and disease', *Annu Rev Biochem*, 84: 435-64.

Landgraf, P., E. R. Antileo, E. M. Schuman, and D. C. Dieterich. 2015. 'BONCAT: metabolic labeling, click chemistry, and affinity purification of newly synthesized proteomes', *Methods Mol Biol*, 1266: 199-215.

Lane, T. J., and V. S. Pande. 2013. 'Inferring the rate-length law of protein folding', *PLoS One*, 8: e78606.

Lazzari, E., and G. Meroni. 2016. 'TRIM32 ubiquitin E3 ligase, one enzyme for several pathologies: From muscular dystrophy to tumours', *Int J Biochem Cell Biol*, 79: 469-77.

Lee, J. G., S. Takahama, G. Zhang, S. I. Tomarev, and Y. Ye. 2016. 'Unconventional secretion of misfolded proteins promotes adaptation to proteasome dysfunction in mammalian cells', *Nat Cell Biol*, 18: 765-76.

Lee, M. J., T. Tasaki, K. Moroi, J. Y. An, S. Kimura, I. V. Davydov, and Y. T. Kwon. 2005. 'RGS4 and RGS5 are in vivo substrates of the N-end rule pathway', *Proc Natl Acad Sci U S A*, 102: 15030-5.

Lee, S. H., J. H. Choi, N. Lee, H. R. Lee, J. I. Kim, N. K. Yu, S. L. Choi, S. H. Lee, H. Kim, and B. K. Kaang. 2008. 'Synaptic protein degradation underlies destabilization of retrieved fear memory', *Science*, 319: 1253-6.

Lee, Y. C., M. Srajer Gajdosik, D. Josic, and S. H. Lin. 2012. 'Plasma membrane isolation using immobilized concanavalin A magnetic beads', *Methods Mol Biol*, 909: 29-41.

Li, N., C. L. Kuo, G. Paniagua, H. van den Elst, M. Verdoes, L. I. Willems, W. A. van der Linden, M. Ruben, E. van Genderen, J. Gubbens, G. P. van Wezel, H. S. Overkleeft, and B. I. Florea. 2013. 'Relative quantification of proteasome activity by activity-based protein profiling and LC-MS/MS', *Nature protocols*, 8: 1155-68.

Lin, D. T., Y. Makino, K. Sharma, T. Hayashi, R. Neve, K. Takamiya, and R. L. Huganir. 2009. 'Regulation of AMPA receptor extrasynaptic insertion by 4.1N, phosphorylation and palmitoylation', *Nature neuroscience*, 12: 879-87.

Lin, Y., B. L. Bloodgood, J. L. Hauser, A. D. Lapan, A. C. Koon, T. K. Kim, L. S. Hu, A. N. Malik, and M. E. Greenberg. 2008. 'Activity-dependent regulation of inhibitory synapse development by Npas4', *Nature*, 455: 1198-204.

Liu, Q. Y., J. X. Lei, M. Sikorska, and R. Liu. 2008. 'A novel brain-enriched E3 ubiquitin ligase RNF182 is up regulated in the brains of Alzheimer's patients and targets ATP6V0C for degradation', *Mol Neurodegener*, 3: 4.

Lopez Salon, M., L. Morelli, E. M. Castano, E. F. Soto, and J. M. Pasquini. 2000. 'Defective ubiquitination of cerebral proteins in Alzheimer's disease', *J Neurosci Res*, 62: 302-10.

Lu, Y., K. Christian, and B. Lu. 2008. 'BDNF: a key regulator for protein synthesis-dependent LTP and long-term memory?', *Neurobiol Learn Mem*, 89: 312-23.

Mabb, A. M., H. S. Je, M. J. Wall, C. G. Robinson, R. S. Larsen, Y. Qiang, S. A. Correa, and M. D. Ehlers. 2014. 'Triad3A regulates synaptic strength by ubiquitination of Arc', *Neuron*, 82: 1299-316.

Maier, T., M. Guell, and L. Serrano. 2009. 'Correlation of mRNA and protein in complex biological samples', *FEBS Lett*, 583: 3966-73.

Malenka, R. C., and R. A. Nicoll. 1999. 'Long-term potentiation--a decade of progress?', *Science*, 285: 1870-4.

Margolis, S. S., J. Salogiannis, D. M. Lipton, C. Mandel-Brehm, Z. P. Wills, A. R. Mardinly, L. Hu, P. L. Greer, J. B. Bikoff, H. Y. Ho, M. J. Soskis, M. Sahin, and M. E. Greenberg. 2010. 'EphB-mediated degradation of the RhoA GEF Ephexin5 relieves a developmental brake on excitatory synapse formation', *Cell*, 143: 442-55.

Marin, P., K. L. Nastiuk, N. Daniel, J. A. Girault, A. J. Czernik, J. Glowinski, A. C. Nairn, and J. Premont. 1997. 'Glutamate-dependent phosphorylation of elongation factor-2 and inhibition of protein synthesis in neurons', *J Neurosci*, 17: 3445-54.

McShane, E., C. Sin, H. Zauber, J. N. Wells, N. Donnelly, X. Wang, J. Hou, W. Chen, Z. Storchova, J. A. Marsh, A. Valleriani, and M. Selbach. 2016. 'Kinetic Analysis of Protein Stability Reveals Age-Dependent Degradation', *Cell*, 167: 803-15 e21.

Mei, F., G. Nagappan, Y. Ke, T. C. Sacktor, and B. Lu. 2011. 'BDNF facilitates L-LTP maintenance in the absence of protein synthesis through PKMzeta', *PLoS One*, 6: e21568.

Melville, M. W., A. J. McClellan, A. S. Meyer, A. Darveau, and J. Frydman. 2003. 'The Hsp70 and TRiC/CCT chaperone systems cooperate in vivo to assemble the von Hippel-Lindau tumor suppressor complex', *Mol Cell Biol*, 23: 3141-51.

Meng, L., R. Mohan, B. H. Kwok, M. Elofsson, N. Sin, and C. M. Crews. 1999a. 'Epoxomicin, a potent and selective proteasome inhibitor, exhibits in vivo antiinflammatory activity', *Proc Natl Acad Sci U S A*, 96: 10403-8.

———. 1999b. 'Epoxomicin, a potent and selective proteasome inhibitor, exhibits in vivo antiinflammatory activity', *Proceedings of the National Academy of Sciences of the United States of America*, 96: 10403-8.

Mills, E. W., J. Wangen, R. Green, and N. T. Ingolia. 2016. 'Dynamic Regulation of a Ribosome Rescue Pathway in Erythroid Cells and Platelets', *Cell Rep*, 17: 1-10.

Morishima, Y., Y. Gotoh, J. Zieg, T. Barrett, H. Takano, R. Flavell, R. J. Davis, Y. Shirasaki, and M. E. Greenberg. 2001. 'Beta-amyloid induces neuronal apoptosis via a mechanism that involves the c-Jun N-terminal kinase pathway and the induction of Fas ligand', *J Neurosci*, 21: 7551-60.

Murata, S., Y. Takahama, and K. Tanaka. 2008. 'Thymoproteasome: probable role in generating positively selecting peptides', *Curr Opin Immunol*, 20: 192-6.

Nathans, D. 1964. 'Puromycin Inhibition of Protein Synthesis: Incorporation of Puromycin into Peptide Chains', *Proc Natl Acad Sci U S A*, 51: 585-92.

Nathans, D., and A. Neidle. 1963. 'Structural requirements for puromycin inhibition of protein synthesis', *Nature*, 197: 1076-7.

Nestler, Eric J., Steven E. Hyman, David M. Holtzman, and Robert C. Malenka. 2015. *Molecular neuropharmacology : a foundation for clinical neuroscience* (The McGraw-Hill Companies, Inc.: New York).

Newman, R. H., P. Whitehead, J. Lally, A. Coffer, and P. Freemont. 1996. '20S human proteasomes bind with a specific orientation to lipid monolayers in vitro', *Biochimica et biophysica acta*, 1281: 111-6.

Ng, D. T., and P. Walter. 1994. 'Protein translocation across the endoplasmic reticulum', *Curr Opin Cell Biol*, 6: 510-6.

Nicoll, R. A., and K. W. Roche. 2013. 'Long-term potentiation: peeling the onion', *Neuropharmacology*, 74: 18-22.

Obeng, E. A., L. M. Carlson, D. M. Gutman, W. J. Harrington, Jr., K. P. Lee, and L. H. Boise. 2006. 'Proteasome inhibitors induce a terminal unfolded protein response in multiple myeloma cells', *Blood*, 107: 4907-16.

Ogg, S. C., and P. Walter. 1995. 'SRP samples nascent chains for the presence of signal sequences by interacting with ribosomes at a discrete step during translation elongation', *Cell*, 81: 1075-84.

Ortega, Z., M. Diaz-Hernandez, and J. J. Lucas. 2007. 'Is the ubiquitin-proteasome system impaired in Huntington's disease?', *Cell Mol Life Sci*, 64: 2245-57.

Ostroff, L. E., B. Botsford, S. Gindina, K. K. Cowansage, J. E. LeDoux, E. Klann, and C. Hoeffer. 2017. 'Accumulation of Polyribosomes in Dendritic Spine Heads, But Not Bases and Necks, during Memory Consolidation Depends on Cap-Dependent Translation Initiation', *J Neurosci*, 37: 1862-72.

Ostroff, L. E., J. C. Fiala, B. Allwardt, and K. M. Harris. 2002. 'Polyribosomes redistribute from dendritic shafts into spines with enlarged synapses during LTP in developing rat hippocampal slices', *Neuron*, 35: 535-45.

Pande, V. S. 2014. 'Understanding protein folding using Markov state models', *Adv Exp Med Biol*, 797: 101-6.

Park, S., C. Lee, P. Sabharwal, M. Zhang, C. L. Meyers, and S. Sockanathan. 2013. 'GDE2 promotes neurogenesis by glycosylphosphatidylinositol-anchor cleavage of RECK', *Science*, 339: 324-8.

Patel, T. P., K. Man, B. L. Firestein, and D. F. Meaney. 2015. 'Automated quantification of neuronal networks and single-cell calcium dynamics using calcium imaging', *Journal of neuroscience methods*, 243: 26-38.

Patrick, G. N., B. Bingol, H. A. Weld, and E. M. Schuman. 2003. 'Ubiquitin-mediated proteasome activity is required for agonist-induced endocytosis of GluRs', *Current biology : CB*, 13: 2073-81.

Pechmann, S., F. Willmund, and J. Frydman. 2013. 'The ribosome as a hub for protein quality control', *Mol Cell*, 49: 411-21.

Peebles, C. L., J. Yoo, M. T. Thwin, J. J. Palop, J. L. Noebels, and S. Finkbeiner. 2010. 'Arc regulates spine morphology and maintains network stability in vivo', *Proc Natl Acad Sci U S A*, 107: 18173-8.

Pines, J., and C. Lindon. 2005. 'Proteolysis: anytime, any place, anywhere?', *Nature cell biology*, 7: 731-5.

Plotkin, J. B., H. Robins, and A. J. Levine. 2004. 'Tissue-specific codon usage and the expression of human genes', *Proc Natl Acad Sci U S A*, 101: 12588-91.

Powers, T., and P. Walter. 1996. 'The nascent polypeptide-associated complex modulates interactions between the signal recognition particle and the ribosome', *Curr Biol*, 6: 331-8.

Protter, D. S., and R. Parker. 2016. 'Principles and Properties of Stress Granules', *Trends Cell Biol*, 26: 668-79.

Protter, D. S. W., B. S. Rao, B. Van Treeck, Y. Lin, L. Mizoue, M. K. Rosen, and R. Parker. 2018. 'Intrinsically Disordered Regions Can Contribute Promiscuous Interactions to RNP Granule Assembly', *Cell Rep*, 22: 1401-12.

Prouty, W. F., and A. L. Goldberg. 1972. 'Fate of abnormal proteins in E. coli accumulation in intracellular granules before catabolism', *Nat New Biol*, 240: 147-50.

Prouty, W. F., M. J. Karnovsky, and A. L. Goldberg. 1975. 'Degradation of abnormal proteins in Escherichia coli. Formation of protein inclusions in cells exposed to amino acid analogs', *J Biol Chem*, 250: 1112-22.

Rabl, J., D. M. Smith, Y. Yu, S. C. Chang, A. L. Goldberg, and Y. Cheng. 2008. 'Mechanism of gate opening in the 20S proteasome by the proteasomal ATPases', *Mol Cell*, 30: 360-8.

Ramachandran, K. V., and S. S. Margolis. 2017. 'A mammalian nervous-system-specific plasma membrane proteasome complex that modulates neuronal function', *Nat Struct Mol Biol*, 24: 419-30.

Ramaswami, M., J. P. Taylor, and R. Parker. 2013. 'Altered ribostasis: RNA-protein granules in degenerative disorders', *Cell*, 154: 727-36.

Richburg, J. H., J. L. Myers, and S. B. Bratton. 2014. 'The role of E3 ligases in the ubiquitin-dependent regulation of spermatogenesis', *Semin Cell Dev Biol*, 30: 27-35.

Rinetti, G. V., and F. E. Schweizer. 2010. 'Ubiquitination acutely regulates presynaptic neurotransmitter release in mammalian neurons', *The Journal of neuroscience : the official journal of the Society for Neuroscience*, 30: 3157-66.

Rivkin, E., A. L. Kierszenbaum, M. Gil, and L. L. Tres. 2009. 'Rnf19a, a ubiquitin protein ligase, and Psmc3, a component of the 26S proteasome, tether to the acrosome membranes and the head-tail coupling apparatus during rat spermatid development', *Dev Dyn*, 238: 1851-61.

Roberts, R. B., and L. B. Flexner. 1969. 'The biochemical basis of long-term memory', *Q Rev Biophys*, 2: 135-73.

Robertson, J. H., and D. N. Wheatley. 1979. 'Pools and protein synthesis in mammalian cells', *Biochem J*, 178: 699-709.

Rock, K. L., D. J. Farfan-Arribas, J. D. Colbert, and A. L. Goldberg. 2014. 'Re-examining class-I presentation and the DRiP hypothesis', *Trends Immunol*, 35: 144-52.

Rock, K. L., C. Gramm, L. Rothstein, K. Clark, R. Stein, L. Dick, D. Hwang, and A. L. Goldberg. 1994. 'Inhibitors of the proteasome block the degradation of most cell

proteins and the generation of peptides presented on MHC class I molecules', *Cell*, 78: 761-71.

Rosales, O., C. Opazo, E. S. Diaz, J. V. Villegas, R. Sanchez, and P. Morales. 2011. 'Proteasome activity and proteasome subunit transcripts in human spermatozoa separated by a discontinuous Percoll gradient', *Andrologia*, 43: 106-13.

Sanchez, R., M. Deppe, M. Schulz, P. Bravo, J. Villegas, P. Morales, and J. Risopatron. 2011. 'Participation of the sperm proteasome during in vitro fertilisation and the acrosome reaction in cattle', *Andrologia*, 43: 114-20.

Sasanami, T., K. Sugiura, T. Tokumoto, N. Yoshizaki, H. Dohra, S. Nishio, S. Mizushima, G. Hiyama, and T. Matsuda. 2012. 'Sperm proteasome degrades egg envelope glycoprotein ZP1 during fertilization of Japanese quail (Coturnix japonica)', *Reproduction*, 144: 423-31.

Sato, Y., N. Watanabe, N. Fukushima, S. Mita, and T. Hirata. 2011. 'Actin-independent behavior and membrane deformation exhibited by the four-transmembrane protein M6a', *PLoS One*, 6: e26702.

Scheetz, A. J., A. C. Nairn, and M. Constantine-Paton. 2000. 'NMDA receptor-mediated control of protein synthesis at developing synapses', *Nat Neurosci*, 3: 211-6.

Schmidt, M., and D. Finley. 2014. 'Regulation of proteasome activity in health and disease', *Biochimica et biophysica acta*, 1843: 13-25.

Schratt, G. M., E. A. Nigh, W. G. Chen, L. Hu, and M. E. Greenberg. 2004. 'BDNF regulates the translation of a select group of mRNAs by a mammalian target of rapamycin-phosphatidylinositol 3-kinase-dependent pathway during neuronal development', *J Neurosci*, 24: 7366-77.

Schreiber, J., M. J. Vegh, J. Dawitz, T. Kroon, M. Loos, D. Labonte, K. W. Li, P. Van Nierop, M. T. Van Diepen, C. I. De Zeeuw, M. Kneussel, R. M. Meredith, A. B. Smit, and R. E. Van Kesteren. 2015. 'Ubiquitin ligase TRIM3 controls

hippocampal plasticity and learning by regulating synaptic gamma-actin levels', *J Cell Biol*, 211: 569-86.

Schubert, U., L. C. Anton, J. Gibbs, C. C. Norbury, J. W. Yewdell, and J. R. Bennink. 2000. 'Rapid degradation of a large fraction of newly synthesized proteins by proteasomes', *Nature*, 404: 770-4.

Schwanhausser, B., D. Busse, N. Li, G. Dittmar, J. Schuchhardt, J. Wolf, W. Chen, and M. Selbach. 2011. 'Global quantification of mammalian gene expression control', *Nature*, 473: 337-42.

Schwanhausser, B., J. Wolf, M. Selbach, and D. Busse. 2013. 'Synthesis and degradation jointly determine the responsiveness of the cellular proteome', *Bioessays*, 35: 597-601.

Sell, G. L., and S. S. Margolis. 2015. 'From UBE3A to Angelman syndrome: a substrate perspective', *Front Neurosci*, 9: 322.

Sell, G. L., T. B. Schaffer, and S. S. Margolis. 2017. 'Reducing expression of synapse-restricting protein Ephexin5 ameliorates Alzheimer's-like impairment in mice', *J Clin Invest*.

Shao, S., K. von der Malsburg, and R. S. Hegde. 2013. 'Listerin-dependent nascent protein ubiquitination relies on ribosome subunit dissociation', *Mol Cell*, 50: 637-48.

Shatz, C. J. 2009. 'MHC class I: an unexpected role in neuronal plasticity', *Neuron*, 64: 40-5.

Shin, S. M., N. Zhang, J. Hansen, N. Z. Gerges, D. T. Pak, M. Sheng, and S. H. Lee. 2012. 'GKAP orchestrates activity-dependent postsynaptic protein remodeling and homeostatic scaling', *Nat Neurosci*, 15: 1655-66.

Siegel, V. 1995. 'A second signal recognition event required for translocation into the endoplasmic reticulum', *Cell*, 82: 167-70.

Sin, N., K. B. Kim, M. Elofsson, L. Meng, H. Auth, B. H. Kwok, and C. M. Crews. 1999. 'Total synthesis of the potent proteasome inhibitor epoxomicin: a useful tool for understanding proteasome biology', *Bioorg Med Chem Lett*, 9: 2283-8.

Smith, M. J., and G. L. Koch. 1989. 'Multiple zones in the sequence of calreticulin (CRP55, calregulin, HACBP), a major calcium binding ER/SR protein', *EMBO J*, 8: 3581-6.

Sontag, E. M., R. S. Samant, and J. Frydman. 2017. 'Mechanisms and Functions of Spatial Protein Quality Control', *Annu Rev Biochem*, 86: 97-122.

Speckmann, T., P. V. Sabatini, C. Nian, R. G. Smith, and F. C. Lynn. 2016. 'Npas4 Transcription Factor Expression Is Regulated by Calcium Signaling Pathways and Prevents Tacrolimus-induced Cytotoxicity in Pancreatic Beta Cells', *J Biol Chem*, 291: 2682-95.

Steward, O., and P. M. Falk. 1991. 'Selective localization of polyribosomes beneath developing synapses: a quantitative analysis of the relationships between polyribosomes and developing synapses in the hippocampus and dentate gyrus', *J Comp Neurol*, 314: 545-57.

Steward, O., and W. B. Levy. 1982. 'Preferential localization of polyribosomes under the base of dendritic spines in granule cells of the dentate gyrus', *J Neurosci*, 2: 284-91.

Steward, O., and P. Worley. 2001. 'Localization of mRNAs at synaptic sites on dendrites', *Results Probl Cell Differ*, 34: 1-26.

Tai, H. C., H. Besche, A. L. Goldberg, and E. M. Schuman. 2010. 'Characterization of the Brain 26S Proteasome and its Interacting Proteins', *Front Mol Neurosci*, 3.

Tai, H. C., and E. M. Schuman. 2008a. 'Ubiquitin, the proteasome and protein degradation in neuronal function and dysfunction', *Nat Rev Neurosci*, 9: 826-38.

———. 2008b. 'Ubiquitin, the proteasome and protein degradation in neuronal function and dysfunction', *Nature reviews. Neuroscience*, 9: 826-38.

Tcherkezian, J., P. A. Brittis, F. Thomas, P. P. Roux, and J. G. Flanagan. 2010. 'Transmembrane receptor DCC associates with protein synthesis machinery and regulates translation', *Cell*, 141: 632-44.

Thrift, R. N., D. W. Andrews, P. Walter, and A. E. Johnson. 1991. 'A nascent membrane protein is located adjacent to ER membrane proteins throughout its integration and translation', *J Cell Biol*, 112: 809-21.

Tsai, N. P. 2014. 'Ubiquitin proteasome system-mediated degradation of synaptic proteins: An update from the postsynaptic side', *Biochim Biophys Acta*, 1843: 2838-42.

Tsurumi, C., N. Ishida, T. Tamura, A. Kakizuka, E. Nishida, E. Okumura, T. Kishimoto, M. Inagaki, K. Okazaki, N. Sagata, and et al. 1995. 'Degradation of c-Fos by the 26S proteasome is accelerated by c-Jun and multiple protein kinases', *Mol Cell Biol*, 15: 5682-7.

Tsvetkov, P., G. Asher, A. Paz, N. Reuven, J. L. Sussman, I. Silman, and Y. Shaul. 2008. 'Operational definition of intrinsically unstructured protein sequences based on susceptibility to the 20S proteasome', *Proteins*, 70: 1357-66.

Tsvetkov, P., N. Reuven, C. Prives, and Y. Shaul. 2009. 'Susceptibility of p53 unstructured N terminus to 20 S proteasomal degradation programs the stress response', *J Biol Chem*, 284: 26234-42.

Tsvetkov, P., N. Reuven, and Y. Shaul. 2009. 'The nanny model for IDPs', *Nat Chem Biol*, 5: 778-81.

Turner, G. C., and A. Varshavsky. 2000. 'Detecting and measuring cotranslational protein degradation in vivo', *Science*, 289: 2117-20.

Uechi, H., J. Hamazaki, and S. Murata. 2014. 'Characterization of the testis-specific proteasome subunit alpha4s in mammals', *J Biol Chem*, 289: 12365-74.

Vabulas, R. M., and F. U. Hartl. 2005. 'Protein synthesis upon acute nutrient restriction relies on proteasome function', *Science*, 310: 1960-3.

van Meer, G., D. R. Voelker, and G. W. Feigenson. 2008. 'Membrane lipids: where they are and how they behave', *Nature reviews. Molecular cell biology*, 9: 112-24.

van Weering, J. R., E. Brown, T. H. Sharp, J. Mantell, P. J. Cullen, and P. Verkade. 2010. 'Intracellular membrane traffic at high resolution', *Methods Cell Biol*, 96: 619-48.

Vilchez, D., L. Boyer, I. Morantte, M. Lutz, C. Merkwirth, D. Joyce, B. Spencer, L. Page, E. Masliah, W. T. Berggren, F. H. Gage, and A. Dillin. 2012. 'Increased proteasome activity in human embryonic stem cells is regulated by PSMD11', *Nature*, 489: 304-8.

Vitolo, O. V., A. Sant'Angelo, V. Costanzo, F. Battaglia, O. Arancio, and M. Shelanski. 2002. 'Amyloid beta -peptide inhibition of the PKA/CREB pathway and long-term potentiation: reversibility by drugs that enhance cAMP signaling', *Proc Natl Acad Sci U S A*, 99: 13217-21.

von der Malsburg, K., S. Shao, and R. S. Hegde. 2015. 'The ribosome quality control pathway can access nascent polypeptides stalled at the Sec61 translocon', *Mol Biol Cell*, 26: 2168-80.

Wade, B. E., C. E. Wang, S. Yan, K. Bhat, B. Huang, S. Li, and X. J. Li. 2014. 'Ubiquitin-activating enzyme activity contributes to differential accumulation of mutant huntingtin in brain and peripheral tissues', *J Neurosci*, 34: 8411-22.

Wang, F., L. A. Durfee, and J. M. Huibregtse. 2013. 'A cotranslational ubiquitination pathway for quality control of misfolded proteins', *Mol Cell*, 50: 368-78.

Wang, H. R., Y. Zhang, B. Ozdamar, A. A. Ogunjimi, E. Alexandrova, G. H. Thomsen, and J. L. Wrana. 2003. 'Regulation of cell polarity and protrusion formation by targeting RhoA for degradation', *Science*, 302: 1775-9.

Werner, H., L. Dimou, M. Klugmann, S. Pfeiffer, and K. A. Nave. 2001. 'Multiple splice isoforms of proteolipid M6B in neurons and oligodendrocytes', *Mol Cell Neurosci*, 18: 593-605.

West, A. E., W. G. Chen, M. B. Dalva, R. E. Dolmetsch, J. M. Kornhauser, A. J. Shaywitz, M. A. Takasu, X. Tao, and M. E. Greenberg. 2001. 'Calcium regulation of neuronal gene expression', *Proc Natl Acad Sci U S A*, 98: 11024-31.

Wheatley, D. N. 2011. 'Protein balance: a fundamental question of cell biology needing reappraisal', *Cell Biol Int*, 35: 453-5.

Wheatley, D. N., M. R. Giddings, and M. S. Inglis. 1980. 'Kinetics of degradation of "short-" and "long-lived" proteins in cultured mammalian cells', *Cell Biol Int Rep*, 4: 1081-90.

Wheatley, D. N., S. Grisolia, and J. Hernandez-Yago. 1982. 'Significance of the rapid degradation of newly synthesized proteins in mammalian cells: a working hypothesis', *J Theor Biol*, 98: 283-300.

Wheatley, D. N., and M. S. Inglis. 1980. 'An intracellular perfusion system linking pools and protein synthesis', *J Theor Biol*, 83: 437-45.

Wheeler, J. R., T. Matheny, S. Jain, R. Abrisch, and R. Parker. 2016. 'Distinct stages in stress granule assembly and disassembly', *Elife*, 5.

Wickner, S., M. R. Maurizi, and S. Gottesman. 1999. 'Posttranslational quality control: folding, refolding, and degrading proteins', *Science*, 286: 1888-93.

Wiedmann, B., H. Sakai, T. A. Davis, and M. Wiedmann. 1994. 'A protein complex required for signal-sequence-specific sorting and translocation', *Nature*, 370: 434-40.

Wilson, A. C., B. N. Dugger, D. W. Dickson, and D. S. Wang. 2011. 'TDP-43 in aging and Alzheimer's disease - a review', *Int J Clin Exp Pathol*, 4: 147-55.

Winter, M. B., F. La Greca, S. Arastu-Kapur, F. Caiazza, P. Cimermancic, T. J. Buchholz, J. L. Anderl, M. Ravalin, M. F. Bohn, A. Sali, A. J. O'Donoghue, and C. S. Craik. 2017. 'Immunoproteasome functions explained by divergence in cleavage specificity and regulation', *Elife*, 6.

Wu, B., C. Eliscovich, Y. J. Yoon, and R. H. Singer. 2016. 'Translation dynamics of single mRNAs in live cells and neurons', *Science*, 352: 1430-5.

Wu, S., K. L. Hyrc, K. L. Moulder, Y. Lin, T. Warmke, and B. J. Snider. 2009. 'Cellular calcium deficiency plays a role in neuronal death caused by proteasome inhibitors', *J Neurochem*, 109: 1225-36.

Wu, W. K., V. Volta, C. H. Cho, Y. C. Wu, H. T. Li, L. Yu, Z. J. Li, and J. J. Sung. 2009. 'Repression of protein translation and mTOR signaling by proteasome inhibitor in colon cancer cells', *Biochem Biophys Res Commun*, 386: 598-601.

Wunder, C., J. Lippincott-Schwartz, and H. Lorenz. 2010. 'Determining membrane protein topologies in single cells and high-throughput screening applications', *Current protocols in cell biology / editorial board, Juan S. Bonifacino ... [et al.]*, Chapter 5: Unit 5 7.

Xia, Z., H. Dudek, C. K. Miranti, and M. E. Greenberg. 1996. 'Calcium influx via the NMDA receptor induces immediate early gene transcription by a MAP kinase/ERK-dependent mechanism', *J Neurosci*, 16: 5425-36.

Yang, Z., and D. J. Klionsky. 2010. 'Mammalian autophagy: core molecular machinery and signaling regulation', *Curr Opin Cell Biol*, 22: 124-31.

Yokota, N., Y. Harada, and H. Sawada. 2010. 'Identification of testis-specific ubiquitin-conjugating enzyme in the ascidian Ciona intestinalis', *Mol Reprod Dev*, 77: 640-7.

Yonashiro, R., E. B. Tahara, M. H. Bengtson, M. Khokhrina, H. Lorenz, K. C. Chen, Y. Kigoshi-Tansho, J. N. Savas, J. R. Yates, S. A. Kay, E. A. Craig, A. Mogk, B. Bukau, and C. A. Joazeiro. 2016. 'The Rqc2/Tae2 subunit of the ribosome-associated quality control (RQC) complex marks ribosome-stalled nascent polypeptide chains for aggregation', *Elife*, 5: e11794.

Zhang, M., C. M. Pickart, and P. Coffino. 2003. 'Determinants of proteasome recognition of ornithine decarboxylase, a ubiquitin-independent substrate', *EMBO J*, 22: 1488-96.

Zhang, Y., K. Chen, S. A. Sloan, M. L. Bennett, A. R. Scholze, S. O'Keeffe, H. P. Phatnani, P. Guarnieri, C. Caneda, N. Ruderisch, S. Deng, S. A. Liddelow, C. Zhang, R. Daneman, T. Maniatis, B. A. Barres, and J. Q. Wu. 2014. 'An RNA-sequencing transcriptome and splicing database of glia, neurons, and vascular cells of the cerebral cortex', *J Neurosci*, 34: 11929-47.

Zhao, J., G. A. Garcia, and A. L. Goldberg. 2016. 'Control of proteasomal proteolysis by mTOR', *Nature*, 529: E1-2.

Zhao, J., B. Zhai, S. P. Gygi, and A. L. Goldberg. 2015. 'mTOR inhibition activates overall protein degradation by the ubiquitin proteasome system as well as by autophagy', *Proc Natl Acad Sci U S A*, 112: 15790-7.

Zhu, P. P., A. Patterson, B. Lavoie, J. Stadler, M. Shoeb, R. Patel, and C. Blackstone. 2003. 'Cellular localization, oligomerization, and membrane association of the hereditary spastic paraplegia 3A (SPG3A) protein atlastin', *The Journal of biological chemistry*, 278: 49063-71.

Zimmerman, S., and P. Sutovsky. 2009. 'The sperm proteasome during sperm capacitation and fertilization', *J Reprod Immunol*, 83: 19-25.

## Curriculum Vitae


| | |
|---|---|
| **Name** | Kapil Vishveshwar Ramachandran |
| **Date of Birth** | May 17, 1991 |
| **Place of Birth** | Austin, Texas |
| **Mailing Address** | 2125 E Lombard St<br>Baltimore, MD 21231 |
| **Phone** | 512-426-0093 |
| **Email** | kramachandran517@gmail.com |


**Education**

| | | |
|---|---|---|
| PhD | expected 2018 | Biological Chemistry<br>Johns Hopkins School of Medicine<br>Baltimore, MD<br>Thesis advisor: Seth S. Margolis, Ph.D. |
| Bachelor of Science<br>Neuroscience | 2008-2012 | Duke University<br>Trinity College of Arts and Sciences |

**Professional experience**

| | | |
|---|---|---|
| Research rotations | 2012-2013 | Advisors: Craig M. Montell, Ph.D<br>Erika L, Matunis, Ph.D.<br>Seth S. Margolis, Ph.D. |
| Undergraduate research | 2008-2012 | Geoffrey S. Pitt, M.D, Ph.D |
| High School research | 2006-2008 | Nigel S. Atkinson, Ph.D |

**Publications**

**Ramachandran KV***, Fu JM, Schaffer T, Na C-H, Margolis SS*. Activity-dependent degradation of the immediate early nascentome by the neuronal membrane proteasome. Manuscript in review, Molecular Cell, 2018. *Co-Corresponding Authors

**Ramachandran KV*** and Margolis SS*. A nervous system-specific plasma membrane proteasome complex that modulates neuronal function. Nature Structural and Molecular Biology, April 2017. doi: 10.1038/nsmb.3389. *Co-Corresponding Authors

See: News In Depth, Science, March 31, 2017

Cover article, NSMB April 2017

Andersen ND, **Ramachandran KV**, Bao MM, Kirby ML, Pitt GS, Hutson MR. Calcium signaling regulates ventricular hypertrophy during development independent of contraction or blood flow. J Mol Cell Cardiol. 2015 Mar; 80:1-9.

Stine RL, Greenspan LJ, **Ramachandran KV**, Matunis EL. Coordinate regulation of stem cell competition by Slit-Robo and JAK-STAT signaling in the *Drosophila* testis. Plos Genetics, 2014 Nov 6; 10(11):e1004713

**Ramachandran KV**, Hennessey JA, Barnett AS, Yin X, Stadt HA, Yazawa M, Dolmetsch RE, Kirby ML, Pitt GS. Calcium influx through L-type $Ca_V1.2$ $Ca^{2+}$ channels regulates mandibular development. J Clin Invest. 2013;123(4):1638-46.

**Ramachandran KV** and Margolis SS. Neurons talking trash – implications from the discovery of the neuronal membrane proteasome to nervous system biology. Manuscript in preparation, invited "Think again" review at Bioessays.

**Ramachandran KV*** and Margolis SS*. Neuronal membrane proteasomes generate peptides that are protective against abeta-induced neurotoxicity. Manuscript in preparation, 2018. *Co-Corresponding Authors

**Talks**

Invited Lecture to the Directors of the National Institute of Health (NIH) and National Institute of Drug Abuse (NIDA), 2008

Invited lecture to the public at North Carolina Museum of Life and Science, 2009

Invited lecture at University of Texas at Austin, 2012

Talk at FASEB: Ion Channel Regulation, 2013

Seminar talk at Department of Biological Chemistry, Johns Hopkins School of Medicine, 2015

Talk at Biochemistry, Cellular, and Molecular Biology Program Retreat, Johns Hopkins School of Medicine, 2015

Seminar talk at Department of Neuroscience, Johns Hopkins School of Medicine, 2016

Seminar talk at Department of Biological Chemistry, Johns Hopkins School of Medicine, 2016

Talk at Cold Spring Harbor Conference on Protein Homeostasis in Health and Disease, 2016

Talk at Gordon Research Conference – Cell Biology of the Neuron, 2016

Talk at American Society for Biochemistry and Molecular Biology (ASBMB), 2017

Seminar at Weizmann Institute of Science, Israel (Host: Dr. Michal Sharon), 2017

Seminar at Harvard Medical School, Dept of Cell Biology (Host: Dr. Alfred Goldberg), 2017

**Posters**

Poster Presentation at 49$^{th}$ Annual Drosophila Conference in San Diego., 2008

Poster Presentation at 38th Society for Neuroscience Conference, Washington DC., 2008

Poster at Weinstein Conference, 2012

FASEB: Calcium and Cell Function., 2013

BCMB Program Retreat Poster, Johns Hopkins School of Medicine, 2014

BCMB Graduate Program Recruiting Poster session, Johns Hopkins School of Medicine, 2015

Biological Chemistry Retreat Poster, Johns Hopkins School of Medicine, 2016

Posters at Cold Spring Harbor Conference on Protein Homeostasis in Health and Disease, 2016

Poster at Keystone Symposia – Synapses and Circuits, 2017

**Grants**

2011: Duke University Dean's Research Fellowship

2012: Weinstein Award

2013: NSF Graduate Research Fellowship

2016: Cold Spring Harbor travel award

2018: Harvard Society of Fellows, Junior Fellow

**Service and activities**

2010-2012 Duke University Board of Trustees, Academic Affairs Counsel

2014 Sara Bellum Public Outreach for STEM education

2014 Advisor for the NSF for STEM education, outreach

2014-2015 Advisor for NSF and USAID on International Research Development

2013-2016 Recruitment Leader and Coordinator for Johns Hopkins BCMB graduate program

2017 Teaching Graduate Ethics Course: Scientific Record Keeping, Data Management